DEVELOPMENT OF A

MULTI-FREQUENCY INTERFEROMETER TELESCOPE FOR RADIO ASTRONOMY

(MITRA)

Master of Engineering: Electrical

Thesis

by

Dominique Guelord Kumamputu Ingala

DEVELOPMENT OF A

MULTI-FREQUENCY INTERFEROMETER TELESCOPE FOR RADIO ASTRONOMY

(MITRA)

Submitted to the Department of Electronic Engineering in the Faculty of Engineering and the Built Environment at the Durban University of Technology, in fulfilment of the academic requirements for the Degree

Master of Engineering: Electrical

By

Dominique Guelord Kumamputu Ingala

March 2015

Mr SD MacPherson Supervisor	Date
Dr O Sokoya Co-supervisor	Date

Plagiarism Declaration

I hereby declare that the contents of this thesis, entitled **Development of a Multi-frequency Interferometer Telescope for Radio Astronomy (MITRA),** is a true reflection of my own work, and that this thesis has not been submitted, in whole or part, for a degree to any other University or Institution.

Dominique G.K. Ingala

Student Number: 20929809

Dedication

Special words of dedication to my parents: Mr. Claude Ingala and Mrs. Philomène Anger.

The truth is what my parents have taught me.

Acknowledgments

The goal of this project would have not been achieved without the contribution of many individuals. The list of acknowledgments will not be exhaustive. First of all, I sincerely thank Mr. S.D. MacPherson for supervising this project. His guidance and cooperation during this research were much appreciated. Acknowledgment must be extended to Mr. G. van Vuuren for suggestions on the development and implementation of this project. Thanks also to Prof. G. Beehary of the University of Mauritius for valuable discussions during the course of the project. Mr. J. Kaganda and Ms. Z. Chiliza are acknowledged for their assistance during the construction stage.

Many thanks are sent to the subject librarian Mrs. A. Finlayson for her assistance in finding relevant literature related to this research, especially for organizing free training on research tools such as EndNote.

Special acknowledgment is addressed to Prof. A. van Ardenne and the Organizing Committee of the URSI-Session for their support for my participation in the IEEE Africon 2013 Conference and for the publication of my article in IEEE Xplore.

I am grateful to Dr. N. Oozeer and the Local Organizing Committee of the 2nd Synthesis Imaging School for Radio Astronomy organized by the SKA-SA. I am also grateful to Dr. A. van der Byl and the Organizing Committee of the High Performance Signal Processing Workshop at the University of Cape Town. Attending these events was very important for my studies.

I will remember those who brought up various signs of encouragement, especially my uncles Mr. Antoine Bulu and Lally Anger for their financial contributions for the sake of my studies.

Abstract

This dissertation describes the development and construction of the Multi-frequency Interferometer Telescope for Radio Astronomy (MITRA) at the Durban University of Technology. The MITRA station consists of 2 antenna arrays separated by a baseline distance of 8 m. Each array consists of 8 Log-Periodic Dipole Antennas (LPDAs) operating from 200 MHz to 800 MHz. The design and construction of the LPDA antenna and receiver system is described. The receiver topology provides an equivalent noise temperature of 113.1 K and 55.1 dB of gain. The Intermediate Frequency (IF) stage was designed to produce a fixed IF frequency of 800 MHz. The digital Back-End and correlator were implemented using a low cost Software Defined Radio (SDR) platform and Gnu-Radio software. Gnu-Octave was used for data analysis to generate the relevant received signal parameters including total power, real, and imaginary, magnitude and phase components. Measured results show that interference fringes were successfully detected within the bandwidth of the receiver using a Radio Frequency (RF) generator as a simulated source. This research was presented at the IEEE Africon 2013 / URSI Session Mauritius, and published in the proceedings.

List of Acronyms

ADC : Analog-to-Digital Converter

ASIC : Application Specific Integrated Circuit

AUT : Antenna Under Test

BCR : Berkeley Cognitive Radio

BPF : Band-Pass Filter

DAC : Digital-to-Analog Converter

DB : Daughter Board

dBi : Decibel with respect to an isotropic antenna

DDC : Digital Down Converter

DSP : Digital Signal Processing

DUC : Digital Up Converter

EH : East-Horizontal

EW : East-West

FFT : Fast Fourier Transform

FIR : Finite Impulse Response

FM : Frequency Modulation

FPGA : Field Programmable Gate Array

GBT : Green Bank Telescope

GPL : General Public Licence

GPS : Global Positioning System

GRC : GnuRadio Companion

GUI : Graphical User Interface

HPBW : Half Power Bandwidth

ID : Identification

IEEE : Institute of Electrical and Electronic Engineers

IF : Intermediate Frequency

IP : Internet Protocol

IRL : Isotropic Received Level

KUAR : Kansas University Agile Radio

LED : Light Emitting Diode

LNA : Low Noise Amplifier

LO : Local Oscillator

LPCAD : Log Periodic Computer-Aided Drawing

LPDA : Log Periodic Dipole Antenna

LPF : Low Pass Filter

MAC : Media Access Control

MARS : Maynooth Adaptable Radio System

MIMO : Multiple Inputs Multiple Outputs

MITRA : Multi-frequency Interferometer Telescope for Radio Astronomy

NATR : National Antenna Test Range

NIC : Network Interface Card

NICT : National Institute of Information and Communication Technology

NRAO : National Radio Astronomy Observatory

NS : North-South

PC : Personal Computer

PLL : Phase Locked Loop

PPS : Pulse Per Second

RF : Radio Frequency

RFI : Radio Frequency Interference

RFID : Radio Frequency Identification

ROACH : Reconfigurable Open Architecture Computing Hardware

rms : Root Mean Squared

RX : Receiver

SDR : Software Defined Radio

SKA : Square Kilometre Array

SKA-SA : Square Kilometre Array – South Africa

SNR : Signal-to-Noise Ratio

SPI : Serial Peripheral Interface

TX : Transmitter

UHD : USRP Hardware Driver

USRP : Universal Software Radio Peripheral

VLBA : Very Long Baseline Array

VLBI : Very Long Baseline Interferometer

VNA : Vector Network Analyzer

VSWR : Voltage Standing Wave Ratio

WH : West-Horizontal

List of Figures

List of Tables

List of Annexures

Table of Contents

Chapter 1: General Introduction

1.1. Project background and overview

This project concerns the development of a Multi-frequency Interferometer Telescope for Radio Astronomy (MITRA). MITRA is an international collaborative project between the University of Mauritius (UoM) and the Durban University of Technology (DUT). MITRA functions initially as a two element interferometer. Each element is a station of 16 antennas. The first element is located at Bras d'Eau, Poste de Flacq, Mauritius and the second at DUT. Both elements, separated by a distance of 2400 km, will be used to form a very long baseline interferometer (VLBI). Each station will be independently controlled. The purpose of this research was to develop the DUT station of the MITRA project.

1.2. Definition of concepts

A telescope for radio astronomy is defined as a radio system designed to collect electromagnetic radiation from the universe so as to permit the radiation to be analyzed [1]. Radio telescopes are used to study naturally occurring radio emission from stars, galaxies, quasars and other astronomical objects at specific frequencies [2].

The frequency range in radio astronomy is defined by three factors: atmospheric transparency, technology, and fundamental limitations imposed by quantum noise. The Earth's atmosphere absorbs electromagnetic radiation at most infrared, ultraviolet, X-ray, and gamma ray wavelengths. There are only two atmospheric windows suitable for ground-based astronomy: the radio wave band and the visible wave band. The two atmospheric windows constitute the

frequency ranges of the electromagnetic spectrum in which most radiation reaches the ground [3].

The visible wave band is relatively narrow in terms of logarithmic frequencies or wavelengths. Early astronomical observing was limited to visible objects: stars, clusters, galaxies of stars, hot ionized gas, and objects shining by reflected starlight (planets, moons) [3].

The radio window is much wider than the visible window. It includes a wide range of astronomical sources, including thermal and non-thermal radiation mechanisms. The atmosphere is not perfectly transparent at any radio frequency. The Earth's ionosphere prevents ground-based observations at frequencies below 10 MHz (λ = 30 m). Cosmic radio waves having frequencies below 10 MHz are usually reflected back into space by the Earth's ionosphere. The radio window is exceptionally broad from 10 MHz to 1 THz [3].

The MITRA telescope is a multi-frequency interferometer. By definition, an interferometer is an instrument that achieves high angular resolution by combining signals from at least two separated telescopes or two antenna arrays [3]. The angular resolution of a telescope is the smallest angle between two distinct objects that can be resolved. It is the ability of a telescope to distinguish fine detail.[4].

Angular resolution is one of the basic requirements of a telescope. It depends on the size of the telescope aperture. To be useful as a radio telescope, the antenna must have a large effective aperture. The ideal radio telescope should have a large collecting area to detect faint sources [3, 5].

For parabolic dish telescopes, the resolution depends on the dish diameter (see Equation 1.1). The bigger the dish, the higher the resolution. The construction of a large diameter dish becomes an engineering challenge, especially if the dish needs to be fully steerable because the mechanical structure, control system, and maintenance become more demanding.

The angular resolution of single-dish radio telescopes is often inadequate. The radio band is too wide (five decades in wavelength) to be covered effectively by a single telescope design [3, 5]. The angular resolution θ is given by Equation 1.1 [6]:

$$\theta = 1.22 \cdot \frac{\lambda}{D} \qquad \text{[rad]} \tag{1.1}$$

The inadequateness of a single-dish telescope regarding the angular resolution can be demonstrated using some practical examples.

The Hartebeesthoek 26 m diameter radio telescope is currently equipped with receivers to cover the 18 cm, 13 cm, 6 cm, 5 cm, 4.5 cm, 3.5 cm, and 2.5 cm wavelength bands [7].

At 18 cm wavelength, the telescope in this study should provide an angular resolution of 0.0084 radians or 1 742.44 arcsec.

The Green Bank Telescope (GBT) is the world largest fully steerable single-dish telescope. It is a 100 m diameter dual offset Gregorian reflector radio telescope operating in the frequency range 100 MHz to 115 GHz (wavelength = 3 m to 2.6 mm). For this telescope, the 18 cm wavelength is covered by the L-Band (1.15-1.73 GHz) receiver [8].

At 18 cm wavelength, the GBT telescope should provide an angular resolution of 0.0021 radians or 453.03 arcsec.

It can be seen that at the same wavelength, the angular resolution of the Hartebeestoek telescope is 3.84 times lower than the resolution of the Green Bank Telescope. This is exactly the proportion between 26 m and 100 m dish diameters.

The Very Long Baseline Array (VLBA) is an array of ten parabolic antennas at different stations distributed over the United States. Several other radio telescopes often participate in VLBI observing in conjunction with the VLBA. At the 18 cm wavelength band, the VLBA array provides an angular resolution of 4.3 milliarcsec [9].

Using Equation 1.1, the VLBA telescope would theoretically require a parabolic antenna with a diameter of 10 534 km. Building such a telescope would not be possible.

This distance (10 534 km) is approximately the baseline between the Mauna Kea (MK) station in the USA and the Effelsberg (EB) station in Germany when the VLBA operates in VLBI observation [9].

The surface brightness and angular size of radio sources span an even wider range, so a combination of single telescopes and aperture-synthesis interferometers are needed to detect and image them. It is not practical to build a single telescope that is even close to optimum for all of radio astronomy. Interferometer techniques are used to provide larger dimensions to the total aperture so as to improve the resolution [3, 5].

Radio telescopes vary widely, but they all have two basic components: a radio antenna and a sensitive radio receiver. The sensitivity of a radio telescope is the ability to measure weak sources of radio emission. It depends on the collecting area and efficiency of the antenna, and the sensitivity of the radio receiver used to detect signals. For broadband continuum emission, the sensitivity also depends on the bandwidth of the receiver. Because cosmic radio sources are extremely weak, radio telescopes are usually large and only the most sensitive radio receivers are used. Moreover, weak cosmic signals can be easily masked by terrestrial radio interference, and great effort is taken to protect radio telescopes from artificial human related interference [2].

As part of the specifications the MITRA telescope will not operate at a single frequency. It will be operational for a range of frequencies from 200 MHz to 800 MHz. A number of interesting astrophysical emissions and phenomena can be analyzed in this band: galaxy evolution, radio galaxy physics, clusters of galaxies, black holes, relics of radio emission, gas and star formation [10].

1.3. Brief science case for MITRA

Presently most radio telescopes carrying out low frequency observations are found in the northern hemisphere. Important objects for study, e.g. the centre of the Milky Way and the Large and Small Magellanic clouds (LMC & SMC) are only visible from the southern hemisphere. A large percentage of astronomical objects radiate more strongly at lower frequencies as received from the southern hemisphere, which is where MITRA will operate from. The MITRA telescope will be able to address the following areas of research [11]:

- Solar: flares, coronal mass ejections.

Solar flares and coronal mass ejections are important factors in the variation of space weather and the danger they pose to satellites and power grids. This solar emission is generally stronger at lower frequencies, where the low frequency array can observe and monitor them.

- The Milky Way and the galactic centre star forming regions.

  It is important to study our galaxy, the Milky Way, as it is the building block of the large scale structures in the Universe. It is speculated that a super massive black hole is found at the galactic centre and radio observations suggest its existence. More low frequency observations are required. Also low frequency observations of star forming regions can give important insights into their formation and the chemistry of the Milky Way.

- Clusters of galaxies.

  Clusters are strong radio emitters. They can be used to trace baryonic matter in the universe. More accurate maps of clusters may help to identify the underlying dark energy in the universe.

- Pulsars.

  Pulsars are rapidly rotating neutron stars. Insights into condensed matter physics can be derived from observations of pulsars. Pulsar profiles change with frequency. Monitoring pulsars over a wide frequency range can lead to new discoveries of hitherto unknown mechanisms, for example science from observations of the glitches occurring in the Vela pulsar.

- Supernova Remnants.

A better analysis of supernova remnants can be gained by observing the interaction of shock waves with the cosmic plasma and dust using this low frequency array. Furthermore, the interstellar medium can also be studied by this interaction.

- Transient sources.

  There is great interest in understanding transient sources. Low frequency target-of-opportunity observations of such objects will provide data necessary to better understand them.

- Spectral and recombination line observations.

  Spectral and recombination line observations afford observers the opportunity to study the astro-chemistry of the Milky Way and other objects.

- Study of spectral indices of sources.

  Galaxy type identification is greatly improved through the study of spectral indices of radio sources. Low frequency spectral index studies that can be performed by this new array will provide statistical information on various galaxy populations.

- Interstellar scintillation: lower end of spectrum.

  Interstellar scintillation is important in the study of interstellar plasma.

- Jupiter.

  Radio emission from Jupiter peaks at about 22 MHz. Observations of Jupiter's emission at higher frequencies can assist in the study of its magnetic fields.

- Ionospheric and Space Weather.

  The radio study of ionospheric mechanisms can provide crucial data on space weather.

1.4. Proposed MITRA signal chain

The MITRA telescope was implemented following the general block diagram shown in Figure 1.1. The MITRA telescope signal chain consists of 2 segments. The outdoor segment or Front-End segment consists of two antenna arrays separated by a distance of 8 metres. Each array is a set of eight dual-polarized log-periodic dipole antennas (LPDAs). The LPDAs provide dual polarized outputs which are filtered and amplified. The indoor segment consists of the Intermediate Frequency (IF) stage and the Digital Back-End. Each antenna array is formed using an 8-way combiner [12]. By grouping the antennas into an array, the directivity is increased [13].

After the combiner, a fibre optic transmitter is used to convert the RF signal to a fibre optic signal. Four fibre optic cables are used to transport the signals to the indoor segment. The first operation in the indoor segment is the optical-to-RF conversion using a fibre optic receiver.

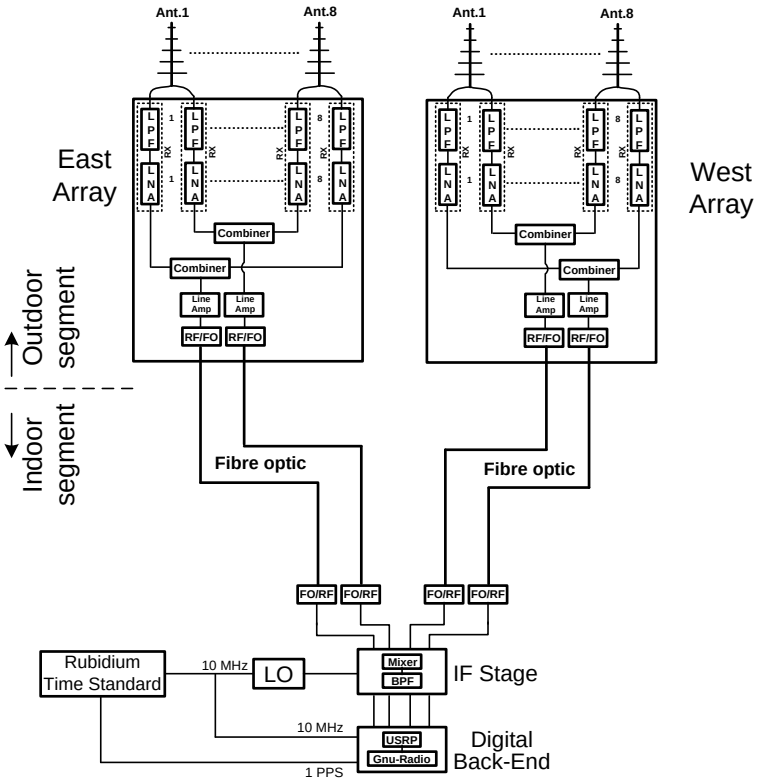

Figure 1.1. General block diagram of the MITRA telescope

The IF stage is designed to have 800 MHz as the system IF. The Digital Back-End section was implemented in Software Defined Radio (SDR) architecture. The Universal Software Radio Peripheral (USRP) and Gnu-Radio software is used for the Digital Back-End. A GPS-disciplined Rubidium time standard is used for time synchronization and phase coherence.

Chapter 2: Design and Construction of the Dual-polarized Log-periodic Dipole Antenna (LPDA)

2.1. Introduction

This chapter focuses on the design and construction of the dual-polarized log-periodic antenna (LPDA) for the MITRA array. The design process started with a single-polarized LPDA. The concept of a dual-polarized LPDA was implemented in the construction phase [13].

The LPDA is a series-fed array of parallel wire dipoles of successively increasing lengths outward from the feed point at the apex [14]. The LPDA introduces a radiation pattern and directivity typically between 7 and 15 dBi. However the driven element shifts with the frequency. This is why the LPDA offers a wide bandwidth. The reason for this antenna being called a log-periodic antenna is that its input impedance is a periodic function of the logarithm of the frequency. Other parameters that undergo similar variations include the radiation pattern, directivity and beamwidth [15].

2.2. Fundamental considerations

Figure 2.1 shows the geometric dimensions of the log-periodic dipole antenna [15]. The LPDA consists of many dipoles of different lengths. Each element is connected to the source. The antenna is divided into the so-called active region and inactive regions. The role of a specific dipole element is linked to the operating frequency: If its length, L, is approximately half a wavelength, it is an active dipole and within the active region. If its length is greater than half a wavelength, it is in an inactive region and acts as a reflector. If its length is less than half a wavelength, it is also in an inactive region but acts as a director. The highest frequency is

basically determined by the shortest dipole length (L_N) while the lowest frequency is determined by the longest dipole length (L_1) [15].

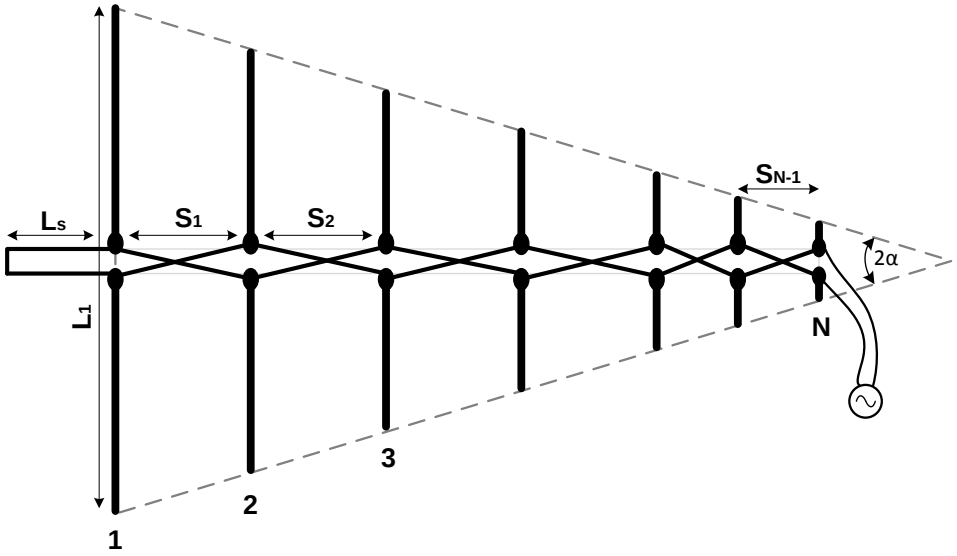

Figure 2.1. Geometric dimensions of the LPDA

For the geometrical dimension analysis, the following notations are used:

L_s: the length of the boom before the first element,

L_n: the length of the element n, where $n = 1, 2, 3, \ldots$

S_n: the spacing between elements n and $n + 1$;

d_n: the diameter of the element n;

g_n: the physical gap between the poles of the element n.

They are related to the scaling factor τ in Equation 2.1.

$$\tau = \frac{L_2}{L_n} = \frac{L_{n+1}}{L_n} = \frac{S_{n+1}}{S_n} = \frac{d_{n+1}}{d_n} = \frac{g_{n+1}}{g_n} < 1 \tag{2.1}$$

and the spacing factor σ in Equation 2.2.

$$\sigma = \frac{S_1}{2L_1} = \frac{S_n}{2L_n} < 1 \tag{2.2}$$

As shown in Figure 2.1, two straight lines through the dipole ends form an angle 2α, which is a characteristic of the frequency-independent structure. The angle α is called the apex angle of the log-periodic antenna, which is a key design parameter and can be found from Equation 2.3.

$$\alpha = tan^{-1}\left(\frac{(L_n - L_{n-1})}{2S_n}\right) = tan^{-1}\left(\frac{L_n(1-\tau)}{2S_n}\right) = tan^{-1}\left(\frac{(1-\tau)}{4\sigma}\right) \tag{2.3}$$

These relations hold true for any n. From the operational principle of the antenna and the frequency point of view, Equation 2.1 corresponds to:

$$\tau = \frac{L_{n+1}}{L_n} = \frac{f_n}{f_{n+1}} \tag{2.4}$$

Where f_n is the resonant frequency of element n. Taking the logarithm of both sides, we have:

$$log(\tau) = log(f_n) - log(f_{n+1}) \tag{2.5}$$

$$log(f_{n+1}) = log(f_n) - log(\tau) \tag{2.6}$$

This means that the resonant frequency in log scale is increased by every $|log(\tau)|$. Thus, the performance of the antenna is periodic in a logarithmic fashion, hence the name log-periodic antenna.

The relation between the directivity as a function of the scaling factor τ and the spacing factor σ is summarized in Table 2.1. This table can be used to compute the physical dimensions. It is apparent that the higher the directivity the larger the scaling factor and spacing factor, but the smaller the apex value.

Another important aspect of the design is the antenna input impedance which can be tuned by changing the diameter d of the element and the feeding gap g between the two poles [15].

$$g = d.cosh(Z_0/120) \tag{2.7}$$

Where Z_0 is the characteristic impedance of the feed line.

Table 2.1. Optimum design data for the LPDA

Directivity (dBi)	**Scaling factor τ**	**Spacing factor σ**	**Apex angle α**
7	0.782	0.138	21.55°
7.5	0.824	0.146	16.77°
8	0.865	0.157	12.13°
8.5	0.892	0.165	9.29°
9	0.918	0.169	6.91°
9.5	0.935	0.174	5.33°
10	0.943	0.179	4.55°
10.5	0.957	0.182	3.38°
11	0.964	0.185	2.79°

In practice, the most likely scenario is that the design frequency range is given from f_{min} to f_{max}. The following equations may be employed for the design [15]:

$$L_1 \geq \frac{\lambda_{max}}{2} = \frac{c}{f_{min}} \tag{2.8}$$

$$L_N \geq \frac{\lambda_{min}}{2} = \frac{c}{f_{max}} \tag{2.9}$$

$$\frac{f_{min}}{f_{max}} = \frac{L_N}{L_1} = \tau \frac{L_{N-1}}{L_1} = \tau^{N-1} \tag{2.10}$$

$$N = \left(\frac{log\left(\frac{f_{min}}{f_{max}}\right)}{log(\tau)} \right) + 1 \tag{2.11}$$

where *c* is the velocity of an electromagnetic wave in free space.

A design example in [15] has demonstrated that the calculated number of elements (in Equation 2.11) must be increased by 2. This is a precautionary measure to make sure that the desired directivity will be achieved [15].

Once the physical dimensions are obtained, it is desirable to find the radiation pattern. The best approach for this is to use a software package to complete this task [15].

The antenna feed should be shorted at a distance L_s behind the longest element L_1. The short acts as a reflector. Its distance from L_1 can be calculated from Equation 2.12 [15]. This corresponds to the section of the boom before the longest element L_1 also known as a shorting stub [16].

$$L_s = \frac{L_1}{4} \tag{2.12}$$

When the spacing between elements is determined using Equation 2.2, the total length L_t of the antenna is given by Equation 2.13.

$$L_t = L_s + \sum_{n}^{N-1} S_n \tag{2.13}$$

In theory, the dipole diameter and feed gap at an element should also be scaled as indicated in Equation 2.1, but in practice this is sometimes hard to achieve [15] as it complicates the physical construction of the antenna.

2.3. MITRA LPDA physical dimensions (Calculation)

The MITRA antenna was designed based on the following parameters:

- f_{min} = 200 MHz
- f_{max} = 800 MHz
- directivity G = 8.5 dBi (average value in Table 2.1)
- scaling factor τ = 0.892
- spacing factor σ = 0.165
- diameter of element: 6 mm
- Boom width: 15 mm

Applying Equation 2.11, the number of elements gives N = 13 elements. As stated in Section 2.2, the calculated number of elements should be increased by 2 to achieve optimum performance. The total number of elements is therefore:

$$N = 15 \text{ elements}$$

Using Equation 2.8 and Equation 2.2, the element lengths as well as the distance between elements were calculated and are shown in Table 2.2.

Using Equation 2.12, the distance to the shorting stub was calculated as:

$$L_s = 18.8 \text{ cm}$$

Applying Equation 2.13, the total antenna length, from the longest to the shortest element, was calculated as:

$$L_t = 1.8 \text{ m}$$

Including the shorting bar, the overall antenna length is 2 m. Figure 2.2 shows the physical dimensions of the MITRA LPDA.

Table 2.2. Calculated element lengths and distance between elements

Element length (cm)		Spacing (cm)	
L_1	75.0	S_1	24.8
L_2	66.9	S_2	22.1
L_3	59.7	S_3	19.7
L_4	53.2	S_4	17.6
L_5	47.5	S_5	15.7
L_6	42.4	S_6	14.0
L_7	37.8	S_7	12.5
L_8	33.7	S_8	11.1
L_9	30.1	S_9	9.9
L_{10}	26.8	S_{10}	8.8
L_{11}	23.9	S_{11}	7.9
L_{12}	21.3	S_{12}	7.0
L_{13}	19.0	S_{13}	6.3
L_{14}	17.0	S_{14}	5.6
L_{15}	15.1	S_{15}	----

2.4. Simulation and optimization

LPCAD software [17] was used to verify the physical dimensions calculated in Section 2.3. The same design parameters discussed in Section 2.3 were considered. The element length and spacing were computed, and are given in Table 2.3. For example, L_1 is the total dipole length of the longest element 1. The spacing S_1 is the distance between elements 1 and 2. It can be seen that the simulated results correlate with the calculated ones [12].

The LPCAD file was exported into 4nec2 antenna design software [18] for simulation. It should be mentioned that the simulator was not able to design a dual-polarized LPDA. Figure 2.3 shows a single-polarized LPDA antenna under simulation. A ground plane was used and the antenna was mounted vertically. The number of elements (15) is the same as determined from the calculation in Section 2.3.

Figure 2.4 shows the simulated result of the Voltage Standing Wave Ratio (VSWR) between 200-800 MHz. It can be seen that across the band the average value of the VSWR is below 2.

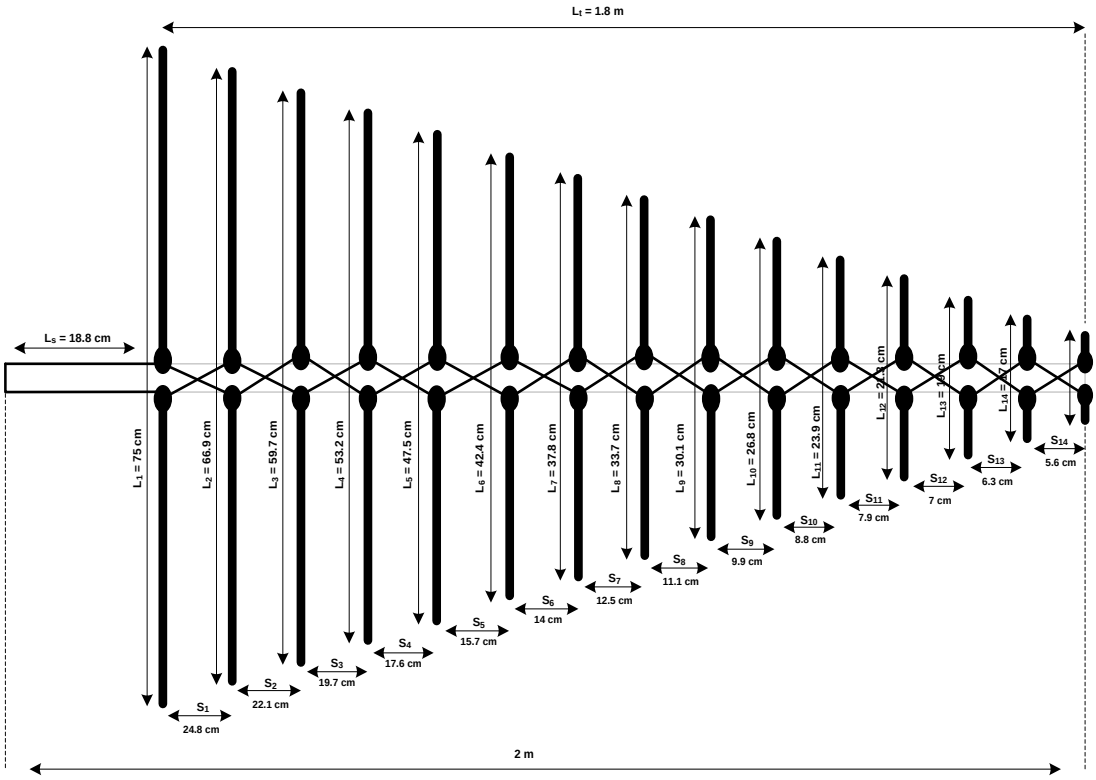

Figure 2.2. Physical dimensions of the MITRA LPDA

Table 2.3. LPDA dimensions

Length (m)		Spacing (m)	
L_1	0.765	S_1	0.252
L_2	0.682	S_2	0.225
L_3	0.609	S_3	0.201
L_4	0.543	S_4	0.179
L_5	0.484	S_5	0.16
L_6	0.432	S_6	0.143
L_7	0.385	S_7	0.127
L_8	0.344	S_8	0.113
L_9	0.307	S_9	0.101
L_{10}	0.273	S_{10}	0.09
L_{11}	0.244	S_{11}	0.08
L_{12}	0.218	S_{12}	0.072
L_{13}	0.194	S_{13}	0.064
L_{14}	0.173	S_{14}	0.057
L_{15}	0.154	----	----

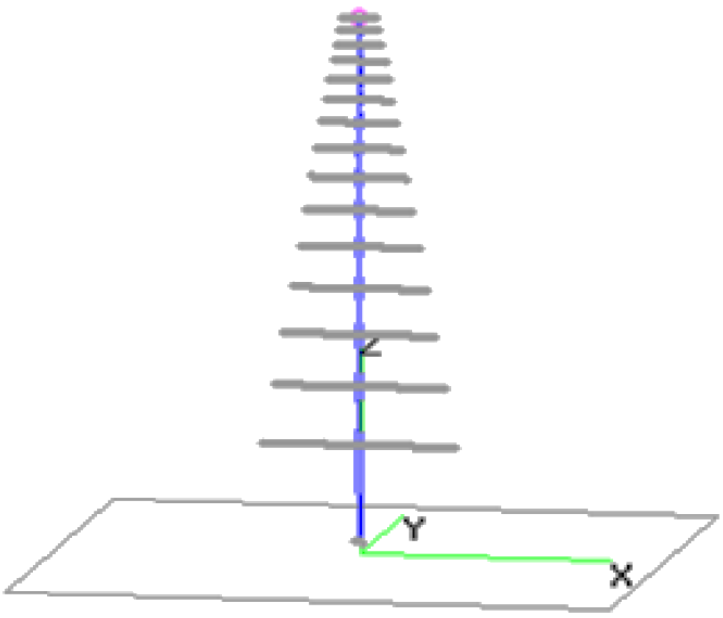

Figure 2.3. MITRA antenna under simulation

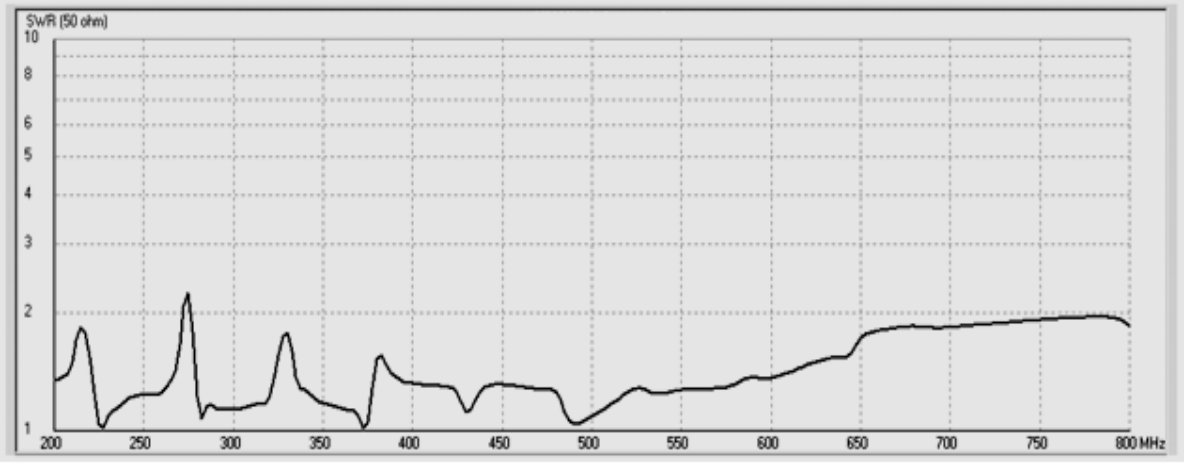

Figure 2.4. Simulated VSWR result between 200-800 MHz

The simulated plot of the radiation pattern at 300 MHz is shown in Figure 2.5. A maximum directivity of 9.49 dBi was obtained at 300 MHz. The simulated plot shows a half-power beamwidth (HPBW) of 80°. Simulated polar plots at other frequencies (200, 400, 500, 600, 700 and 800 MHz) are shown from Figure 2.6 to Figure 2.11. Figure 2.12 shows the simulated result of the gain between 200 MHz to 800 MHz. The presence of more side and back lobes can be observed as the frequency increases. There is a minimum gain of 7.35 dB at 800 MHz and a

maximum gain of 11.24 dB at 330 MHz. The simulated results demonstrate a reduced performance of the LPDA at the upper limit of the operational frequency band.

2.5. Construction

Any electromagnetic wave can be decomposed into two orthogonal polarized components. If the wave is essentially random (noise generated by blackbody radiation for example) the two orthogonal components will vary rapidly in intensity but have equal powers when averaged over long times. Such radiation is called unpolarized. Blackbody radiation is unpolarized. Most astronomical sources are unpolarized or nearly so [19].

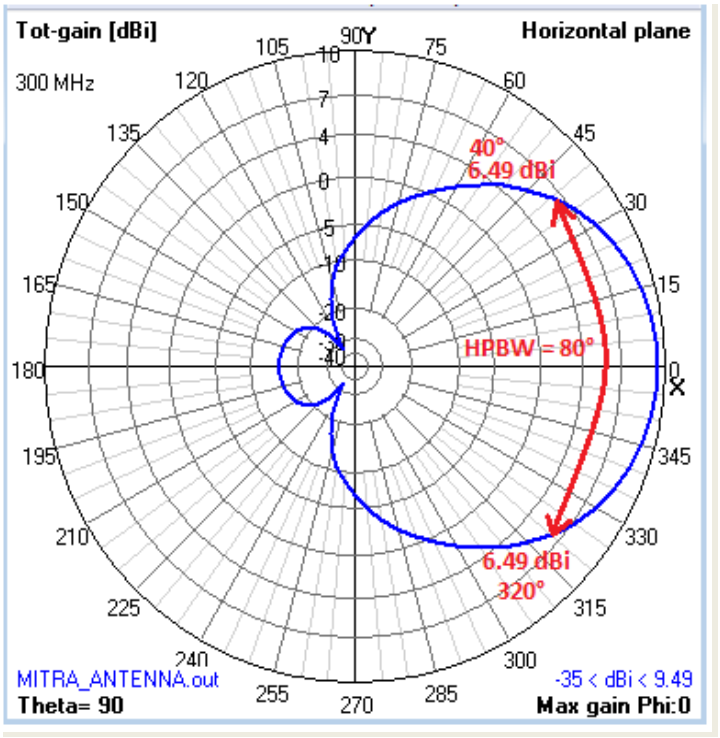

Figure 2.5. Simulated plot of the radiation pattern at 300 MHz

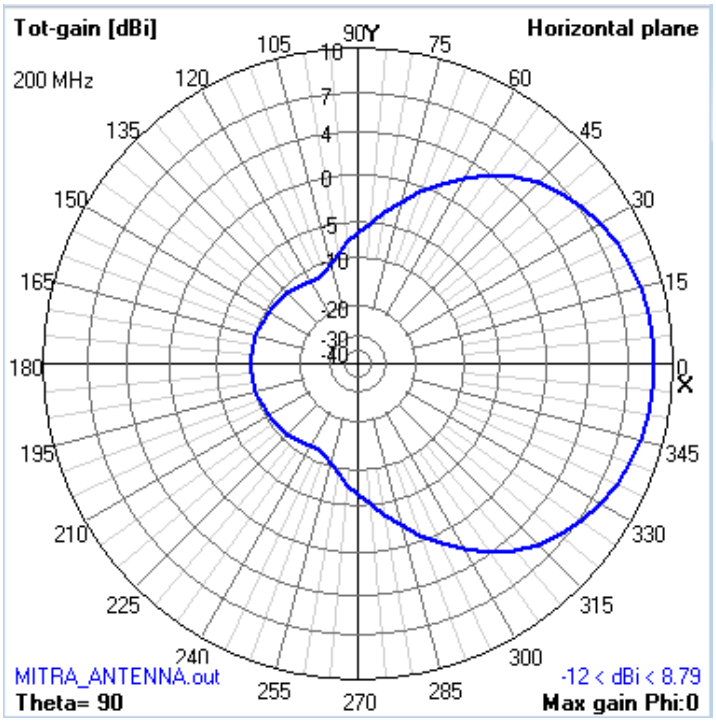

Figure 2.6. Simulated plot of the radiation pattern at 200 MHz

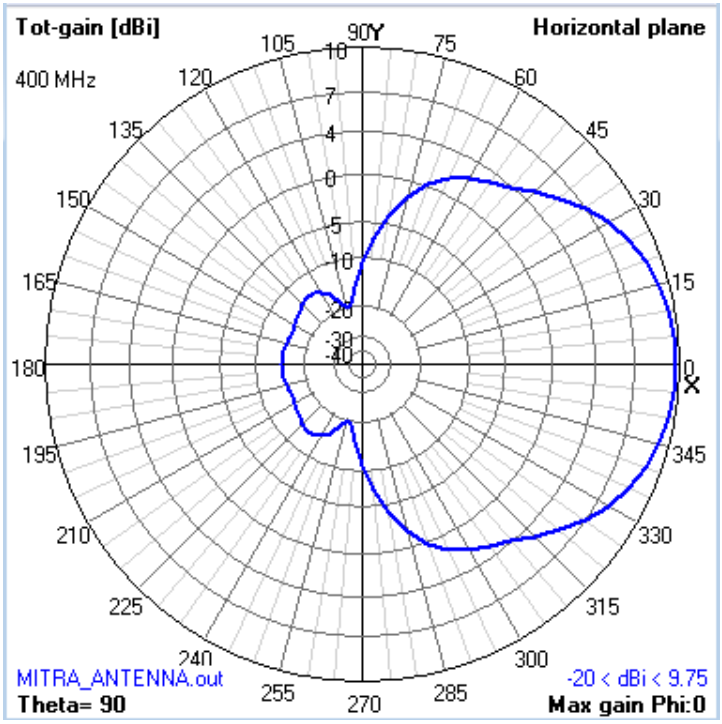

Figure 2.7. Simulated plot of the radiation pattern at 400 MHz

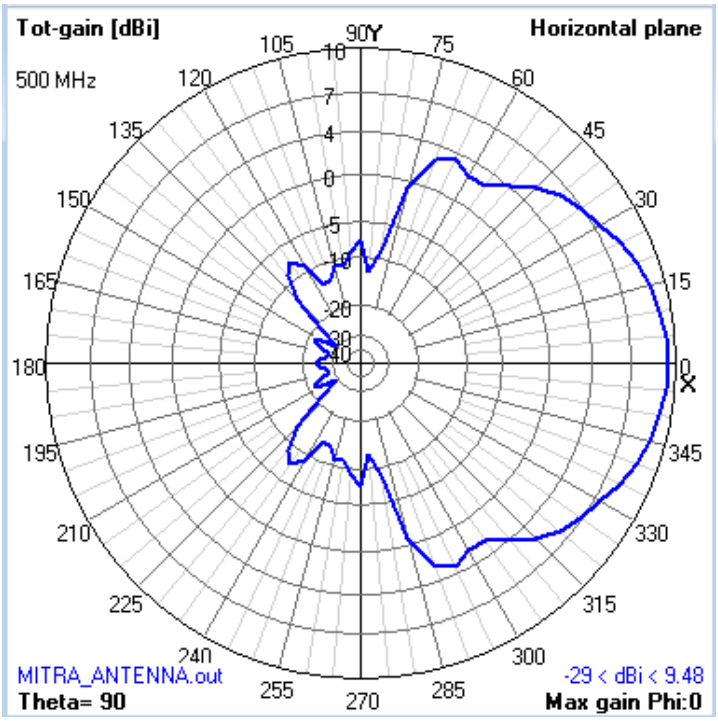

Figure 2.8. Simulated plot of the radiation pattern at 500 MHz

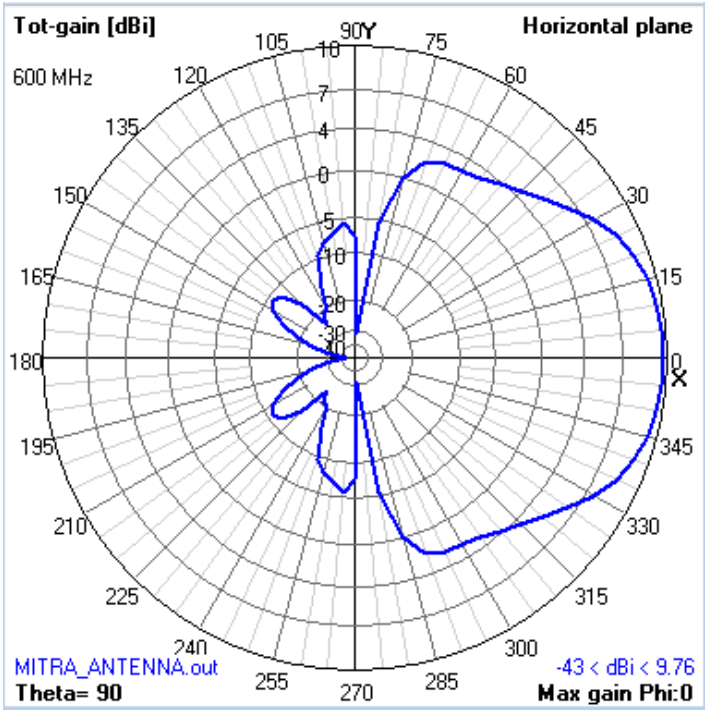

Figure 2.9. Simulated plot of the radiation pattern at 600 MHz

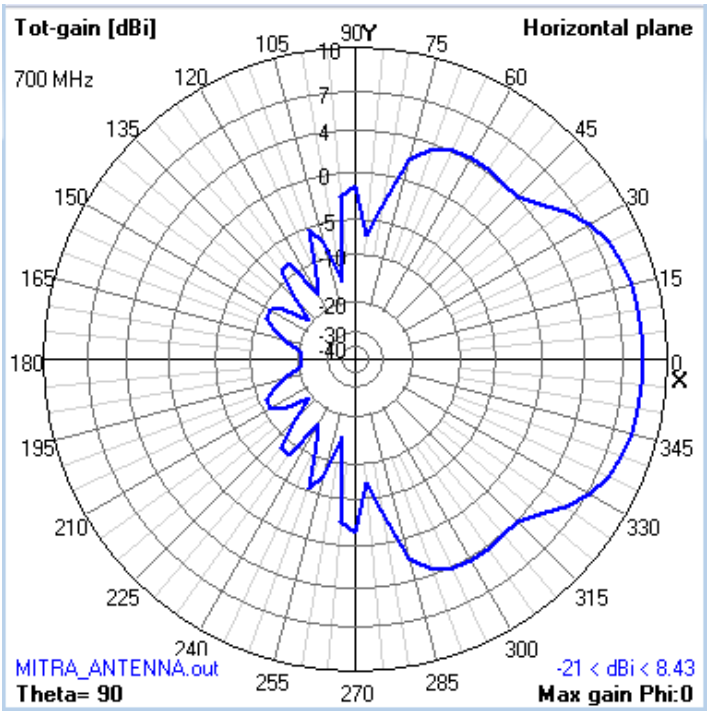

Figure 2.10. Simulated plot of the radiation pattern at 700 MHz

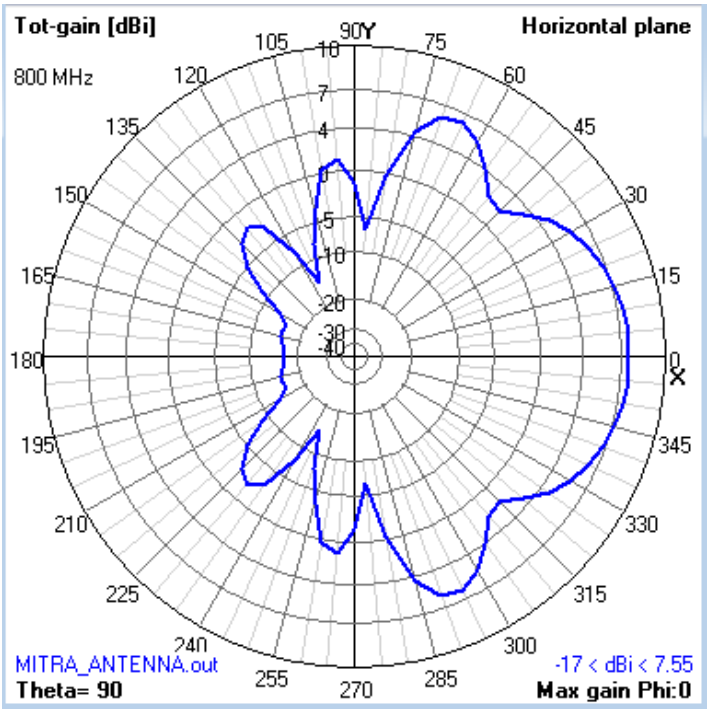

Figure 2.11. Simulated plot of the radiation pattern at 800 MHz

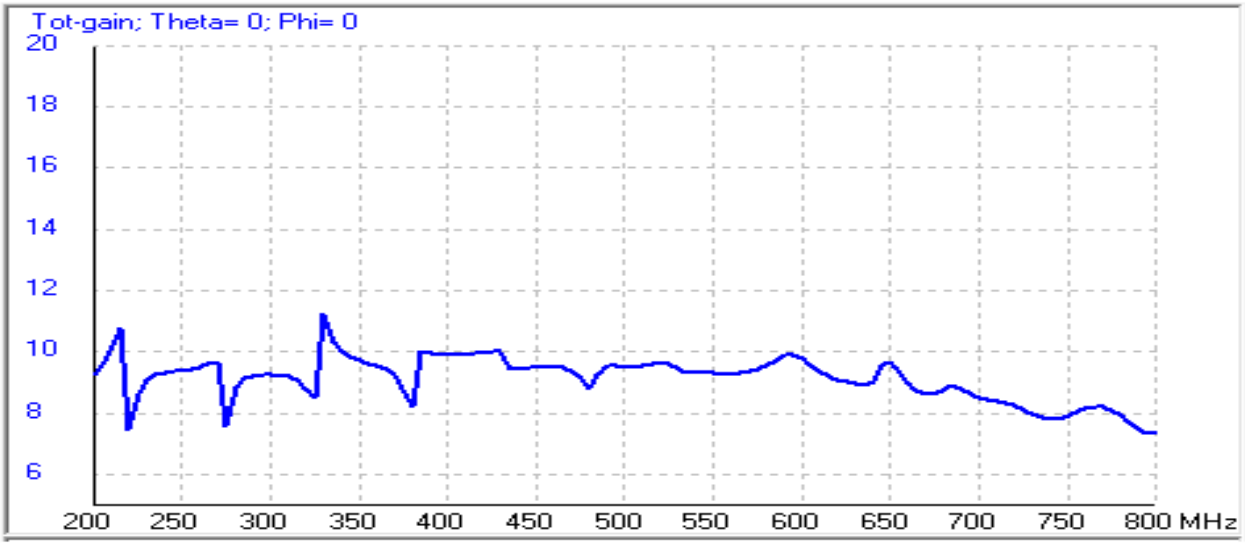

Figure 2.12. Simulated antenna gain

Any antenna with a single output collects only one of the two polarizations from an electromagnetic wave. For example, a linear dipole antenna collects radiations only from the linear polarization whose electric field is parallel to the antenna elements. Electric fields perpendicular to the dipole antenna do not produce current in the antenna. The linear dipole is completely insensitive to the linear polarization perpendicular to its elements. A pair of crossed dipoles is needed to collect power from both orthogonal polarizations simultaneously [19].

For this reason, the MITRA antenna was designed as a dual-polarized log-periodic dipole antenna. Each MITRA antenna consists of two identical LPDA antennas (LPDA 1 and LPDA 2) oriented at 90°. In order to have the two antennas oriented symmetrically at 90°, each LPDA was divided into two distinct sections (A-B and C-D) as shown in Figure 2.13.

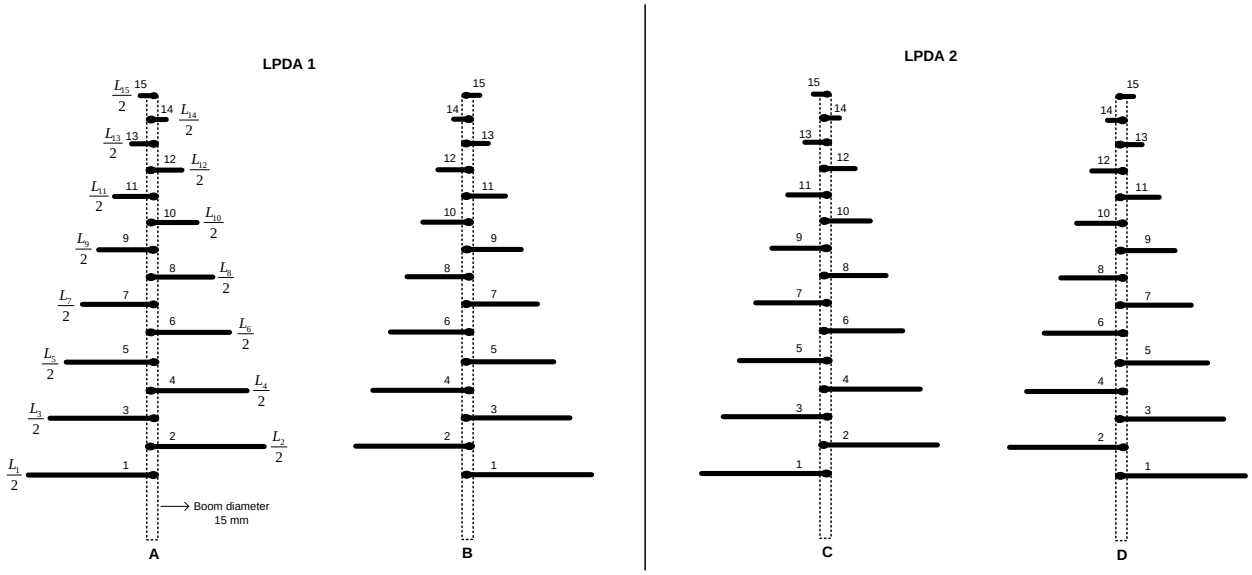

Figure 2.13. LPDA 1 and LPDA 2 sections

The shorting bar in Figure 2.14 was used to assemble the dual-polarized LPDA. It was found that the use of the shorting bar improved the VSWR of the LPDA. The square holes A and B were used to fit the two booms from LPDA 1. The square holes C and D were used to fit the two booms from LPDA 2. Referring to Figure 2.15, the calculated distance between A and B, and between C and D, was 22.32 mm. This distance was enough for a reasonable separation between the booms. The dimensions (in mm) of the shorting bar are given in Figure 2.15.

Spacers shown in Figure 2.16 were used to ensure there was no physical contact between the booms. Cable ties were used to clamp the booms around the spacer in order to ensure the booms did not make physical contact. The design dimensions (in mm) of the plastic spacer are shown in Figure 2.17. The square base shown in Figure 2.18 was designed to support the antenna structure. The design dimensions (in mm) are given in Figure 2.19.

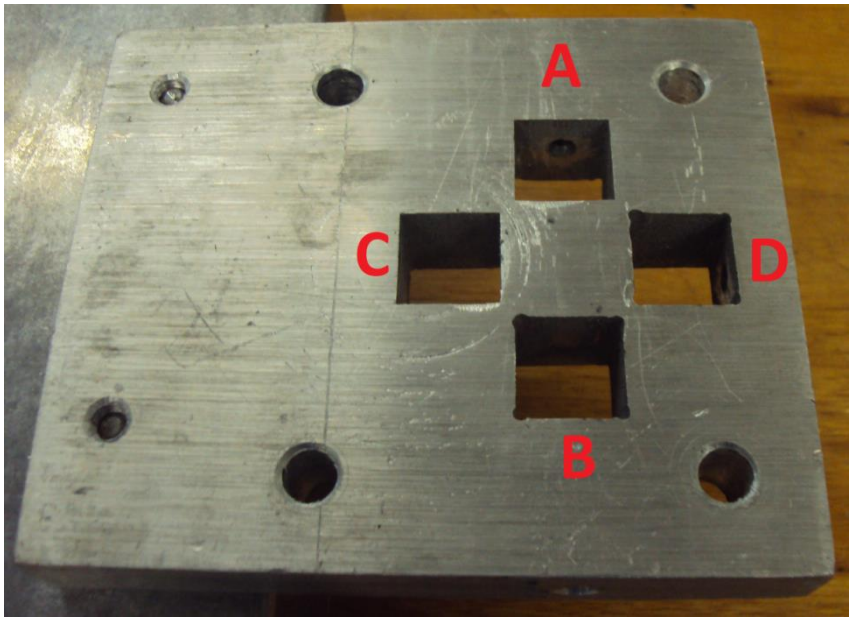

Figure 2.14. Shorting bar

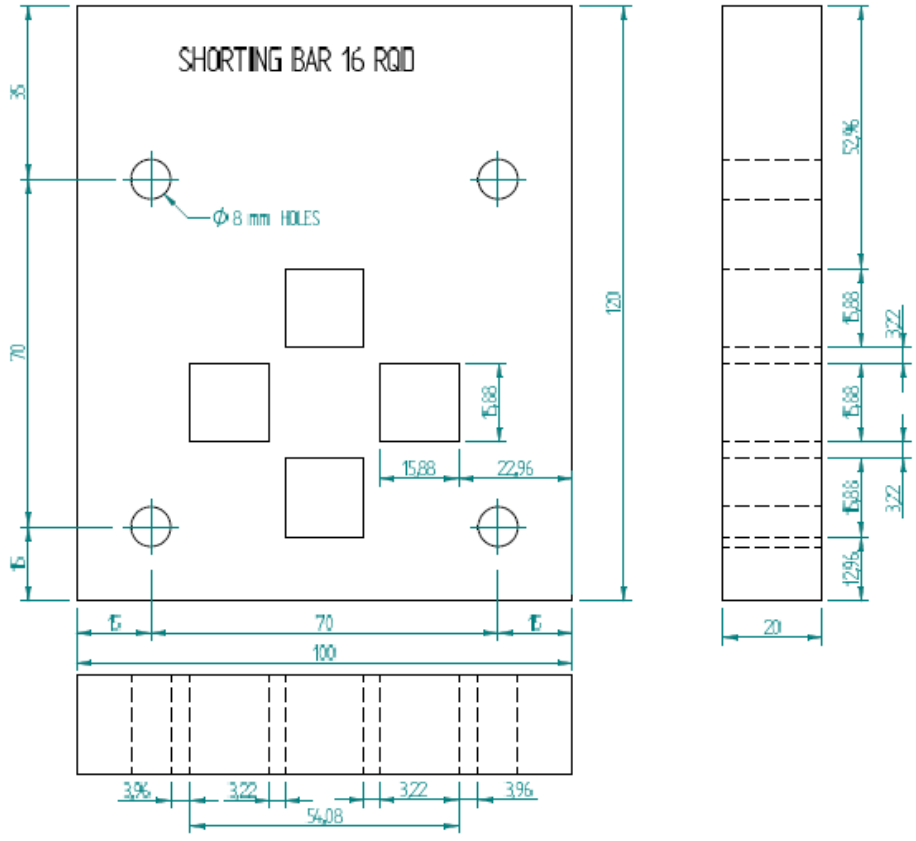

Figure 2.15. Dimensions (in mm) of the shorting bar

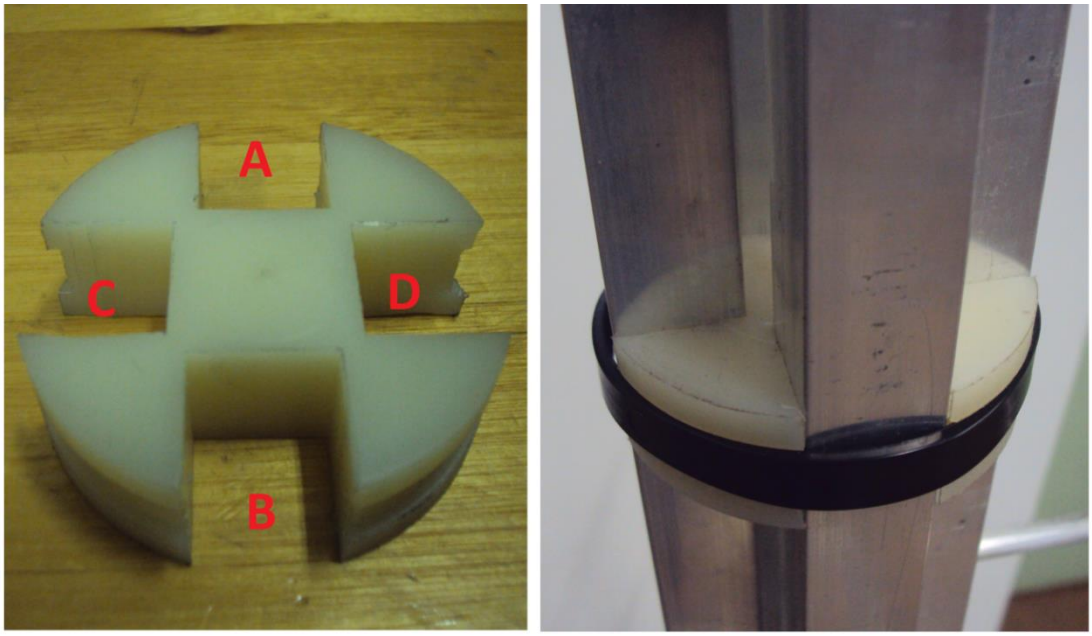

Figure 2.16. Plastic spacer

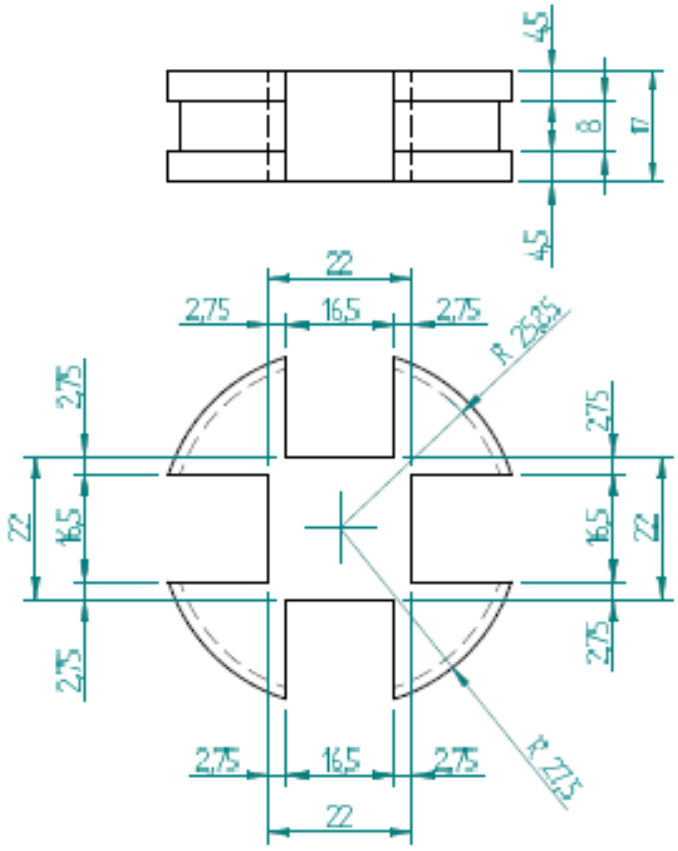

Figure 2.17. Dimensions (in mm) of the spacer

Figure 2.18. Antenna base

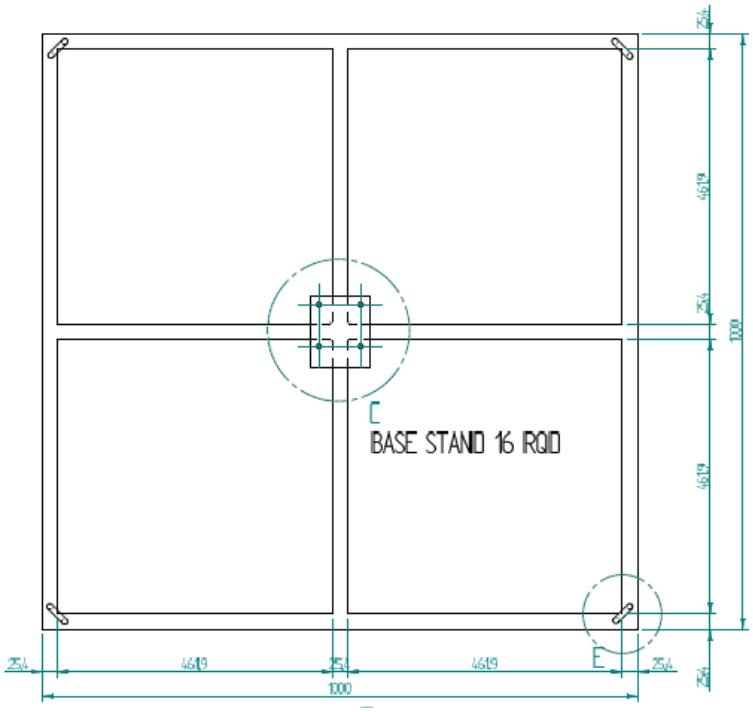

Figure 2.19. Antenna base design dimensions (in mm)

Stay-wires were used to protect the antenna against wind loading. The final design model of the dual-polarized LPDA is shown in Figure 2.20.

2.6. Cabling

As shown in Figure 2.1, the LPDA feed point is located at the shortest element. Two RF cables were used to feed the MITRA antenna. The two LPDAs (LPDA 1 and LPDA 2) are separately fed.

Double-shielded coaxial cable (LMR-195) was used to feed the antennas. The cable outer jacket was stripped for the entire length of the boom and the cable was fed inside one of the antenna booms. The coaxial outer conductor is thus shorted to the inside of the boom. In addition there are solid electrical connections at each end of the boom to the coaxial outer conductor. This arrangement produces an infinite balun [20].

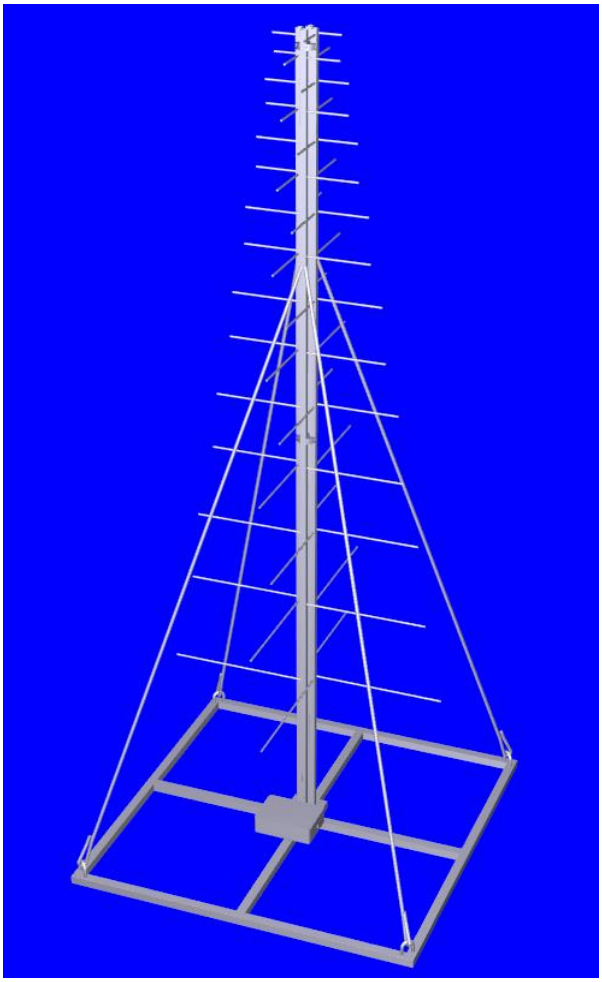

Figure 2.20. Design model of the MITRA Dual-polarized LPDA

As shown in Figure 2.21, each feeder-boom was made with a cavity where the stripped part of the coaxial cable penetrates inside the boom. This cavity was made 15 cm above the ground plane. A screw, nut and threaded bracket were used to clamp the stripped part of the cable

against the boom for good grounding. For waterproofing, self-amalgamating tape was used to seal the cavity and the clamping point.

It was found that careful positioning of the cable at the antenna feed point was required to improve the VSWR. Any loop in the cable degrades the antenna performance. As shown in Figure 2.22, a U-notch cut was made at the inside of each boom. To ensure good grounding at the feed point, screws and threaded brackets were used to clamp the stripped part of the cable against the feeder-boom.

The braiding shield was extended to 30 mm beyond the clamping point. Heat-shrink tubing was used to cover the remaining braiding shield and the dielectric. This arrangement is shown in Figure 2.23.

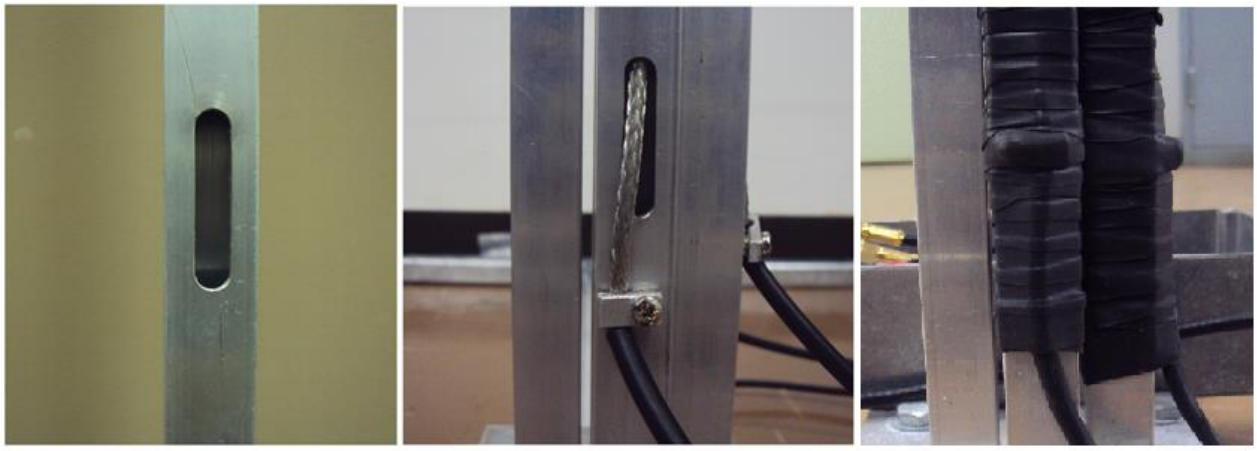

Figure 2.21. Feeder-boom cavity, cable clamping, and waterproofing seal

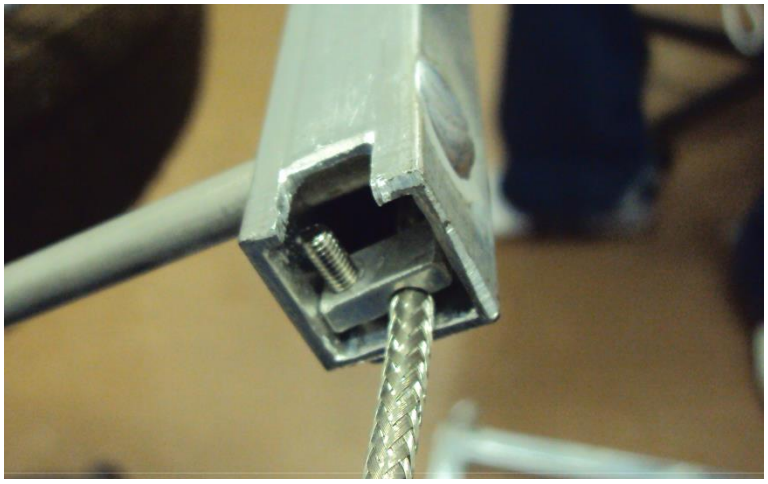

Figure 2.22. Antenna boom with U-notch cut

The solid core of the cable was used to make an electrical connection between the corresponding booms (A-B and C-D). Screws and threaded brackets were used to clamp the solid core against the boom at the feed point. Cable positioning is shown in Figure 2.24.

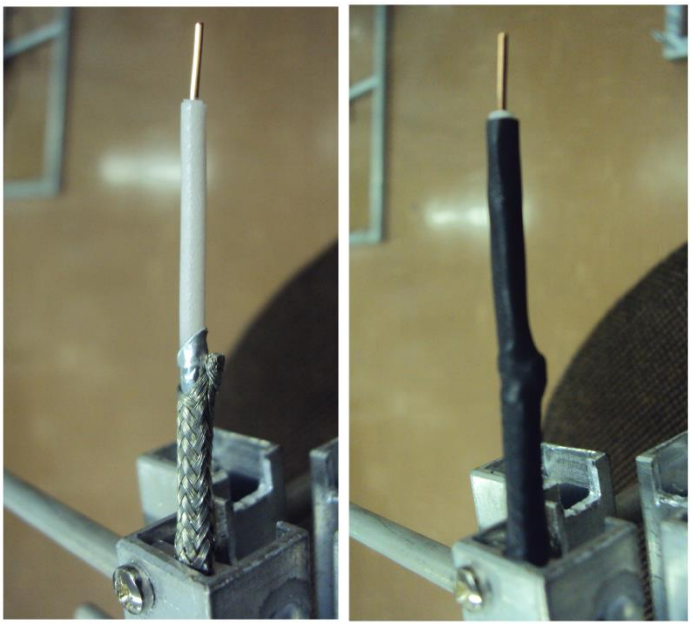

Figure 2.23. Feed point preparation

A plastic cover was used at the top end of the antenna for waterproofing. This cover was fabricated using the bottom of a 0.5 litre coke bottle. As shown in Figure 2.25, the waterproof

cover was painted with bitumen to provide ultra-violet (UV) light protection. The mounting of this waterproof cover on the antenna is shown in Figure 2.25. Figure 2.26 shows the completed MITRA antenna. Two concrete blocks were used to support the antenna against wind loading.

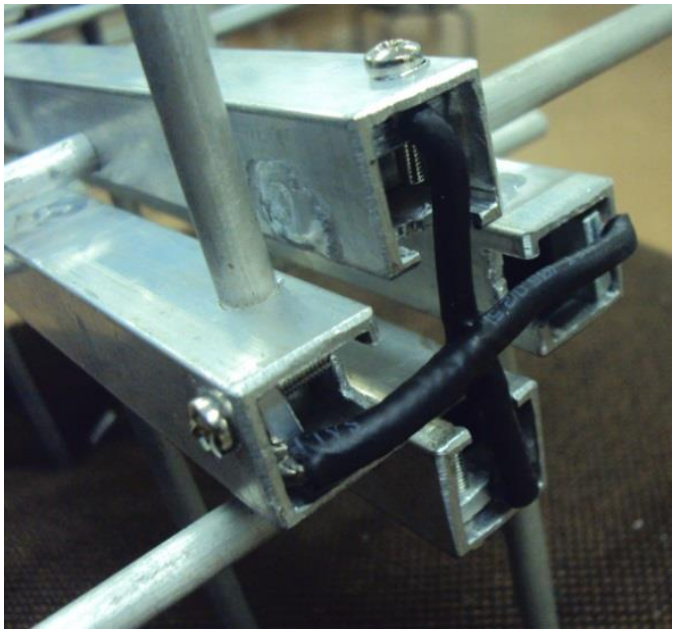

Figure 2.24. Cable positioning at the antenna feed point

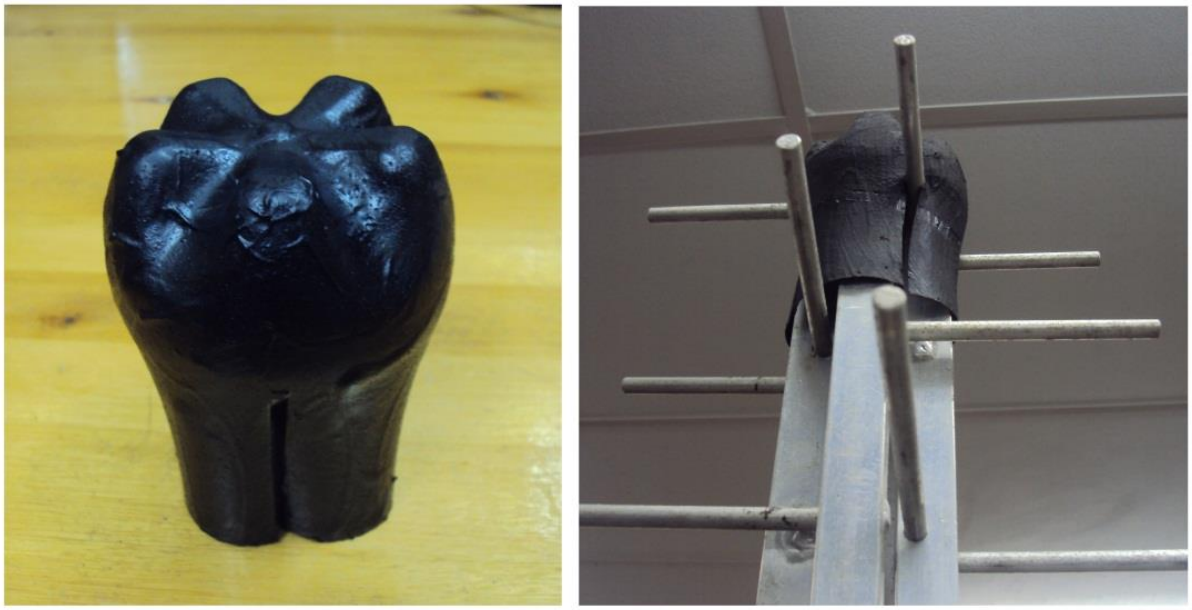

Figure 2.25. Antenna cover and cover mounting

Figure 2.26. The constructed antenna

2.7. Testing and Measurement

The antenna for the MITRA project was tested at the South African National Antenna Test Range (NATR) at Paardefontein. The two output cables from the MITRA antenna were respectively labeled antenna 1 and antenna 2. Three measurements were performed: VSWR, radiation pattern and gain. The measurement was conducted following the procedure described by Baker [21]. This is the standard method applied at the NATR test range.

2.7.1. VSWR measurement

The VSWR measurement was performed using a Vector Network Analyser (VNA) calibrated from 100 MHz to 1 GHz. The antenna was positioned vertically. Figure 2.27 shows the measured

result of the VSWR. The plot shows two traces for the orthogonal polarizations (North-South (NS) and East-West (EW)). The average value of VSWR is less than 2.5 between 200 MHz to 650 MHz. Above 650 MHz the antenna response degrades. This is possibly a consequence of the antenna element dimensions becoming comparable to the boom dimensions at the higher frequency limits [12]. It can be seen that the response correlates for both polarizations.

2.7.2. Radiation pattern measurement

The radiation pattern was measured using a source antenna and the Antenna Under Test (AUT). For this set-up, the distance between source and AUT was 180 m. The source antenna was the ETS-Lindgren 3142 D. The datasheet of this antenna is given Aannexure 1. The height of the source antenna, measured at the antenna boom, was 0.9 m above the ground. The AUT was the MITRA LPDA and it was mounted on top of the Azimuth-Elevation positioner at a height of 14.5 m. A 2 x 2 m metallic ground plane was used with the AUT as shown in Figure 2.28. The measurement set-up is shown in Figure 2.29.

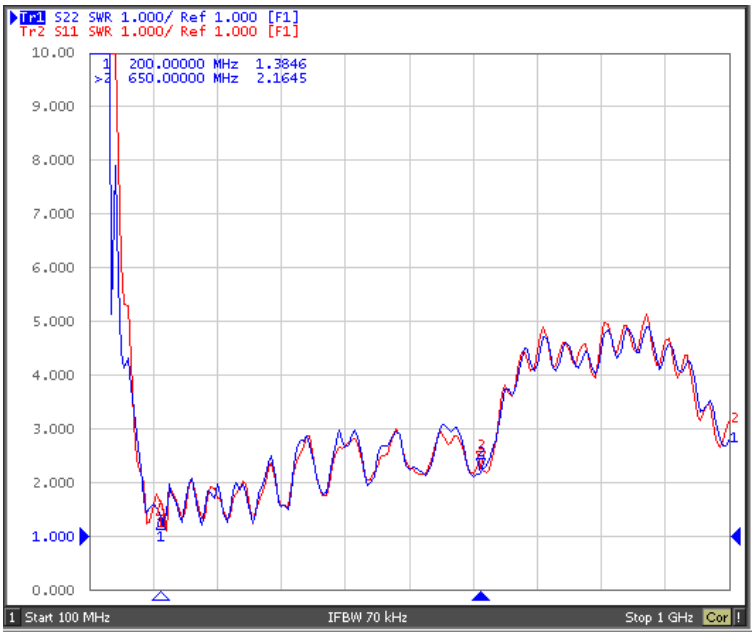

Figure 2.27. Measured result of the VSWR

Figure 2.28. MITRA LPDA with ground plane

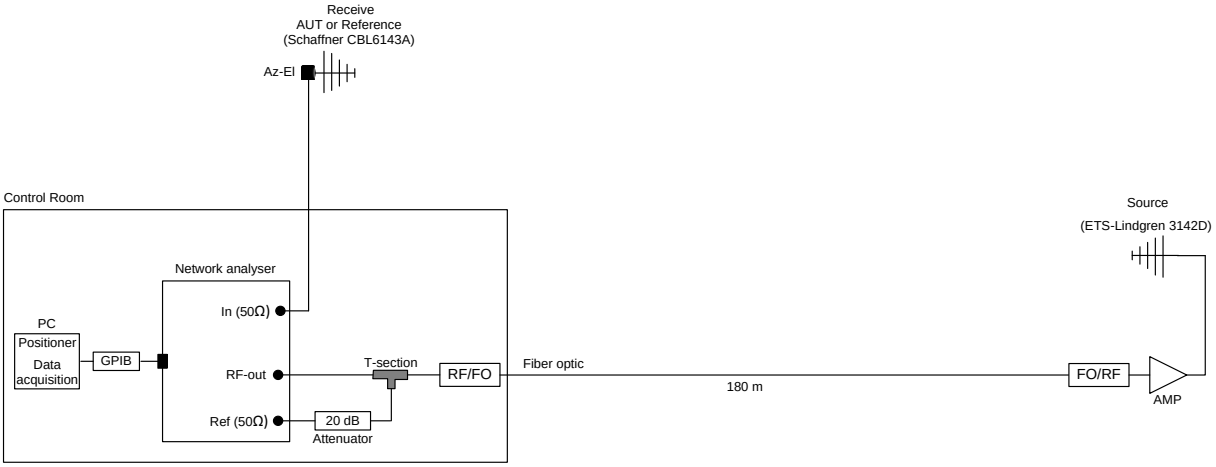

Figure 2.29. Measurement set-up for radiation pattern

The measurement was performed in three steps:

- Test 1: Co-polarization test (Vertical-Vertical) for H-Plane pattern. The source and receive antennas were positioned for vertical polarization. The source antenna in vertical polarization is shown in Figure 2.30. For the MITRA antenna, LPDA 1 was positioned for vertical polarization.
- Test 2: Co-polarization test (Horizontal-Horizontal) for E-Plane pattern. The source antenna was positioned in horizontal polarization. Without rotating the AUT, LPDA 2 was connected to the measurement system as it was already oriented in the horizontal plane for Test 1.
- Test 3: Cross-polarization test (Vertical-Horizontal). The source antenna was rotated back to vertical polarization. Without rotating the AUT, LPDA 2 was again used as it was still oriented in the horizontal plane as in Test 1 and in Test 2.

Figure 2.31 shows the measured result of the radiation pattern at 300 MHz for Test 1. The measured plot shows a half-power beamwidth (HPBW) of 84°, which gives a 4° difference compared to the simulated result in Figure 2.5.

For Test 1, the radiation patterns for other frequencies (200 MHz, 400 MHz, 500 MHz, 600 MHz, 700 MHz and 800 MHz) are shown from Figure 2.32 to Figure 2.37 respectively. The presence of side lobes is possibly caused by the arrangement of the coaxial cables running to the control room. The response also degrades towards the upper limit of the frequency band.

The radiation patterns for Test 2 from 200 MHz to 800 MHz (in step of 100 MHz) are shown from Figure 2.38 to Figure 2.44. Again it can be seen that the response degrades at the upper limit of the frequency band.

For Test 3, the radiation patterns of the frequencies from 200 MHz to 800 MHz (in step of 100 MHz) are shown from Figure 2.45 to Figure 2.51. Cross-polarization should be minimized for optimum operation.

The minimum cross-polarization rejection can be calculated as the difference between the maximum S_{21} (dB) values from Test 1 (co-polarization Vertical-Vertical) and Test 3 (cross-polarization Vertical-Horizontal). Test 1 and Test 3 were considered as the source antenna was in the same orientation in both measurements. From the radiation pattern plots, the maximum S_{21} (dB) values were measured at 180°. The cross polarization rejection shown in Table 2.4 shows that the performance of the antenna degrades towards the boundary of the operational frequency band.

Figure 2.30. Source antenna (ETS-Lindgren 3142D) for vertical polarization

2.7.3. Gain measurement and calculation

The gain measurement procedure used was the gain transfer method, which is a relative measurement described mathematically in Equation 2.14 [21, 22].

$$G_{(AUT,dBi)} = G_{(Ref,dBi)} + D_{(dB)} \tag{2.14}$$

$G_{(Ref,dBi)}$ is the gain of the reference antenna expressed in dBi and provided by the manufacturer. D is the relative difference between the highest value of S_{21} (dB) measured with the reference antenna and the highest value of S_{21} (dB) measured with the AUT. The reference and AUT antennas are positioned for the same polarization.

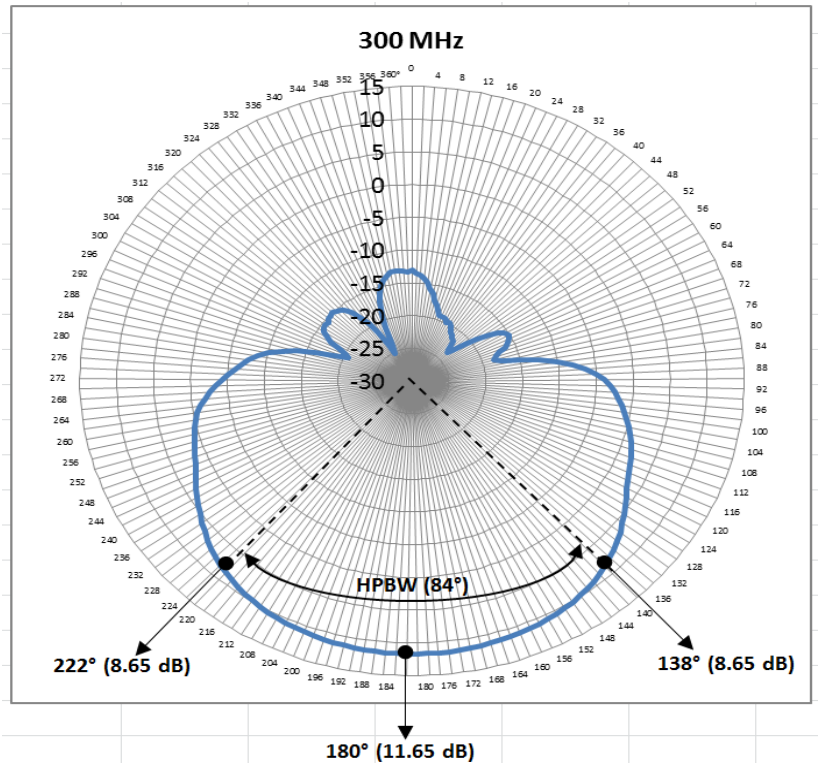

Figure 2.31. Radiation pattern of co-polarization (Vertical-Vertical) at 300 MHz (Test 1)

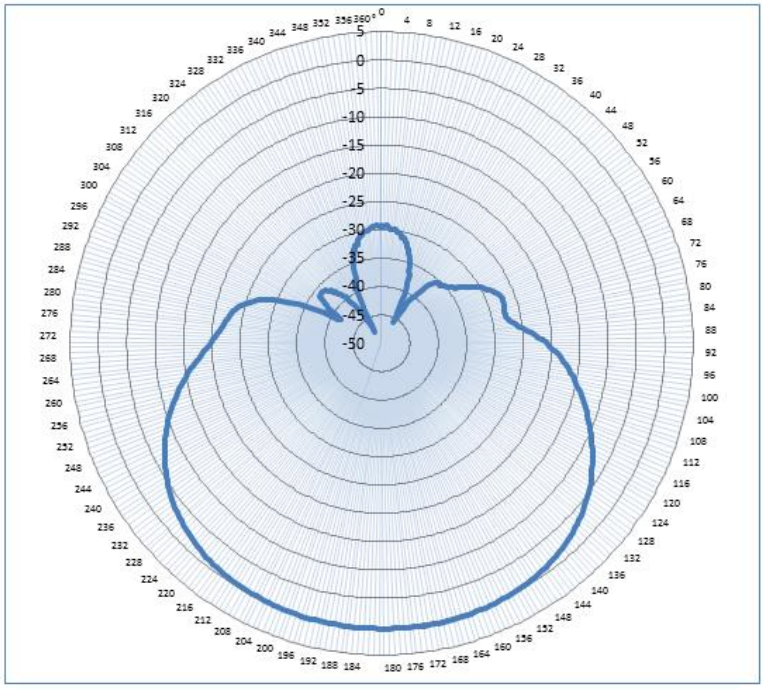

Figure 2.32. Radiation pattern of co-polarization (Vertical-Vertical) at 200 MHz (Test 1)

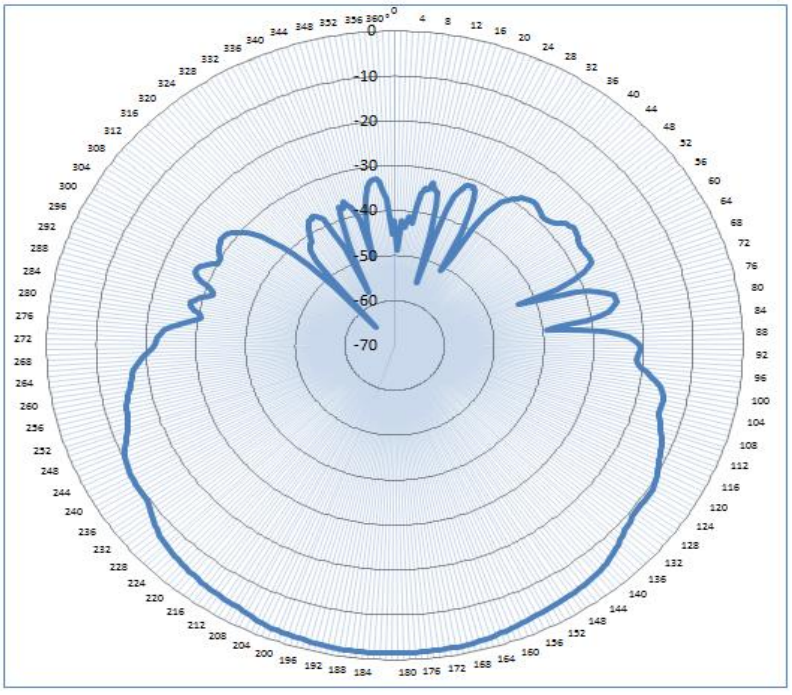

Figure 2.33. Radiation pattern of co-polarization (Vertical-Vertical) at 400 MHz (Test 1)

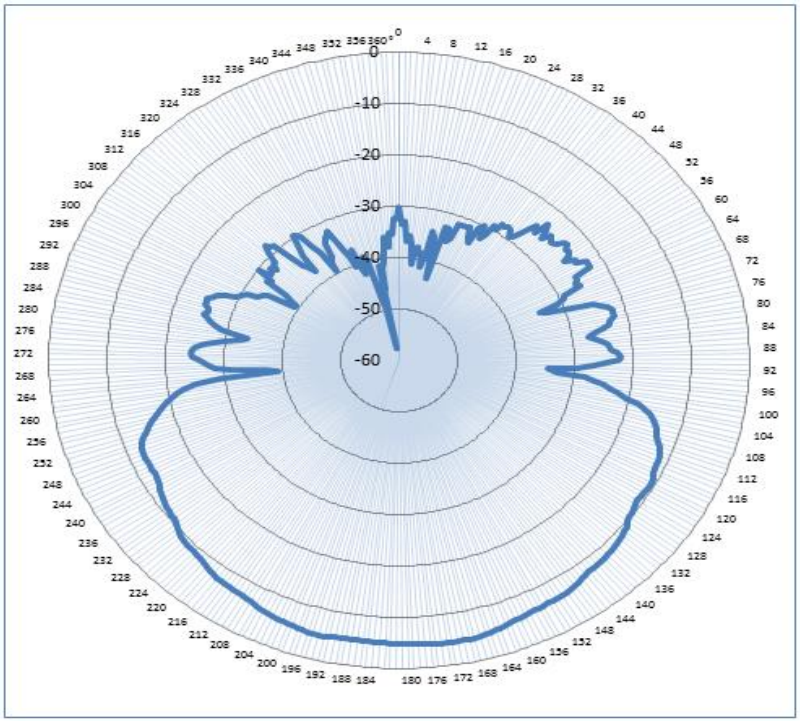

Figure 2.34. Radiation pattern of co-polarization (Vertical-Vertical) at 500 MHz (Test 1)

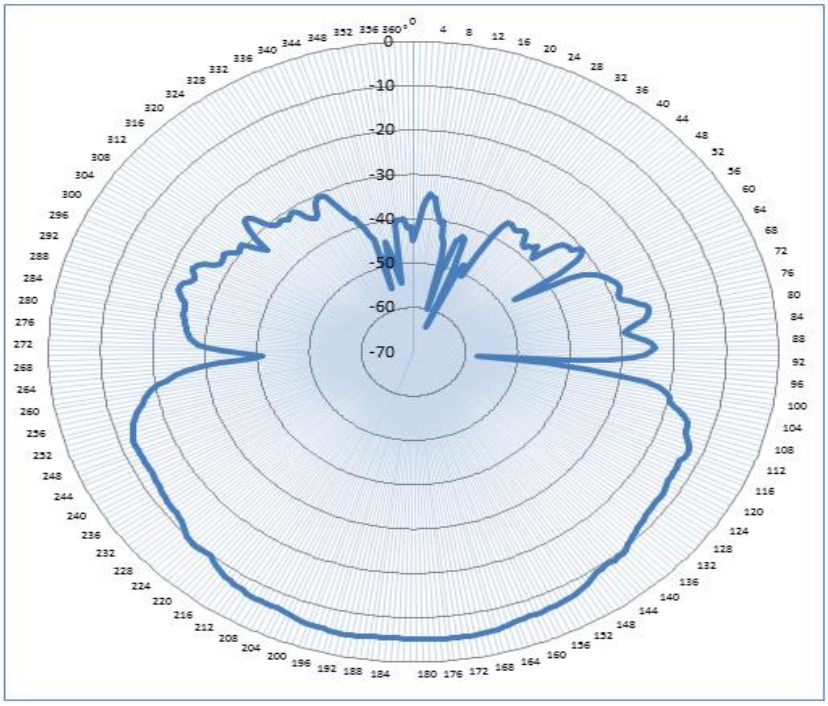

Figure 2.35. Radiation pattern of co-polarization (Vertical-Vertical) at 600 MHz (Test 1)

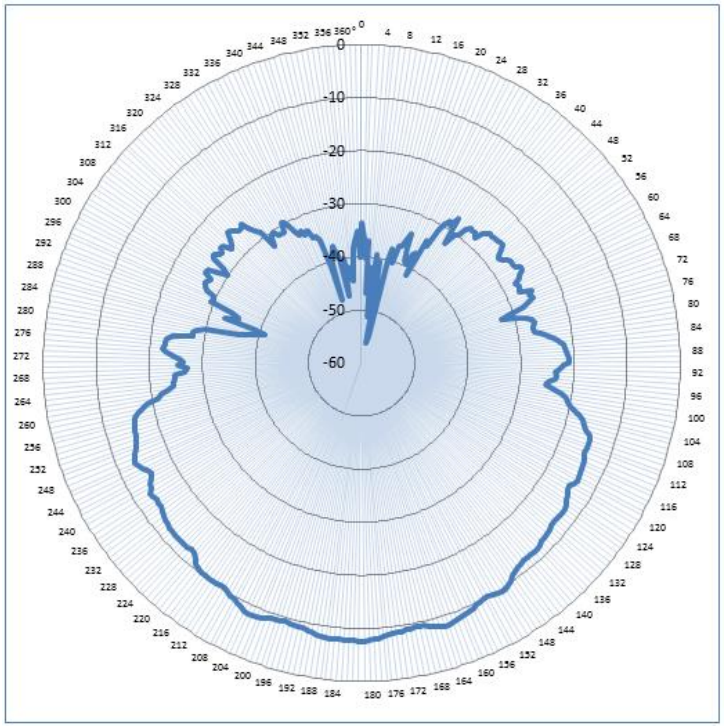

Figure 2.36. Radiation pattern of co-polarization (Vertical-Vertical) at 700 MHz (Test 1)

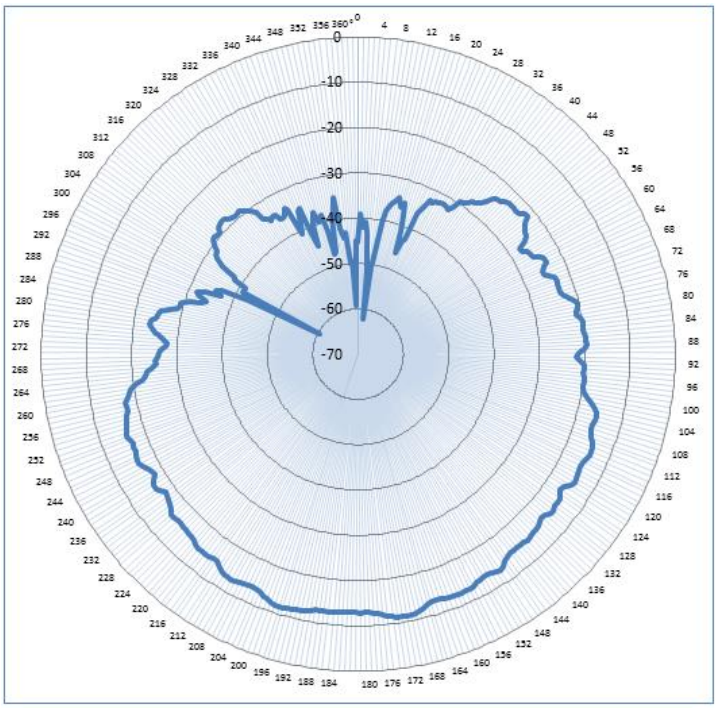

Figure 2.37. Radiation pattern of co-polarization (Vertical-Vertical) at 800 MHz (Test 1)

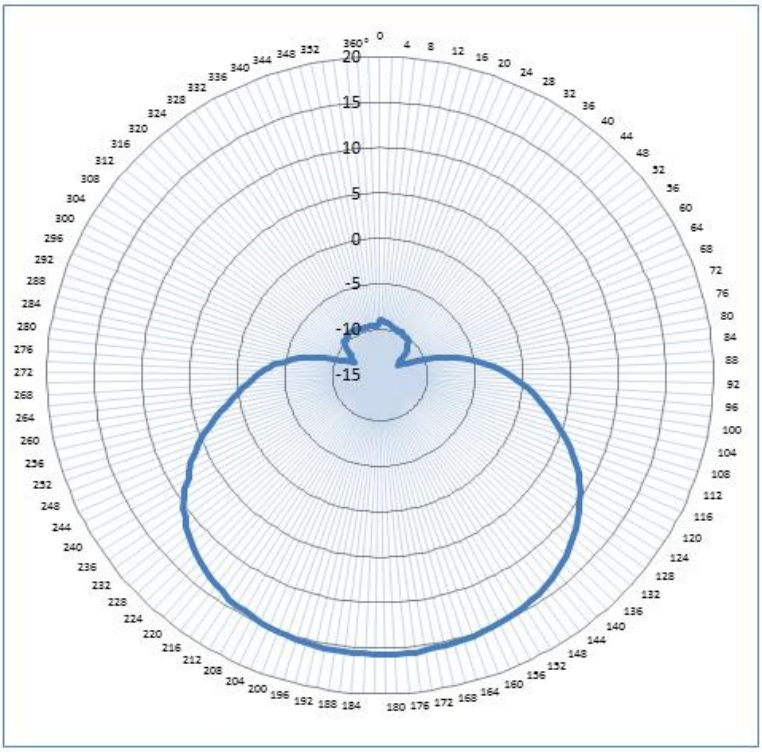

Figure 2.38. Radiation pattern of co-polarization (Horizontal-Horizontal) at 200 MHz (Test 2)

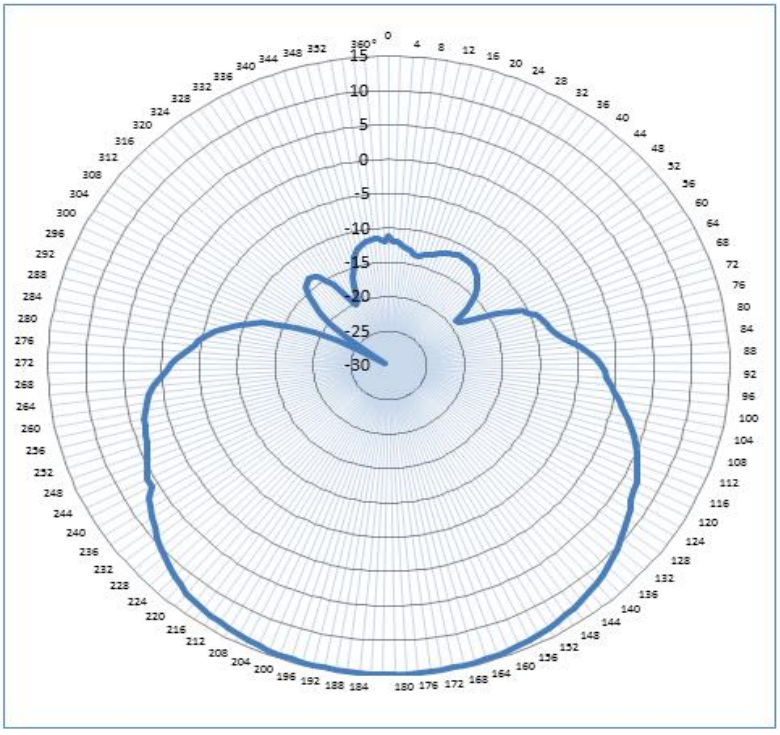

Figure 2.39. Radiation pattern of co-polarization (Horizontal-Horizontal) at 300 MHz (Test 2)

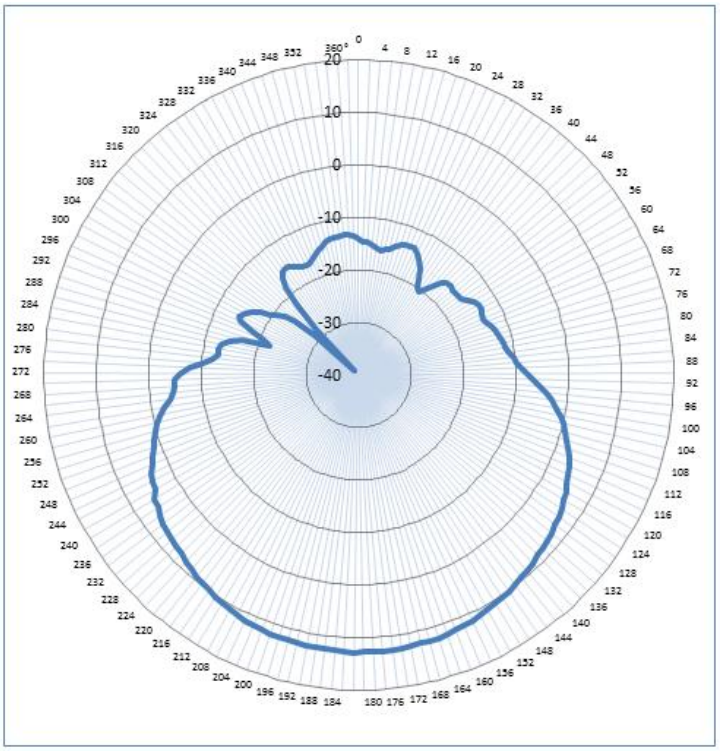

Figure 2.40. Radiation pattern of co-polarization (Horizontal-Horizontal) at 400 MHz (Test 2)

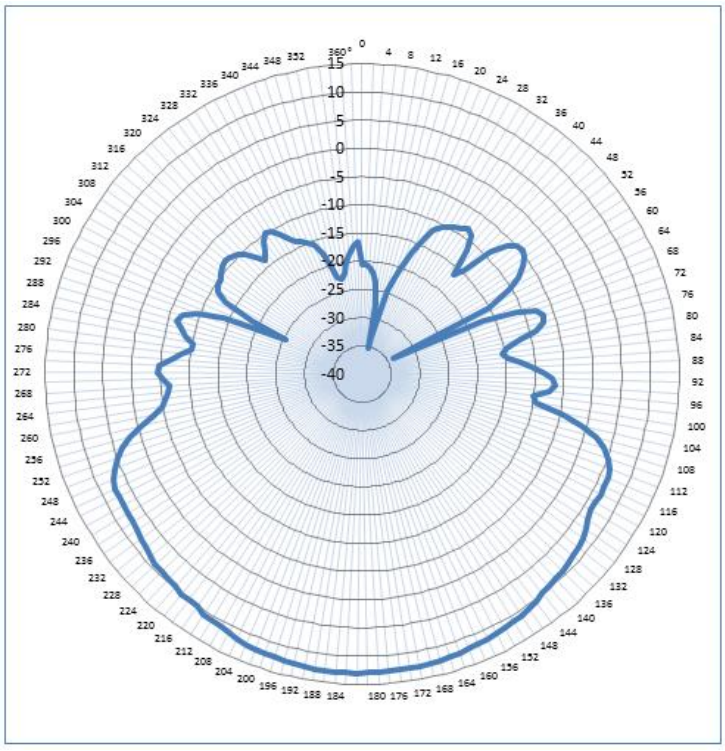

Figure 2.41. Radiation pattern of co-polarization (Horizontal-Horizontal) at 500 MHz (Test 2)

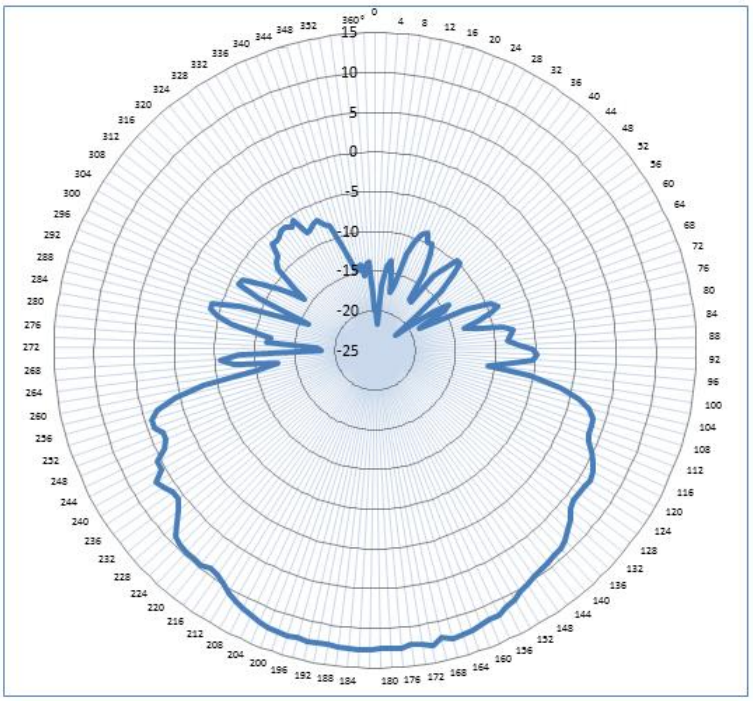

Figure 2.42. Radiation pattern of co-polarization (Horizontal-Horizontal) at 600 MHz (Test 2)

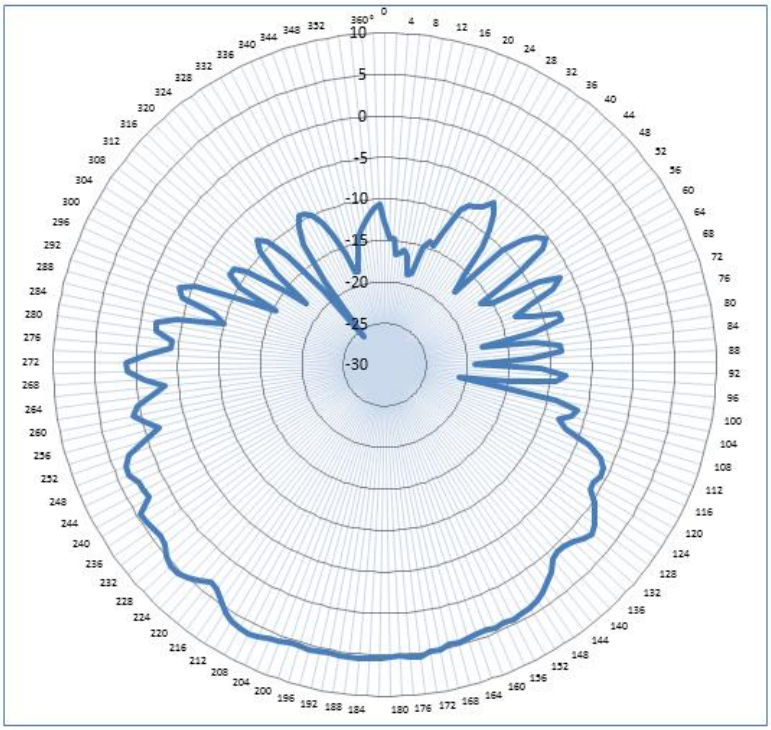

Figure 2.43. Radiation pattern of co-polarization (Horizontal-Horizontal) at 700 MHz (Test 2)

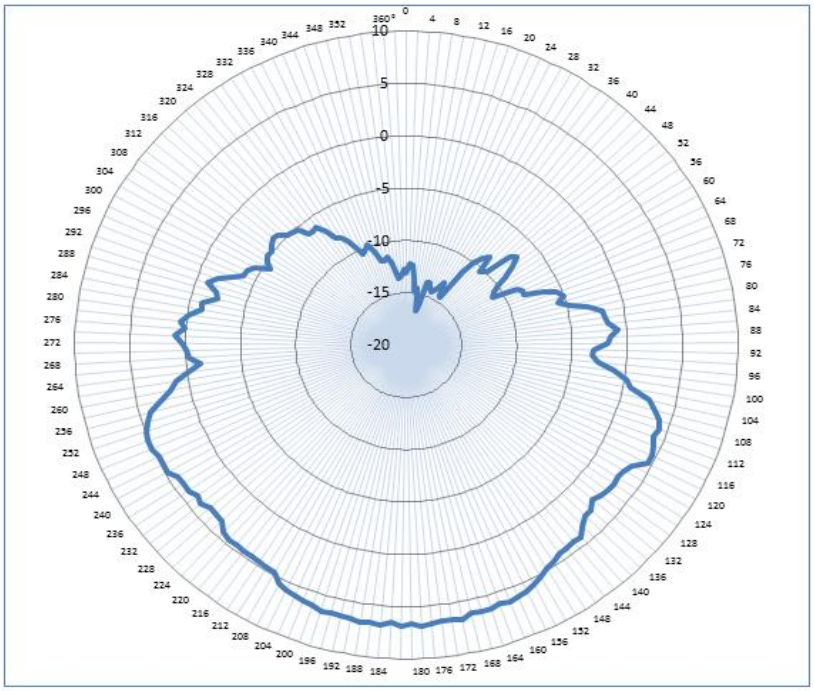

Figure 2.44. Radiation pattern of co-polarization (Horizontal-Horizontal) at 800 MHz (Test 2)

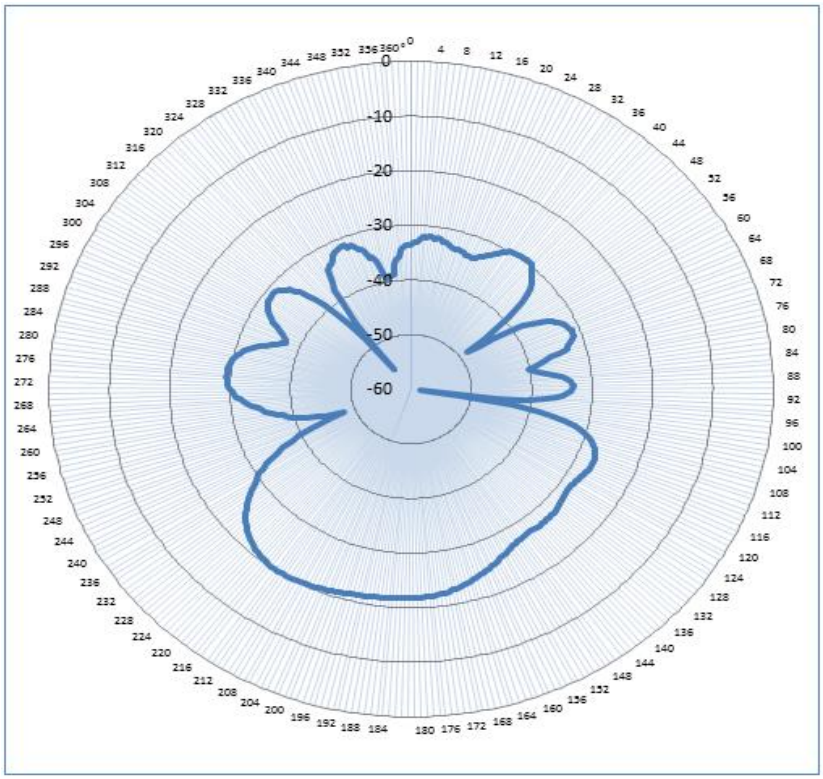

Figure 2.45. Radiation pattern of cross-polarization (Vertical-Horizontal) at 200 MHz (Test 3)

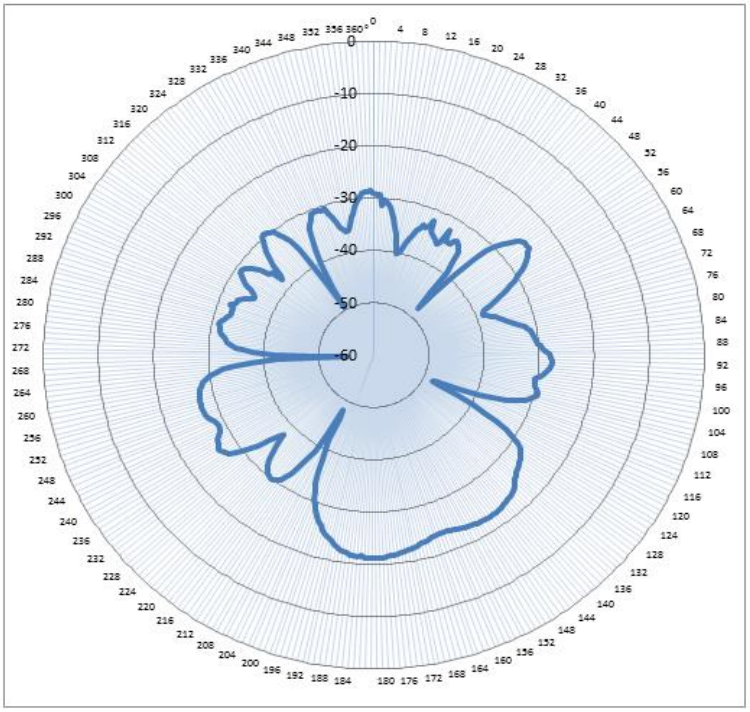

Figure 2.46. Radiation pattern of cross-polarization (Vertical-Horizontal) at 300 MHz (Test 3)

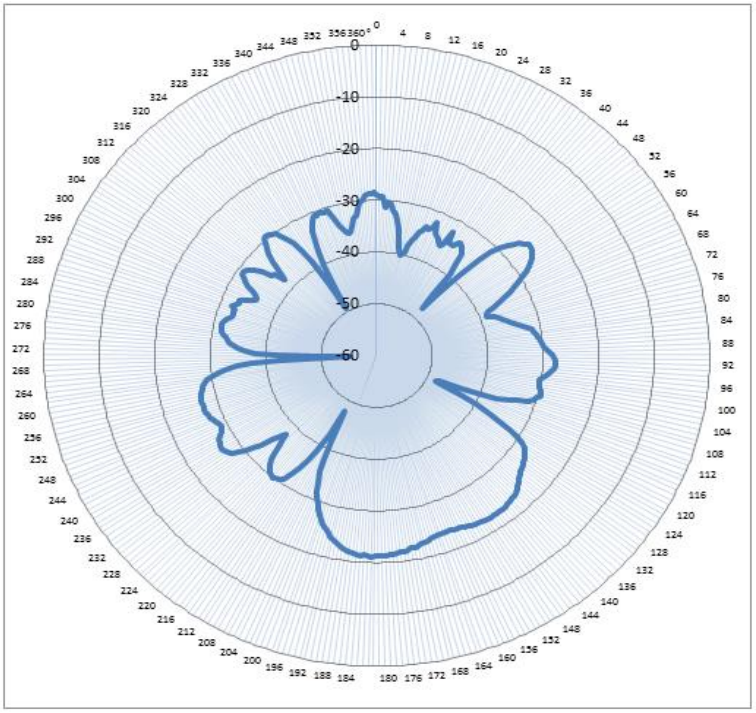

Figure 2.47. Radiation pattern of cross-polarization (Vertical-Horizontal) at 400 MHz (Test 3)

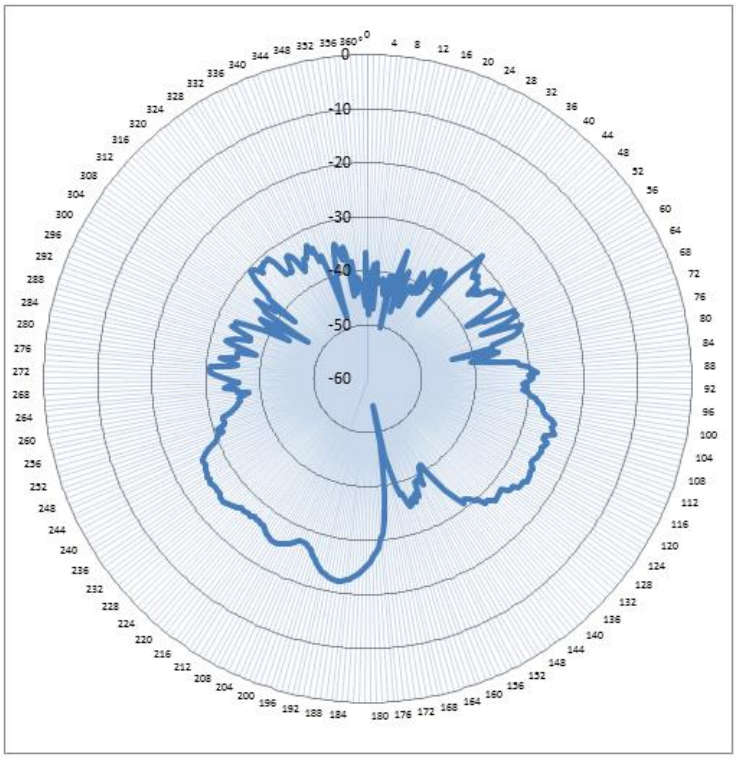

Figure 2.48. Radiation pattern of cross-polarization (Vertical-Horizontal) at 500 MHz (Test 3)

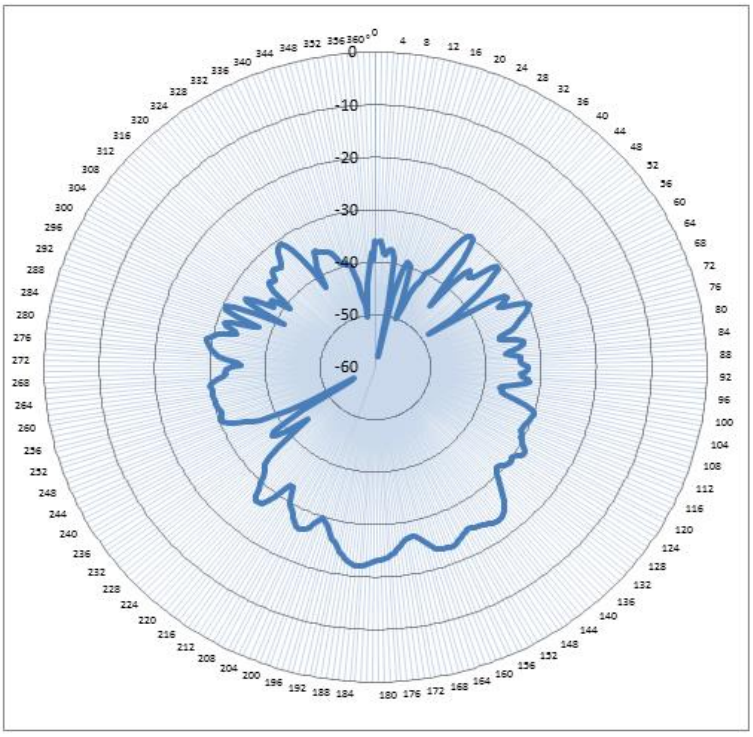

Figure 2.49. Radiation pattern of cross-polarization (Vertical-Horizontal) at 600 MHz (Test 3)

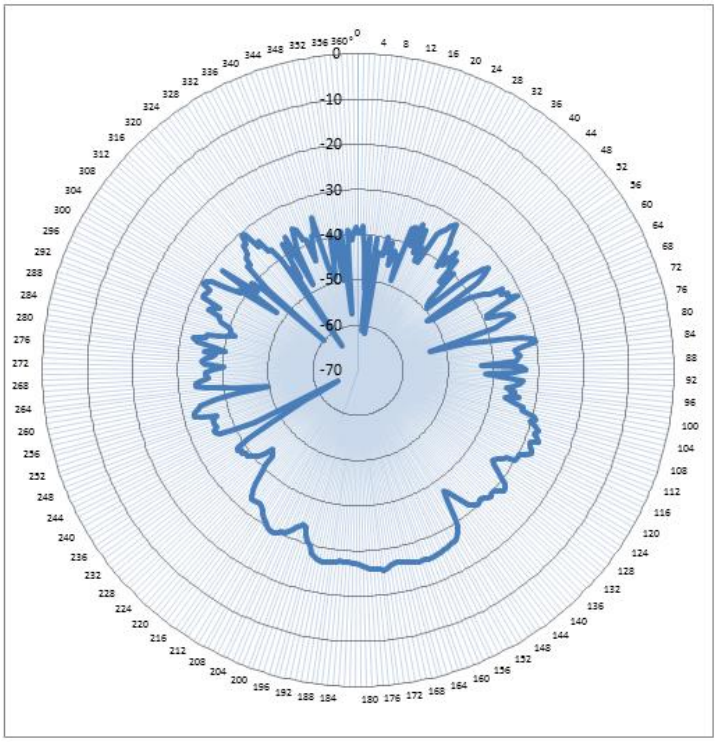

Figure 2.50. Radiation pattern of cross-polarization (Vertical-Horizontal) at 700 MHz (Test 3)

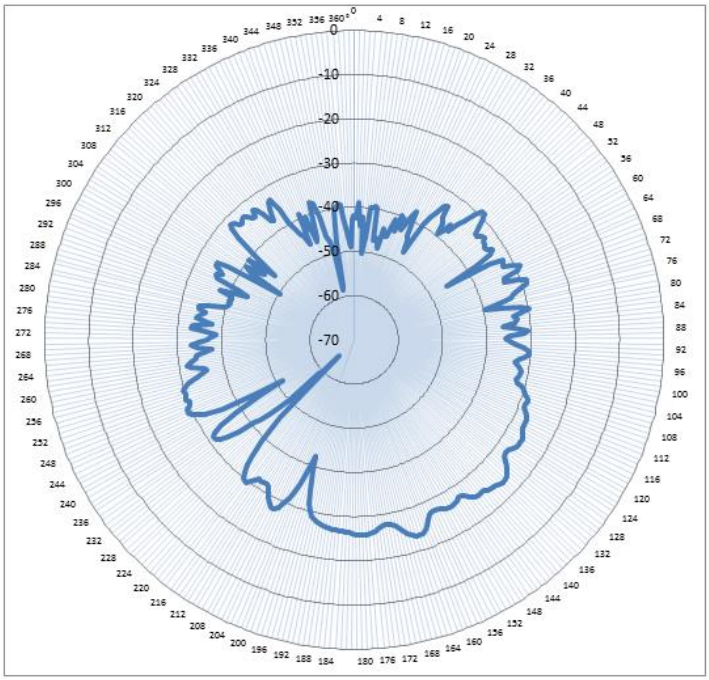

Figure 2.51. Radiation pattern of cross-polarization (Vertical-Horizontal) at 800 MHz (Test 3)

Table 2.4. Cross-polarization rejection

Angle (°)	Frequency (MHz)	Test 1 S_{21} (dB)	Test 3 S_{21} (dB)	Polarization Rejection (dB)
180	200	0.39	-21.79	22.18
180	300	-1.49	-21.21	19.72
180	400	-1.5	-19.28	17.78
180	500	-4.83	-26.04	21.21
180	600	-5.24	-23.14	17.9
180	700	-7.58	-26.99	19.41
180	800	-12.88	-25.84	12.96

The same ground plane was used for both AUT and reference measurements. The source antenna was the ETS-Lindgren 3142 D and the reference antenna was the Schaffner CBL6143A. The datasheet of the reference antenna is given in Annexure 2. The gain measurement was only done for co-polarization measurements. Two measurements were performed with the reference antenna:

- Test 4: Vertical-Vertical. The source and reference antennas were positioned for vertical polarization. The reference antenna in vertical polarization is shown Figure 2.52.
- Test 5: Horizontal-Horizontal. The source and reference antennas were positioned for horizontal polarization.

For example, at 300 MHz, the gain of the reference antenna is 6.61 dBi as specified in the datasheet (Annexure 2). The maximum value of S_{21}(dB) of the AUT was measured as -1.29 dB for co-polarization vertical-vertical (H-plane) in Test 1. At 300 MHz, the maximum value of S_{21}(dB) of the reference antenna was measured as -2.78 dB for co-polarization vertical-vertical (H-plane) in Test 4. Using Equation 2.14, the gain of the AUT for H-plane is calculated as follows:

$$G_{(AUT,\ dBi)} = 6.61 \text{ dBi} + [-1.29-(-2.78)] = 8.1 \text{ dBi}$$

Figure 2.52. Reference antenna (Schaffner CBL6143A) in vertical polarization

At 300 MHz, the maximum value of S_{21}(dB) of the AUT was measured as 1.91 dB for co-polarization horizontal-horizontal (V-plane) in Test 2. At 300 MHz, the maximum value of S_{21}(dB) of the reference antenna was measured as 0.23 dB for co-polarization horizontal-horizontal (V-plane) in Test 5. Using Equation 2.14, the gain of the AUT for V-plane is calculated as follows:

$$G_{(AUT,\ dBi)} = 6.61 \text{ dBi} + [1.91-(0.23)] = 8.29 \text{ dBi}$$

The data set for these measurements between 200 MHz to 800 MHz (in steps of 100 MHz) is shown in Table 2.5. The gain for E and H planes between 200 MHz to 800 MHz are plotted in Figure 2.53. It can be seen that in both planes the results show good correlation. The gain degrades at the upper limit of the frequency band as expected.

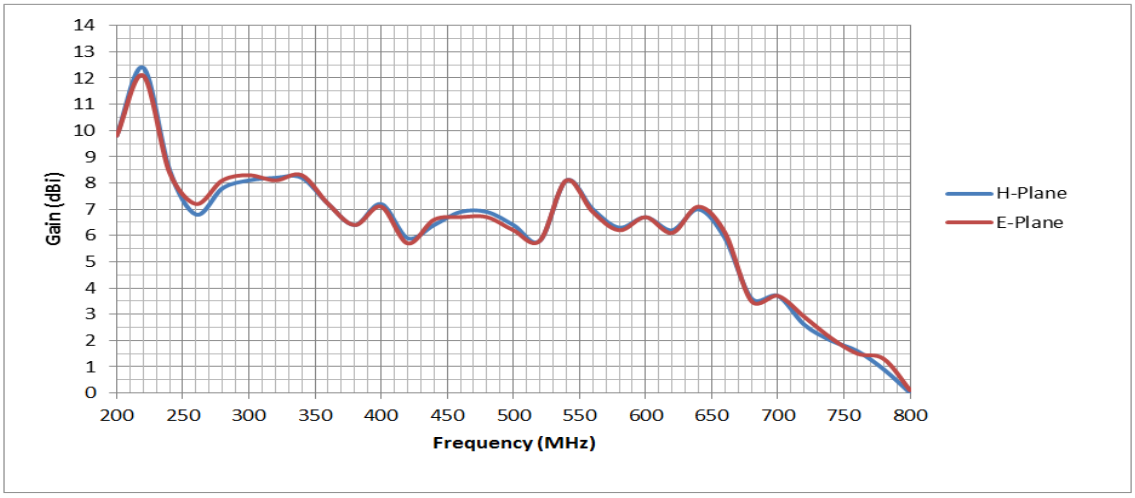

Figure 2.53. Measured result of the MITRA antenna gain for E and H planes

Table 2.5. Result of the gain measurement of the MITRA antenna

Frequency	Test 1 (AUT)	Test 2 (AUT)	Test 4 (Ref. Ant*)	Test 5(Ref. Ant)	Ref. Ant Gain	AUT H-Plane	AUT E-Plane
MHz	H-Plane(dB)	E-Plane (dB)	H-Plane (dB)	E-Plane (dB)	Spec. (dBi)*	Gain (dBi)	Gain (dBi)
200	0.42	2.25	-3.53	-1.66	5.84	9.79	9.75
220	2.52	4.19	-4.97	-3.08	4.87	12.36	12.14
240	0.63	2.64	-1.34	0.79	6.52	8.49	8.37
260	-1	1.12	-1.95	-0.23	5.82	6.77	7.17
280	0.27	2.51	-0.73	1.17	6.76	7.76	8.10
300	-1.29	1.91	-2.78	0.23	6.61	8.10	8.29
320	-0.4	2.11	-1.98	0.6	6.62	8.20	8.13
340	-1	1.84	-2.56	0.21	6.65	8.21	8.28
360	-1.58	0.94	-2.2	0.31	6.60	7.22	7.23
380	-2.69	-0.02	-2.64	0.04	6.45	6.40	6.39
400	-1.41	0.9	-2.24	0.25	6.42	7.25	7.07
420	-2.38	-0.07	-1.78	0.77	6.49	5.89	5.65
440	-2.98	0	-2.82	-0.06	6.52	6.36	6.58
460	-2.58	-0.2	-2.83	-0.24	6.68	6.93	6.72
480	-3.12	-1.11	-3.17	-0.96	6.88	6.93	6.73
500	-4.39	-2.15	-4.08	-1.66	6.71	6.40	6.22
520	-4.95	-2.48	-3.95	-1.48	6.77	5.77	5.77
540	-4.33	-1.78	-5.62	-3.03	6.81	8.10	8.06
560	-5.57	-2.7	-5.73	-2.72	6.86	7.02	6.88
580	-4.62	-2.13	-4.44	-1.9	6.47	6.29	6.24
600	-4.99	-2.73	-4.94	-2.67	6.78	6.73	6.72
620	-4.6	-2.79	-3.9	-2.01	6.89	6.19	6.11
640	-3.37	-1.05	-3.25	-1.11	7.09	6.97	7.15
660	-5.37	-2.99	-3.94	-1.75	7.38	5.95	6.14
680	-6.61	-4.49	-2.77	-0.6	7.43	3.59	3.54
700	-7.58	-5.14	-3.6	-1.17	7.67	3.69	3.70
720	-8.43	-6.08	-3.22	-1.15	7.81	2.60	2.88
740	-11.23	-9.08	-5.23	-3.19	7.97	1.97	2.08
760	-11.68	-9.61	-5.21	-3.12	8.02	1.55	1.53
780	-11	-8.67	-3.73	-1.81	8.14	0.87	1.28
800	-11.23	-9.27	-3.1	-1.23	8.17	0.04	0.13

*Ref. Ant: Reference Antenna

*Spec.: Gain specification of the reference antenna (Annexure 2)

Chapter 3: MITRA Front-End

3.1. Introduction

As shown in Figure 1.1, the MITRA Front-End is part of the out-door segment. The Front-End consists of two identical arrays of dual-polarized LPDAs. The two arrays are in an East-West configuration. Each antenna array is a set of eight individual antennas. Antenna 1 is located towards the South, and antenna 8 towards North. Each MITRA antenna gives two output signals for orthogonal polarizations. The two outputs are conventionally called North-South (NS) and East-West (EW). After the combiner, two signals from each array are sent to the Back-End. The four signals are conventionally called: NS-E (North-South output in the East array), EW-E (East-West output in the East array), NS-W (North-South output in the West array), and EW-W (East-West South output in the West array).

3.2. MITRA Array Development

The block diagram for the MITRA Front-End at the DUT station is shown in Figure 3.1. Each antenna polarization is equipped with a low-pass filter (LPF) and low noise amplifier (LNA). Two combiners are used to group the eight NS and eight EW signals. Line amplifiers (Line Amp) are used to compensate for the poor noise figure of the fibre optic transmitter (28 dB) and are used to convert the RF signals to optical signals for transmission to the control room [12]. The datasheet of the RF-to-Fibre converter is provided in Annexure 3. Figure 3.2 shows the view of the Front-End after construction.

3.3. MITRA Array Front-End Noise Temperature and Gain Calculation

The Front-End gain and noise temperature were calculated up to the RF-to-Fibre converter. As shown in Figure 3.1, the Front-End consists of four identical beamformers. A single beamformer is shown in Figure 3.3. The low-pass filter (LPF) is inserted at the input of the low-noise amplifier (LNA). The Durban University of Technology (DUT) MITRA station is located in an environment where the presence of radio frequency interference (RFI) is prominent. The LPF is inserted before the LNA to attenuate the out of band RFI and thus prevent the LNAs from being driven into their non-linear region.

An array system may be represented by an equivalent receiver consisting of a cascade of two-port networks for which the gain and noise temperature can be calculated. When considering array systems with multiple antenna inputs and receiver channels, the gain and noise temperature are calculated from the equivalent system where the array is replaced by an equivalent two-port network amplifier, followed by a passive lossy two-port network with a gain that is equal to the uncorrelated gain of the combiner.

This gain is calculated from the loss in the individual branch of the combiner and the combination of all equal input powers with equal weight. In this calculation the noise contribution of any lossy component should be taken into account. To keep the calculation simple and straightforward, the antenna noise contribution and the noise coupling between antenna elements will be neglected [23].

Figure 3.3 shows the equivalent signal chain of this single beamformer with associated gain and equivalent noise temperature of each stage. As shown in the datasheet of the splitter in

Annexure 4, the average insertion loss of the splitter is 10 dB measured between the common port and the individual ports. The combiner gain of 9 dB (due to 8 inputs) was used to calculate the resultant total loss of the combiner of 1 dB as described by Woestenburg [23]. Having 1 dB insertion loss, the resultant gain of the combiner gives 8 dB. It should be mentioned that this approach is applicable only for the calculation of the system noise temperature as the noise temperature can be evaluated between one single port and the common port. The datasheet of the low-pass filter (LPF) is provided in Annexure 5. The datasheet of the low-noise amplifier (LNA) is given in Annexure 6. The datasheet of the line amplifier is given in Annexure 7.

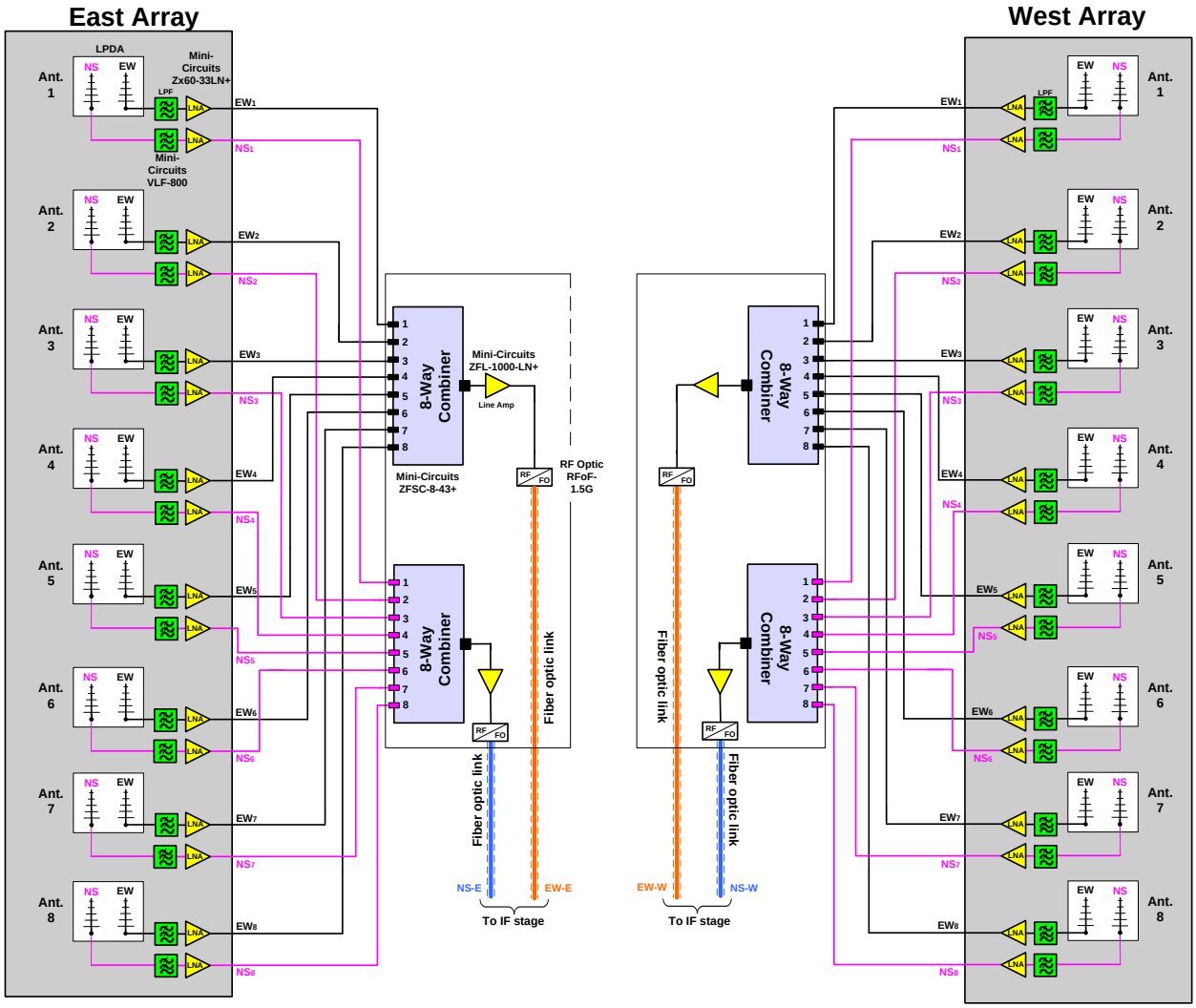

Figure 3.1. Block diagram of the MITRA Front-End

The equivalent noise factor F_e can be calculated by applying Friis's formula in Equation 3.1 [24] and the equivalent noise temperature T_e can be calculated from Equation 3.2.

$$F_e = F_1 + \frac{F_2 - 1}{G_1} + \frac{F_3 - 1}{G_1 G_2} + \frac{F_4 - 1}{G_1 G_2 G_3} + \frac{F_5 - 1}{G_1 G_2 G_3 G_4} \tag{3.1}$$

$$T_e = (F_1 - 1)T_0 \,[\mathrm{K}] \tag{3.2}$$

Figure 3.2. MITRA Front-End view

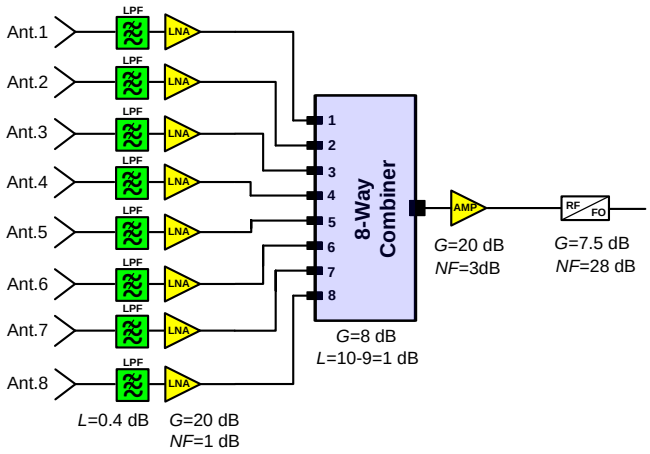

Figure 3.3. Single beam former of the MITRA Front-End

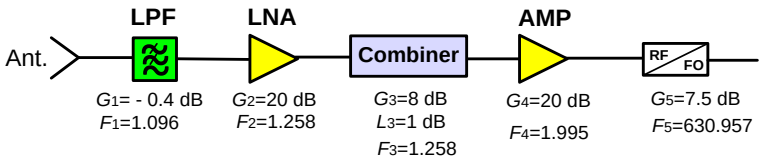

Figure 3.4. Equivalent system for noise temperature calculation

The LPF provides 0.4 dB insertion loss between 200 MHz to 800 MHz, which corresponds to a noise factor of 1.096. The LNA provides 20 dB gain (100 in linear value) and a noise figure of 1 dB (1.258 noise factor). The line amplifier provides 20 dB gain (with a 12 V supply) and a noise figure of 3 dB (1.995 noise factor). The RF-to-Fibre converter (RF/FO) provides 7.5 dB gain and a noise figure of 28 dB (630.957 noise factor).

From Equation 3.1, the MITRA equivalent noise factor gives:

$$F_e = 1.096 + \frac{1.258 - 1}{0.912} + \frac{1.258 - 1}{0.912 \times 100} + \frac{1.995 - 1}{0.912 \times 100 \times 6.3} + \frac{930.957 - 1}{0.912 \times 100 \times 6.3 \times 100} = 1.39$$

The system noise figure is $NF = 1.44$ dB

Using Equation 3.2, the MITRA equivalent noise temperature gives:

$$T_e = (1.39 - 1)290 = 113.1 \ [\mathrm{K}]$$

Referring to Figure 3.4, the Front-End gain gives $G_e = 55.1$ dB

3.4. Sensitivity Equation

The sensitivity, or minimum detectable temperature, of a radio telescope is equal to the rms noise temperature of the system as given by Equation 3.3 [25]. Equation 3.3 is also referred to as the sensitivity equation [7].

$$\Delta T_{rms} = \frac{K_r\, T_{sys}}{\sqrt{\Delta\nu\; t\; n}} \quad [\mathrm{K}] \tag{3.3}$$

where ΔT_{rms} = rms noise temperature

K_r = sensitivity constant of the instrument. $K_r = 1$ for simple instrument

$\Delta\nu =$ receiver bandwidth

t = integration time, which is the length of time for which the signal is averaged

n = number of records averaged

The calculation of the system noise temperature T_{sys} should include the sky noise temperature T_{sky}. It has been shown that at a frequency of 350 MHz, the sky temperature can be estimated as 100 K [26]. The average artificial human made noise T_{man} between 200 MHz and 900 MHz in a business area has been shown to be approximately 10 dB above the thermal noise (kT_0B) [27]. With that, Equation 3.4 can be used to calculate T_{sys}.

$$T_{sys} = (F_e - 1)T_0 + T_{sky} + T_{man} \quad [\mathrm{K}] \tag{3.4}$$

$$T_{sys} = (1.39 - 1)290 + 100 + 2900 = 3113 \text{ K}$$

For $\Delta\nu = 10$ MHz and assuming the product $tn = 1$, the MITRA sensitivity gives:

$$\Delta T_{rms} = \frac{3113}{\sqrt{10 \times 10^6}} = 0.98 \text{ K}$$

The smallest change in the antenna temperature ΔT_{min} that can realistically be detected is normally taken as three times the rms noise [7].

$$\Delta T_{min} = 3 \times \Delta T_{rms} = 2.95 \text{ K}$$

3.5. Minimum Detectable Flux Density Estimation

The minimum detectable flux density ΔS_{min} can be calculated from Equation 3.5, where k is Boltzmann's constant (1.38x10^{-23} joule K^{-1}), A_e is the effective aperture of the antenna and N_a is the number of antennas [7, 28].

$$\Delta S_{min} = \frac{3\ K_r\ k\ T_{sys}}{A_e\sqrt{N_a(N_a-1)\Delta\nu\ t\ n}} 10^{26} \quad [\text{Jy}] \tag{3.5}$$

The effective aperture area of an antenna is given in Equation 3.6, where D is the directivity of the antenna. The maximum effective aperture as defined does not include the effect of losses in the antenna, which can be accounted for by replacing D with G, the gain of the antenna [29].

$$A_e = \frac{\lambda^2}{4\pi} D = \frac{\lambda^2}{4\pi} G \quad [\text{m}^2] \tag{3.6}$$

For the purpose of the effective aperture calculation, the gain of the antenna and the gain of the combiner are considered. At 350 MHz, the gain of the MITRA antenna is 7.5 dBi (see Figure 2.53). The gain of the combiner is 8 dB (9 dB gain for 8 inputs and 1 dB insertion loss). With the MITRA array configuration, the value of G should be the cascaded gain from the antenna and the combiner. With that, G becomes:

$$G = 7.5 + 8 = 15.5 \text{ dB}$$

The antenna effective aperture is:

$$A_e = \frac{(0.857)^2}{4\pi} 35.5 = 2.07\ \text{m}^2$$

Using Equation 3.5, the minimum detectable flux density is:

$$\Delta S_{min} = \frac{3\,K_r\,k\,T_{sys}}{A_e\sqrt{N_a(N_a-1)\Delta\nu\,t\,n}}10^{26} = \frac{3\times 1\times 1.38\times 10^{-23}\times 3113}{2.07\sqrt{2\times 10\times 10^6}}\times 10^{26} = 1392 \quad [\text{Jy}]$$

At 300 MHz the flux density of the Sun is approximately equal to 10^5 Jy [25, 30]. With that, the calculated value of the minimum detectable flux density of 1392 Jy shows that the Sun should be able to be detected with the MITRA station in the business area of an urban environment.

3.6. Fringe width

The fringe width FW for a baseline B is given by Equation 3.7

$$FW = 1.02\frac{\lambda}{B} \quad [\text{rad}] \tag{3.7}$$

At 350 MHz, the fringe width of the MITRA arrays (8 m baseline) gives $FW = 0.11$ rad $= 6.3°$. For a source moving at 1° in 4 minutes, it will take 25.2 minutes to produce one fringe.

Chapter 4: MITRA IF Stage and Back-End

4.1. Introduction

The intermediate frequency (IF) and the Back-End stages are part of the in-door segment of the MITRA Radio Telescope. The purpose of this chapter is to discuss this in-door segment. As shown in Figure 4.1, the IF stage was implemented using analog components to produce an IF at 800 MHz. The digital Back-End was developed using a software defined radio (SDR) technique.

4.2. IF stage

The IF stage was designed to perform three operations: the Fibre-to-RF conversion, frequency translation, and band-pass filtering. The signal delivered from the Front-End was in the optical domain. The first task in the IF stage was the Optic-to-RF conversion using the fibre receiver (RFoF-2G). The datasheet of this product is provided in Annexure 7.

The system IF is 800 MHz. High-side injection on the mixer was implemented to ensure good image frequency rejection. The datasheet of the mixer (ZX-05-11X+) is shown in Annexure 8. The presence of the LO frequency and image frequencies within the operating band will affect the observation and need to be eliminated. The high IF frequency results in an image frequency range which extends from 1.8-2.4 GHz. These image frequencies are rejected by the low-pass filter (LPF) preceding the LNA's in the Front-End [12]. This LPF has a cut-off frequency of 800 MHz. The performance of the LPF is discussed in Chapter 7.

4.3. Digital Back-End

The digital Back-End consists of USRP networked devices in conjunction with the SBX RF daughter board. A summary of the USRP specifications is as follows [31]:

- FPGA: Xilinx Spartan 3A-DSP.
- ADC sample rate: 100 Msps.
- ADC resolution: 14 bits.
- DAC sample rate: 400 Msps.
- DAC resolution: 16 bits.
- Gigabit Ethernet interface.
- Bandwidth: 50 MHz (in the receive direction) and 25 MHz (in the transmit direction).
- Full duplex.
- MIMO capability with up to 8 antennas.
- 10 MHz external reference clock and 1 PPS source inputs.
- Software compatibility: Gnu-Radio, LabVIEW and Simulink.

The datasheet of the USRP network series is provided in Annexure 9. USRP devices take two reference signals in order to synchronize clocks and sampling time [32]:

- A 10 MHz reference to provide a single frequency reference for both devices.
- A 1 pulse-per-second (1PPS) to synchronize the sampling time across devices.

A MIMO configuration can be implemented for applications requiring multiple USRP devices operating synchronously. A MIMO cable transmits an encoded time message from one device to another. For a system to be considered MIMO capable, each channel in the radio must meet

two requirements: the sample clocks must be synchronized, and the sample time must be aligned when any DSP operations occur. This is achieved by sharing a common 10 MHz reference and 1 PPS signal to two or more devices [33].

Beamforming or direction finding applications require a knowledge of the phase relationships between multiple channels. While all Ettus daughter boards can be used in a MIMO configuration, this does not necessarily imply there is a phase alignment between the RF chains of one or more daughter boards [34].

In this context, phase alignment implies a minimal phase difference between multiple channels. Phase ambiguities are caused by the phased-locked loop (PLL). These phase ambiguities can generally be calibrated by measuring the phase difference and compensating for it. Filters, mixers, amplifiers and other components produce phase variations that vary with time, temperature, mechanical conditions, etc. These errors will not change with each PLL retune but may change over time and temperature variation [33].

With regard to phase ambiguities, the BasicRX, BasicTX, LFRX and LFTX USRP daughter boards are exceptions to this, since they do not include local oscillators that contribute to phase ambiguity between channels. The SBX daughter board utilizes an RF PLL that includes a resynchronization feature, which can be used to align the local oscillators across multiple SBXs and multiple USRP hardware devices. Using the UHD (USRP Hardware Driver), timed SPI commands can drive this re-synchronization feature. The use of any other daughter board requires channel-to-channel phase calibration after each PLL re-tune. Therefore, the SBX board

is the preferred solution for beam-forming applications [34]. The SBX board features are listed below:

- Frequency range: 400 MHz to 4.4 GHz.
- Bandwidth: 40 MHz.
- Transceiver: TX/RX Full duplex.
- MIMO capability.
- Time and phase synchronizations.

Figure 4.2 illustrates a block diagram where a MIMO cable is used to synchronize 2 USRP devices in a master-slave configuration. RF signals can be applied to each USRP respectively. A single 10 MHz reference and a single 1 PPS signals are applied to the master device [33]. The master USRP is connected to the host via a Gigabit Ethernet connection. The slave USRP is configured to accept its frequency and timing reference from the master USRP via the MIMO cable.

Larger MIMO systems can be realized utilizing the external 10 MHz reference and 1 PPS inputs. Figure 4.3 shows a block diagram where 4 USRP devices can be used in a 4x4 configuration. A distribution amplifier can be used to split a common 10 MHz reference and 1 PPS signal [33].

For the MITRA Back-End, the correlation operation was performed in the host computer using Gnu-radio Companion software. USRP setup and correlator design are discussed in Chapter 5 and Chapter 6.

4.4. Time and Frequency Standards

The clocks at VLBI stations must be synchronized accurately enough to avoid time-consuming searches for interference fringes. Precise frequency standards of interest for VLBI include crystal

oscillators and atomic frequency standards such as rubidium vapor cells, caesium-beam resonators, and hydrogen masers (Microwave Amplification Stimulated by Emission of Radiation). Atomic frequency standards incorporate crystal oscillators that are phase-locked or frequency-locked to the atomic process so that short-term performance becomes that of the crystal oscillator. Atomic frequency standards are based on the detection of an atomic or molecular resonance [28].

The rubidium standards have the advantage of being small, inexpensive, and readily transportable. They are sometimes used for VLBI below 1 GHz, where the ionosphere dominates system stability. At higher frequencies the use of rubidium standards results in degraded performance [28].

Caesium frequency standards are larger and substantially more expensive than rubidium standards. Because of their low signal-to-noise ratio, their short-term stability is poor. Thus, they are not used in VLBI for controlling local oscillators. However, they provide long-term stability and are used to monitor time [28].

A Hydrogen maser is used for applications that require extreme frequency stability, low phase noise, and long service life. Hydrogen masers operate on the principal that when hydrogen atoms are provided the proper environment, they emit radiation of a precise frequency of 1420 MHz (hydrogen emission line). Phase locking this extremely small power, high purity, signal to a very high performance quartz oscillator, provides the user with incredible long-term stability as well as excellent phase noise. Active masers are typically four times more stable than passive hydrogen masers, and one-hundred times more stable than high performance caesium.

Standard hydrogen masers provide low phase noise outputs that enable higher resolution measurements in VLBI applications and provide improved reference signals for master timing systems. A commercial maser, for example the MHM 2010™ by Symmetricom®, provides multiple 5, 10, 100 MHz outputs and 1PPS [35].

As shown in Figure 4.1, a Rubidium GPS disciplined Time standard is used in the MITRA Digital Back-End. The datasheet of the Rubidium GPS10RBN is shown in Annexure 10. The 10 MHz clock reference is split five ways so as to distribute the same clock reference where needed. The datasheet of the 5-way 0° splitter is given in Annexure 11. The 1 PPS signal is split using a 4-way splitter so as to distribute the same 1 PPS where needed. The datasheet of the 4-way 0° splitter is provided in Annexure 12.

Accurate frequency and time information can be obtained from the GPS satellite signal. On board each satellite is a caesium frequency standard. The Rubidium GPS10RBN incorporates a 12-channel GPS receiver which uses time information to discipline a 10 MHz rubidium oscillator. Over short periods, the GPS signal is very unstable and has large jitter superimposed on it. The GPS signal must be averaged over very long periods (days) before this jitter can be reduced to acceptable levels. Over short-periods the rubidium stability is very good, thousands of times better than the GPS signal. But rubidium oscillators drift over time, and even after a few months, the error of the rubidium oscillator may become unacceptable. The GPS10RBN is a 10 MHz, GPS disciplined, rubidium frequency standard. It combines the short-term stability of an atomic rubidium frequency standard with the long-term stability and traceability of the GPS set of satellites. The GPS10RBN receives the GPS signal and averages this signal over a very long

time. This long average time is then used to update or correct the frequency of the rubidium oscillator [36].

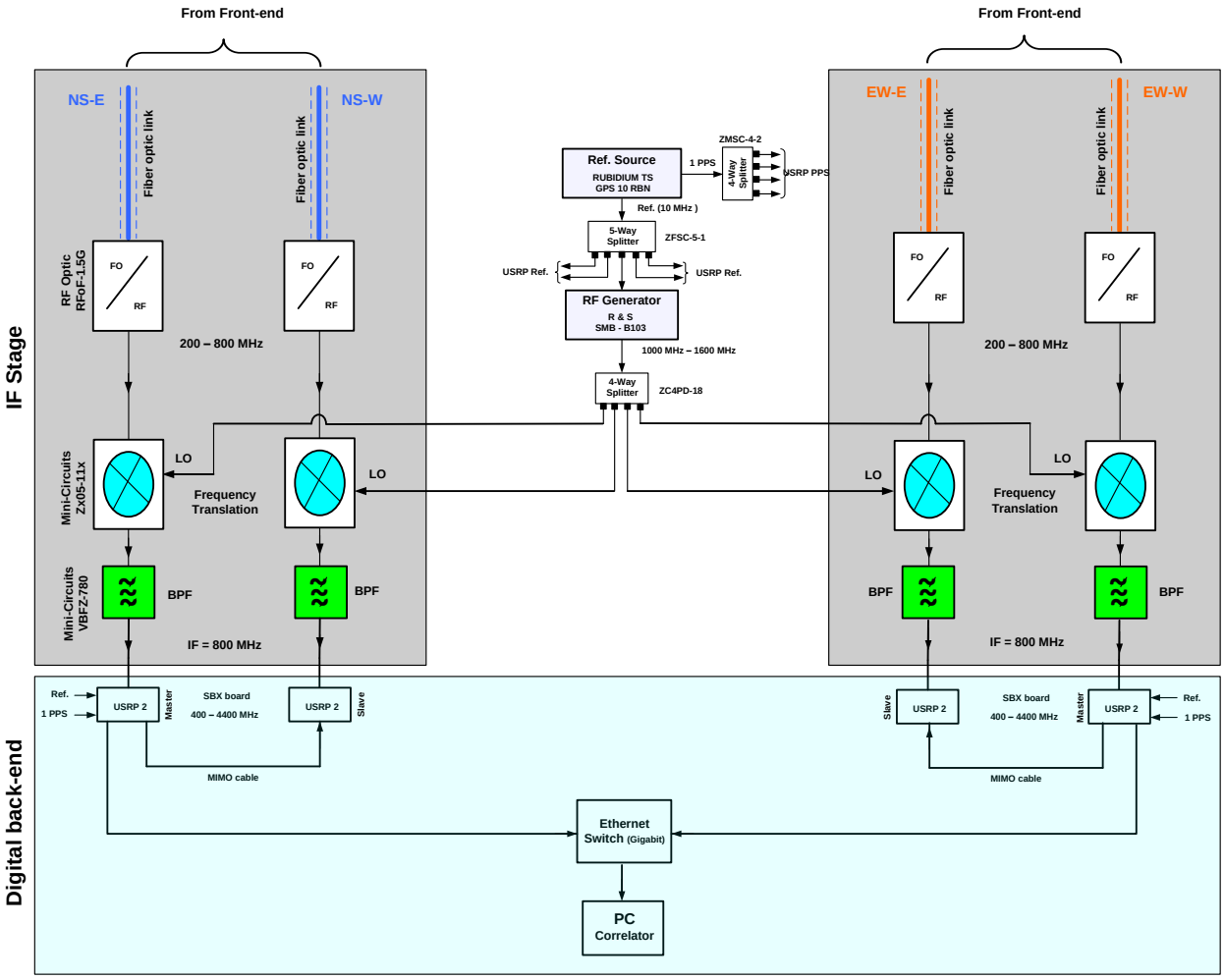

Figure 4.1. Block diagram of the IF stage and Back-End segment

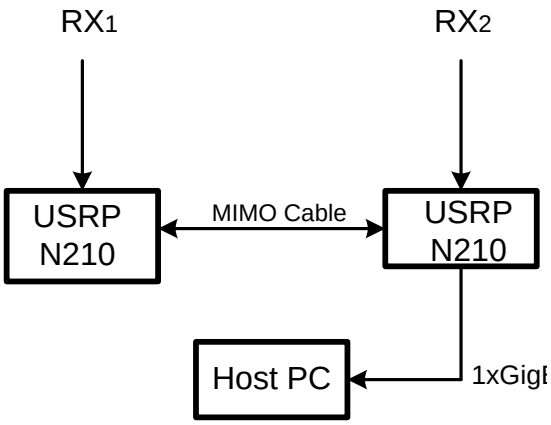

Figure 4.2. USRP devices in a 2x2 master-slave configuration

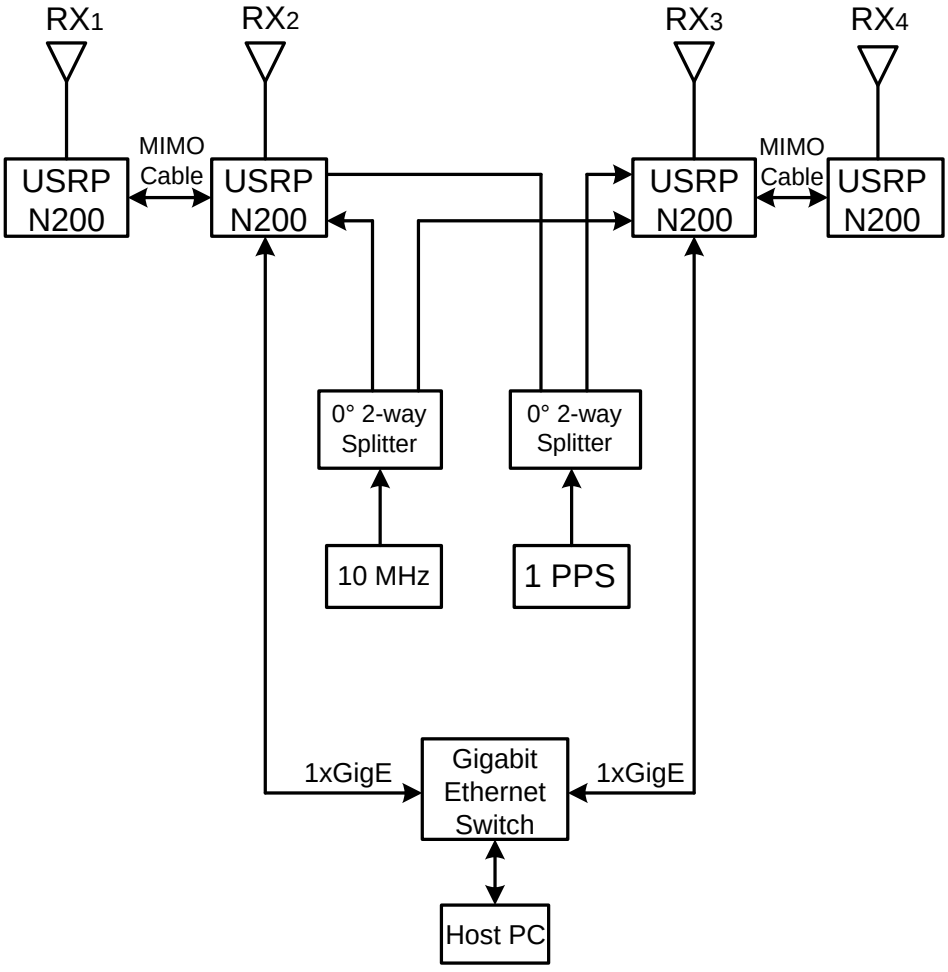

Figure 4.3. USRP devices in a 4 x 4 configuration system

Chapter 5: Introduction to Software Defined Radio and USRP setup

5.1. Introduction

This chapter introduces the Software Defined Radio (SDR) system with particular attention to the Gnu-Radio Software. Experiments demonstrate how to set up the Universal Software Radio Peripheral (USRP). The USRP-1 will be discussed and the USRP-2 will then be introduced. Attention will be focused on the receiver setup. RF signal generators are used to simulate the system.

5.2. Software Defined Radio and Gnu-Radio Software

The SDR forum defines SDR as a radio system in which some or all of the physical layer functions are software defined. This implies that the architecture is flexible so that the radio may be configured. That is, the SDR is a multifunctional, programmable, and easy to upgrade radio that can support a variety of services and standards while at the same time providing a low-cost power-efficient solution [37].

The block diagram of a SDR receiver is shown in Figure 5.1 [38]. The RF tuner converts the analog RF signals to analog IF frequencies. The analog-to-digital converter (ADC) digitizes the analog IF signal thereby converting it into digital samples. These samples are fed to the digital down-converter (DDC). The DDC is typically a single monolithic chip or FPGA, and is a key part of the SDR system.

A conventional DDC has three major sections:

- A digital mixer;
- A digital local oscillator;

- A finite impulse response (FIR) low-pass filter.

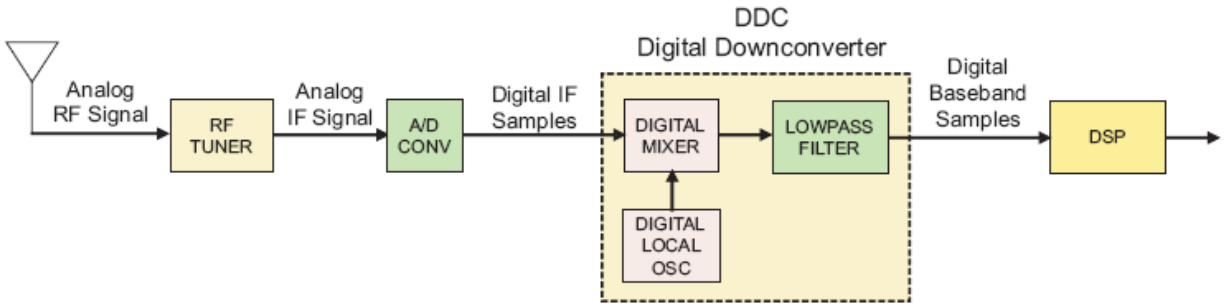

Figure 5.1. Block diagram of a SDR Receiver

The digital mixer and local oscillator translate the digital IF samples down to baseband. The FIR LPF limits the signal bandwidth and acts as a decimating LPF. The digital baseband samples are then fed to a digital signal processing (DSP) block which performs tasks such as demodulation, decoding, etc. Traditionally, these needs have been handled with dedicated Application Specific Integrated Circuits (ASIC) and programmable DSPs.

At the output of the mixer, the high frequency wideband signals from the ADC have been down-converted to DC (zero IF) as complex I and Q components with a frequency shift equal to the local oscillator frequency. In effect, the wideband RF signal can be “slid” around 0 Hz, left and right, simply by tuning the local oscillator. The lower and upper sidebands are preserved. The frequency accuracy and stability are determined entirely by the ADC clock so it is inherently synchronous to the sampling frequency. Since the output of the FIR filter is band limited, the Nyquist theorem allows one to lower the sample rate. The process is called decimation. The clear benefit is that decimated signals can be processed more easily, can be transmitted at a lower rate, or stored in less memory. The DDC performs two signal processing operations:

frequency translation with the tuning controlled by the local oscillator, and LPF filtering with the bandwidth controlled by the decimation setting [38].

The complete form of a SDR system requires the combination of software-based signal processing and the enabling hardware components. There exist a large number of experimental SDR systems that have been developed. Some of them are listed below [39, 40]:

- Universal Software Radio Peripheral (USRP)

  The USRP is one of the most popular SDR platforms currently available. It is the hardware system for the Gnu-Radio software.

- Kansas University Agile Radio (KUAR)

  KUAR was designed to be a low-cost experimental SDR system. It utilizes a modified form of Gnu-Radio software.

- National Institute of Information and Communication Technology (NICT)

  NICT is a Japanese SDR system designed to trial the next generation mobile network. A number of commercial standards were implemented, for example, 802.11a/b/g, digital terrestrial broadcasting (Japanese format), WCDMA, and a general OFDM communication scheme.

- Berkeley Cognitive Radio (BCR)

  BCR is based around the Berkeley emulation engine (BEE2). It can connect up to eighteen daughter boards.

- Maynooth Adaptable Radio System (MARS)

MARS was designed to deliver a performance equivalent to that of future mobile telephony base stations and wireless communication standards. The software selected for initial development was IRiS (Implementing Radio in Software).

- PowerSDR

  PowerSDR is software developed specifically for the FlexRadio hardware to produce a competitive amateur transceiver [40].

The majority of SDR products are *audio IF systems.* New SDRs are designed using a final intermediate frequency (usually a third IF) in the audio range. Low-cost audio analog-to-digital converter (ADC) and digital signal processing (DSP) chips allow the designer to provide many advanced features [40].

As stated, the combination of the USRP and Gnu-Radio is one of the most popular SDR systems available today. Gnu-radio is licensed under the GNU General Public Licence (GPL). It is a free software development toolkit that provides signal processing blocks. It can be used with readily-available low-cost external RF hardware to create software-defined radios, or without hardware in a simulation-type environment. Gnu-radio applications are primarily written in the Python programming language, while the supplied performance-critical signal processing path is implemented in C++ [41].

Gnu-radio comes with a complete transmitter and receiver, a software defined spectrum analyser and oscilloscope, a multichannel receiver and a collection of modulators and demodulators. It can be used for a wide range of applications such as [42]:

- Time Division Multiple Access (TDMA).

- Passive radar.
- Radio astronomy.
- Software GPS.
- Amateur radio transceivers.
- RFID detectors.
- Mobile phones.
- Broadcast TV.
- FM radio.
- Satellite navigation.

It is advisable to have a Linux operating system running in the host computer. At the time of writing, Ubuntu 10.11 and Gnu-Radio v3.5.1 were installed.

5.3. Universal Software Radio Peripheral (USRP)

Figure 5.2 shows the block diagram of the USRP-1 [42]. The datasheet of the USRP-1 is provided in Annexure 13.

The USRP-1 consists of:

- Four ADCs (12-bits, 64 Msamples/sec);
- Four DACs (14-bits, 128 Msamples/sec);
- USB2 controller (FX2);
- 2 RX daughter boards;
- 2 TX daughter boards; and

- A Field Programmable Gate Array (FPGA). One of the functions of the FPGA is to perform digital down-conversion (DDC) and digital up-conversion (DUC).

Figure 5.3 shows the block diagram of the USRP networked-series (USRP-2, USRP-N200, USRP-N210). The USRP networked-series (2-N200-N210) are more powerful than the USRP1. The datasheet of the USRP network-series is provided in Annexure 9. The USRP-1 incorporates the FPGA Altera Cyclone, and the USRP-2 has the FPGA Xilinx Spartan 3A [31].

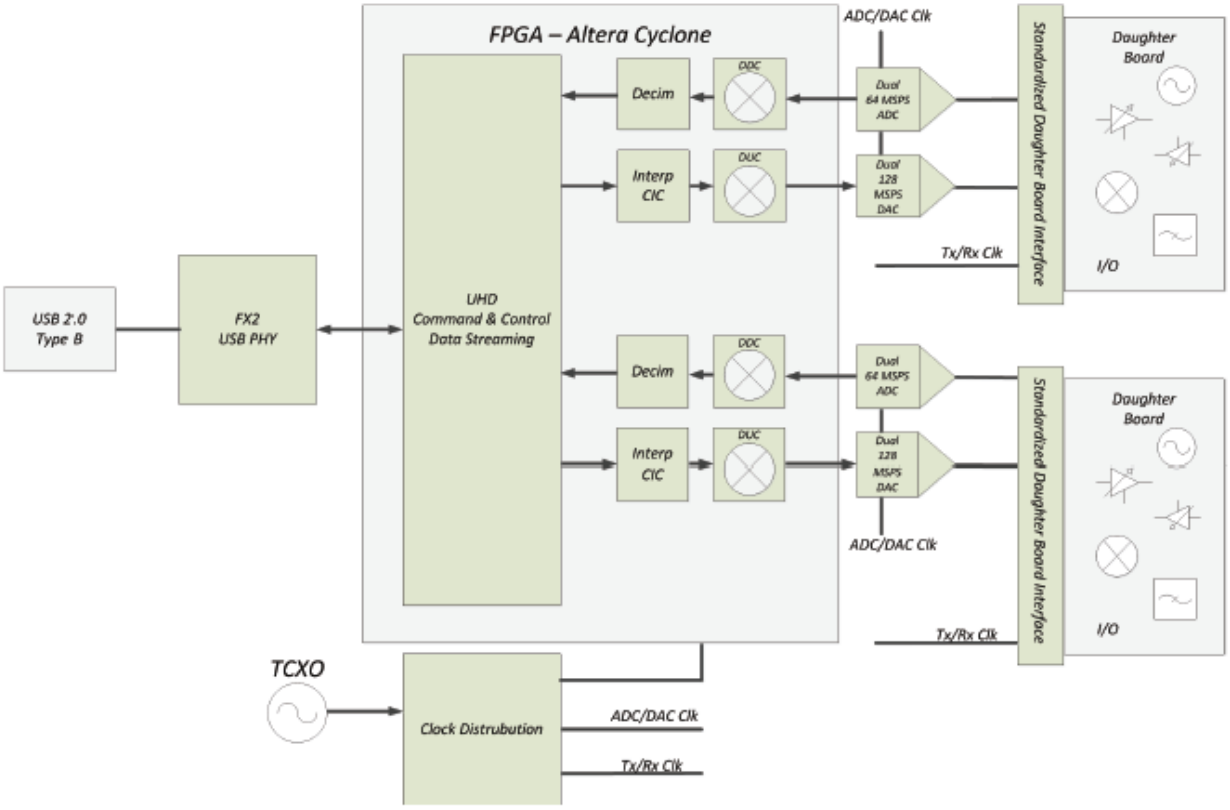

Figure 5.2. USRP-1 block diagram

The USRP-1 has two channels: Channel A and Channel B. Both channels consist of one receiver and one transmitter.

Referring to the block diagrams in Figure 5.2 and Figure 5.3, the USRP devices have two tuning stages [43]:

- RF Front-End: translates between RF and IF. This operation takes place in the daughter board.
- DSP: translates between IF and baseband (normally 0 Hz IF). This translation is implemented by the DDC inside the FPGA.

In a typical case, the user specifies an overall centre frequency for the chain. The RF Front-End will be tuned as close as possible to the centre frequency, as the DSP will account for the error (difference) in tuning between target frequency and actual frequency.

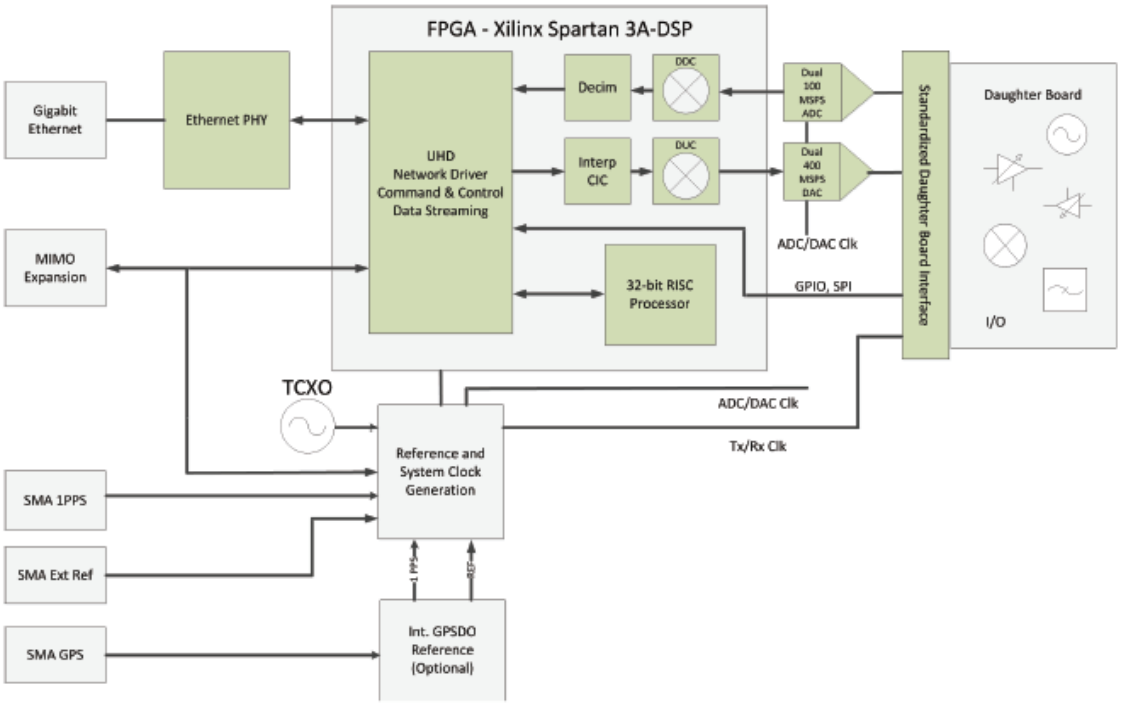

Figure 5.3. USRP-2 block diagram

5.4. Gnu-Radio and USRP

This section explains how to use the USRP-1 in conjunction with the Gnu-Radio software and the DBSRX daughter boards. The DBRX board has the following characteristics:

- Frequency range: 800 MHz to 2.3 GHz.
- Bandwidth: 60 MHz.
- Noise figure: 4-8 dB.
- Type: RX only.

5.4.1. Software and hardware verification

The first step was to test that both software and hardware operate correctly. Software verification was first performed without hardware.

To verify the software installation, two folders called uhd and gnuradio were downloaded. The location of these two folders depends on the installation directory. The uhd and gnuradio folders contain important sub-folders and files for the software to run.

The hardware was tested by checking the communication between the computer and the USRP. This is performed using the Terminal prompt. It is assumed that the USRP is powered and connected to the PC. The Terminal prompt can be opened by typing Ctrl+Alt+T from the key board. There are two methods of testing the hardware from the terminal prompt [44]:

1. Using the “Find-device” command.

   By typing the command “uhd_find_devices” in the Terminal prompt, Gnu-Radio scans the whole system and prints out a list of available USRP mother boards and their addresses in

the system. If the USRP mother board does not work, the Gnu-Radio responds with "*No UHD Devices Found".*

2. Using the "USRP-Probe" command.

   By typing the command "uhd_usrp_probe" in the Terminal prompt, Gnu-Radio scans the system and returns a list of all the devices (mother boards and daughter boards) attached to the system. The properties of each device (name, frequency range, gain, etc.) are also printed.

5.4.2. Gnu-Radio Companion (GRC)

The GRC is the graphical user interface (GUI) which allows the user to implement Gnu-Radio signal processing blocks in a manner similar to Simulink and Labview. The entire interface consists of more than 150 blocks. RF systems can be designed and simulated from the GRC. Any operations that are being executed using hardware can be executed in the same way using the GRC. The constraint here is to place the blocks sequentially, making sure that all the parameters are defined properly [45]. The GRC interface can be opened using two methods:

1. From the Terminal prompt.

   The GRC interface opens by typing the command "gnuradio-companion" in the Terminal prompt. This command is valid for Gnu-Radio v3.5.1. Previous versions of Gnu-Radio used the command "grc" in the Terminal.

2. From the GRC file.

   By double-clicking on the file called "gnuradio-companion". In Gnu-Radio v3.5.1, this file is located in the directory:/gnuradio/grc/scripts. It is advisable to copy this file and paste it in the computer desktop as a shortcut. The GRC interface is shown in Figure 5.4.

The Work-space is the space in the middle of the GRC window. This is where the system flow graph is designed. The program status window provides the execution sequence of the GRC. Error messages are also reported in the program status window. It also provides some suggestions regarding parameter settings of some stages: sample rate, frequency, antenna section, etc.

By default, the GRC interface opens with two blocks: the Options block and the Variable block. The Options block converts the GRC flow graphs into Python code. The Options block also sets some parameters of the GRC. The most important parameter of the Options block is the ID, which is the name of the Python file to be generated by the current flow graph. By default, the ID is set to “top_block”. By running the flow graph, the GRC automatically generates a Python file called “top_block.py”. This Python file is automatically saved and located at the same directory as the current GRC file. It is advisable to rename the ID otherwise the file generated will be overwritten.

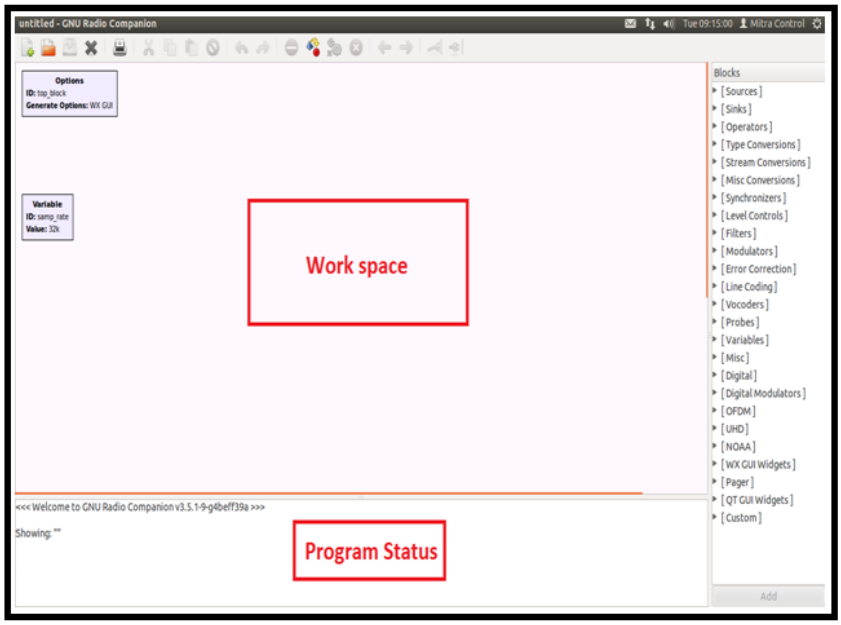

Figure 5.4. GRC interface

The Python file mentioned above can be executed in the Terminal prompt even if the GRC is not opened. This is possible by double-clicking on that Python file and selecting “Run in Terminal”. If the user is familiar with Python programming, the file can be executed as a python file. Also, the code of that Python file can be accessed by opening the file. This is possible by double-clicking on the Python file and selecting “Display”. The Options block is also used to set parameters such as Title, Author, and Description for identification purposes.

The Variable block is normally used to set the sample rate for all the components in the flow graph. This is preferred for applications where all the blocks need the same value of the sample rate.

5.4.3. Single channel operation

As discussed in section 5.3, the USRP-1 mother board has two channels: Channel A and Channel B. Single channel operation refers to applications where only one channel is used. This means the daughter board is plugged into one channel only. Figure 5.5 illustrates the block diagram for single channel operation.

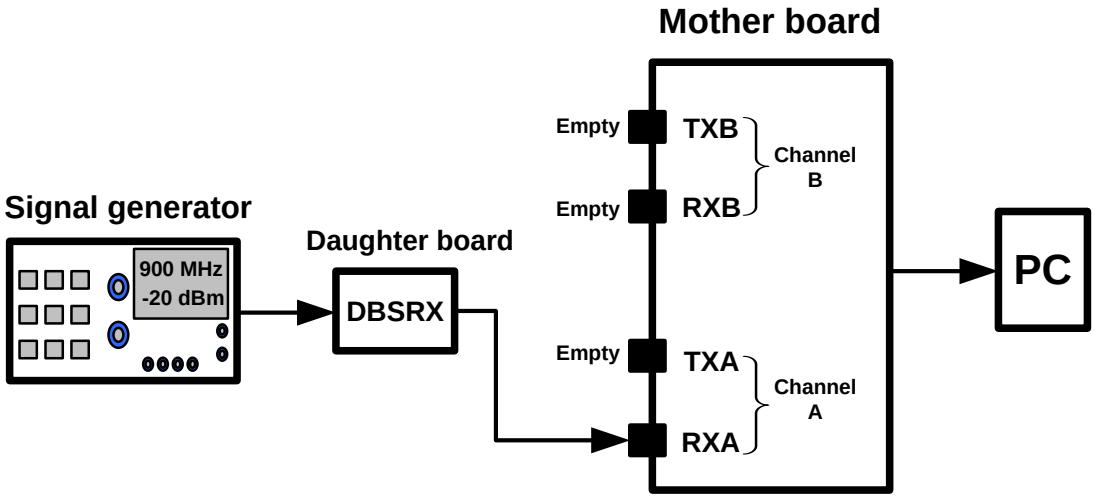

Figure 5.5. Single channel operation

To demonstrate this operation, the USRP-1 and DBSRX daughter boards were set to detect a signal from an external RF signal generator. The signal was set to 900 MHz with an amplitude of -20 dBm. Figure 5.6 shows the flow graph of this application.

The Options block was set as shown in Figure 5.7. The Variable block was used to set all the components in the flow graph to have the same sample rate.

The USRP Source is found under the "*UHD*" menu in the "*Blocks"* panel at the right hand side of the GRC. The FFT Sink is found under the "*WX GUI Widgets"* menu. The two blocks are connected by clicking first on the output of the source, then clicking on the input of the FFT.

For a receiver design, the "UHD: USRP Source" is always the first stage in the flow graph. It controls and sets the USRP as a receiver via the appropriate receiver daughter board. For this experiment, the UHD: USRP Source was set as shown in Figure 5.8.

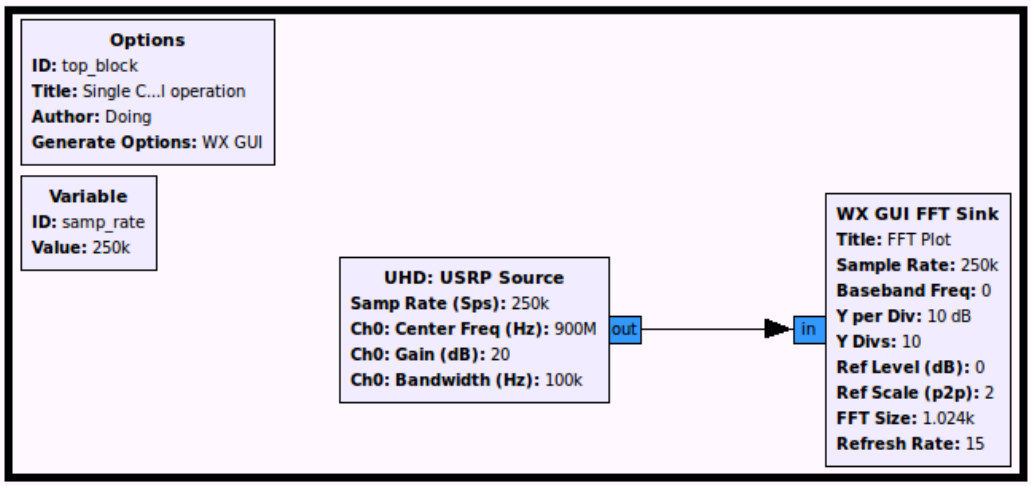

Figure 5.6. GRC designed to detect a signal from a RF signal generator

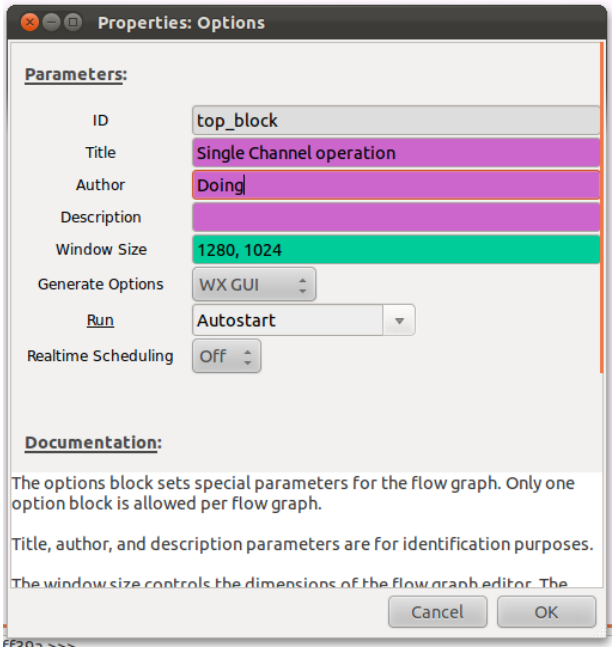

Figure 5.7. Options block settings for single channel operation

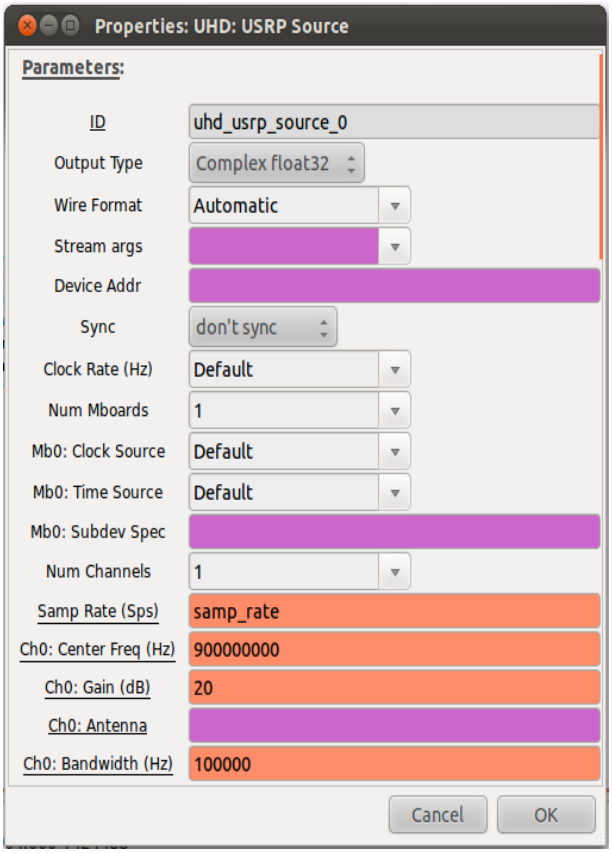

Figure 5.8. USRP Source setup for single channel operation

The setups of the USRP source properties are discussed below:

- **Num Mboards.** Only one mother board was used. It is indexed as “Mb0” (Mother board 0). If two mother boards were used, they would be indexed “Mb0” and “Mb1”.
- **Mb0: Subdev Spec**. This is the mother board sub-device specification. It is used to activate the USRP channel of the mother board. Daughter boards are also referred to as “sub-device”. For this experiment, one daughter board was plugged into channel A and there is no daughter board on Channel B. The unique sub-device is automatically activated. There is no need to set the Mb0: Subdev Spec.
- **Num Channels.** Only one channel is used. It is indexed as “Ch0”. If two channels were used, they would be indexed as “Ch0” and “Ch1”.
- **Samp Rate (Sps):** samp_rate. “samp_rate” is the ID of the variable block component. The USRP Source sample rate will be the value set in the variable block. The sample rate of 250 ksps was suggested by the GRC itself in the program status window.
- **Ch0: Center Freq (Hz):** 900 MHz is the frequency of the signal from the RF generator.
- **Ch0: Gain (dB):** Must be set at a level so as not to over-drive the system. If set improperly, no signal will be appear on the spectrum plots.
- **Ch0: Antenna.** This is the slot name. For example RXA, RXB, TXA, TXB. The daughter board DBSRX has no antenna selection setting.

The “WX GUI FFT Sink” displays the spectrum of the received signal. For this experiment, the “WX GUI FFT Sink” was set as shown in Figure 5.9.

The setups of the FFT Sink properties are discussed below:

- **Type:** Complex. The FFT plot displays a spectrum with positive and negative frequency values. The complex data type carries two components: the real (cos) and the imaginary (sin) components. When plotted in the time domain, data in complex format gives two signals with a 90° phase shift. If the data type was set to *Float*, then only positive frequency values of the spectrum can be displayed. In the time domain, data in float format gives only one signal.
- **Sample Rate:** samp_rate. This is the ID of the variable block. The sample rate of the FFT Sink depends on the value of the variable. Thus the USRP Source and the FFT Sink all have the same sample rate value (250 ksps).
- **Baseband Freq:** 0 as by default. This is to set the centre frequency of the spectrum.

Figure 5.9. FFT Sink setup for single mode operation

As discussed in Section 5.3, the USRP device has two down-conversion stages. The RF Front-end (daughter board) which translates from RF to IF, and the digital-down conversion (within the FPGA) which translates from IF to baseband. It was found that depending on the daughter board type, the IF was 30 MHz or 50 MHz and the baseband was 0 Hz. This is the reason why the FFT Sink parameter, Baseband Freq, discussed above is by default set to 0 Hz. The signal displayed by the FFT Sink is not at the RF frequency. The FFT Sink displays the signal at the baseband frequency.

When the GRC is designed, the Python file of the current flow graph is generated by clicking on the “Generate flow graph” button.  The flow graph is executed by clicking on the “Run” button.  These two controls are found in the GRC tool bar.

The spectrum of the detected signal is shown in Figure 5.10. Data type was set to complex format. Thus FFT plots both positive and negative frequency values. The FFT spectrum span depends on the sample rate. Each side of the spectrum (positive or negative) will have a span that is half the FFT sink sample rate. It can be seen in this case that each side of the spectrum has a span of 125 kHz as the FFT sample rate was set to 250 ksps. It can also be seen that the detected signal is at 4.9 kHz.

It was stated earlier that the baseband should normally be 0 Hz. However, a drift of a few kHz, in this case 4.9 kHz, may occur when the USRP clock source is set to default or internal. After experimentation, it was found that this frequency drift may vary every time the system resets. This situation can be fixed by using an external 10 MHz clock reference source. In this case, the USRP clock source must be set to external.

A frequency modulation experiment was performed using the FM function from the RF signal generator. The 900 MHz carrier was modulated by a 1 kHz signal. The purpose of this experiment was to implement an FM demodulator using the USRP. The flow graph was designed as shown in Figure 5.11.

The USRP Source and the FFT Sink were discussed earlier. The FM demodulator (*FM* Demod) block is found under the *Modulators* menu in the GRC. The FM Demod incorporates a low pass filter and amplifier for the audio signal.

The setup for the FM Demod is discussed below:

- ***Channel Rate:*** was set to 250 ksps as the incoming signal sample rate.
- ***Audio decimation:*** 5. This reduces the audio sample rate by a factor of 5 since most computer sound cards sample at 48 ksps. It can be seen that the sample rate of the Audio Sink is 48 ksps.
- ***Audio Pass:*** Passband frequency of the audio LPF.
- ***Audio Stop:*** Stopband frequency of the audio LPF.

The setup for the FM Demod is discussed below:

- ***Channel Rate:*** was set to 250 ksps as the incoming signal sample rate.
- ***Audio decimation:*** 5. This reduces the audio sample rate by a factor of 5 since most computer sound cards sample at 48 ksps. It can be seen that the sample rate of the Audio Sink is 48 ksps.
- ***Audio Pass:*** Passband frequency of the audio LPF.
- ***Audio Stop:*** Stopband frequency of the audio LPF.

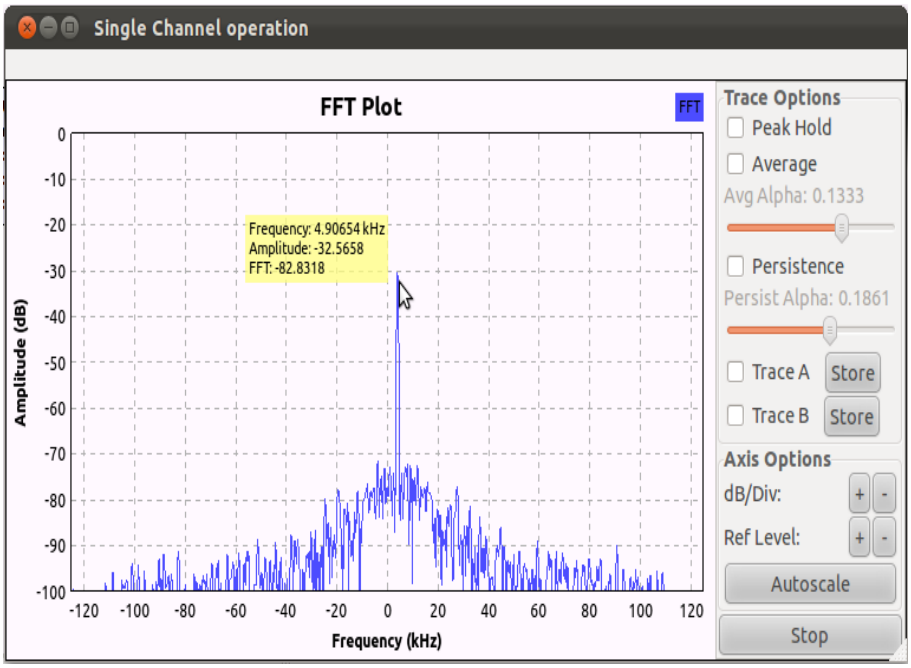

Figure 5.10. Detected signal for the single channel operation

The setup for the FM Demod is discussed below:

- ***Channel Rate:*** was set to 250 ksps as the incoming signal sample rate.
- ***Audio decimation:*** 5. This reduces the audio sample rate by a factor of 5 since most computer sound cards sample at 48 ksps. It can be seen that the sample rate of the Audio Sink is 48 ksps.
- ***Audio Pass:*** Passband frequency of the audio LPF.
- ***Audio Stop:*** Stopband frequency of the audio LPF.

The Audio Sink block controls the computer sound card. This makes the demodulated signal audible from the speakers. The Audio Sink block was set as in Figure 5.12. The Audio Sink is found under the Sinks menu.

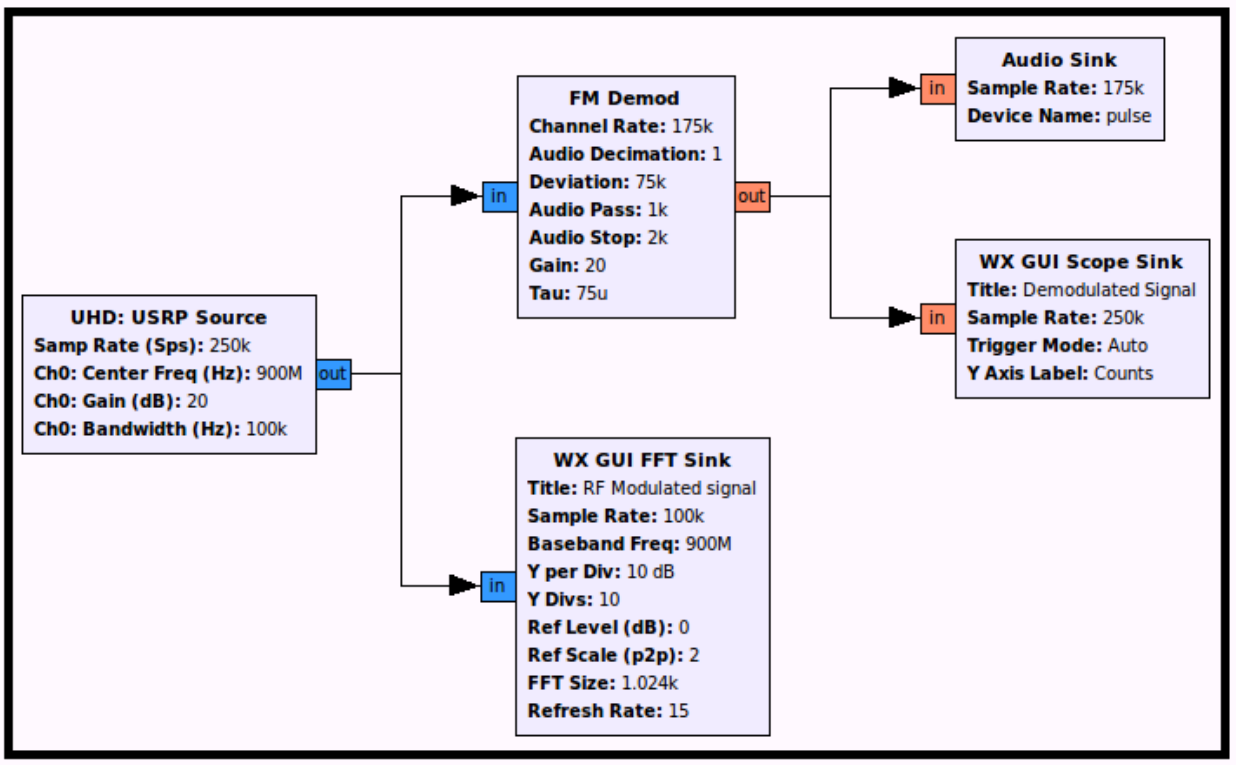

Figure 5.11. FM demodulator flow graph

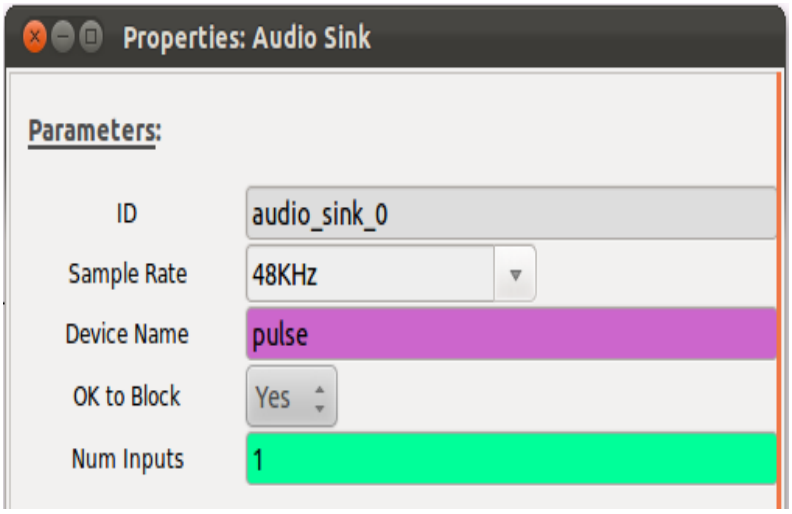

Figure 5.12. Audio Sink Setup

The Audio Sink was setup as follows:

- **Sample Rate:** 48 ksps as most of the computer sound cards sample at 48 ksps.

- **Device Name:** sets the incoming data to match the audio card sampling rate. Device Name can be: pulse, hw:0,0, plughw:0,0, surround51, /dev/dsp. The correct device name is the one which provides an undistorted audio signal from speakers.

If the Audio Sink sample rate is not set correctly, the following messages may appear in the GRC status window:

- "aUaU": audio underrun (not enough samples ready to send to sound card sink).
- "uUuU": USRP underrun (not enough samples ready to send to USRP sink).
- "uOuO": USRP overrun (USRP samples dropped because they were not read in time).

The "WX GUI Scope Sink" is an oscilloscope to display the demodulated signal in the time domain. The Scope Sink sample rate was set to 48 ksps as the output of the FM Demod. The Scope Sink is found under the WX GUI Widgets menu. The data type of Scope Sink was set to *Float* to match the FM Demod output data type.

The spectrum of the modulated carrier was measured and is shown in Figure 5.13. The oscilloscope display of the demodulated signal in provided in Figure 5.14.

It can be seen in Figure 5.14 that the demodulated signal is a sinusoidal signal for which the frequency is calculated below:

$$\frac{1}{170 \times 10^{-3} - 169 \times 10^{-3}} = 1 \text{ kHz}$$

This frequency 1 kHz is equal to the modulating signal frequency from the signal generator.

5.4.4. Multi-channel operation

This refers to applications where both channels of the USRP are used. In this case, signals from two independent signal generators are applied to both channels as shown in Figure 5.15. The flow graph of the dual channel operation is shown in Figure 5.16.

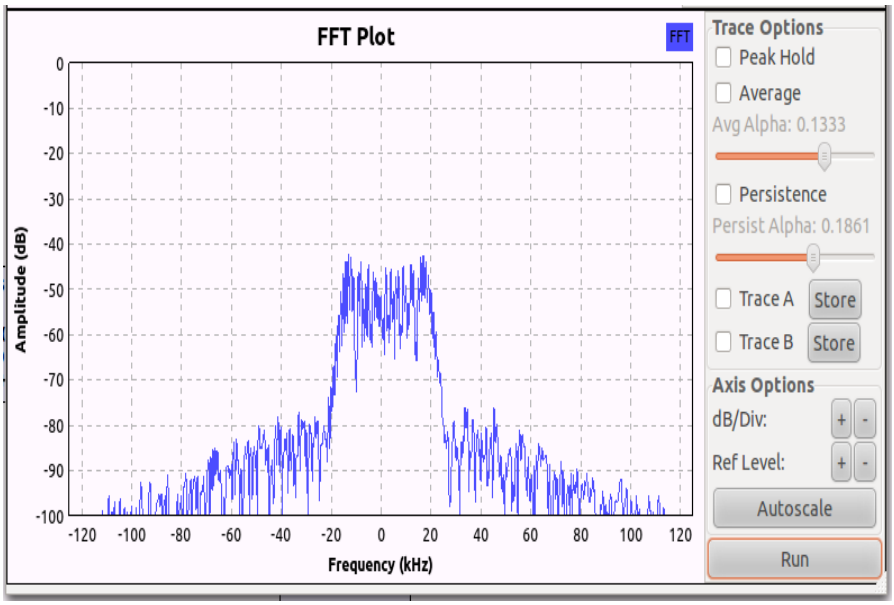

Figure 5.13. FM Modulated carrier at the receiver

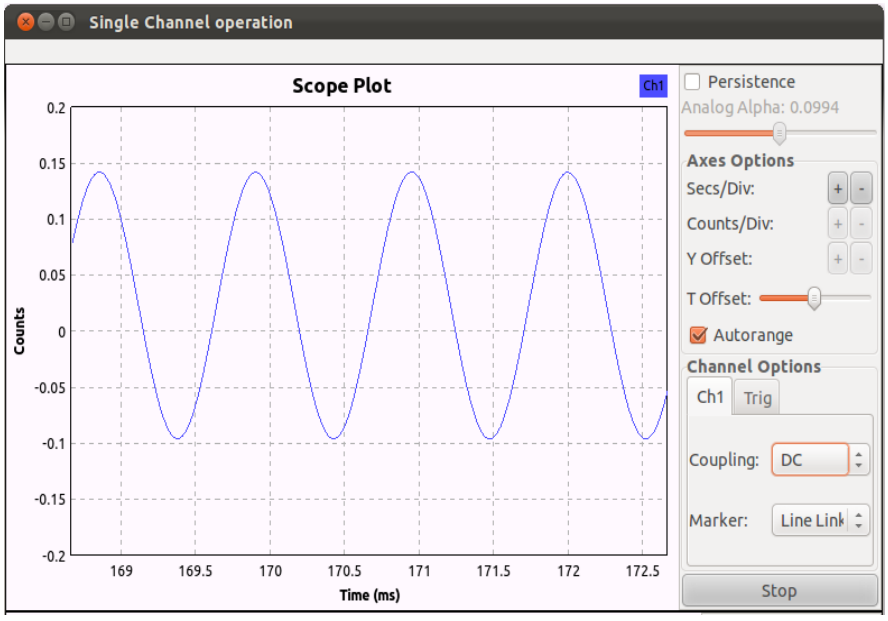

Figure 5.14. Demodulated signal

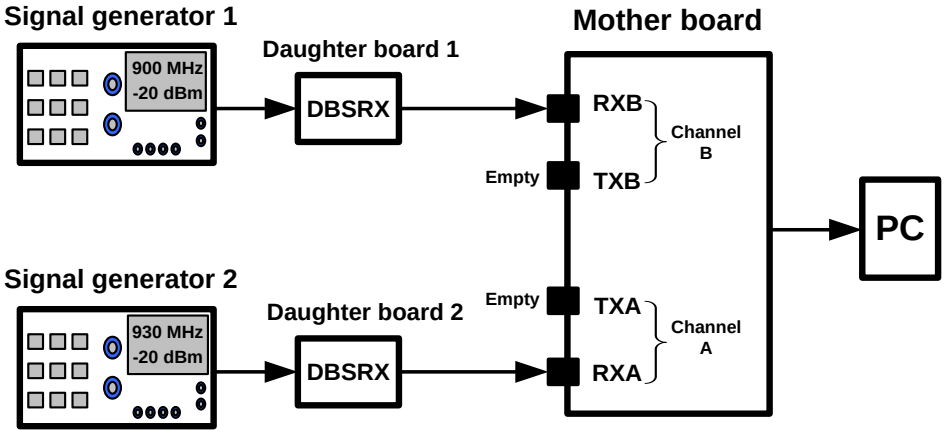

Figure 5.15. Dual channel operation

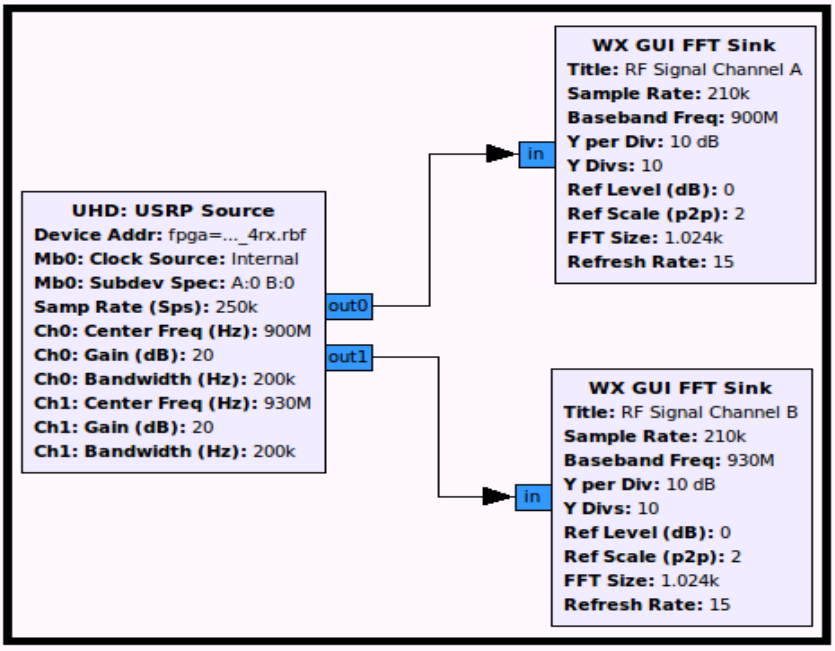

Figure 5.16. Dual channel operation flow graph

The FFT Sinks monitor the output from their respective channels. Both FFT Sinks are set as discussed earlier. The USRP Source settings are shown in Figure 5.17.

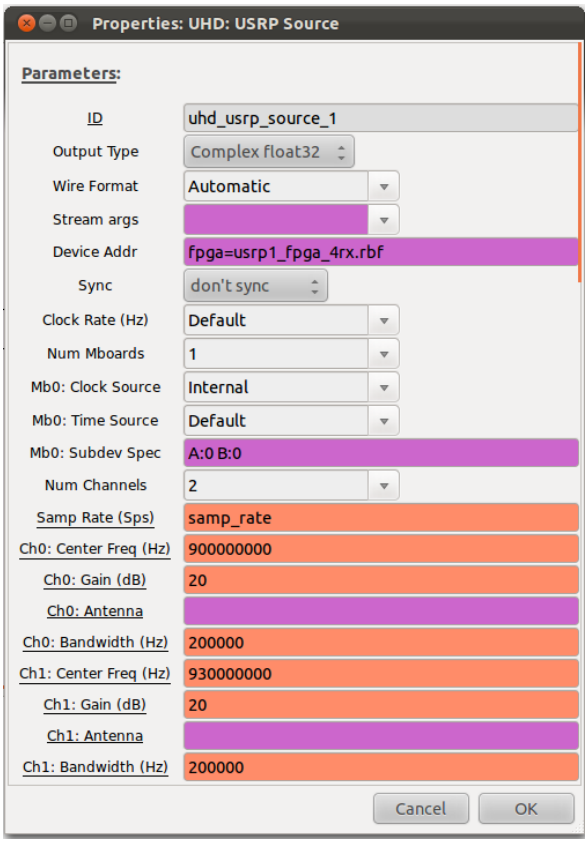

Figure 5.17. USRP Source setup for dual channel operation

USRP Source setup is as follows:

- **Device Addr:** It is recommended that the device address should be "fpga=usrp1_fpga_4rx.rbf" for the application to work properly. It was found that if the Device Addr is left blank, the output signal may be attenuated.
- **Num Mboards:** Only one mother board is used. It is called "Mb0".
- **Mbo: Subdev Spec:** To activate Channel A and Channel B simultaneously, the sub-device specification must be set to "A:0 B:0". When writing this code, the space before "B" must be respected. In this code, A and B mean Channel A and Channel B respectively. The two zeros are to specify the mother board number. The code "A:0 B:0" signifies "channel A of mother board 0, and channel B of mother board 0".
- ***Num Channels:*** Two channels (A and B).

- ***Ch0: Center Freq:*** 900 MHz from signal generator 1.
- ***Ch0:Antenna:*** No antenna selection for the DBSRX daughter board.
- ***Ch1: Center Freq:*** 930 MHz from signal generator 2.

The Spectrum from each channel is shown in Figure 5.18.

5.5. Getting started with the USRP-2

The USRP-2 is a networked-type device. The connection between the USRP-2 and the host PC is established via a 1 Gigabit Ethernet link. The USRP-2 requires a memory card where the booting program (images and firmware) are burnt. This section discusses how to create the booting memory card, and how to set up the network between the PC and the USRP-2 in the Ubuntu operating system.

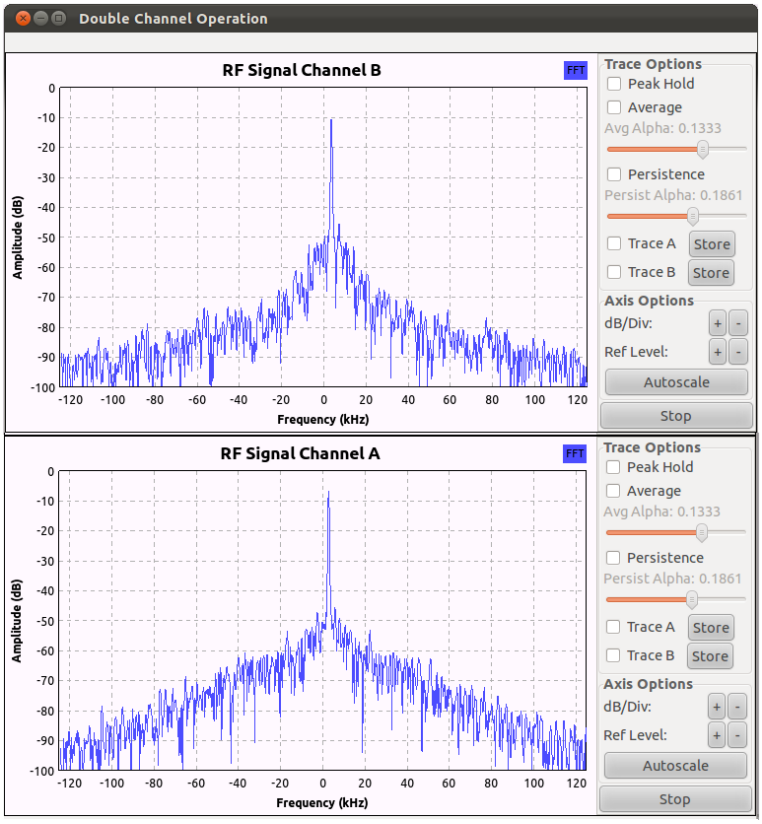

Figure 5.18. Received signals for dual channel operation

5.5.1. Selecting the memory card

The type of the memory card is very critical. Certain types of memory cards will not interface with the USRP-2 [31]. It was found that the SDHC (SanDisk High Capacity) or HC (high capacity) memory cards are not compatible with the USRP-2. Advanced types of memory cards such as SDXC, SDHAI, and UHS may also not work. Memory cards of class 4 and 10 are not advisable. It is recommended to have a standard SanDisk (SD) memory card described as "SD" only. The memory card capacity must be at least 2 GB.

5.5.2. Burning Procedure

The burning process is done using burner software. This graphical user interface (GUI) must be downloaded. Two python files are needed to create the burner: the usrp2_card_burner.py and usrp2_card_burner_gui.py. At the time of writing, these files were downloadable from [46].

After downloading is complete, the two files need to be enabled so that they become executable files. The following commands are used for this conversion:

```
$ sudo chmod +x usrp2_card_burner.py
```

and

```
$ sudo chmod +x usrp2_card_burner_gui.py
```

The prefix $ means the commands are executed in the terminal. The command "sudo" means the process will require the administrator password of the computer.

This experiment was conducted using Ubuntu 11.10. This version has a directory called Home. It is advisable to download and save the python files in the Home directory. By default, the

terminal runs from the Home path. Using another location requires the setup of the directory path properly using the “cd” command.

The process of enabling theses files takes 3 to 5 seconds. A double-click on the relevant file can tell if the file has changed the mode (chmod) from a standard python file to an executable python file.

An additional python tool called “Python tk Package” needed to be installed using the command:

$sudo apt-get install python –tk

The burner GUI must be launched in the terminal by running the command:

$ sudo python usrp2_card_burner_gui.py

Failure to launch the burner GUI in the terminal is an indication that the two python files are not yet enabled, and thus cannot be executed. No further action must be initiated when the GUI is launched or the PC hard drive can be mistakenly formatted. As a precaution, it is advisable to close the burner interface when it is confirmed that the GUI can be launched from the terminal.

The booting programs are referred to as firmware and fpga images. These programs are released every week [31]. It is critical to identify the version of the USRP Hardware Driver (UHD) installed in the PC. Outdated versions of the UHD may not be compatible with the latest released firmware and images. The following command is used to verify the UHD version:

$ uhd_find_devices

The response from this command starts with a statement similar to:

Linux; GNU C++ version 4.6.1; Boost_104601; UHD_003.004.000-1424488

This means the UHD version is *003.004.000-1424488.*

At the time of writing, the images and firmware were downloadable from [47]. This link lists different versions of UHD. The “tar.gz” document should be downloaded. The tar.gz document contains many files. Only the “usrp2_fpga.bin” and “usrp2_fw.bin” files are of interest. The binary file “usrp2_fpga.bin” represents the images. The binary “file usrp2_fw.bin” represents the firmware.

Should the binary files not be accessible, the following commands are used to download the correct version of the UHD automatically:

$sudo “/usr/local/share/uhd/utils/uhd_images_downloader.py”

“sudo/usr/local/share/uhd/images/usrp2_fpga.bin”

The memory card concerned must be identified in order to avoid formatting other device drivers (PC hard drive, USB memory, DVD player, etc.). For this identification, an additional Linux package needs to be installed using the following commands:

$ sudo apt-get update

$ sudo apt-get install sg3-utils

After the installation of the sg3-utils, the memory card can be plugged into the PC via a USB memory card reader or directly through the memory card port (if provided). All the memory drivers installed in the PC should be scanned using the following command:

$ sudo sg_scan –i

As shown in Table 5.1, this command scans and prints out all the memory devices connected in the computer.

Three devices are identified in this example:

- Device 1 identified as “sg0”, is the PC hard drive (ATA)
- Device 2 identified as “sg1”, is the DVD player (hp)
- Device 3 identified as “sg3”, is the memory card (multi-card)

The nomenclature in Table 5.1 may change depending on the number of memory devices connected to the PC. An additional identification code is important. This is determined using the following command:

```
$ sudo sg_map
```

As shown in Table 5.2, this command scans and prints out the identification code of the memory devices connected to the computer.

In Table 5.1, the memory card (device 3) was referred to as “sg2”. With that, the identification code for the memory card in Table 5.2 is “/dev/sdb”. This is the code to use for burning the images and firmware into the memory card. The mapping in Table 5.2 is subject to change depending on the number of memory devices connected to the PC.

The USRP-2 burner GUI can now be launched using the following command:

```
$ sudo python usrp2_card_burner_gui.py
```

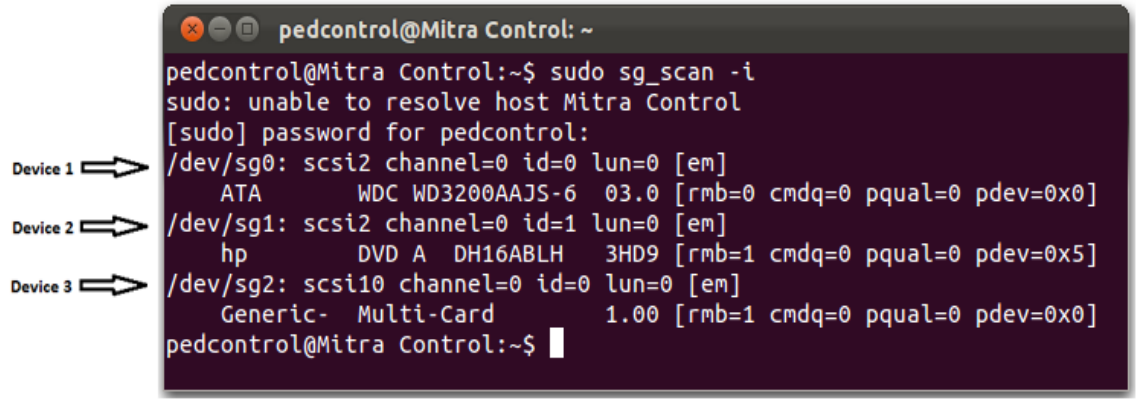

Table 5.1. Available memory devices

Table 5.2. Device identification code

The GUI is shown in Figure 5.19. The image and firmware binary files must be selected accordingly by browsing the directory where the binaries were saved. It was suggested to download and save these files in the Home directory.

A click on “Rescan for devices” button updates the list of the memory devices connected to the PC. It can be seen that the memory card is identified using the same code as shown in Table 5.2. Failure to print the memory card identification code is an indication that the memory card is not compatible with the USRP-2.

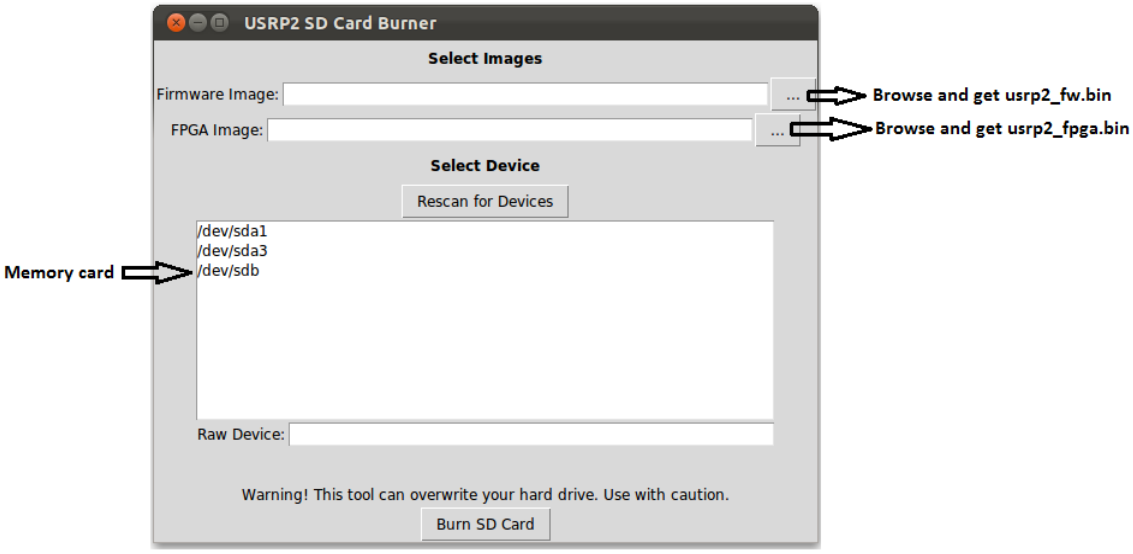

Figure 5.19. USRP2 SD Card burner interface

A click on the "/dev/sdb/" button allows one to select the memory card. This operation must be conducted with caution to make sure that the hard drive or another memory device is not selected. The "Raw Device" bar serves to print the identification code of the selected device.

A click on the "Burn SD Card" button initiates the burning process. This takes 2 to 4 seconds. A message pops up to confirm that burning was successful. The memory card can now be removed from the PC and plugged in to the USRP-2 unit. By powering the USRP-2 device, the six LEDs in the front panel should come on for few seconds. Only LED D and F should remain on. LED D indicates that the firmware was successfully loaded. LED F indicates that the Complex Programmable Logic Device (CPLD) is loaded [31].

5.5.3. Setting the network PC and USRP-2

This network requires the following:

- A Gigabit network interface card;
- A Cat-5 Ethernet cable;

- A RJ-45 connector; and
- IPv4 protocol

It is advisable to make sure that the driver for the Network Interface Card (NIC) is installed in the computer. This installation can be completed in the Windows operating system. In Linux, the NIC is called "*eth"* for Ethernet. The computer may have more than one NIC. In this case, the first NIC is called "*eth0"*, the second NIC is called "*eth1"*, the third is called "*eth2"* and so on [48].

The characteristics of the NIC should be described in order to determine if the NIC complies with the USRP-2 network requirements. In Ubuntu, the "*lshw"* command is used to list the properties of any NIC's installed in the computer:

```
$ sudo lshw –class network
```

This operation takes 2 to 4 seconds depending on the number of NICs in the system. The computer used for this experiment had 2 NICs. The characteristics of these two NICs are listed in Table 5.3.

Attention must be paid to the "logical name" and "capacity" of each NIC. It can be seen that "eth1" is a Gigabit (1 Gbit/s) network interface card. With that, "eth1" is selected for the USRP-2 networking.

The PC and USRP-2 must be connected using a Cat-5 cable. The IP address for the NIC (eth1) must be created in order to have a functional network. By default the USRP-2 IP address is 192.168.10.2 [31].

Following IPv4 protocol, the NIC (eth1) IP address needs to be 192.168.10.1 with a subnet mask of 255.255.255.0. The NIC (eth1) IP address can be configured using the “ifconfig” command as follows:

```
$ sudo ifconfig eth1 192.168.10.1 netmask 255.255.255.0
```

To verify that NIC (eth1) is configured with a proper IP address, the “ifconfig” command can be used as follows. The USRP-2 unit must be powered up first.

```
$ sudo ifconfig eth1
```

Table 5.4 shows that NIC (eth1) has been configured with a correct IP address.

This method is used for a temporary configuration of the NIC. The configuration in Table 5.4 is lost when the USRP-2 reboots. It is advisable to set the NIC IP address for permanent configuration. This can be done manually. A click on the network icon  at the top-right corner of the screen opens a setup window. A click on the “Edit Connections” tab opens a list of available networks (Wired, Wireless, Mobile broadband, etc.). The eth1 NIC is found under the “Wired” network. A double-click on the eth1 network allows editing of the configuration of the USRP-2 network. The setup of the USRP-2 network is done as follows:

- Connection name: changed to “MITRA USRP Network”
- Connect automatically: yes
- Wired:
  - Device MAC address: (eth1) must be selected
  - Cloned MAC addess: No option to change
  - MTU: automatic bytes

- 802.1X Security: No option to change
- IPv4 Settings:
  - Method: Manual
  - Addresses:
    - Address: 192.168.10.1
    - Netmask: 255.255.255.0
    - Gateway: 0.0.0.0
- This setup must be added by clicking on the “Add” button.
  - DNS servers: No option to change
  - Search domains: No option to change
- IPV6 Settings:
  - Method: Ignore

The Firewall may obstruct the USRP-2 network from being established. It is advisable to deactivate the firewall in the system. To do so, the “ufw” (uncomplicated firewall) command can be used.

To disable the firewall: $ sudo ufw disable

To enable the firewall: $ sudo ufw enable

To check the firewall status: $ sudo ufw status

Table 5.3. Characteristics of the NIC's

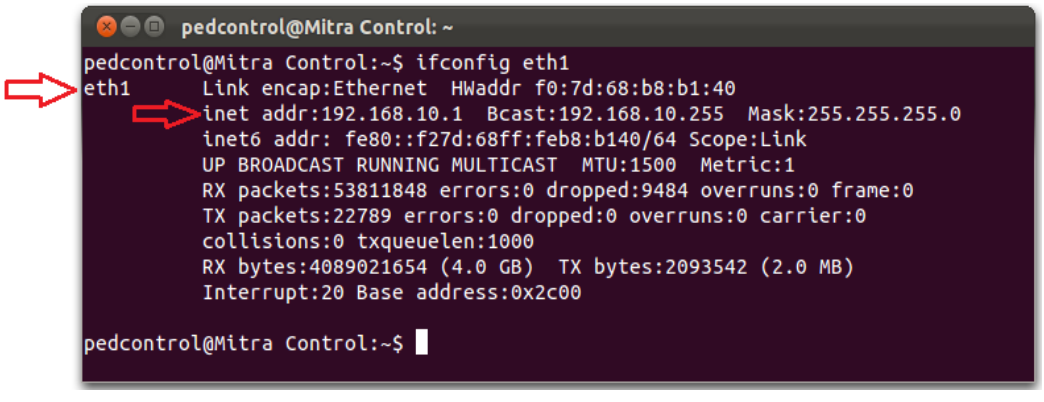

Table 5.4. NIC (eth1) IP configuration

Chapter 6: Correlator Implementation in Gnu-Radio

6.1. Introduction

The purpose of this chapter is to describe the correlator using the GNU-Radio Companion. The correlator is the main component in an interferometer telescope. There exist a number of possible correlator circuits. The simplest type is the adding interferometer in which the voltages of the two antennas are continually added [25]. The problem with the simple adding interferometer is that, in addition to the signal from the source, the output of the receiver contains components from other sources of noise power such as the galactic background radiation, the thermal noise from the ground picked up in the antenna side lobes, and the noise generated in the system.

The introduction of a phase switching interferometer removes many of the unwanted components of the receiver output leaving only the fringe oscillations [28]. In the phase switching system, the phase of one of the two signals is periodically reversed. The signal voltages are multiplied and then time-averaged, which has the effect of filtering out the high frequencies. Averaging a signal modifies the original data set, acting like a low-pass electronic filter, because it reduces the high frequencies in the original signal [49]. The phase-switched interferometer is sometimes referred to as a multiplying interferometer. It produces a fluctuating output signal of average zero called fringe oscillations [25, 28].

For sidereal sources, the variation of the angle θ (see Figure 6.1) with time as the earth rotates generates quasi-sinusoidal fringes at the correlator, which is the output of the interferometer [28].

6.2. The Multiplying Correlator

Figure 6.1 shows the block diagram of a two element multiplying correlator. Signals $v_1(t)$ and $v_2(t)$ are the incoming signal voltages from antenna 1 and antenna 2 respectively. It is assumed that both antennas are pointed in the same direction. A source will induce equal signal voltages into the receivers with a certain phase difference depending on the source direction [25]. The two signals are expected to be of the same frequency since the antennas are pointed at the same source.

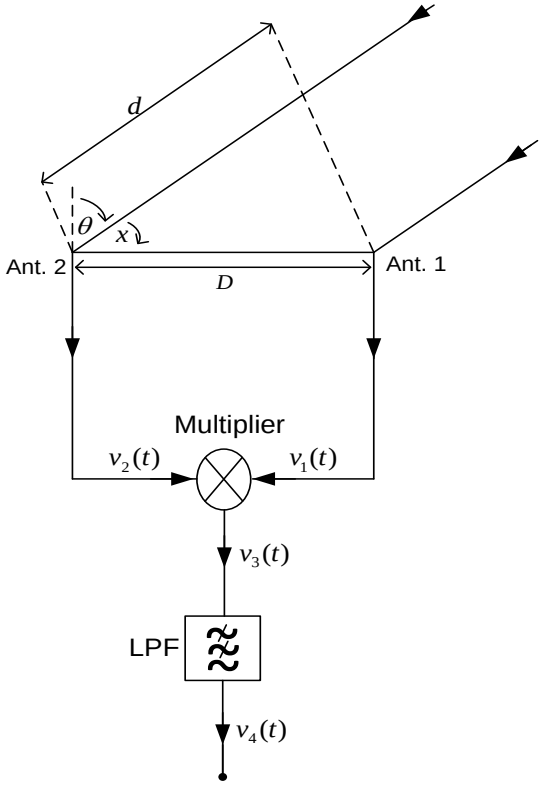

Figure 6.1. Multiplying correlator

The distance d in Figure 6.1 can be derived as follows:

$$\cos(x) = \frac{d}{D} \tag{6.1}$$

$$\theta + x = 90° \Rightarrow x = 90° - \theta \tag{6.2}$$

$$\therefore \cos(90° - \theta) = \frac{d}{D} \tag{6.3}$$

$$\cos(90° - \theta) = \sin(\theta) \tag{6.4}$$

$$\sin(\theta) = \frac{d}{D} \tag{6.5}$$

$$d = D\sin(\theta) \tag{6.6}$$

The wavefront from the source in direction θ reaches Ant. 1 at a time τ_g before it reaches Ant. 2. The variation of the angle θ depends on the earth's rotational velocity. The time τ_g is called the geometric delay and is formulated as follows [12].

$$\tau_g = \frac{D\sin(\theta)}{c} = \frac{d}{c} \quad [\text{s}] \tag{6.7}$$

where c is the velocity of an electromagnetic wave in free space. With the baseline D, observing at angle θ, the delay is τ_g, the frequency is ν, and the phase difference ϕ is formulated in Equation 6.8 [5]:

$$\phi = 2\pi\nu\tau_g = \omega\tau_g \quad [\text{rad}] \tag{6.8}$$

$$\phi = \frac{2\pi\nu D\sin(\theta)}{c} \quad [\text{rad}] \tag{6.9}$$

With $\lambda = \frac{c}{\nu}$, the phase-difference due to the separation of the antennas is expressed as:

$$\phi = \frac{2\pi D\sin(\theta)}{\lambda} \quad [\text{rad}] \tag{6.10}$$

The instantaneous voltages into the multiplier are given as:

$$v_1(t) = V_1\cos(\omega t) \tag{6.11}$$

$$v_2(t) = V_2\cos(\omega(t - \tau_g)) \tag{6.12}$$

The multiplier output gives the signal $v_3(t)$ such that:

$$v_3(t) = V_1 \cos(\omega t) \times V_2 \cos(\omega(t - \tau_g))$$

$$v_3(t) = \frac{V_1 V_2}{2} \left\{ \cos\left[\omega t + \omega(t - \tau_g)\right] + \cos\left[\omega t - \omega(t - \tau_g)\right] \right\}$$

$$v_3(t) = \frac{V_1 V_2}{2} \left\{ \cos\left[\omega t + \omega t - \omega\tau_g)\right] + \cos\left[\omega t - \omega t + \omega\tau_g)\right] \right\}$$

$$v_3(t) = \frac{V_1 V_2}{2} \left\{ \cos(2\omega t - \omega\tau_g) + \cos(\omega\tau_g) \right\} \qquad (6.13)$$

After the LPF in Figure 6.1, the higher frequency component $\cos(2\omega t - \omega\tau_g)$ will be filtered out, giving the signal $v_4(t)$:

$$v_4(t) = \frac{V_1 V_2}{2} \cos(\omega\tau_g) \qquad (6.14)$$

if $V_1 = V_2 = V$, then

$$v_4(t) = \frac{V^2}{2} \cos(\omega\tau_g) \qquad (6.15)$$

The following should be noted:

1. The signal $v_4(t)$ varies between $\frac{V^2}{2}$ and $-\frac{V^2}{2}$

2. The actual peak voltage of the signal at the output of the multiplying correlator is equal to the normalized power calculated using a normalized impedance of 1 Ω.

$$P = V_{rms}{}^2 = \frac{V_p{}^2}{2} \qquad \text{[W]} \qquad (6.16)$$

3. The maximum output power from a 2 element correlator receiver is the same as what would be obtained from a single total power receiver.
4. Non-coherent noise will be eliminated.

The expression $\cos(\omega\tau_g)$ in Equation 6.15 is called the fringe function [28]. The correlator output voltage in Equation 6.16 varies co-sinusoidally with the change of the source direction in the interferometer frame. The sinusoid fringe signal has the fringe phase ϕ expressed in Equation 6.8. The fringe phase is a measure of the source position. Note that the fringe phase and hence measured source position is not affected by small tracking errors of the individual telescopes. It depends on time and time can be measured by clocks with high accuracy [50]. An interferometer whose baseline is horizontal is not affected by the plane-parallel component of atmospheric refraction, which delays the signals reaching both telescopes equally. The response of a two-element interferometer with directive antennas is a co-sinusoid multiplied by the product of the voltage patterns of the individual antennas. Normally the two antennas are identical, so this product is the power pattern of the individual antennas and is called the primary beam. The primary beam is usually a Gaussian much wider than a fringe period. More baselines are required to improve the response of an interferometer. The number of baselines (the distance between the pair of antennas) is expressed in Equation 6.17. The response of the synthesized beam is obtained by averaging the outputs of all pairs [50].

$$N_b = \frac{N_a\left(N_a - 1\right)}{2} \tag{6.17}$$

where N_b is the number of baselines and N_a the number of antennas.

A Microsoft Excel spreadsheet (Annexure 16) was used to demonstrate the operation of the adding and multiplying correlators. Two sinusoidal signals $v_1(t)$ and $v_2(t)$ were created at the same frequency. A varying phase shift ϕ was applied to $v_2(t)$. Figure 6.2 shows the two signals as the phase shift varies.

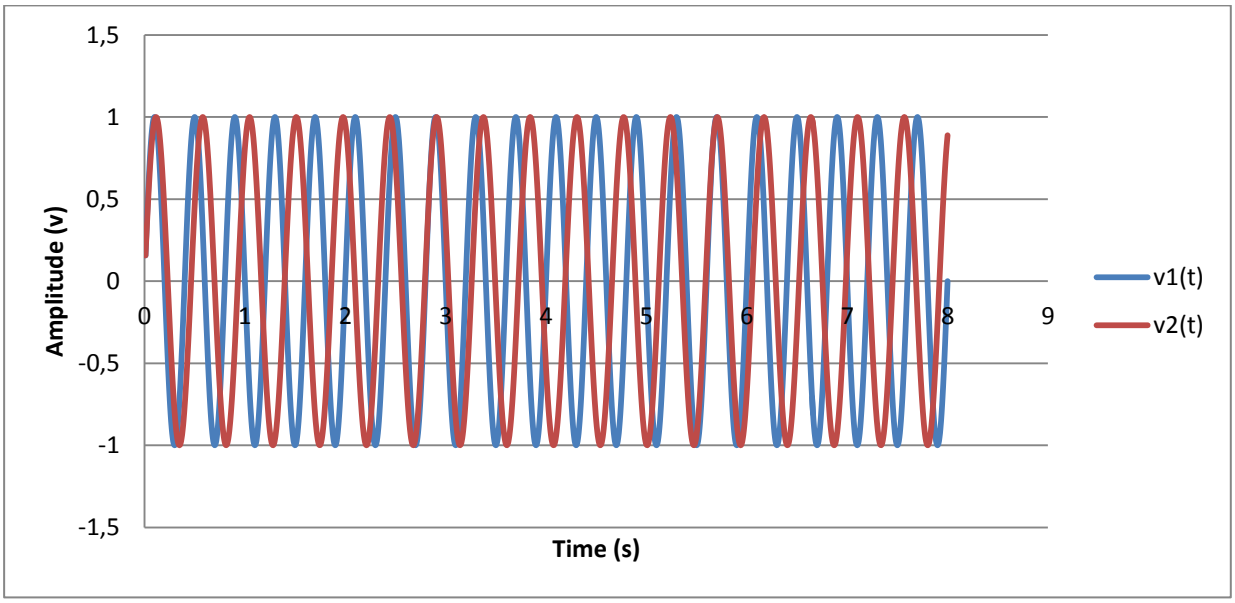

Figure 6.2. Two sinusoidal signals with a varying phase

If $v_1(t)$ and $v_2(t)$ represent the signal voltage as a function of time from the two antennas, the output from a simple adding interferometer (adder followed by a square-law detector) is proportional to $[v_1(t)+v_2(t)]^2$ [51]. Figure 6.3 shows the output of the adding interferometer. The peak points are obtained where $v_1(t)$ and $v_2(t)$ are in phase, and the dips are obtained where $v_1(t)$ and $v_2(t)$ are out of phase.

The voltages $v_1(t)$ and $v_2(t)$ were multiplied to form a multiplying correlator for which the result is shown in Figure 6.4. The exponential smoothing technique was applied to reduce the level of ripple in the correlated data. The damping factor or smoothing constant was set to 0.95. The

action of the multiplying correlator is verified in Figure 6.5 where the two input signals with varying phase are plotted on the same set of axis with the smoothed correlated data. The positive peak is measured where the inputs are in-phase and the negative peak is measured where the inputs are out of phase.

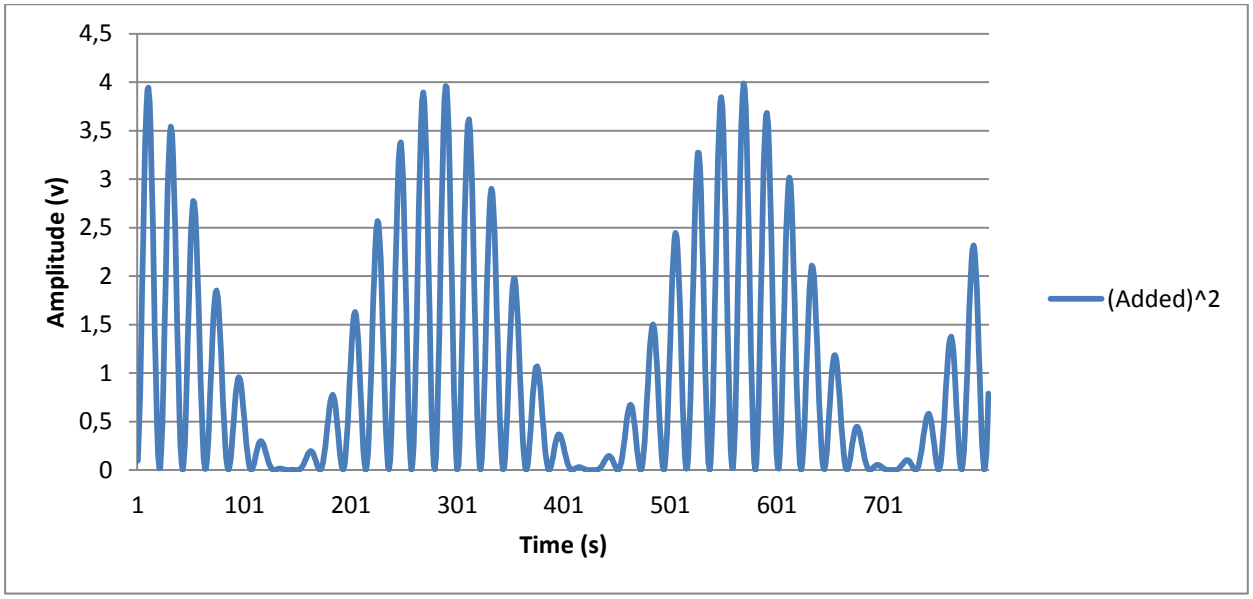

Figure 6.3. Adding correlator

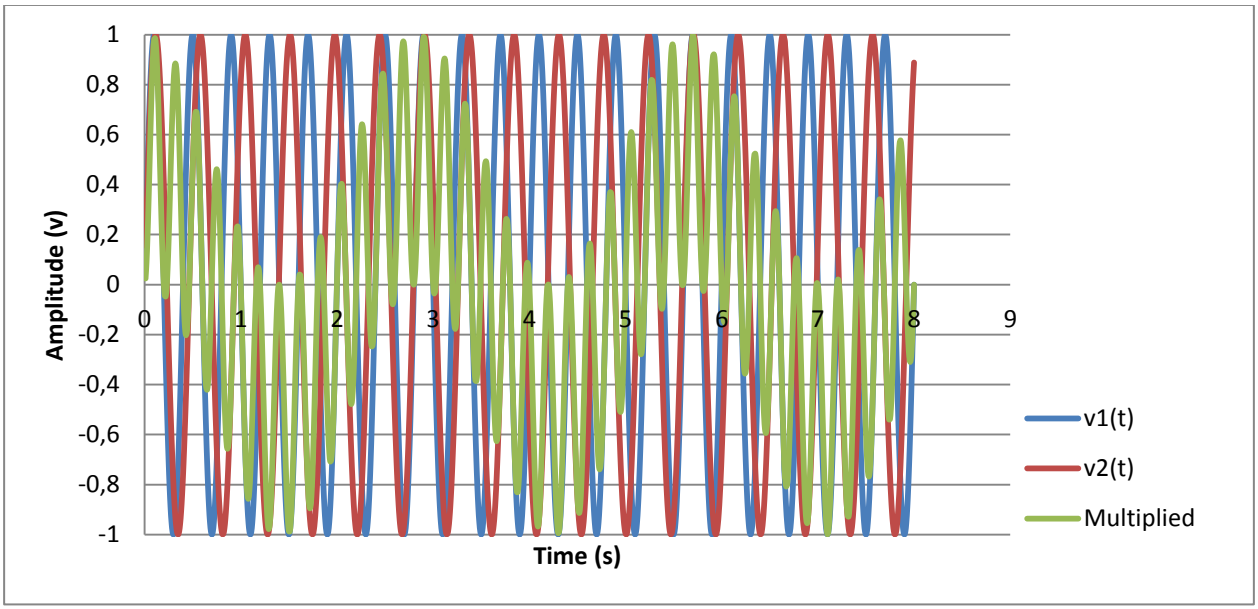

Figure 6.4. Multiplying correlator

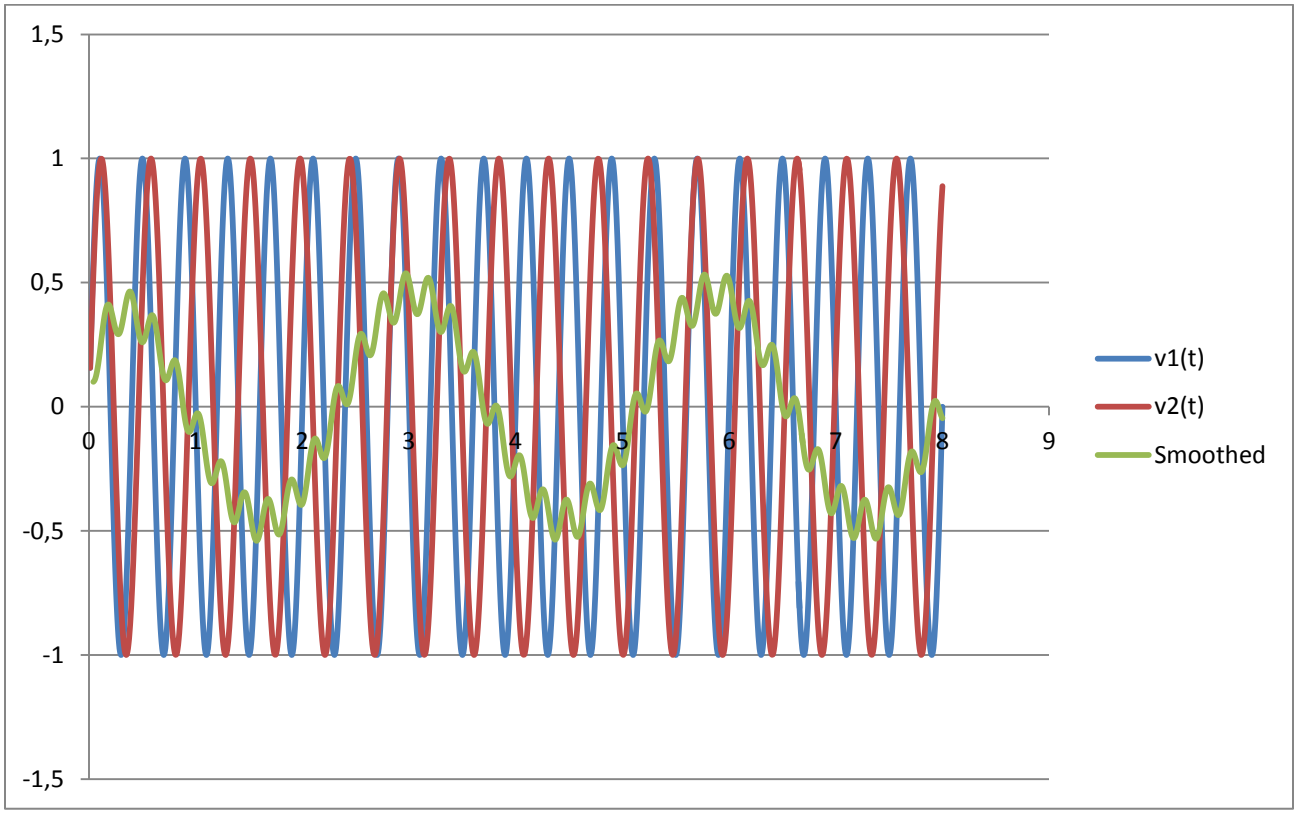

Figure 6.5. Input data and smoothed correlated signal

6.3. Multiplication and Low-Pass Filter Operations

The purpose of this section is to demonstrate that a two-way multiplying correlator can be implemented in Gnuradio-companion. Multiplication and low-pass filtering operations are investigated in Figure 6.6. Two signals of 4 KHz and 10 KHz were multiplied together using the Multiply block which can be found under the Operators menu in the GRC.

The Multiply component was set as shown in Figure 6.7. The IO data type was set to Float for simplicity. This implies that components connected to the multiplier block must also be of float data type. The number of inputs must correspond to the number of signals to multiply. In this case, the number of inputs was 2. By default the vector length was set to 1.

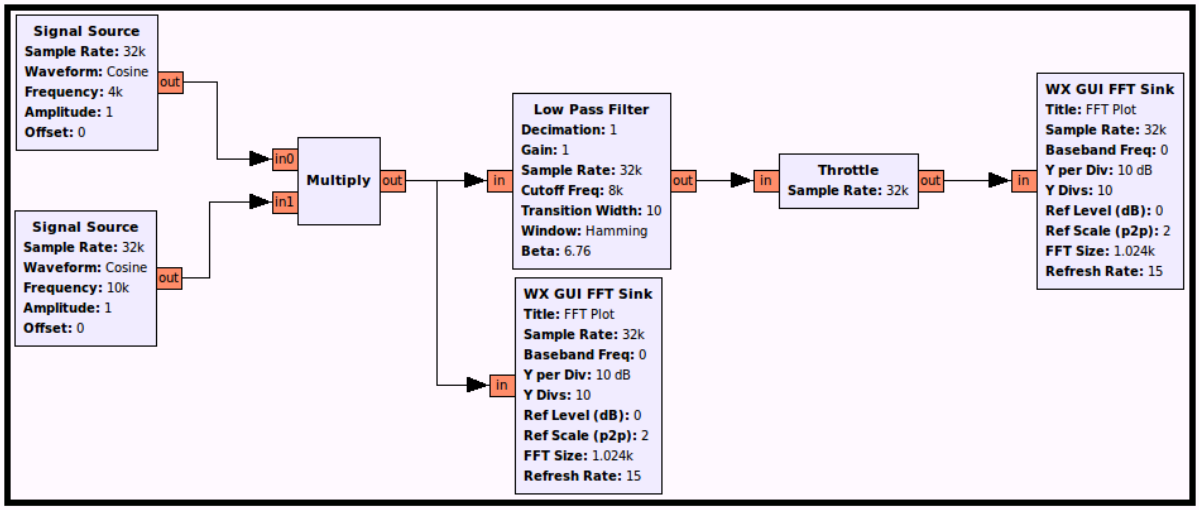

Figure 6.6. Multiplication and low-pass filter operations

The FFT Sink, with a 32 ksps sample rate, provides a spectrum span of 0-16 kHz (half the sample rate), which is wide enough to display both components (6 kHz and 14 kHz) which results from the multiplication. The FFT Sink data type was also set to Float. Figure 6.8 gives the multiplier output spectrum.

The LPF properties were set as shown in Figure 6.9. It can be seen that the data type (FIR Type) was set to float. The sample rate (samp_rate) was also controlled by the variable block. The cut-off frequency (8 kHz) was set to attenuate the 14 kHz component. The LPF operation is demonstrated in Figure 6.10 as the 14 kHz component was attenuated by a factor of 100 dB.

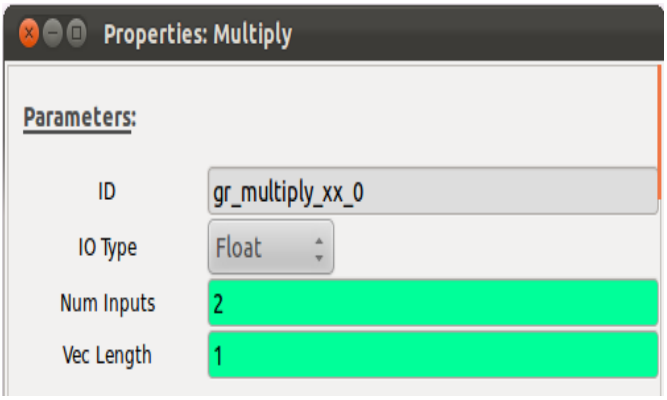

Figure 6.7. Multiply block properties

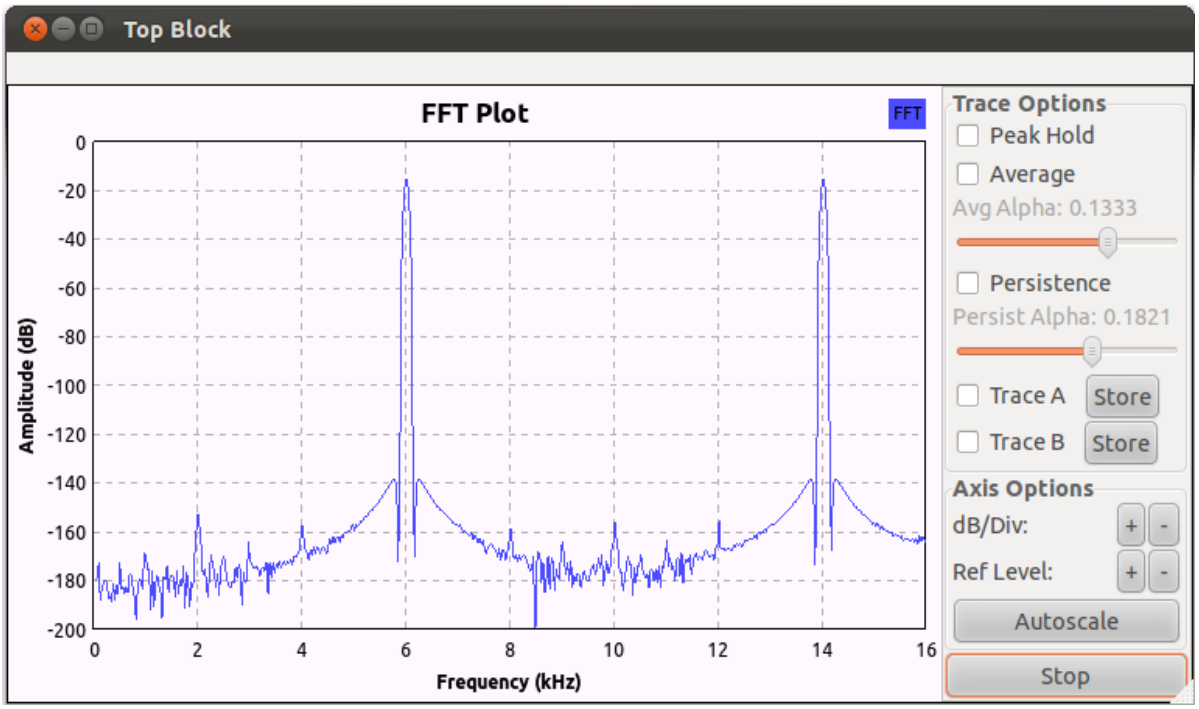

Figure 6.8. Spectrum of the multiplier output

6.4. Multiplying Correlator implemented with the USRP

Two external and independent signal generators were used to simulate the inputs to the correlator with USRP hardware. The signal frequency was 800 MHz produced from each generator. Being unlocked, the two generators provided signals of varying phase-shift. The USRP-2 was used for this experiment. The correlator flow graph is shown in Figure 6.11.

The USRP Source was set to provide a signal in complex data type in the form of $\cos\theta+j\sin\theta$. Two distinct File Sink blocks were inserted to record the raw data captured by the USRP at output 0 and output 1 respectively.

For two frequency-coherent signals, the multiplier output was expected to provide its lowest frequency component at 0 Hz. With that, the low-pass filter cut-off frequency can be set at 1 kHz as in Figure 6.11. The transition width of the LPF was set to 500. This value was optimized in

order to prevent the computer from overrunning and crashing the program. The Multiply Const block was inserted to amplify the correlated signal level for plotting purposes. Another File Sink was inserted to record the correlated signal.

Figure 6.9. Properties of the LPF

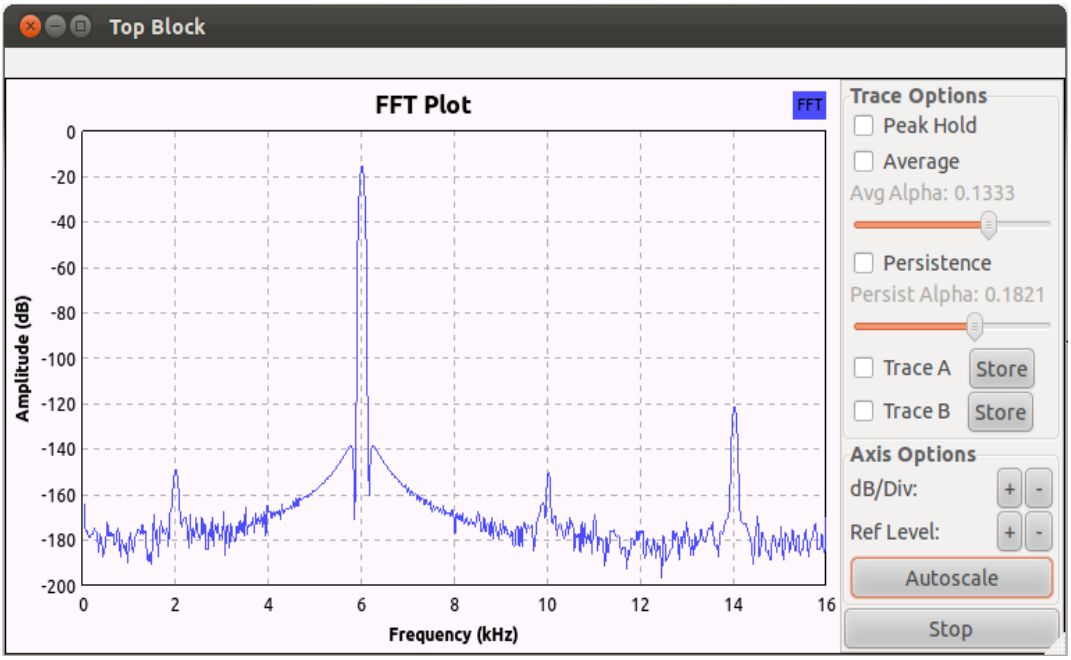

Figure 6.10. LPF output

A Scope Sink was used to monitor the correlated data in the time domain. In complex data format, the real (cosine) and imaginary (sine) components should be automatically plotted on the same set of axes. For simplicity of plotting, the correlated signal was converted to float data format. The raw signals as well as the correlated signal, in float data format, are plotted on the same set of axes in Figure 6.12. The high frequency sinusoids represent the raw data. The low frequency sinusoid is the simulated correlated output signal. It can be seen that the correlated data is a quasi-sinusoidal signal.

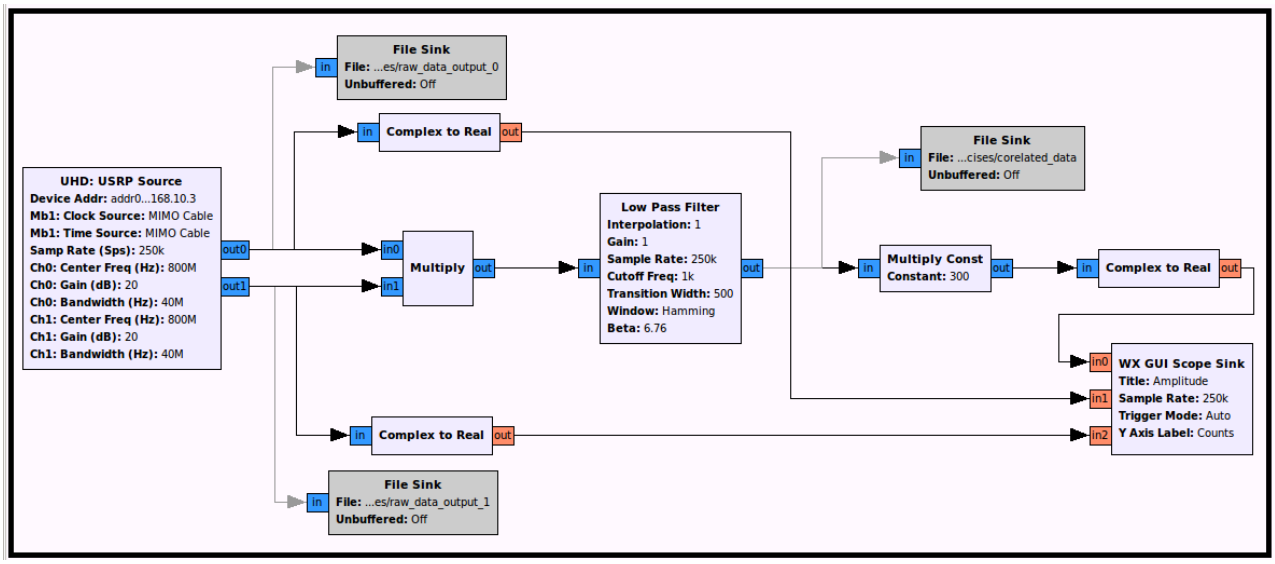

Figure 6.11. Correlator flow graph

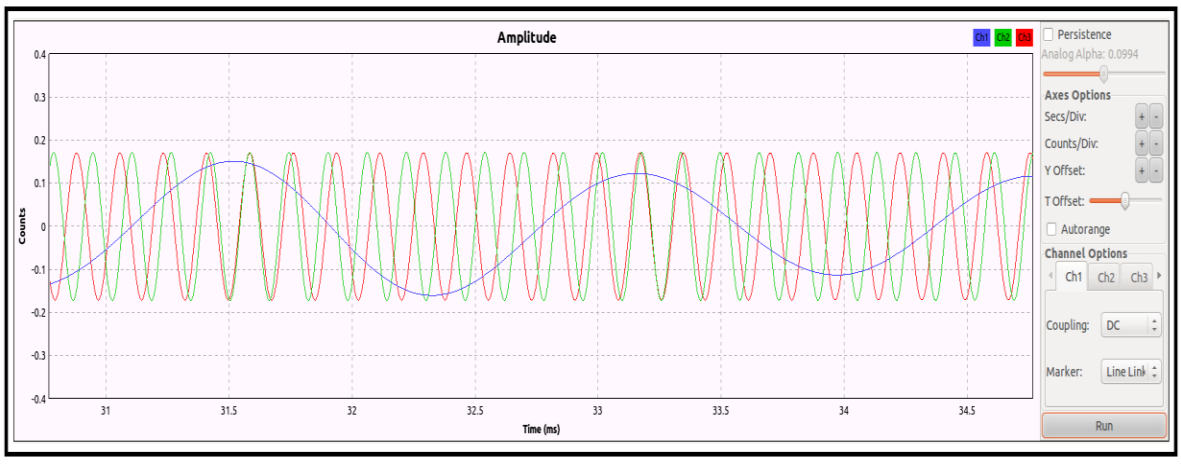

Figure 6.12. Raw data and correlated signal

Chapter 7: MITRA Station System Integration

7.1. Introduction

The purpose of this chapter is to discuss how the components were integrated in the signal chain going from the outdoor segment to the indoor segment. The results of the measurements conducted at various stages will be presented. The setup and performance of relevant components will be discussed. The outdoor and indoor segments were linked via fibre optic cable.

7.2. Single MITRA Antenna

A single LPDA antenna was set to detect RF signals within the operational band. A spectrum analyzer (Rhode & Schwarz FSH4) was used to monitor the received signal at the output of the antenna before the LPF. The North-South (NS) output of antenna 1 in the West array was monitored. The signal received is shown in Figure 7.1. It can be seen that the antenna was able to receive signals below and above the operational frequency band.

7.3. Front-End Low-Pass Filter

The LPF used was the Mini-Circuits VLF-800. The insertion loss of this LPF was measured as shown in Figure 7.2. It can be seen that the actual measured 3 dB cut-off frequency of this LPF is 1.035 GHz.

The LPF was connected to the output of the antenna. The RF signal level measured at the output of the LPF is shown in Figure 7.3. Two markers at 200 MHz and 800 MHz were used to locate the

operational band. This result demonstrates the action of the LPF in the Front-End as the signals above the cut-off frequency are attenuated.

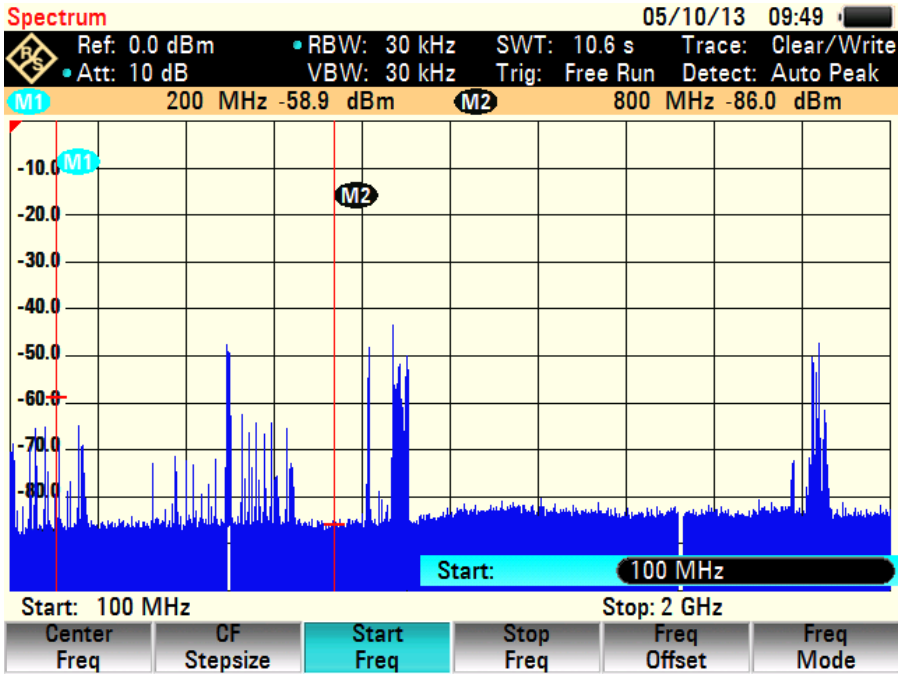

Figure 7.1. RF Signals received by a single LPDA

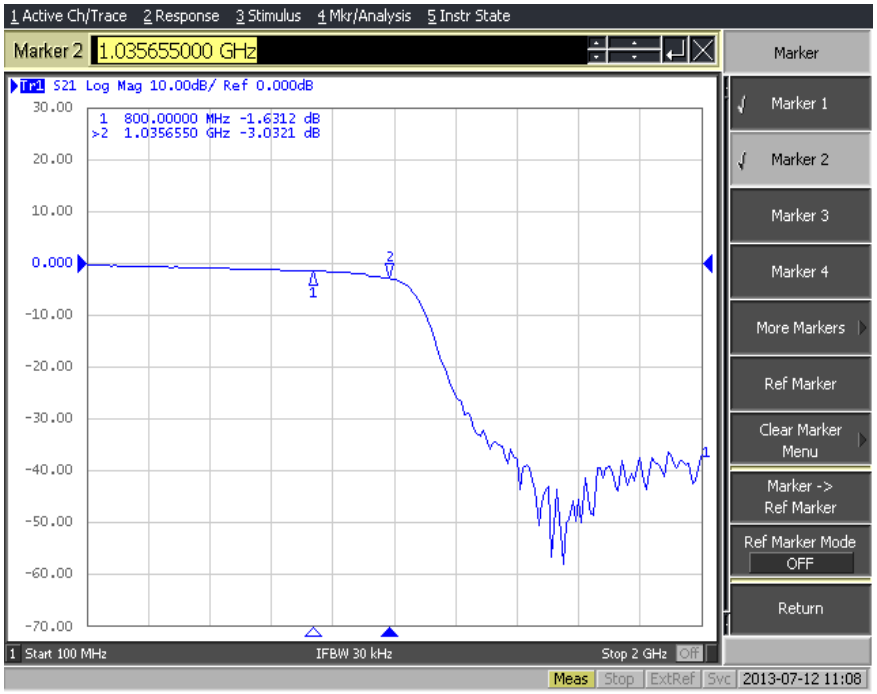

Figure 7.2. Insertion loss response of the LPF

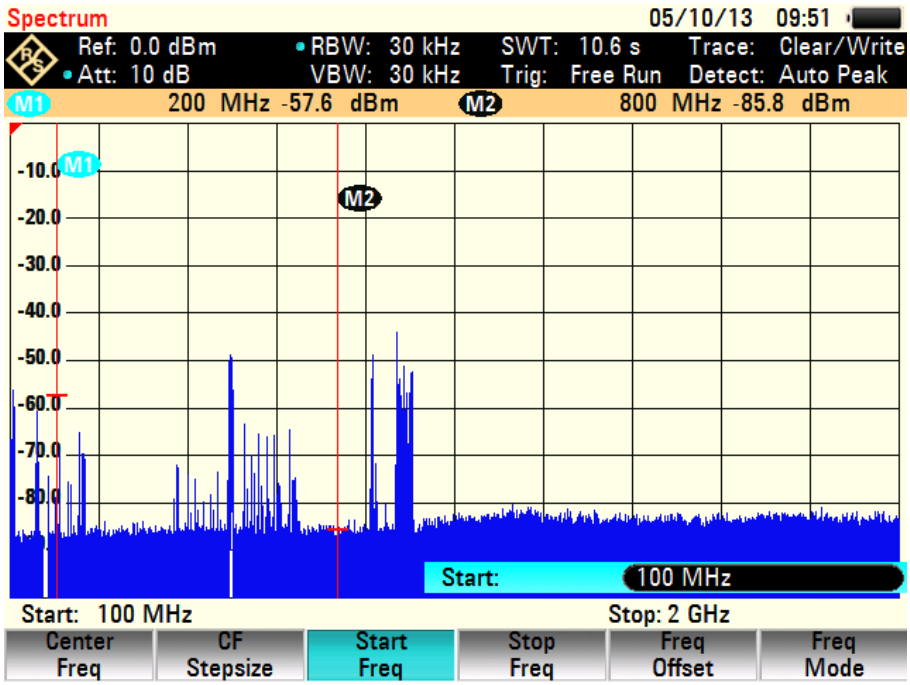

Figure 7.3. Spectrum result of the antenna and LPF cascade

7.4. Low-Noise Amplifier

The LNA used in the Front-End was the Mini-Circuits Zx60-33LN+. The gain response (S21) of this LNA was measured as shown in Figure 7.4. The average gain is approximately 20 dB between 200 MHz and 800 MHz.

The LNA was cascaded with the LPF to form a 2-port network. The measured result of this cascaded system is shown in Figure 7.5. At 800 MHz, the cascade system gives 17.831 dB of gain.

The antenna, LPF and LNA were cascaded. Figure 7.6 shows the spectrum of the signal detected across the operational frequency band. Due to the LNA amplification, the signal level is higher when compared to the spectrum in Figure 7.3 where the signal was measured at the output of the LPF.

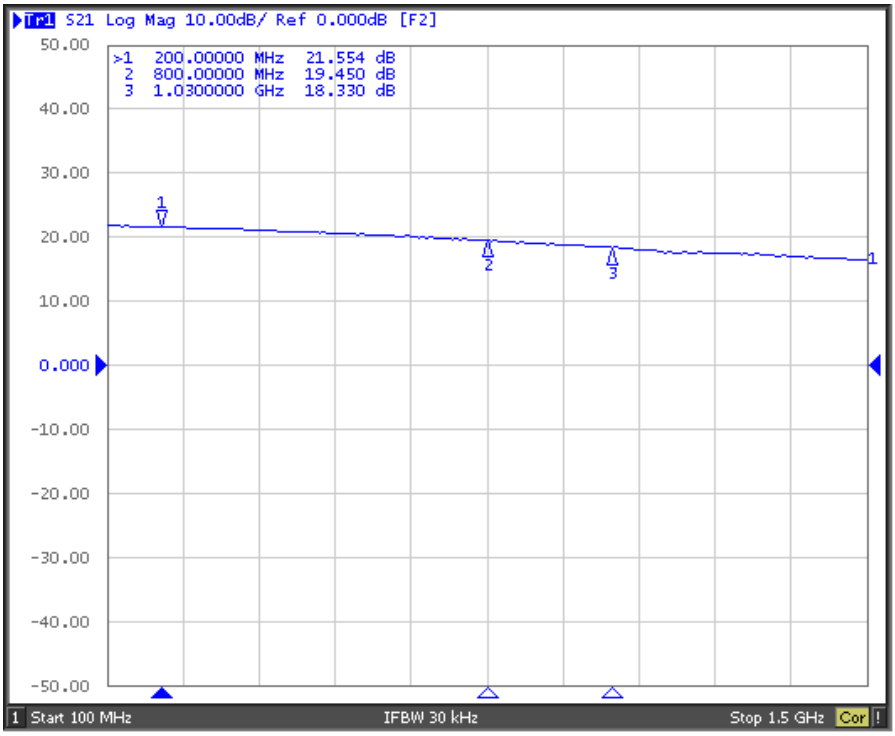

Figure 7.4. Gain response of the LNA

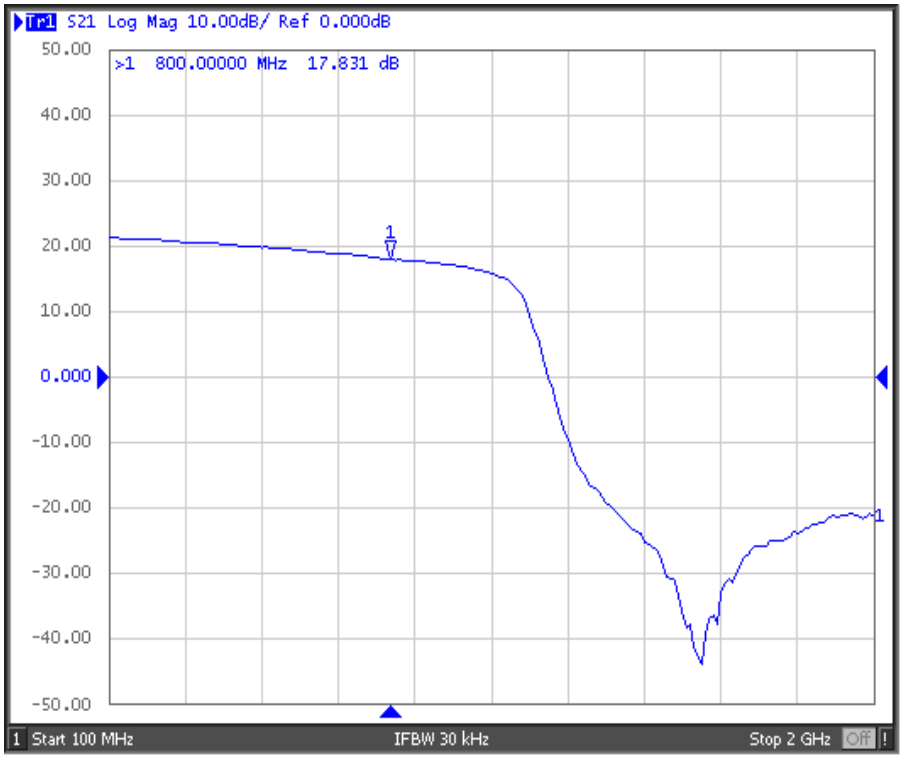

Figure 7.5. Response of the LPF and LNA cascade

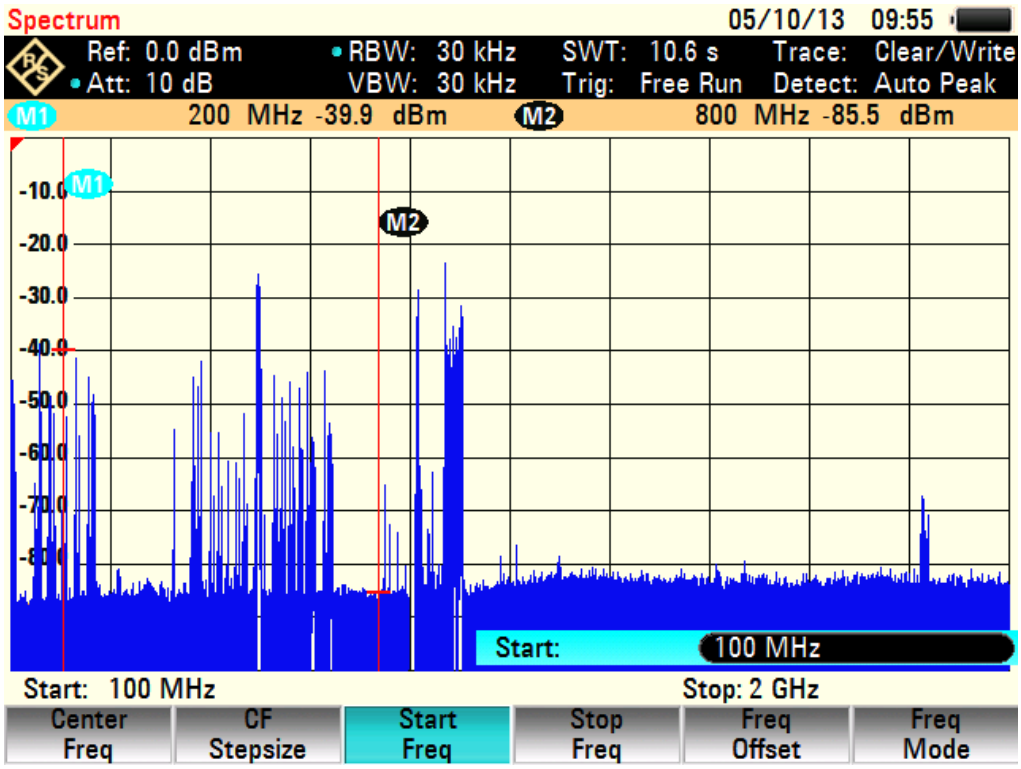

Figure 7.6. Spectrum of the cascade antenna, LPF and LNA

7.5. IF Stage Testing

A simplified diagram of the IF stage is shown in Figure 7.10. Spurious frequency suppression, harmonic rejection, and IF (800 MHz) selection by the band-pass filter (BPF) will be discussed. Measurements were performed at test point A (TP A) and test point B (TP B). The system was tested using an RF signal generator. The RF signal level was set to – 30 dBm. The system output was monitored using a spectrum analyzer. A low-noise RF signal generator (Rohde & Schwarz SMB-B103) was used to produce the LO signal. The LO was set to 7 dBm since the mixer was a level 7 mixer.

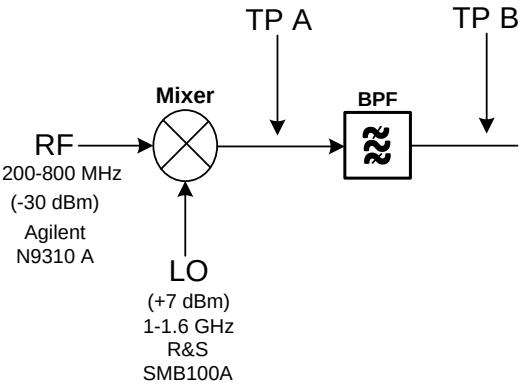

Figure 7.7. IF stage testing system

7.5.1. Mixer Testing

High-side injection was applied. Mixer operation is summarized in Equation 7.1, where F_{out} is the output frequency of the mixer. The IF frequency was calculated using Equation 7.2. The resulting image frequency (F_{im}) was calculated using Equation 7.3. Table 7.1 shows different signal frequencies from the LO and the incoming RF signal, and the corresponding image frequencies. A band-pass filter (BPF) was inserted after the mixer to select the IF. The datasheet of the BPF (Mini-Circuits VBFZ-780) is given in Annexure 14.

$$F_{out} = LO \pm RF \tag{7.1}$$

$$LO = RF + IF \tag{7.2}$$

$$F_{im} = RF + 2.IF \tag{7.3}$$

Overall, the Back-End stage consists of four mixers. All of them were tested under the same conditions and the results were similar. For Test 1, the output of the mixer at TP A is shown in Figure 7.11.

Table 7.1. Lookup Table of the IF stage Frequencies

Test	LO Freq (MHz)	RF Freq (MHz)	IF Freq (MHz)	Image Freq (MHz)
Test 1	1000	200	800	1800
Test 2	1100	300	800	1900
Test 3	1200	400	800	2000
Test 4	1300	500	800	2100
Test 5	1400	600	800	2200
Test6	1500	700	800	2300
Test 7	1600	800	800	2400

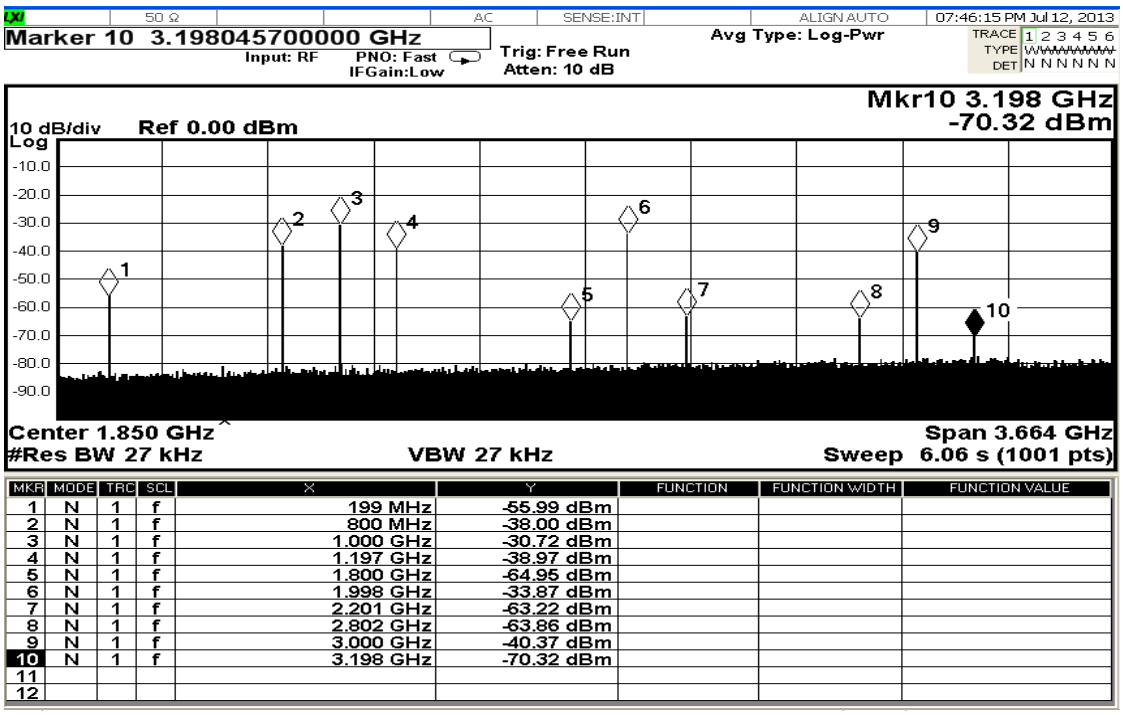

Figure 7.8. Mixer output (F_{out}) when LO = 1 GHz and RF = 200 MHz

- Marker 1: RF input (200 MHz) reproduced at the output of the mixer
- Marker 2: F_{out} calculated as $LO - RF$
- Marker 3: LO input (1000 MHz) reproduced at the output of the mixer
- Marker 4: F_{outt} calculated as $LO + RF$
- Marker 5: F_{im}

- Marker 6: 2nd harmonic of Marker 3
- Marker 7: harmonic calculated as (2x1000 MHz) + 200 MHz
- Marker 8: harmonic calculated as 2x[1000 MHz + (2x200 MHz)]
- Marker 9: 3rd harmonic of Marker 3.
- Marker 10: harmonic calculated as 2x[1000 MHz + (3x200 MHz)]

Further measurements were performed at TP A using the frequency values in Table 1. Results from test 2 to test 7 are respectively shown from Figure 7. 12 to Figure 7. 17.

7.5.2. Band-Pass Filter Testing

The insertion loss of the Band Pass Filter (BPF) is shown in Figure 7.18. The centre frequency of the BPF is measured at 861.1 MHz. The bandwidth of 468.5 MHz was calculated at -3 dB from the centre frequency. The BPF gives an insertion loss of 1.9 dB at 800 MHz.

Measurements were conducted at TP B in Figure 7.10 regarding the frequencies in Table 1. Results are shown from Figure 7. 19 to Figure 7. 25. The impact of the bandwidth of the BPF is visible. The bandwidth of 468.5 MHz is wide enough so that some harmonics will be found in the pass-band. However, these unwanted signals will be attenuated by the digital filter in the SBX daughter board.

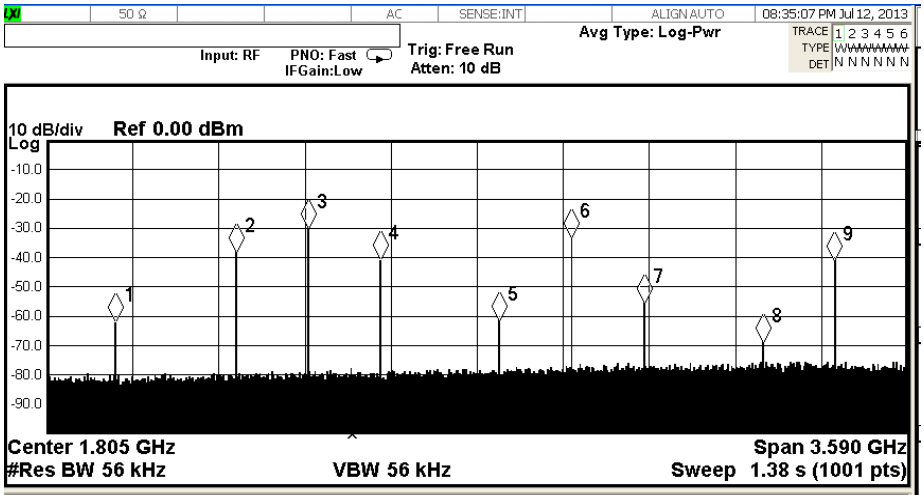

MKR	MODE	TRC	SCL	X	Y	FUNCTION	FUNCTION WIDTH	FUNCTION VALUE
1	N	1	f	298.24 MHz	-62.08 dBm			
2	N	1	f	800.37 MHz	-38.30 dBm			
3	N	1	f	1.102 74 GHz	-30.38 dBm			
4	N	1	f	1.401 98 GHz	-40.89 dBm			
5	N	1	f	1.898 91 GHz	-61.56 dBm			
6	N	1	f	2.199 61 GHz	-33.33 dBm			
7	N	1	f	2.501 90 GHz	-55.49 dBm			
8	N	1	f	2.996 61 GHz	-69.03 dBm			
9	N	1	f	3.297 04 GHz	-41.15 dBm			
10								
11								
12								

Figure 7.9. Mixer output when LO = 1.1 GHz and RF = 300 MHz

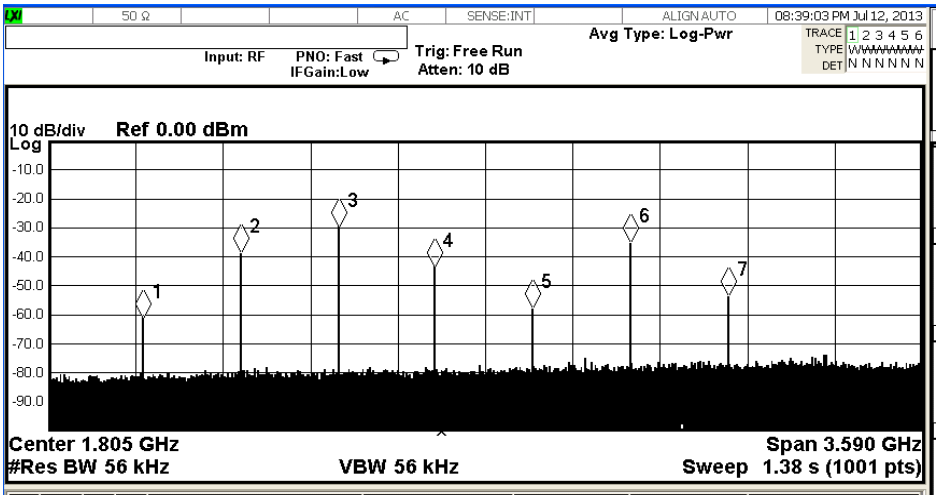

MKR	MODE	TRC	SCL	X	Y	FUNCTION	FUNCTION WIDTH	FUNCTION VALUE
1	N	1	f	398.76 MHz	-61.27 dBm			
2	N	1	f	800.37 MHz	-38.82 dBm			
3	N	1	f	1.203 26 GHz	-29.85 dBm			
4	N	1	f	1.595 84 GHz	-43.58 dBm			
5	N	1	f	1.999 43 GHz	-57.87 dBm			
6	N	1	f	2.400 65 GHz	-35.26 dBm			
7	N	1	f	2.803 46 GHz	-53.56 dBm			
8								
9								
10								
11								
12								

Figure 7.10. Mixer output when LO = 1.2 GHz and RF = 400 MHz

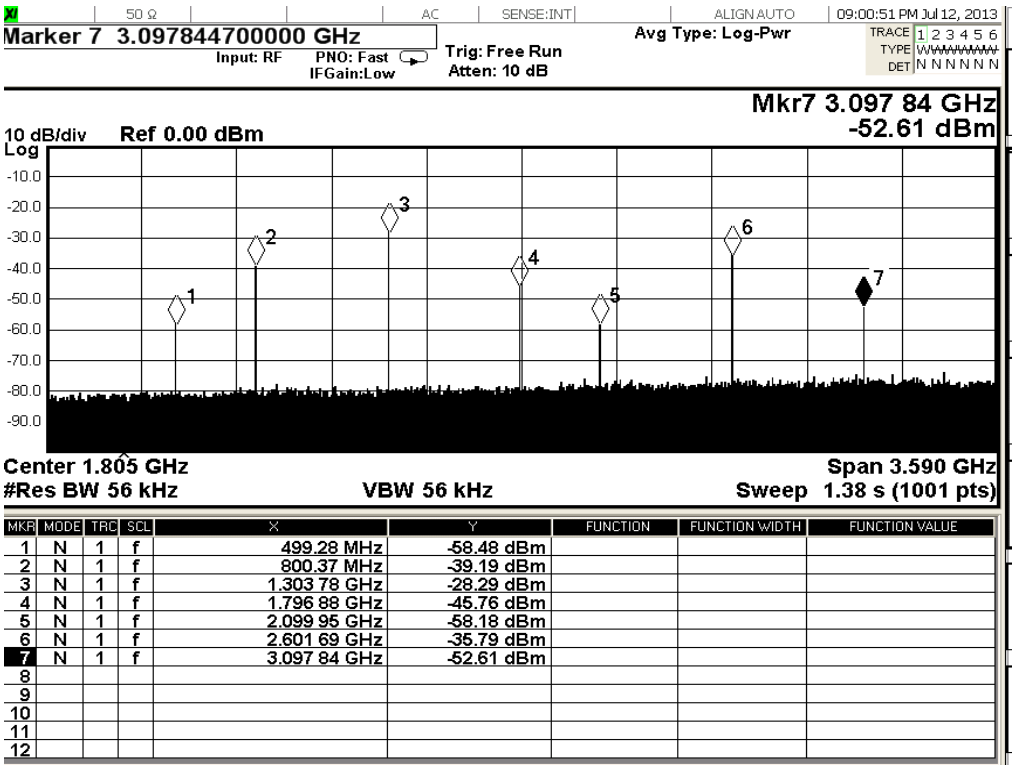

Figure 7.11. Mixer output when LO = 1.3 GHz and RF = 500 MHz

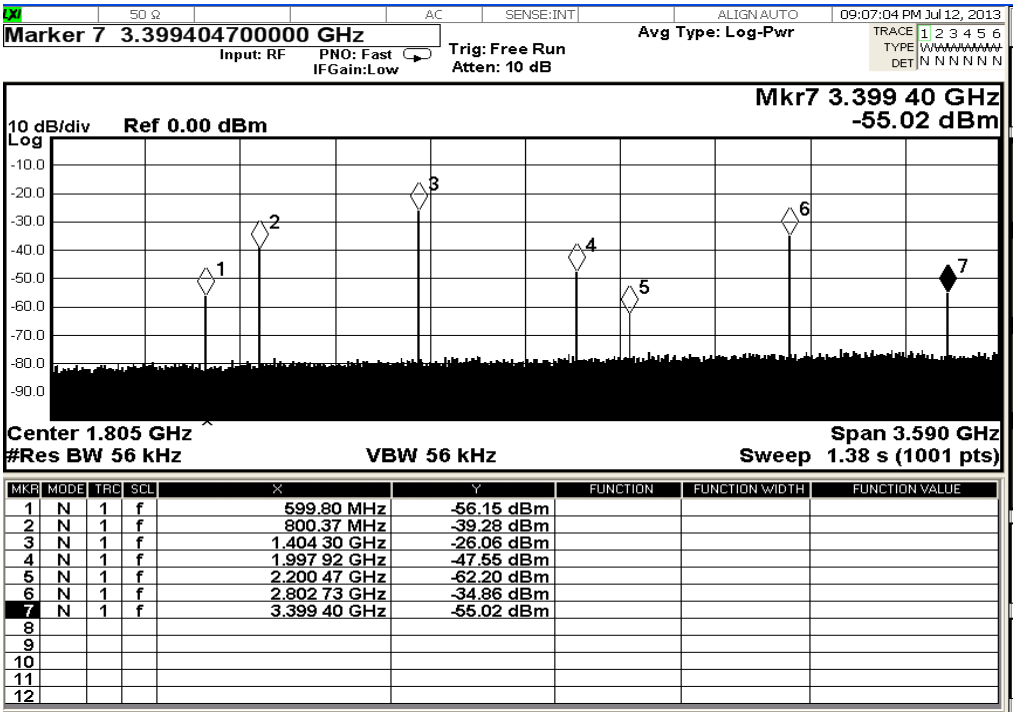

Figure 7.12. Mixer output when LO = 1.4 GHz and RF = 600 MHz

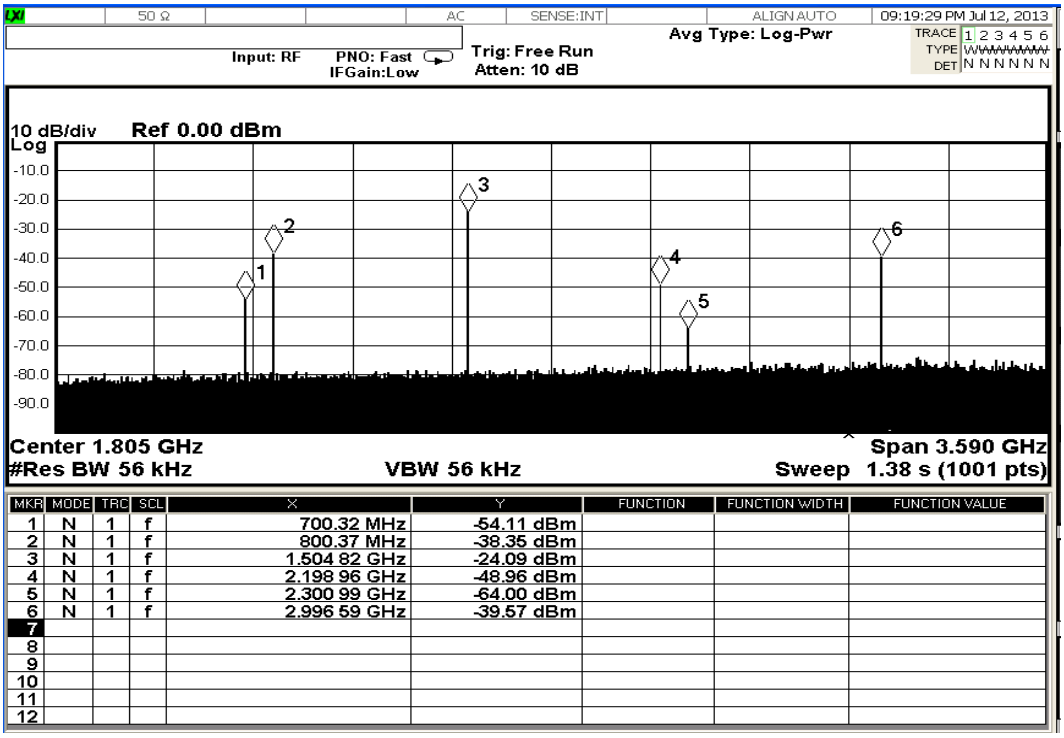

MKR	MODE	TRC	SCL	X	Y	FUNCTION	FUNCTION WIDTH	FUNCTION VALUE
1	N	1	f	700.32 MHz	-54.11 dBm			
2	N	1	f	800.37 MHz	-38.35 dBm			
3	N	1	f	1.504 82 GHz	-24.09 dBm			
4	N	1	f	2.198 96 GHz	-48.96 dBm			
5	N	1	f	2.300 99 GHz	-64.00 dBm			
6	N	1	f	2.996 59 GHz	-39.57 dBm			
7								
8								
9								
10								
11								
12								

Figure 7.13. Mixer output when LO = 1.5 GHz and RF = 700 MHz

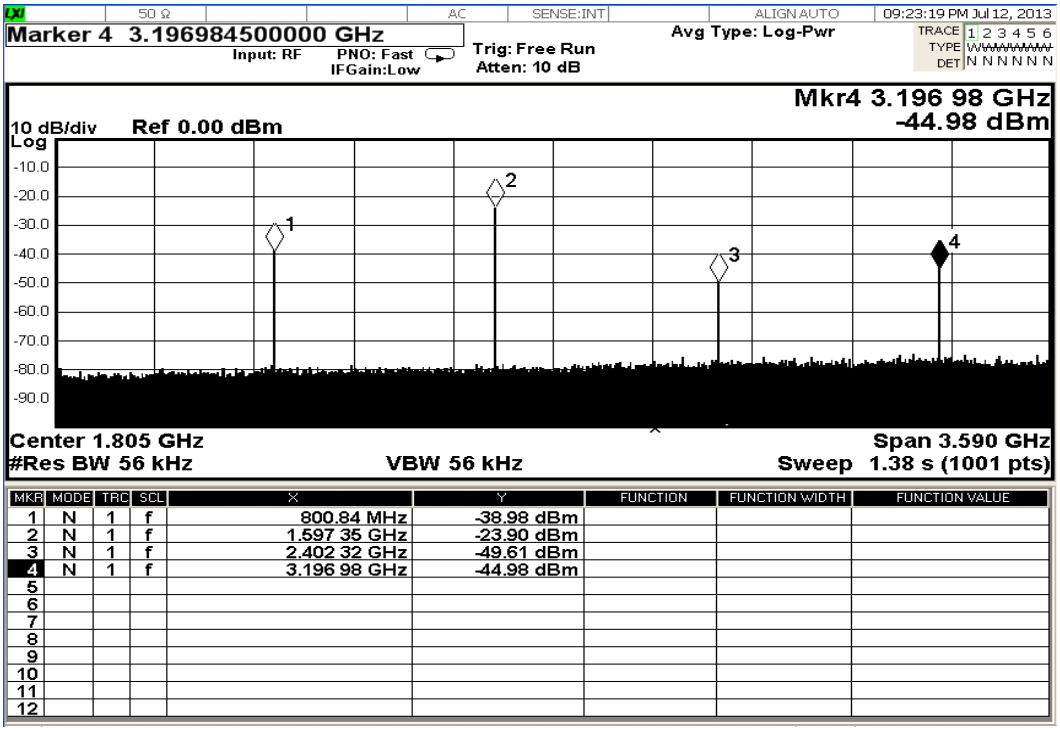

MKR	MODE	TRC	SCL	X	Y	FUNCTION	FUNCTION WIDTH	FUNCTION VALUE
1	N	1	f	800.84 MHz	-38.98 dBm			
2	N	1	f	1.597 35 GHz	-23.90 dBm			
3	N	1	f	2.402 32 GHz	-49.61 dBm			
4	N	1	f	3.196 98 GHz	-44.98 dBm			
5								
6								
7								
8								
9								
10								
11								
12								

Figure 7.14. Mixer output when LO = 1.6 GHz and RF = 800 MHz

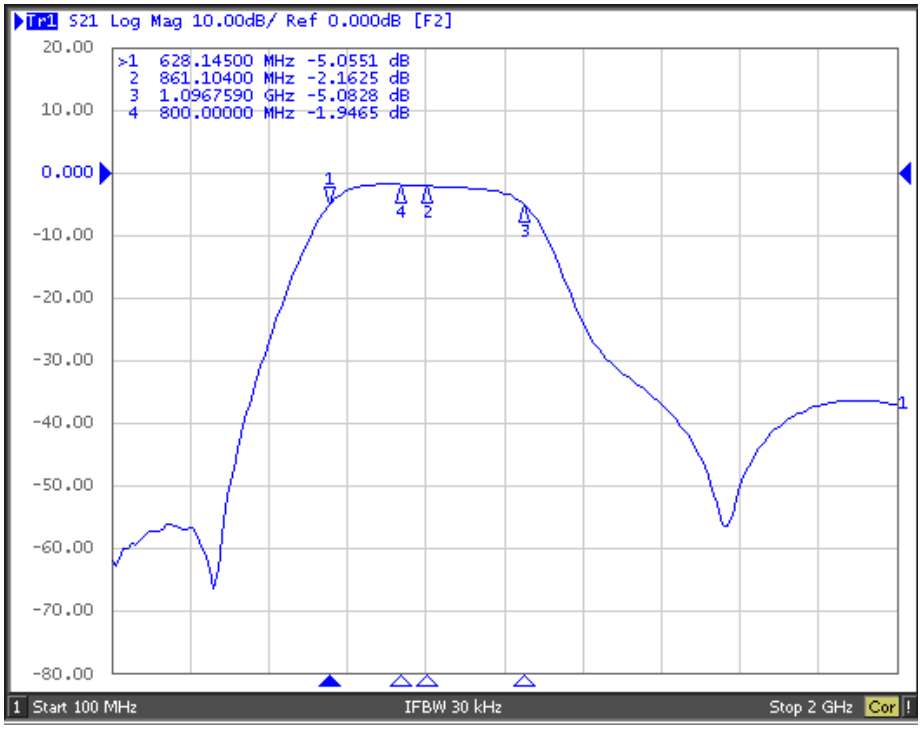

Figure 7.15. Insertion loss the BPF

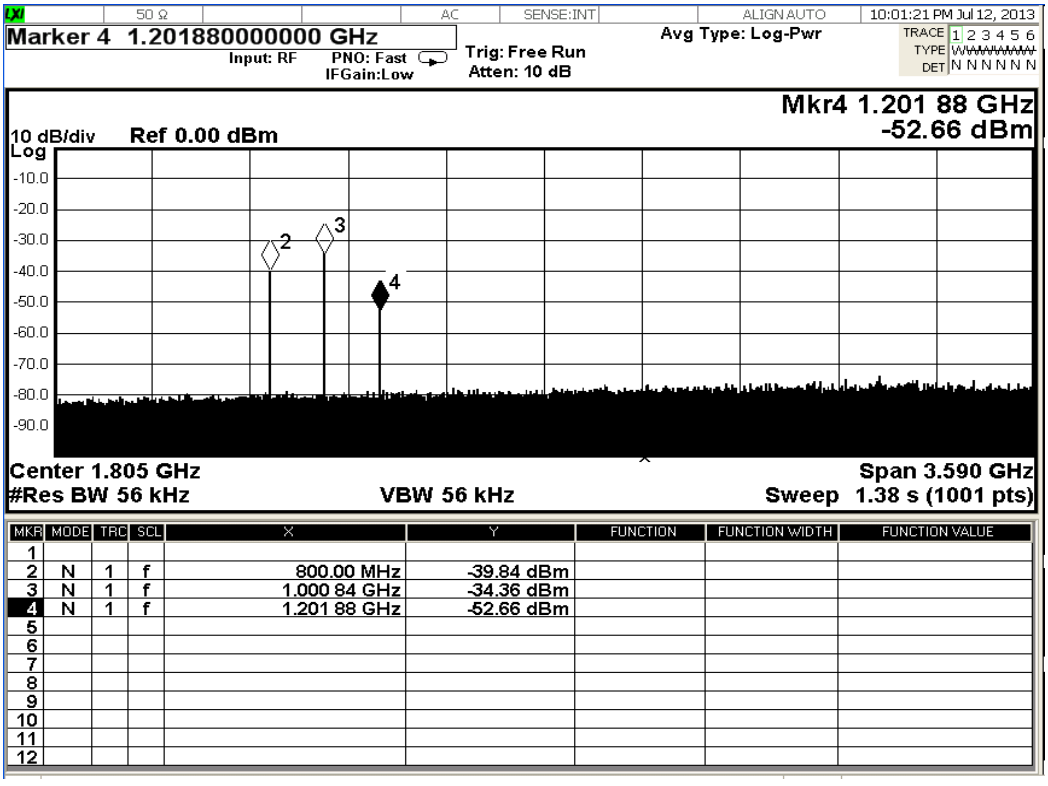

Figure 7.16. BPF output when LO = 1 GHz and RF = 200 MHz

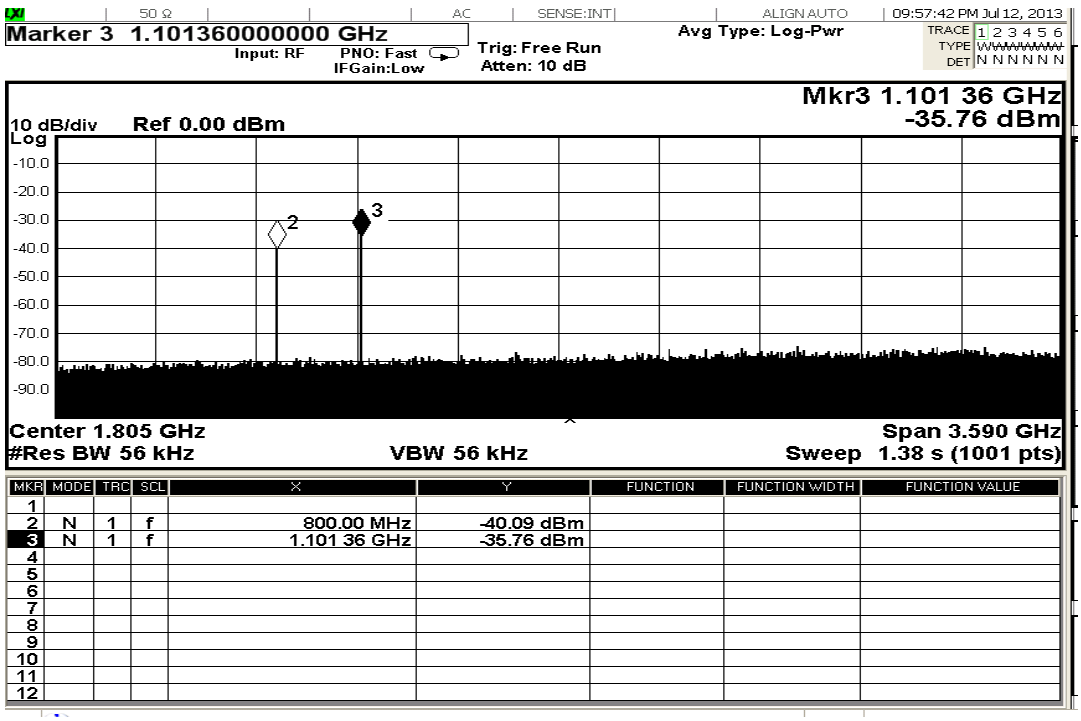

Figure 7.17. BPF output when LO = 1.1 GHz and RF = 300 MHz

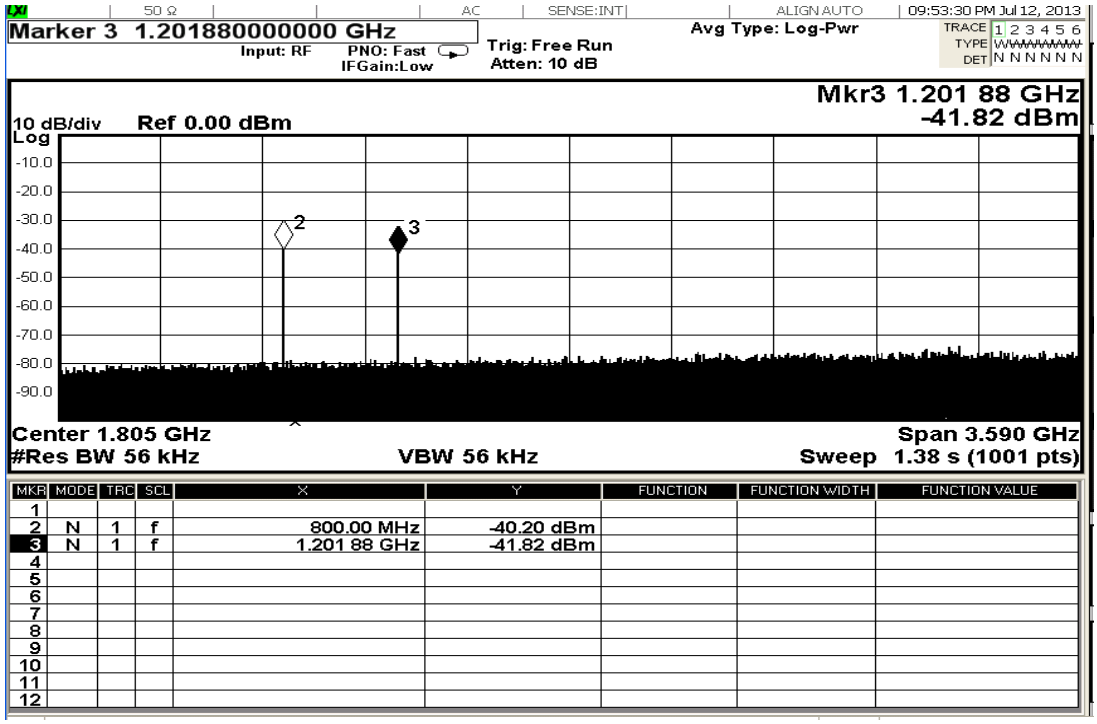

Figure 7.18. BPF output when LO = 1.2 GHz and RF = 400 MHz

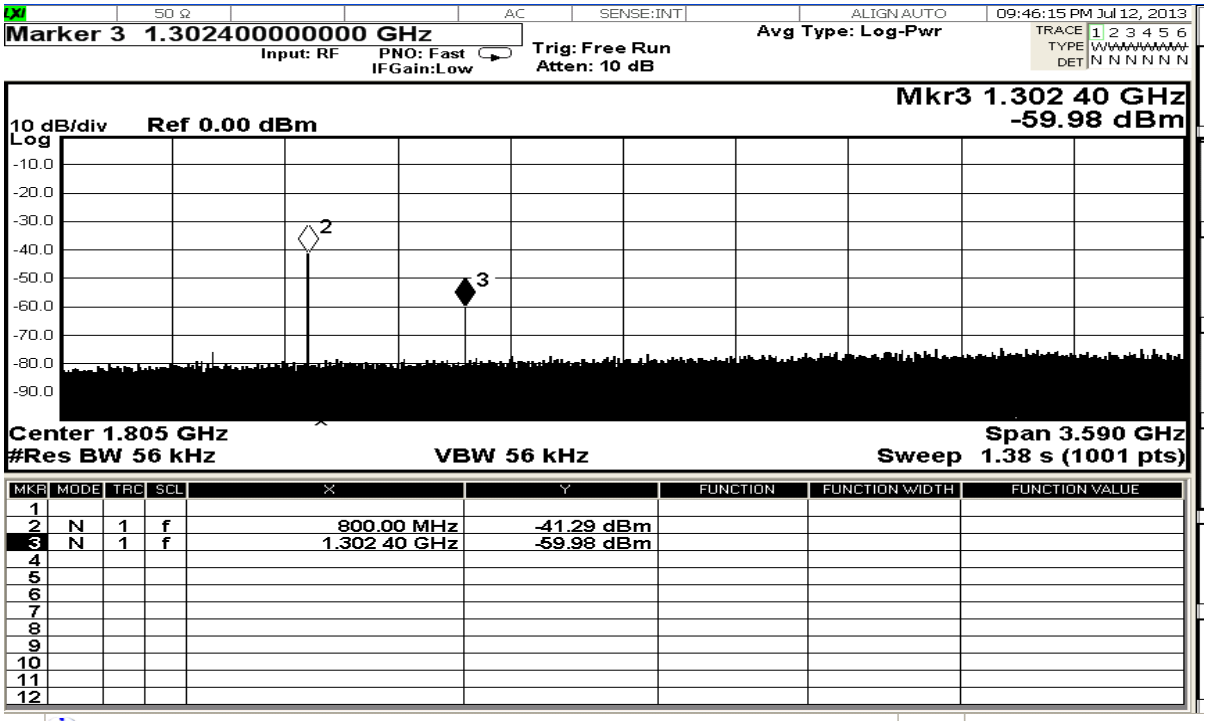

Figure 7.19. BPF output when LO = 1.3 GHz and RF = 500 MHz

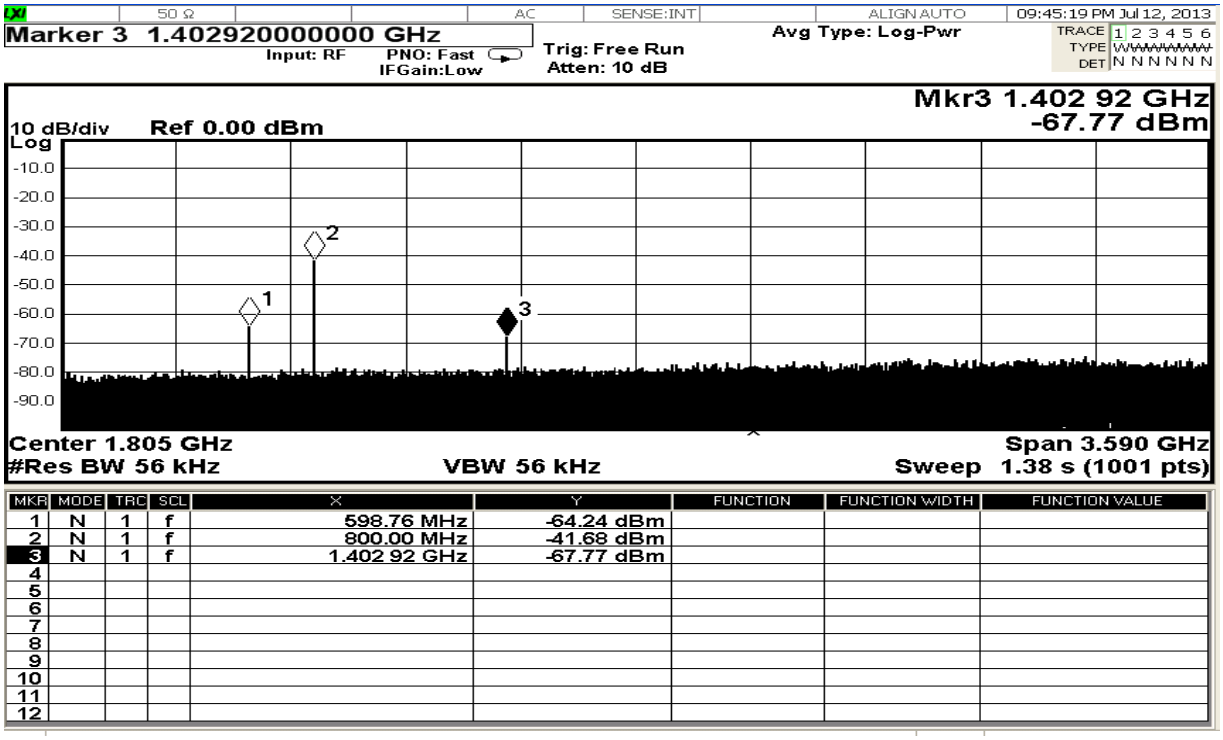

Figure 7.20. BPF output when LO = 1.4 GHz and RF = 600 MHz

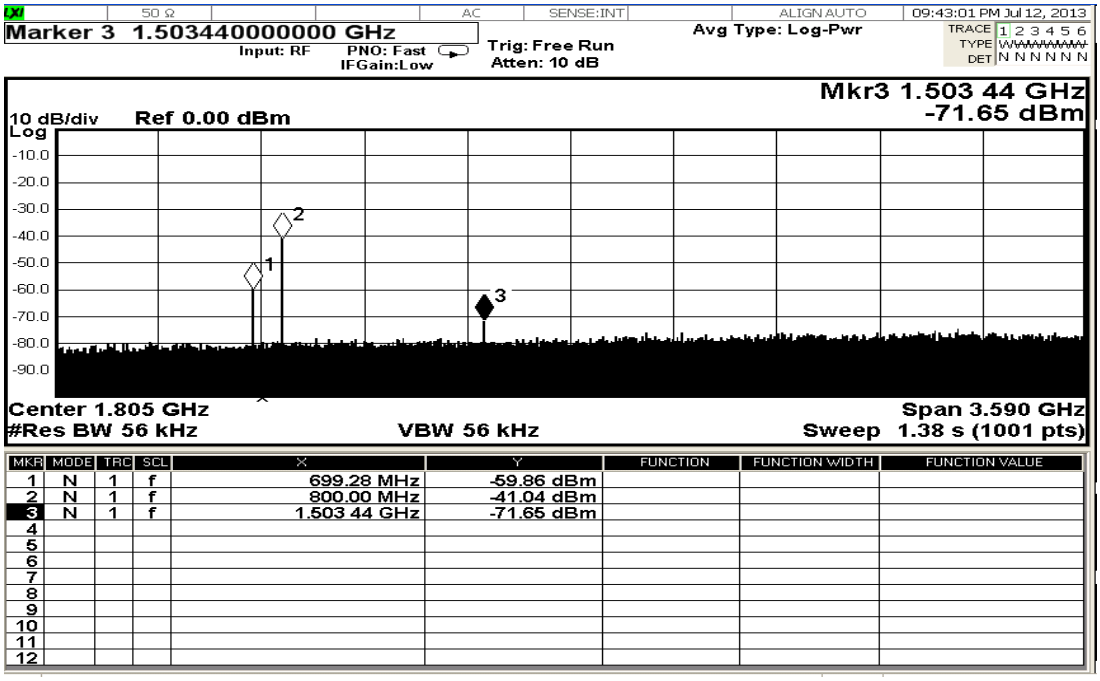

Figure 7.21. BPF output when LO = 1.5 GHz and RF = 700 MHz

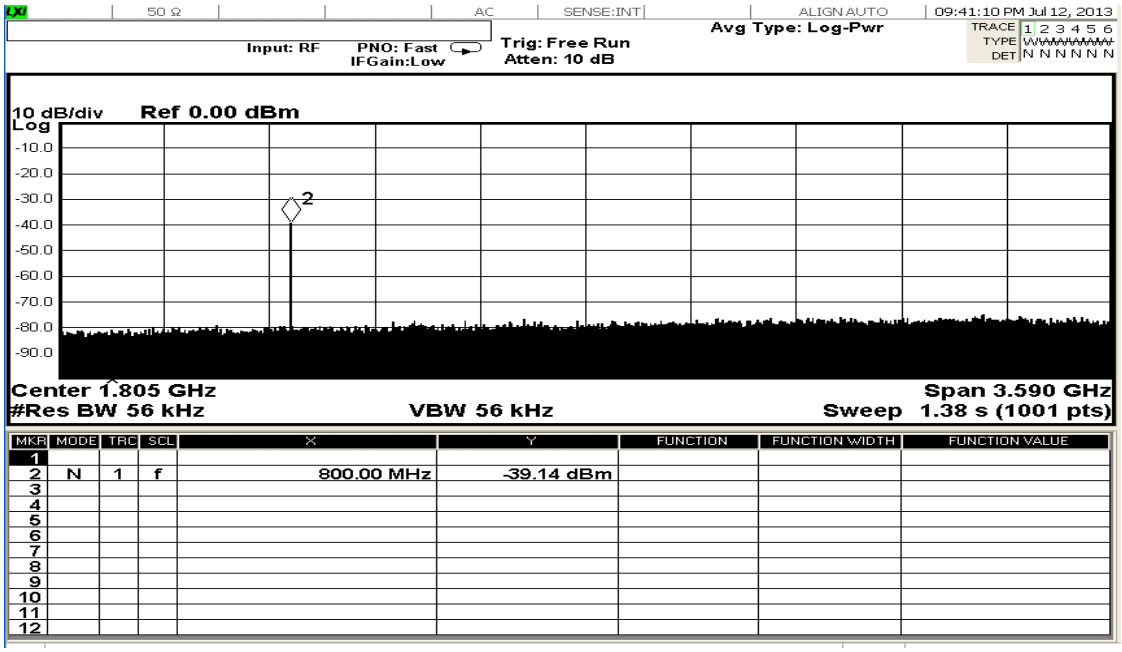

Figure 7.22. BPF output when LO = 1.6 GHz and RF = 800 MHz

The general conclusion is that the IF system operated correctly and unwanted signals were attenuated sufficiently.

7.5.3. Splitter Testing

As shown in Figure4.1, the IF stage consists of four mixers. The LO was produced by an RF signal generator (R&S SMB 100A). The output of the signal generator is split using a 4-way signal splitter (ZC4PD-18-S+) to distribute the LO to the four mixers. The datasheet of this splitter is given in Annexure 15. The output of the splitter was monitored using a spectrum analyzer. The signal level was expected to decrease after the splitter by 3 dB after every split. The input LO level to the mixers must be +7 dBm. It was essential to determine the power of the signal delivered by the signal generator to keep the mixer LO inputs at +7 dBm. A test was conducted between 1000 MHz and 1600 MHz and the results are presented in Table 7.3. The results of the test indicate that the signal generator should provide the LO at an amplitude of +14 dBm.

Table 7.2. Splitter Input and Output

Freq (MHz)	Splitter input (dBm)	Splitter output (dBm)
1000	13.78	7
1100	13.78	7
1200	13.47	7
1300	13.86	7
1400	14.59	7
1500	15	7
1600	15	7

7.6. System Bandwidth Test

The system bandwidth was tested at 202 MHz as no prominent RFI was observed at this frequency as shown in Figure 7.26. A 2-way splitter was connected to the output of the IF stage. The 2 outputs of the splitter were connected to a spectrum analyser and to the USRP respectively. This setup is shown in Figure 7.27. The response from the spectrum analyser is shown in Figure 7.28. The span (10 MHz) of the spectrum analyser was used to indicate the

receiver bandwidth. Figure 7.29 shows the GRC for this exercise. The span of the USRP spectrum is controlled from the variable called ''Samp Rate (Sps)''. The variable ''Bandwidth (Hz)'' controls the resolution bandwidth of the GRC spectrum. This was set to 100 kHz. The maximum span set for the USRP system was also set to 10 MHz. It was found that the USRP system and the performance of the computer used in the Back-End could not handle spans above 10 MHz. Figure 7.30 shows the spectrum of the signal from the USRP. It can be seen that the responses from the spectrum analyser and the GRC (FFT Sink) are similar. With that, a span of 10 MHz was obtained when using the GRC flow graph shown in Figure 7.29.

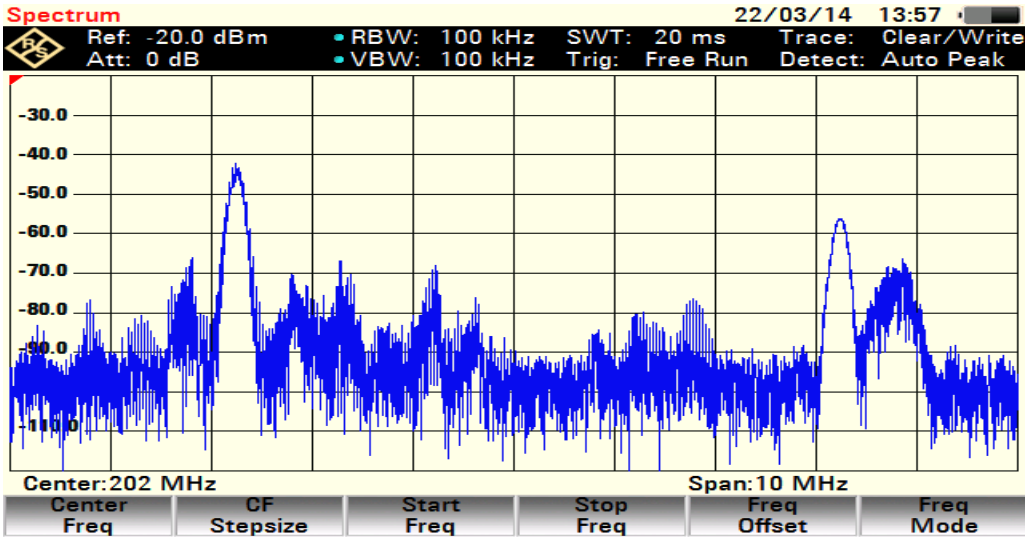

Figure 7.23. RFI at the centre frequency 202 MHz

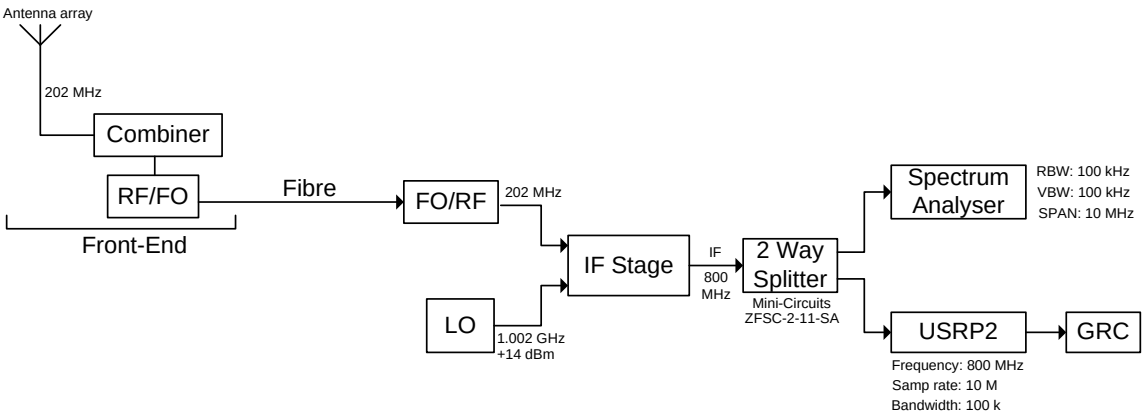

Figure 7.24. Setup for bandwidth testing

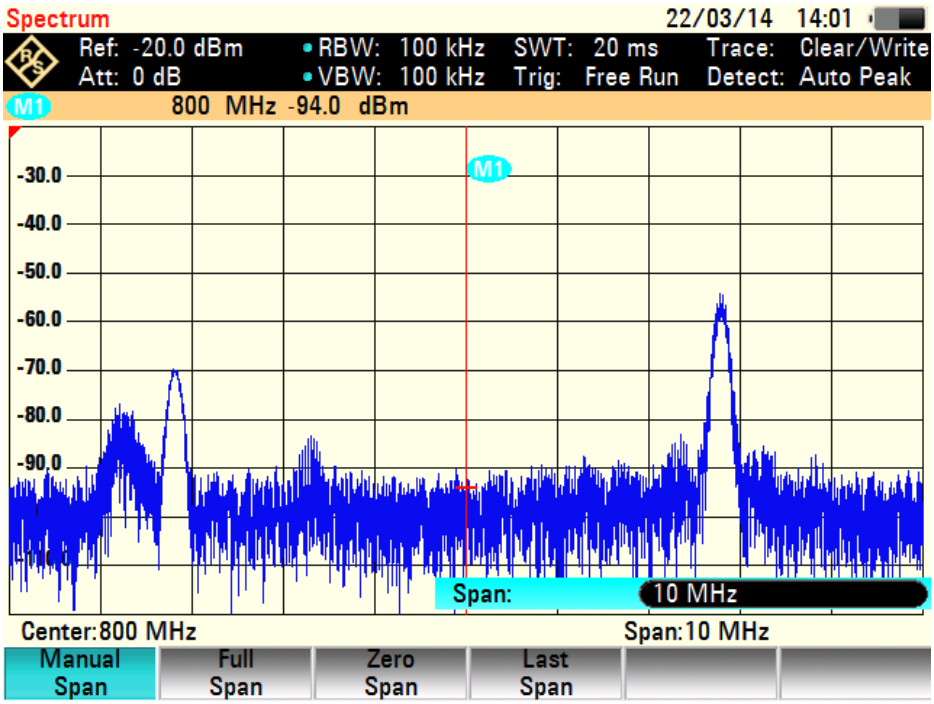

Figure 7.25. Spectrum analyzer response for system bandwidth measurement

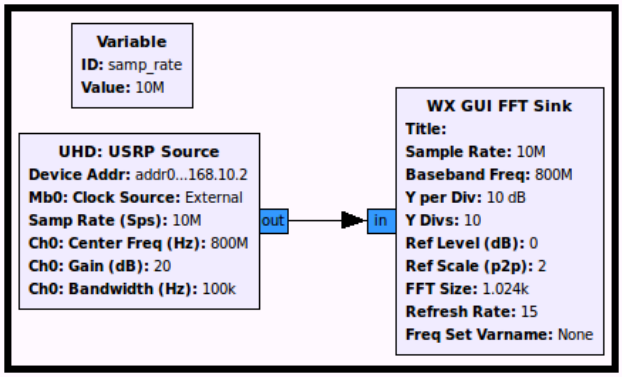

Figure 7.26. GRC setup for system bandwidth-measurement

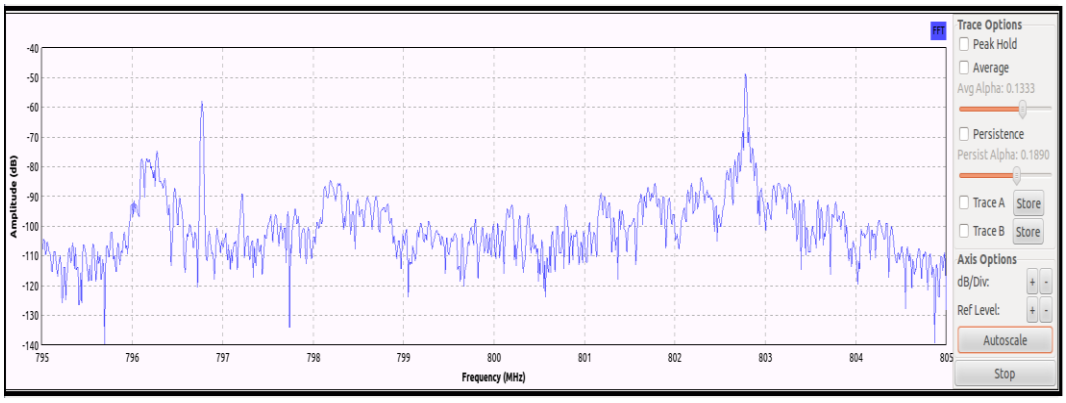

Figure 7.27.GRC (FFT Sink) response for system bandwidth measurement

7.7. Table of Hardware Components

Table 7.3 shows a detailed list of hardware components used in the development of this project.

Table 7.3. Table of Hardware Components

	Designation	Part number	Manufacturer	Quantity
1	Dual-polarized LPDA	N/A	Constructed	16
2	Low-Pass Filter	VLF-800	Mini-Circuits®	32
3	Low-Noise Amplifier	Zx60-33LN+	Mini-Circuits®	32
4	8-way Power Combiner	ZFSC-8-43+	Mini-Circuits®	4
5	RF-to-Fibre Converter	RFoF-2G	Conical RF Optic	4
6	Fibre-to-RF Converter	RFoF-2G	Conical RF Optic	4
7	Mixer	Zx05-11x	Mini-Circuits®	4
8	Band-Pass Filter	VBFZ-780	Mini-Circuits®	4
9	USRP (Mother board)	USRP2/N200/N210	Ettus Research™	4
10	USRP (Daughter board)	SBX	Ettus Research™	4
11	MIMO cable	783076-01	Ettus Research™	2
12	Ethernet Gigabit switch	N/A	N/A	1
13	Frequency-Time Standard	GPS 10 RBN	Precision Test Systems	1
14	5-way Splitter	ZFSC-5-1	Mini-Circuits®	1
15	RF Signal Generator	SMB-B103	Rohde & Schwarz	1
16	4-way Splitter	ZC4PD-18	Mini-Circuits®	1
17	RF Coaxial Cable	LMR-195	N/A	96 m
18	RF Coaxial Cable	RG-58	N/A	320 m
19	Fibre Optic Cable	DTC-9-02VT/V/V	Teldor Cables	100 m

Chapter 8: MITRA Radio Telescope: Proof of Concept

8.1. Introduction

The purpose of this chapter is to prove the concept behind the MITRA project. Two tests were conducted: a walk-by test and a sensitivity comparison test.

In an urban environment, the Radio Frequency Interference (RFI) signals are strong enough to dominate the noise coming from astronomical sources. The RFI was monitored before running the test. This exercise was conducted in order to identify the RFI relatively free portions of the band where radio astronomy observations could be performed.

8.2. RFI Measurement

The North-South (NS) outputs from the West array were used for this experiment. The RFI signals were measured between 200 MHz and 800 MHz in steps of 100 MHz. The results are shown from Figure 8.1 to Figure 8.6. It can be seen that the level of RFI and noise floor are extremely high between 200 MHz and 800 MHz. This makes this location (DUT) to be not suitable for radio astronomy observation between 200 MHz and 800 MHz. However some RFI free frequencies such as 280 MHz, 335 MHz, 433 MHz, and 490 MHz were identified for MITRA system testing.

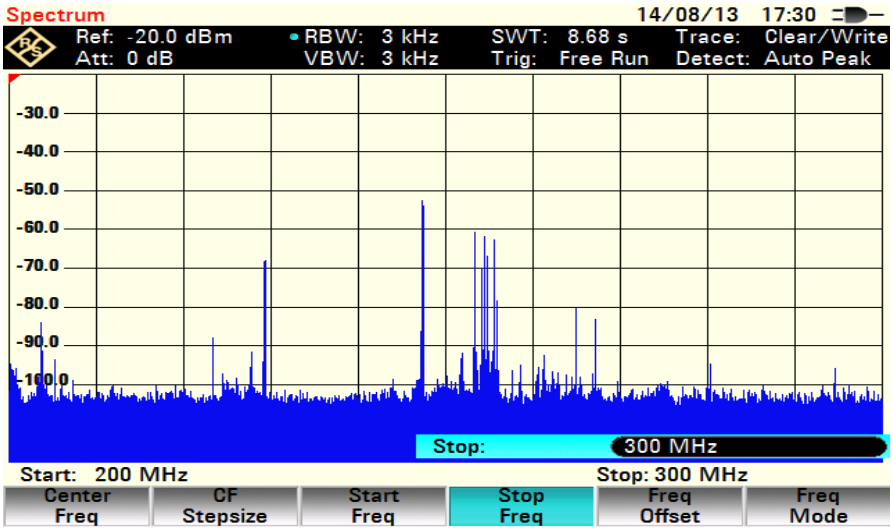

Figure 8.1. RFI between 200 MHzand 300 MHz

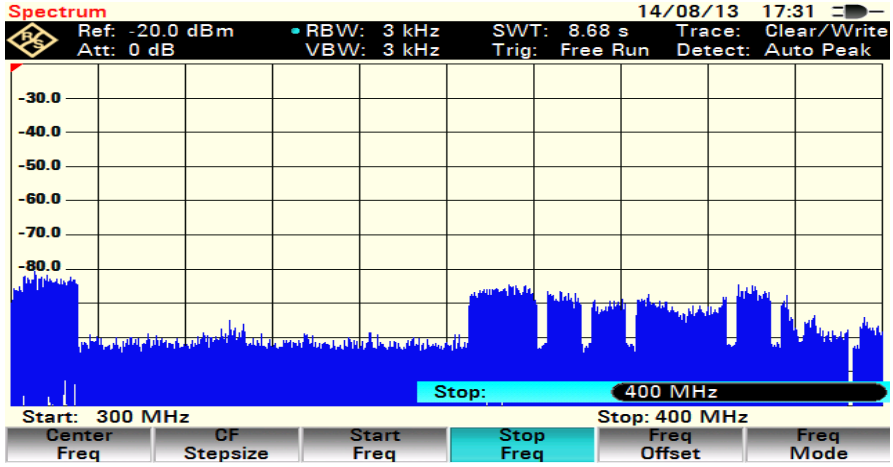

Figure 8.2. RFI between 300 MHz and 400 MHz

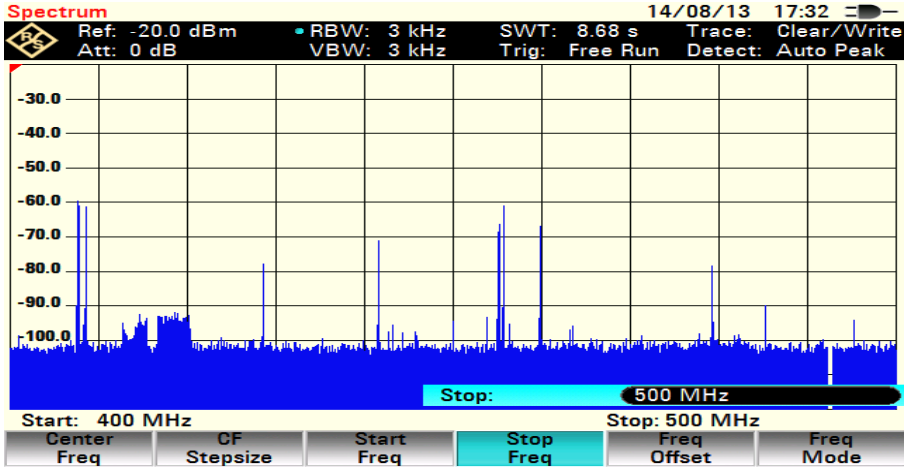

Figure 8.3. RFI between 400 MHz and 500 MHz

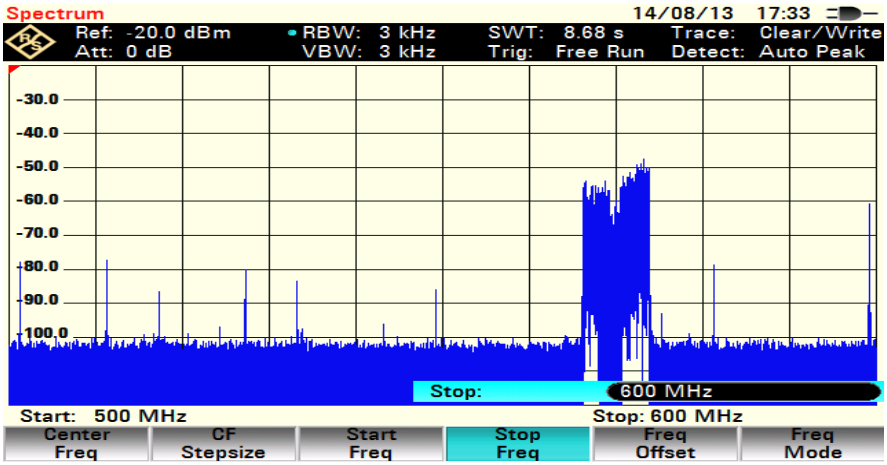

Figure 8.4. RFI between 500 MHz and 600 MHz

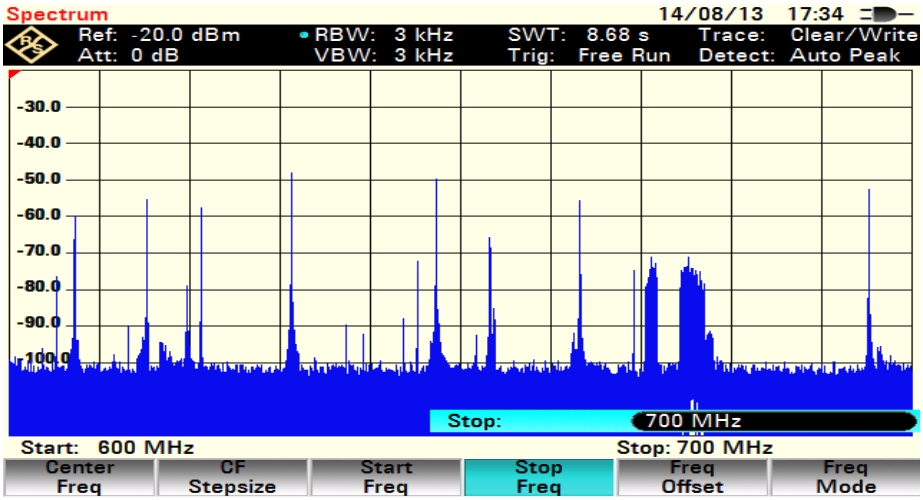

Figure 8.5. RFI between 600 and 700 MHz

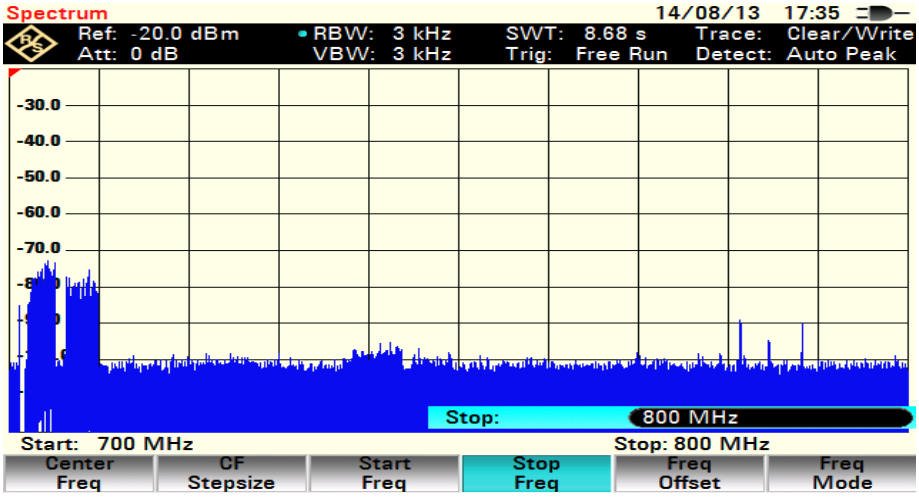

Figure 8.6. RFI between 700 MHzand 800 MHz.

8.3. Walk-By Tests

For this test, an RF signal generator was used to simulate an astronomical source. A dipole antenna was connected to the output of the RF signal generator in order to radiate RF waves toward the MITRA arrays. An operator was tasked to walk with the dipole antenna from east to west and back from west to east. The operator was 5 m away from the antenna arrays. The walking speed was approximately 1 metre per second. The test was performed with the following setup:

- Source: RF signal generator.
- Frequencies: 280 MHz and 335 MHz.
- System sample rate: 250 ksps.
- Data recorded: 250 ksps.
- Front-End feed lines: EW-E and EW-W.
- Back-End LO: 1080 MHz and 1135MHz.

8.3.1. Calibration

An important requirement for interferometry is phase coherence between the relevant components used in the radio telescope signal chain. As discussed in Section 4.3, it was found that there was a phase shift difference between the signals at the outputs of the USRP daughter boards used in the MITRA Back-End. This phase shift difference was caused by the misalignment of the local oscillators of the USRP daughter boards. To correct this misalignment, the mixer section of one of the WBX daughter boards was modified. The 2 USRP daughter boards were arranged in a master-slave topology. The synthesizer outputs from the slave daughter board

were isolated. The synthesizer from the master daughter board was used to distribute the local oscillator signal to the mixer of the slave board.

It was also found that the frequencies of the baseband signals from both USRPs were slightly different. The purpose of this calibration was to verify and correct the frequency offset of the baseband signals. The calibration setup is shown in Figure 8.7. Two RF signal generators were used as the calibrators. The MITRA Front-End was isolated and replaced by the calibrators set to the test frequency. As shown in Figure 8.8, two sliders (Shift_0 and Shift_1) were incorporated in the MITRA flowgraph to allow a real-time adjustment of the centre frequency of the USRP RF channels, thus correcting the frequency offset.

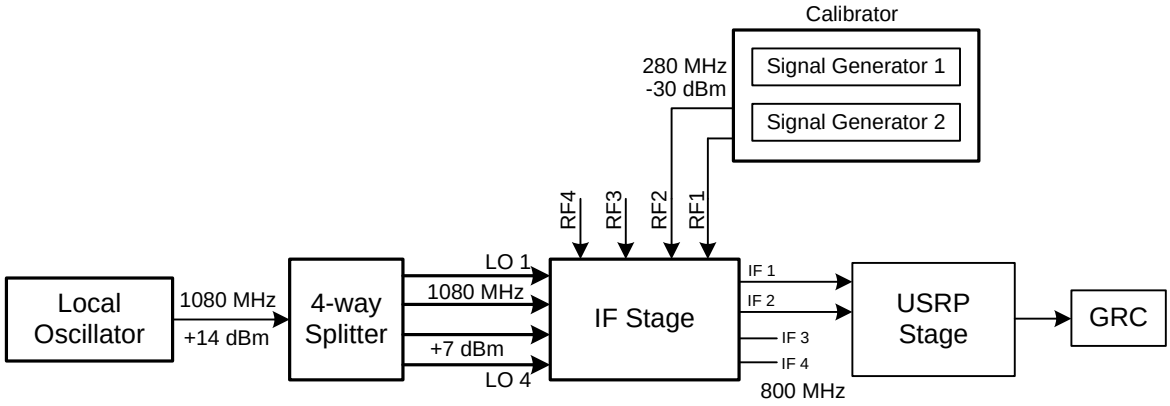

Figure 8.7. Calibration setup

As shown in Figure 8.8, a successful calibration is obtained when the signals of the local oscillators are aligned and of the same frequency. The two high frequency components (green and red) are the raw input data of each respective channel. The low frequency component (blue) is the correlated output signal. The negative peak is measured when the inputs are out of phase, and the positive peak is measured when the inputs are in phase.

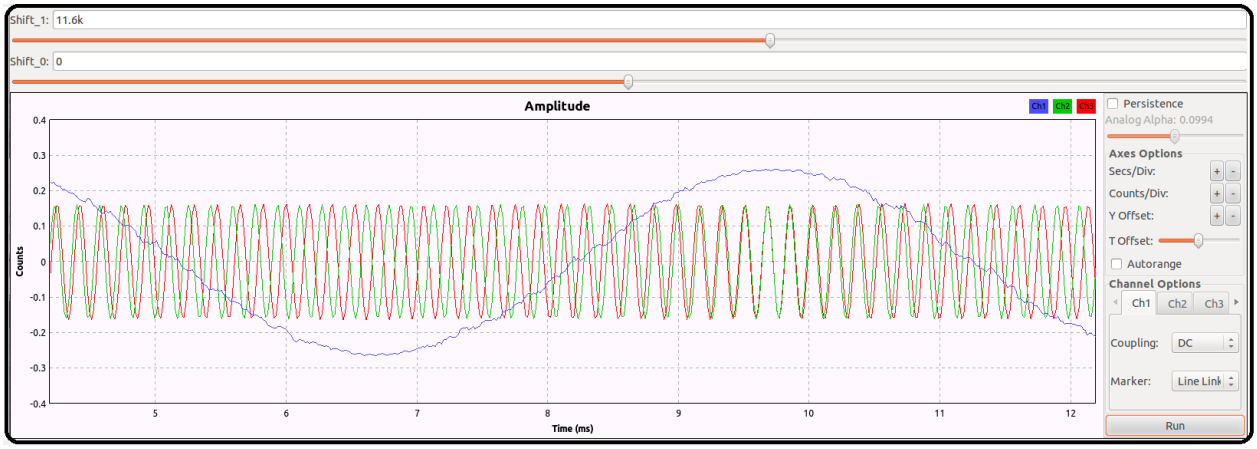

Figure 8.8. Alignment sliders and calibration result

After the calibration process, the Front-End signals can be reconnected to the Back-End as shown in Figure 8.9. This is accomplished without closing the flowgraph and without switching the USRP units off after the calibration process. The calibration process must be verified every time the flowgraph resets and every time the USRP is switched on.

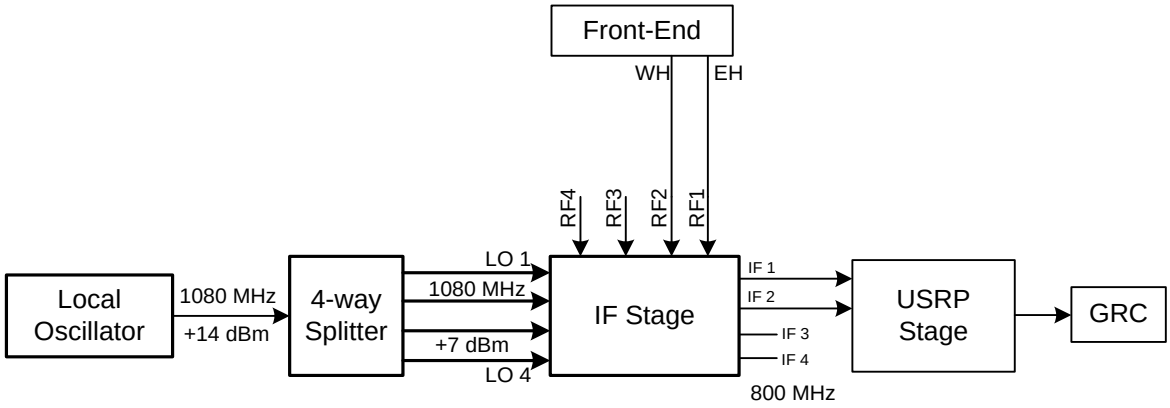

Figure 8.9. Switching to the Front-End

8.3.2. Data Analysis

Gnu Radio Companion (GRC) writes the data into a binary (little endian) format [52]. For the MITRA project, the GRC was set to write the samples as complex binary data. Gnu Octave software was used to read the data stored from the GRC. Octave was launched from the Ubuntu

terminal and was manipulated using terminal prompt commands. In this exercise Octave was mainly used to plot, in the time domain, the dataset for the total duration of the test, and to work out other signal variants such as the real, imaginary, phase, and magnitude components from the complex dataset [53].

8.3.3. Walk-by Test Results (Test at 280 MHz)

The real component of the full dataset of the correlated is shown in Figure 8.10. The time in seconds is marked in red. The test took 110 to 120 seconds. The sudden change of amplitude level around 5 seconds shows the time when the RF signal generator was switched on before the test. The sudden change of amplitude level around 100 seconds shows the time when the RF signal generator was switched off after the test. The signal level in the correlated data varies as the source moves across the arrays. Depending on the source location, a strong signal is measured in the correlated data when the two antenna arrays receive the same signal level from the source, and vice-versa. The 2 antenna arrays receive the same signal level when the source reaches the midpoint of the baseline.

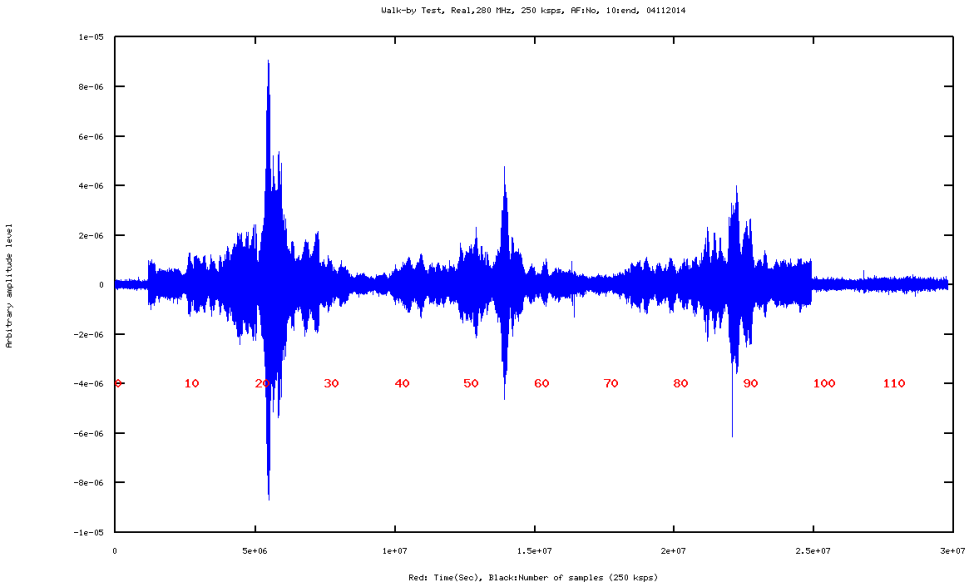

Figure 8.10. Real component of the full dataset of the correlated (280 MHz)

The data section (8 to 36 seconds) around the peak signal level was extracted for analysis. The real component of this dataset is shown in Figure 8.11. The magnitude component of this dataset is shown in Figure 8.12.

The correlated data was furthermore analyzed at the around the peak point. The moving average technique was applied to clean the signal. Figure 8.13 shows the real component of the sinusoidal correlation pattern obtained around the centre of the peak point. The averaged version of the real component is shown in Figure 8.14.

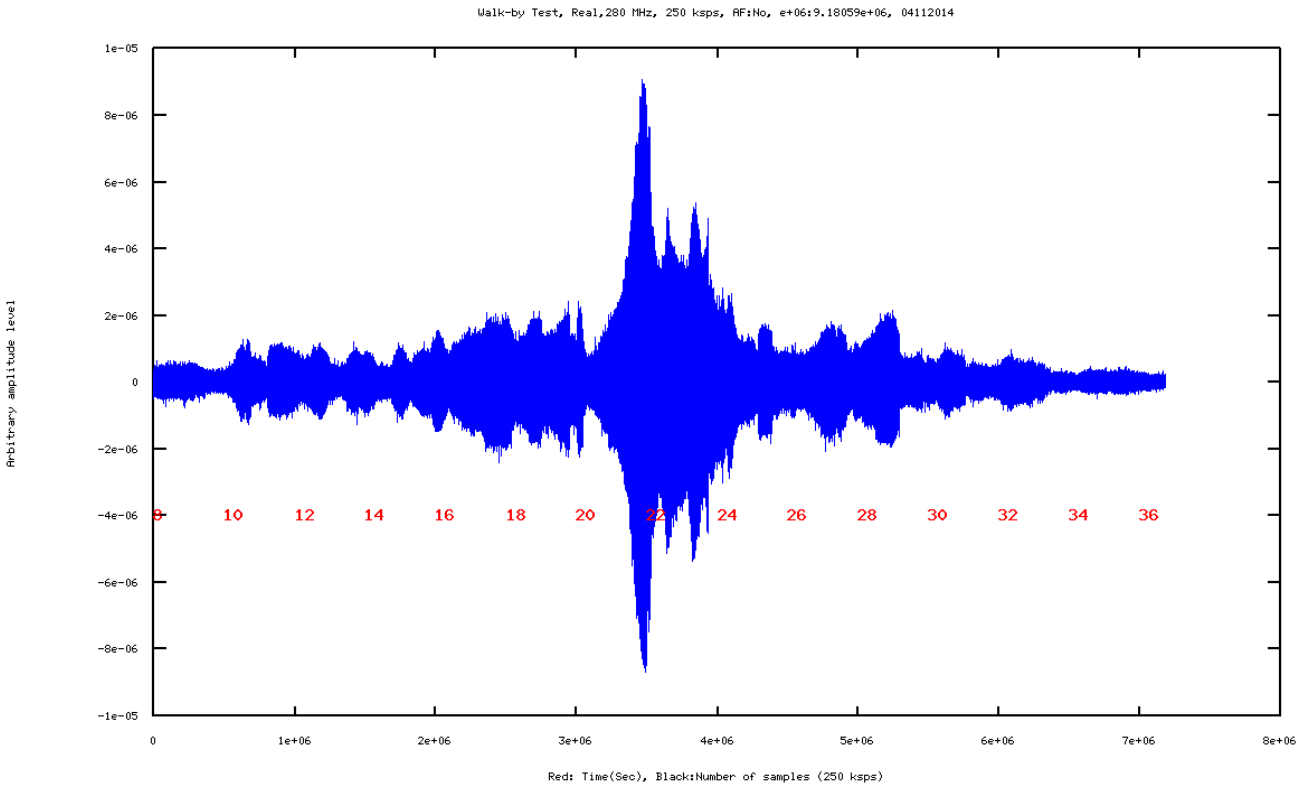

Figure 8.11. Real component of the correlation pattern around the peak signal level (280 MHz)

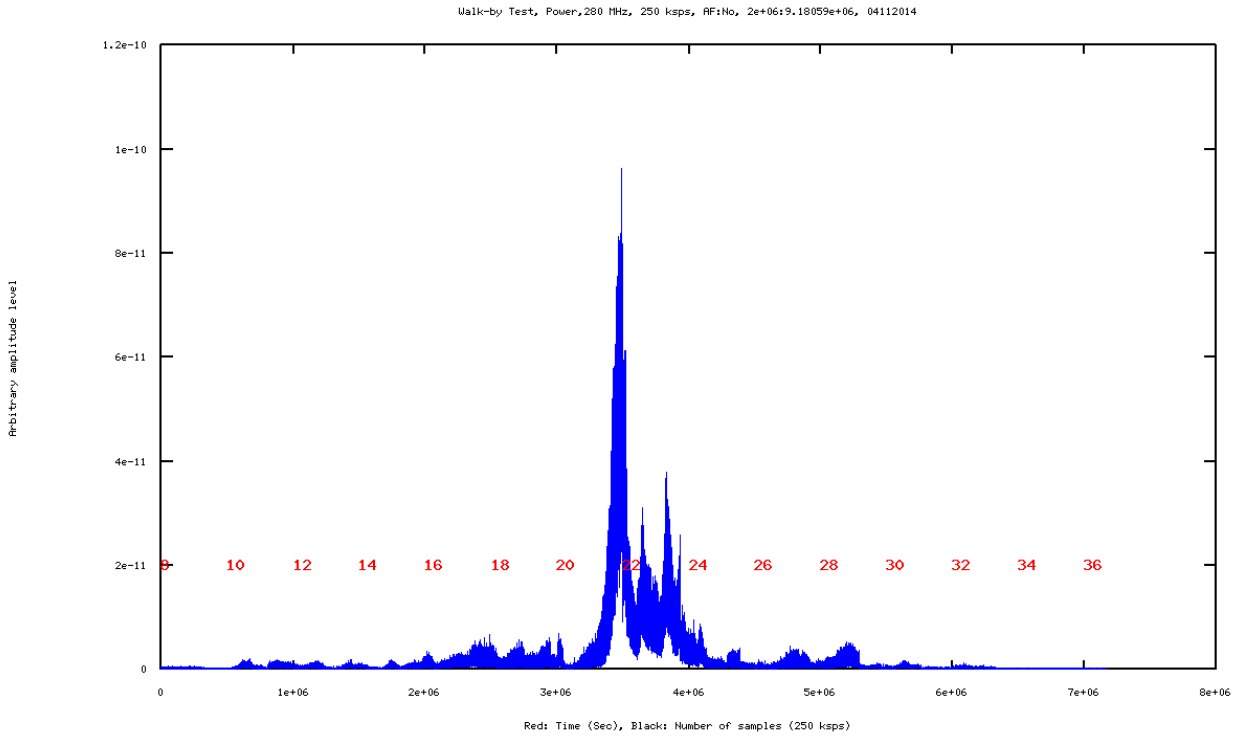

Figure 8.12. Magnitude plot of the dataset around the peak signal level (280 MHz)

The imaginary component of this pattern is shown in Figure 8.15. The averaged version of the imaginary component is shown in Figure 8.16. The real and imaginary components plotted on the same set of axis are shown in Figure 8.17. The averaged version of the real and imaginary components plotted over the same set of axis is shown in Figure 8.18. The phase plot of this correlation pattern is shown in Figure 8.19. The averaged version of the phase component is shown in Figure 8.20. The period of the correlated signal is approximately 1.6 ms.

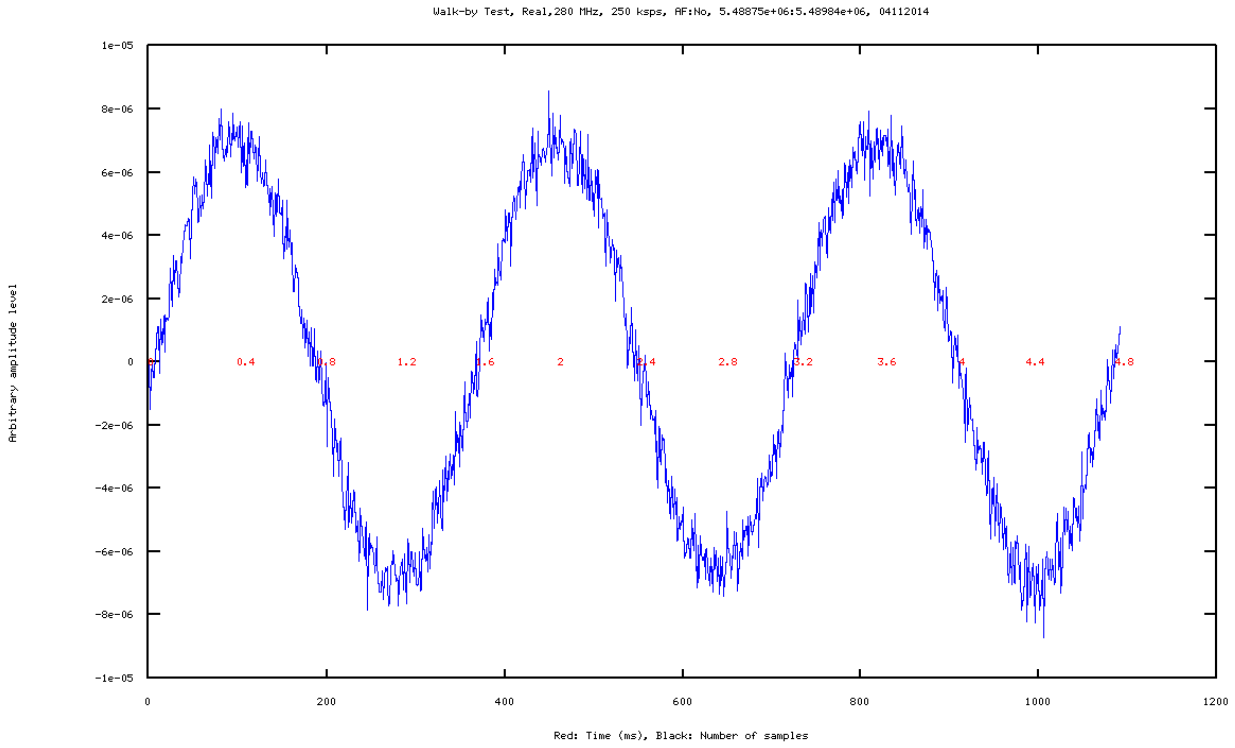

Figure 8.13. Sinusoidal correlation pattern. Real component (280 MHz)

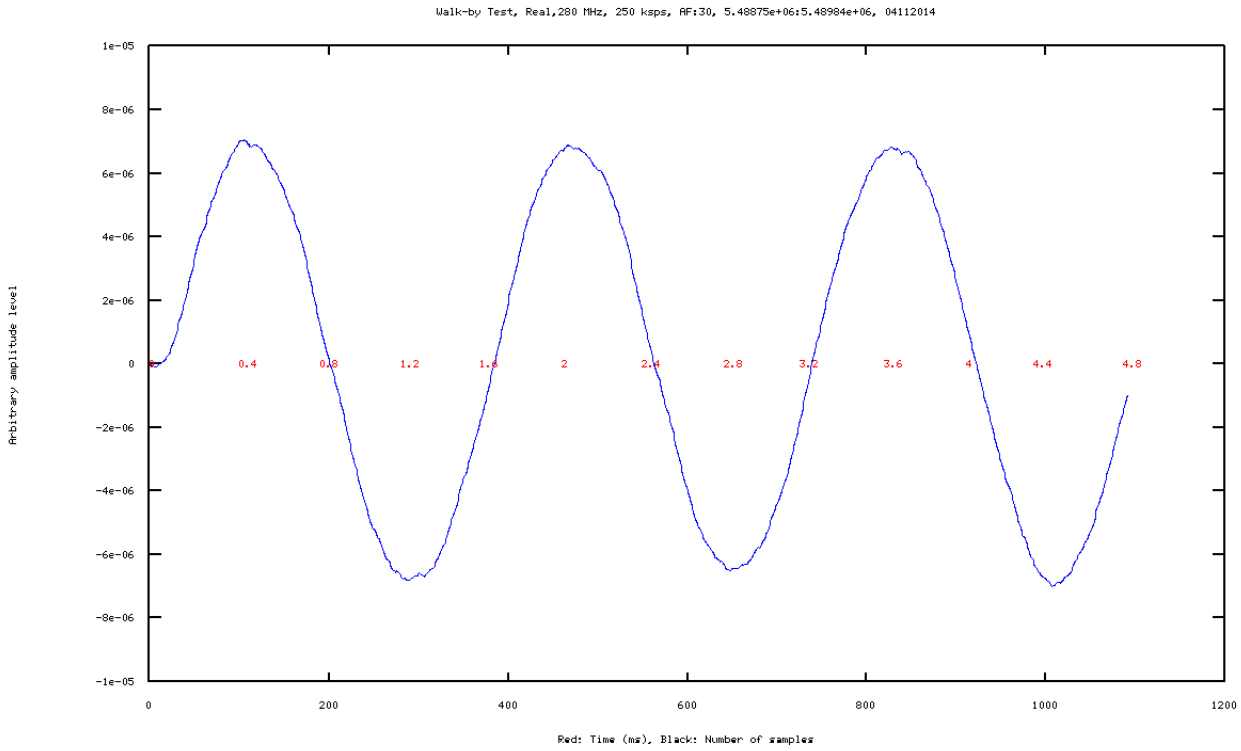

Figure 8.14. Sinusoidal correlation pattern. Real component averaged (280 MHz)

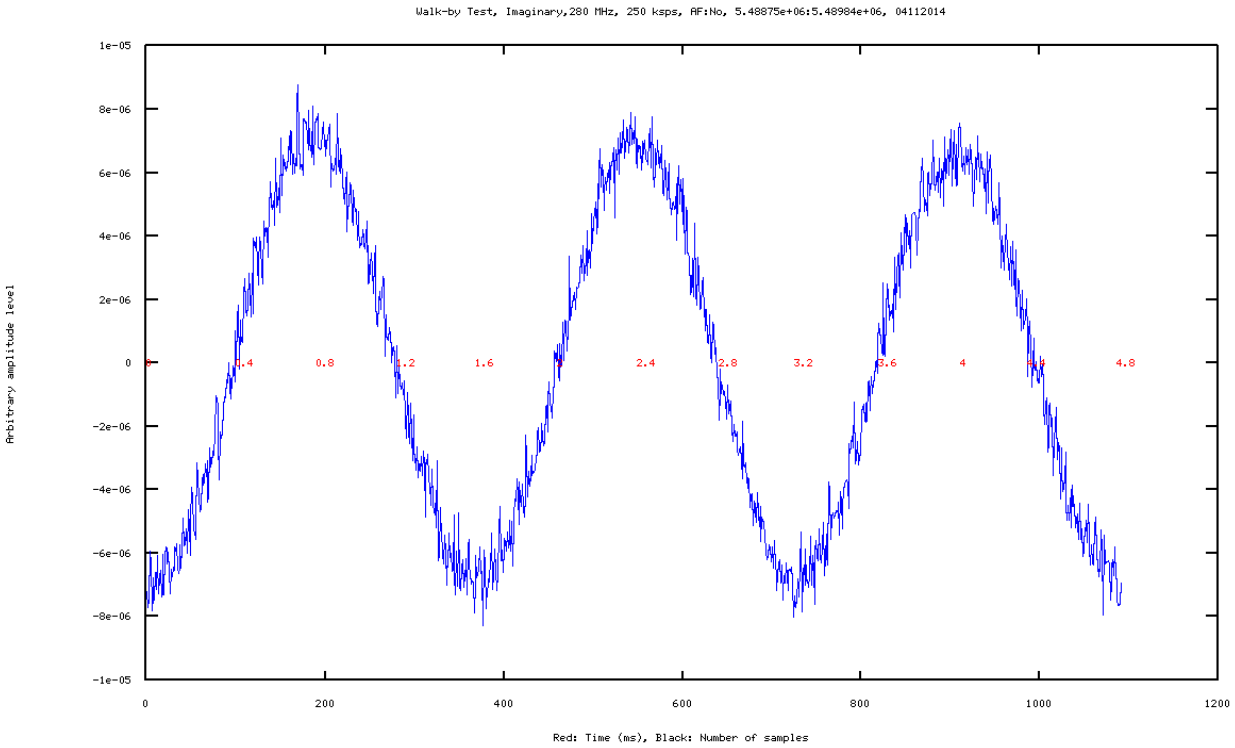

Figure 8.15. Sinusoidal correlation pattern. Imaginary component (280 MHz)

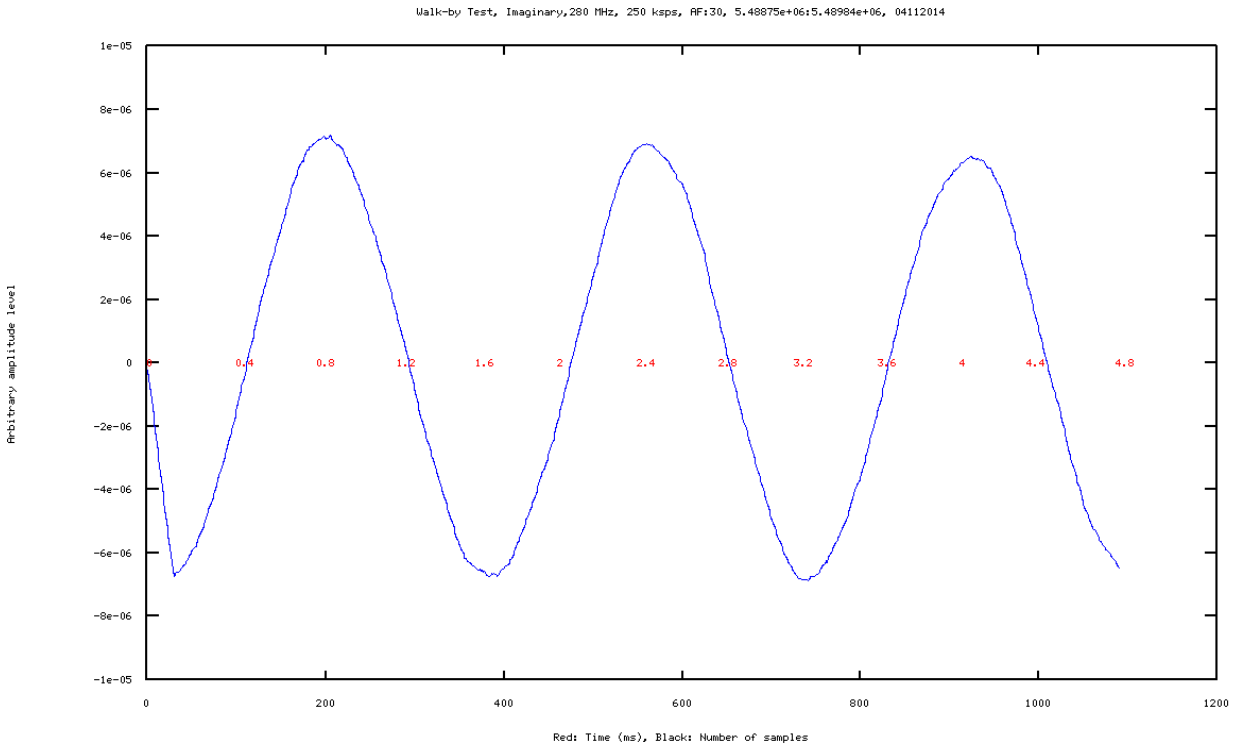

Figure 8.16. Sinusoidal correlation pattern. Imaginary component averaged (280 MHz)

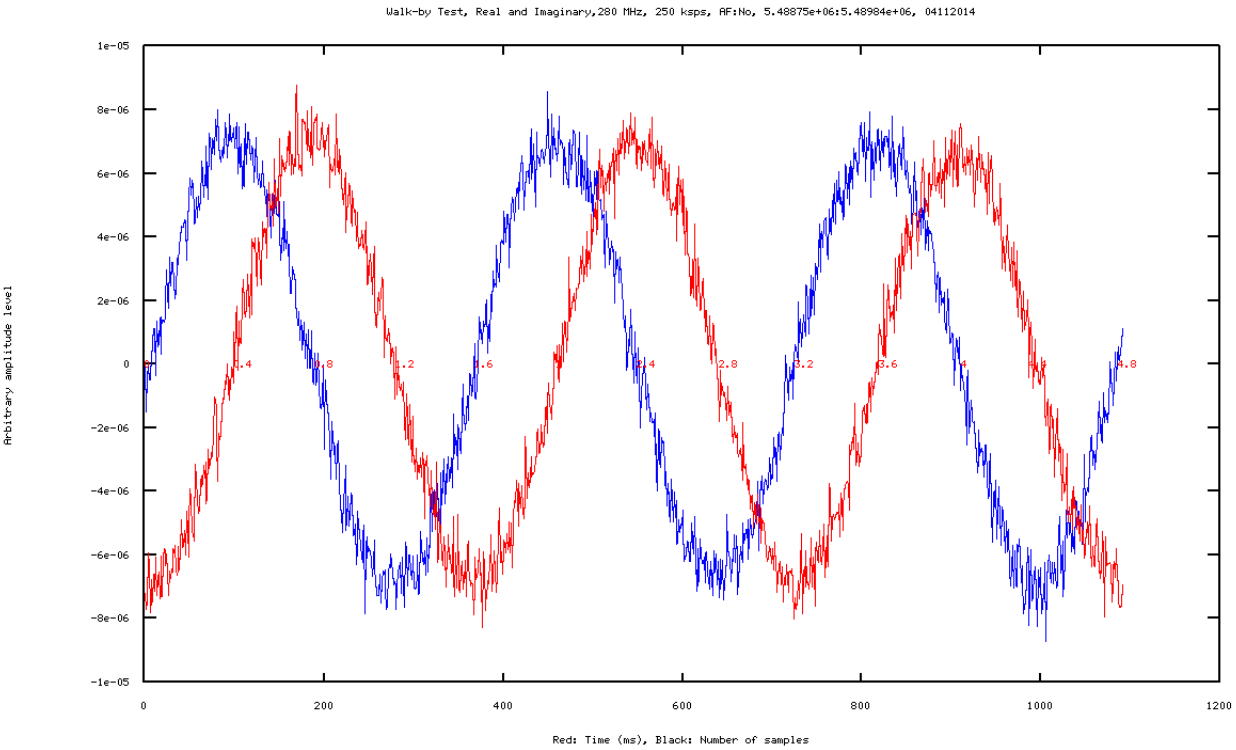

Figure 8.17. Sinusoidal correlation pattern. Real and imaginary components (280 MHz)

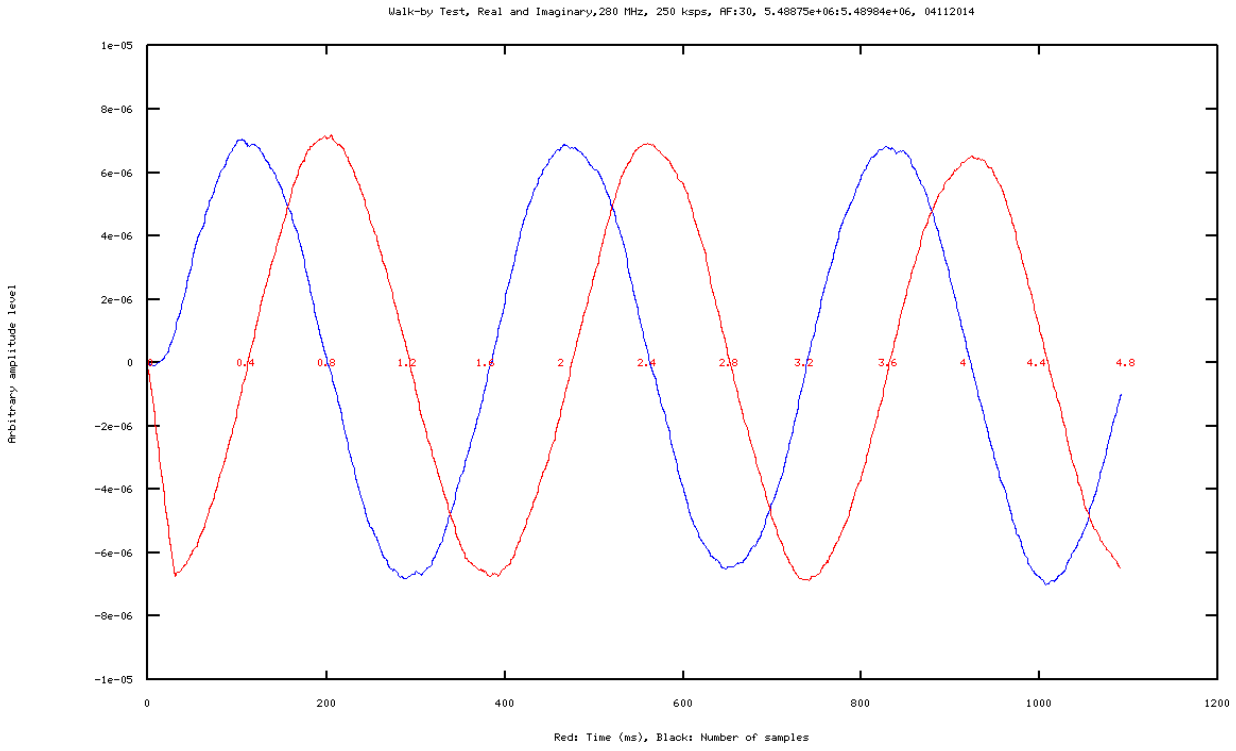

Figure 8.18. Sinusoidal correlation pattern. Real and imaginary component averaged (280 MHz)

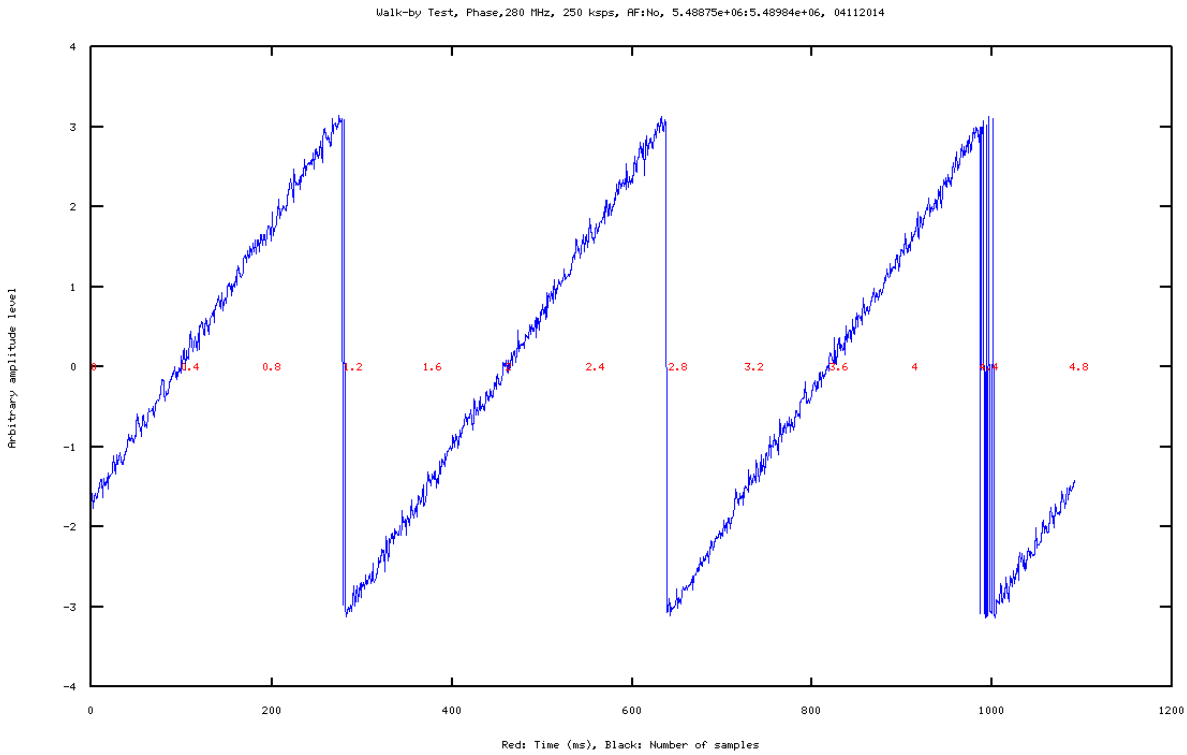

Figure 8.19. Sinusoidal correlation pattern. Phase component (280 MHz)

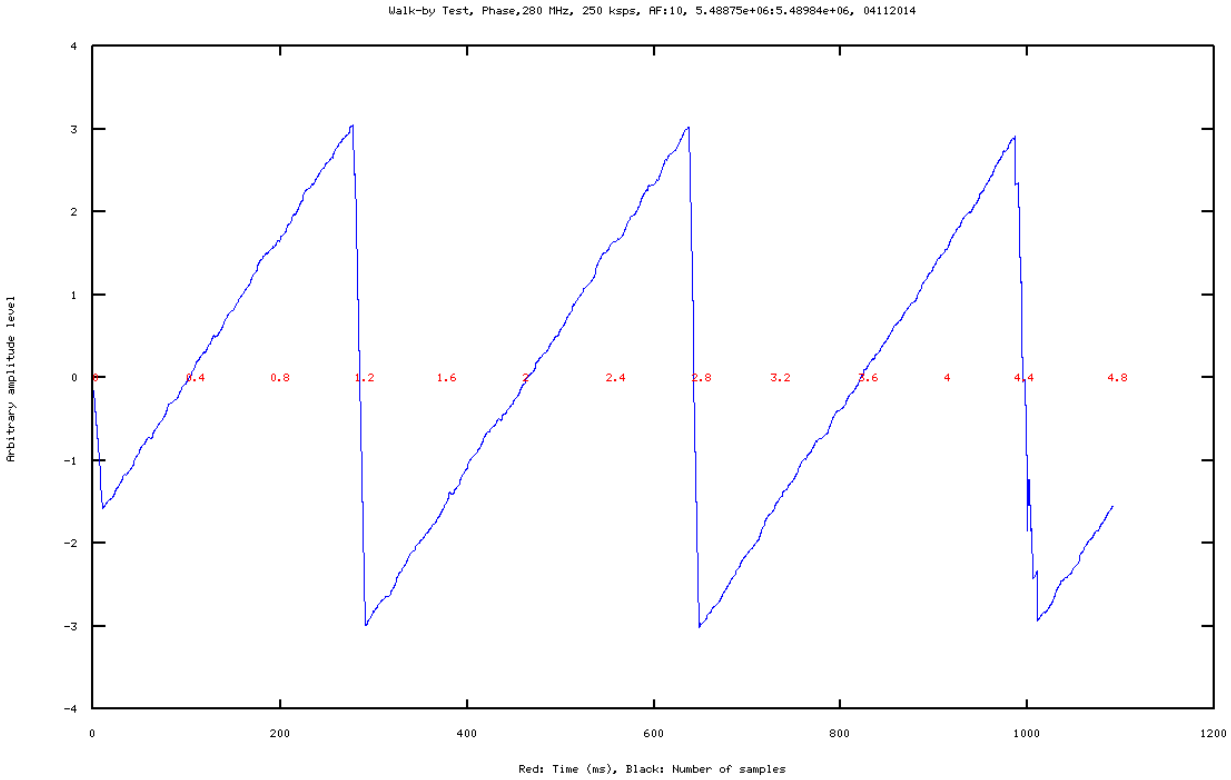

Figure 8.20. Sinusoidal correlation pattern. Phase component averaged (280 MHz)

8.3.4. Walk-by Test Results (Test at 335 MHz)

The real component of the full dataset is shown in Figure 8.21. The signal was also analyzed from approximately 8 to 36 seconds. The real component of this dataset is shown in Figure 8.22. The magnitude component of this dataset is shown in Figure 8.23.

Figure 8.24 shows the real component of the sinusoidal correlation pattern obtained around the centre of the peak point. The averaged version of the real component is shown in Figure 8.25. The imaginary component of this pattern is shown in Figure 8.26. The averaged version of the imaginary component is shown in Figure 8.27. The real and imaginary components plotted on the same set of axis are shown in Figure 8.28. The averaged version of the real and imaginary components plotted over the same set of axis is shown in Figure 8.29. The phase plot of this correlation pattern is shown in Figure 8.30. The averaged version of the phase component is shown in Figure 8.31. The period of the correlated signal is approximately 1.2 ms.

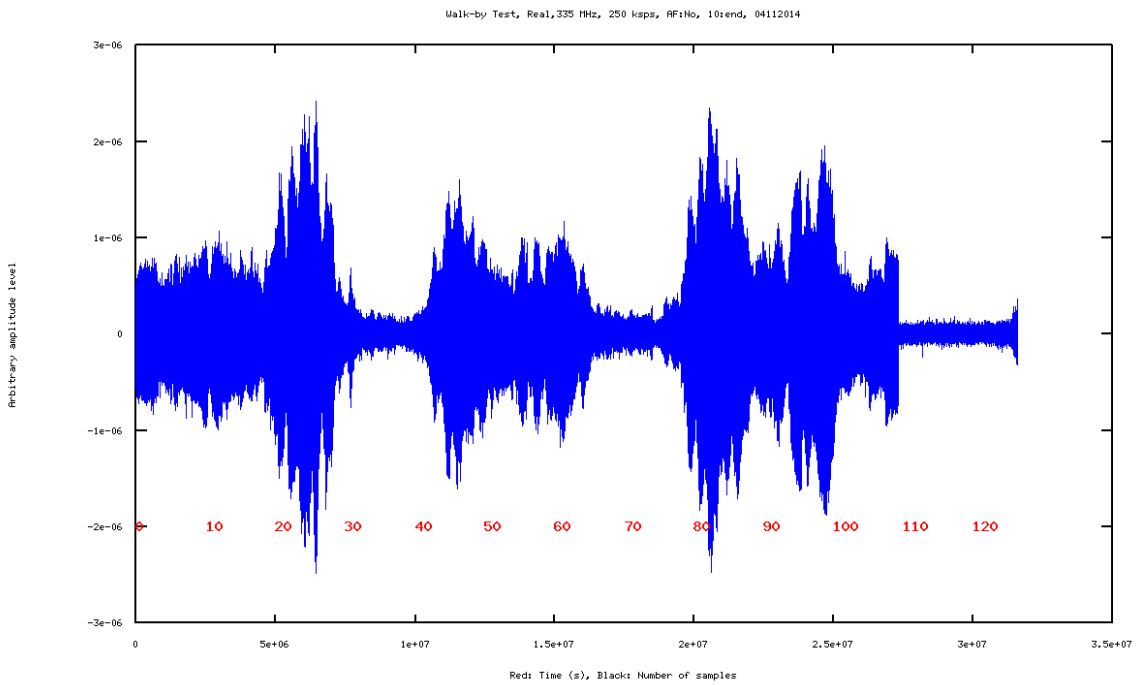

Figure 8.21. Real component of the full dataset of the correlated (335 MHz)

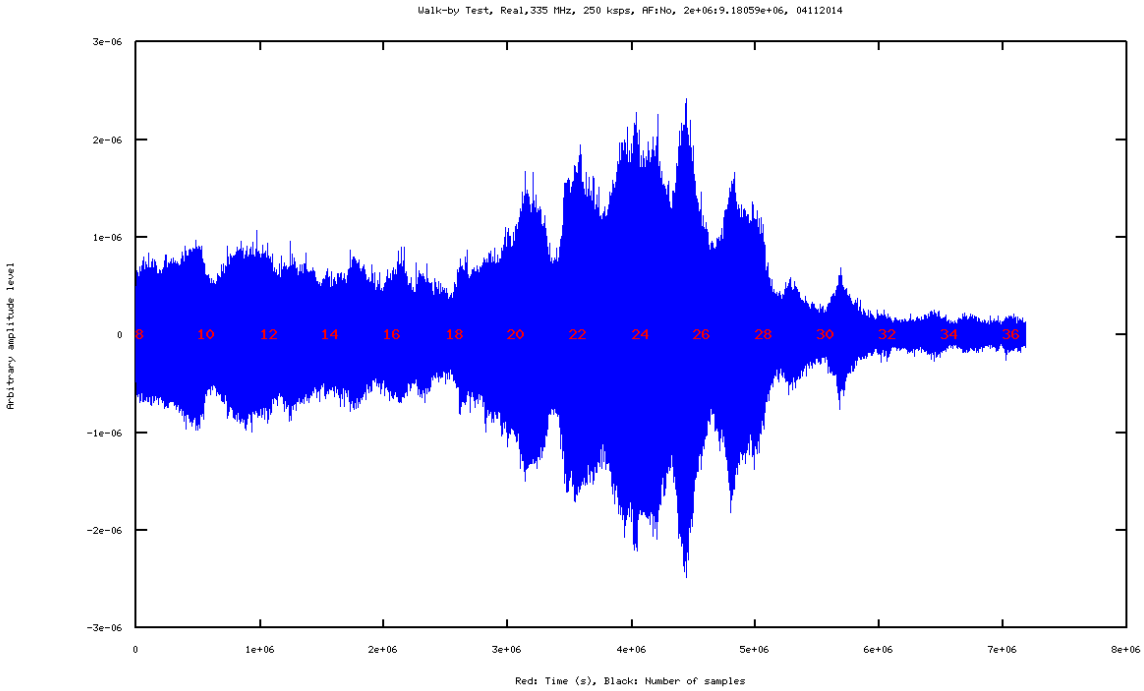

Figure 8.22. Real component of the correlation pattern around the peak signal level (335 MHz)

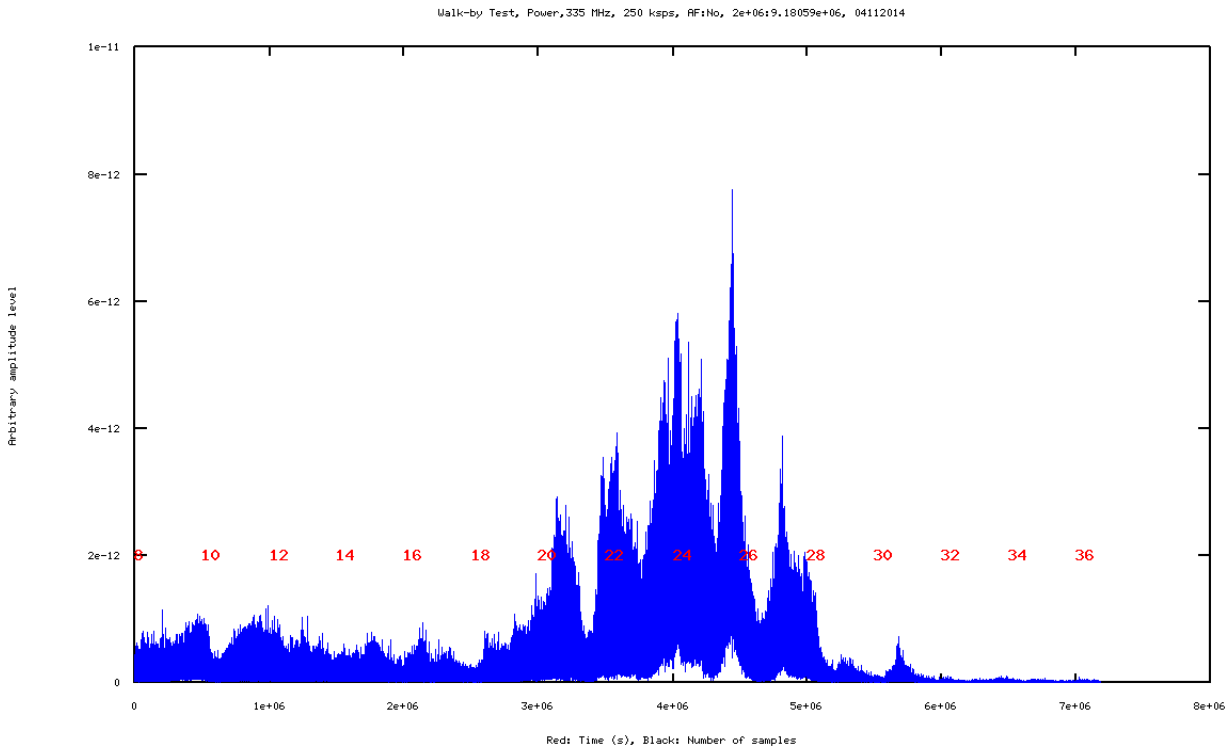

Figure 8.23. Magnitude plot of the dataset around the peak signal level (335 MHz)

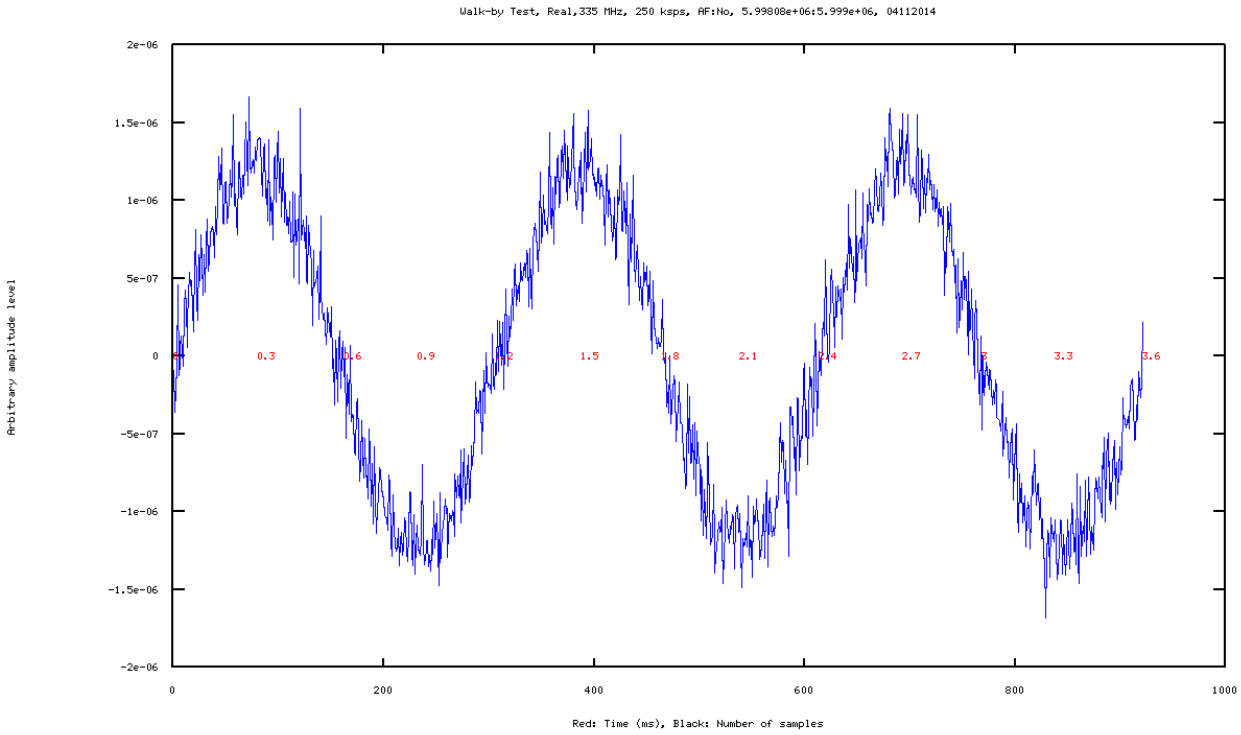

Figure 8.24. Sinusoidal correlation pattern. Real component (335 MHz)

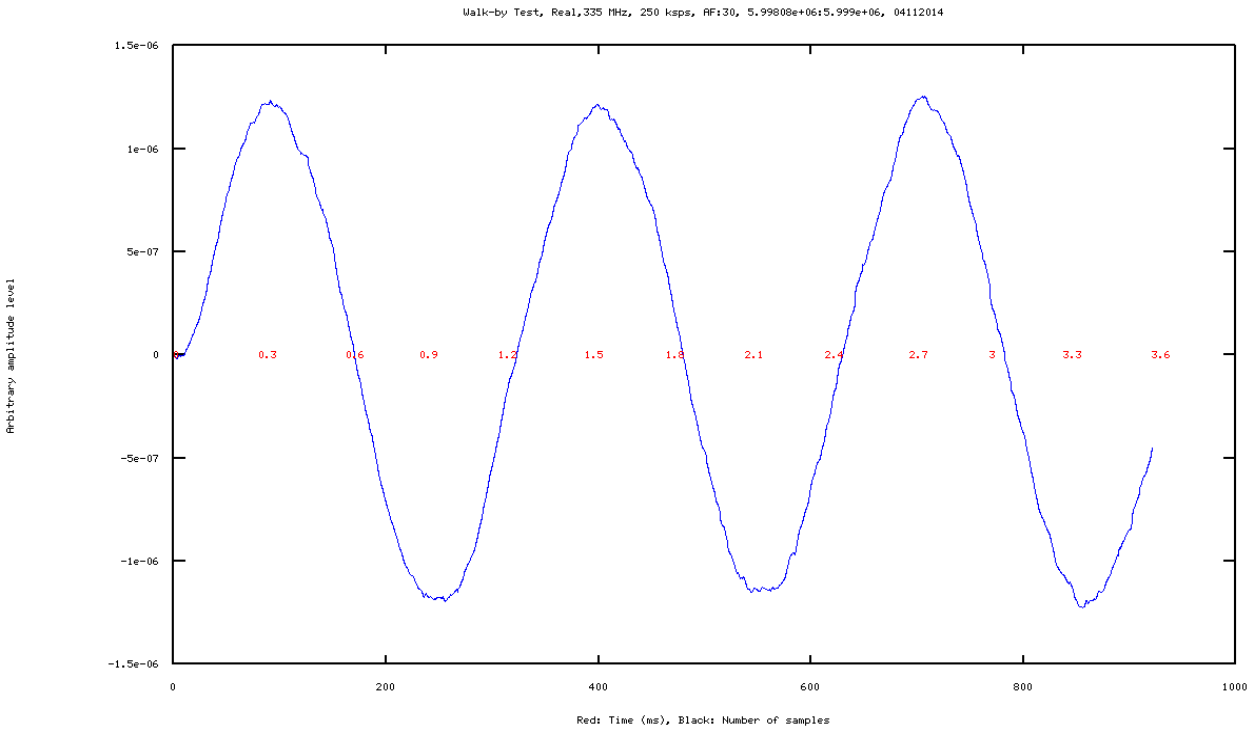

Figure 8.25. Sinusoidal correlation pattern. Real component averaged (335 MHz)

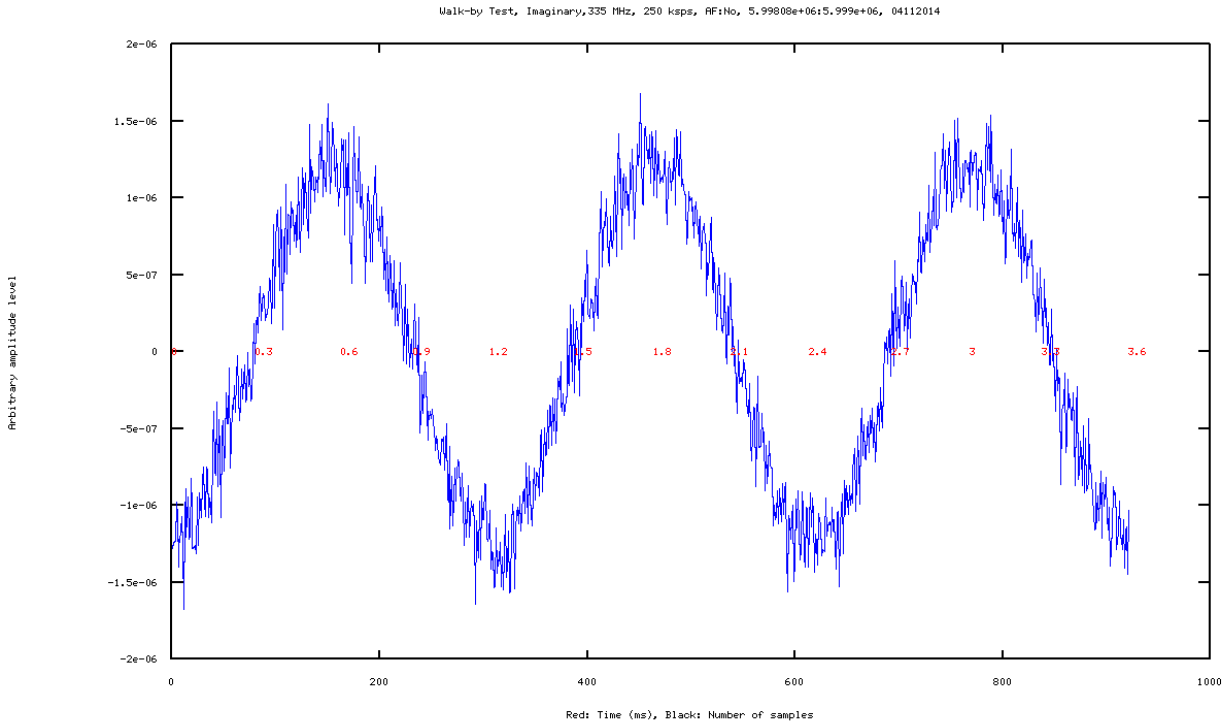

Figure 8.26. Sinusoidal correlation pattern. Imaginary component (335 MHz)

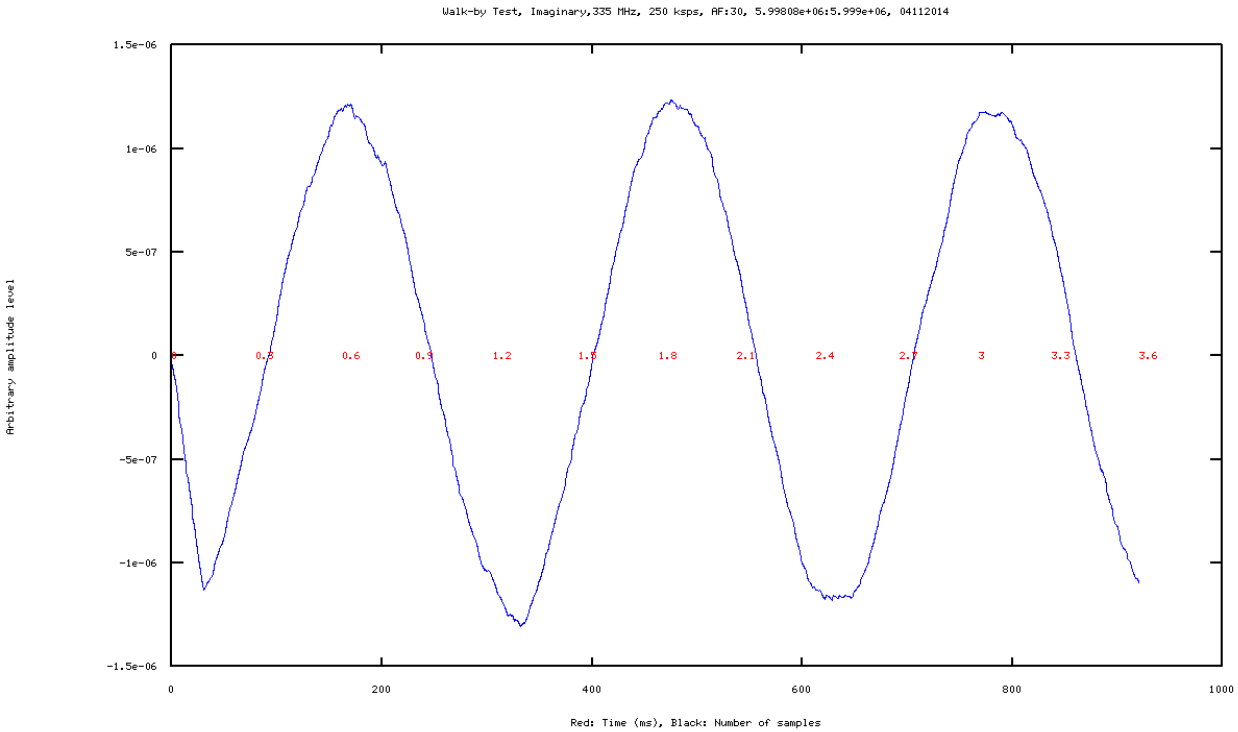

Figure 8.27. Sinusoidal correlation pattern. Imaginary component averaged (335 MHz)

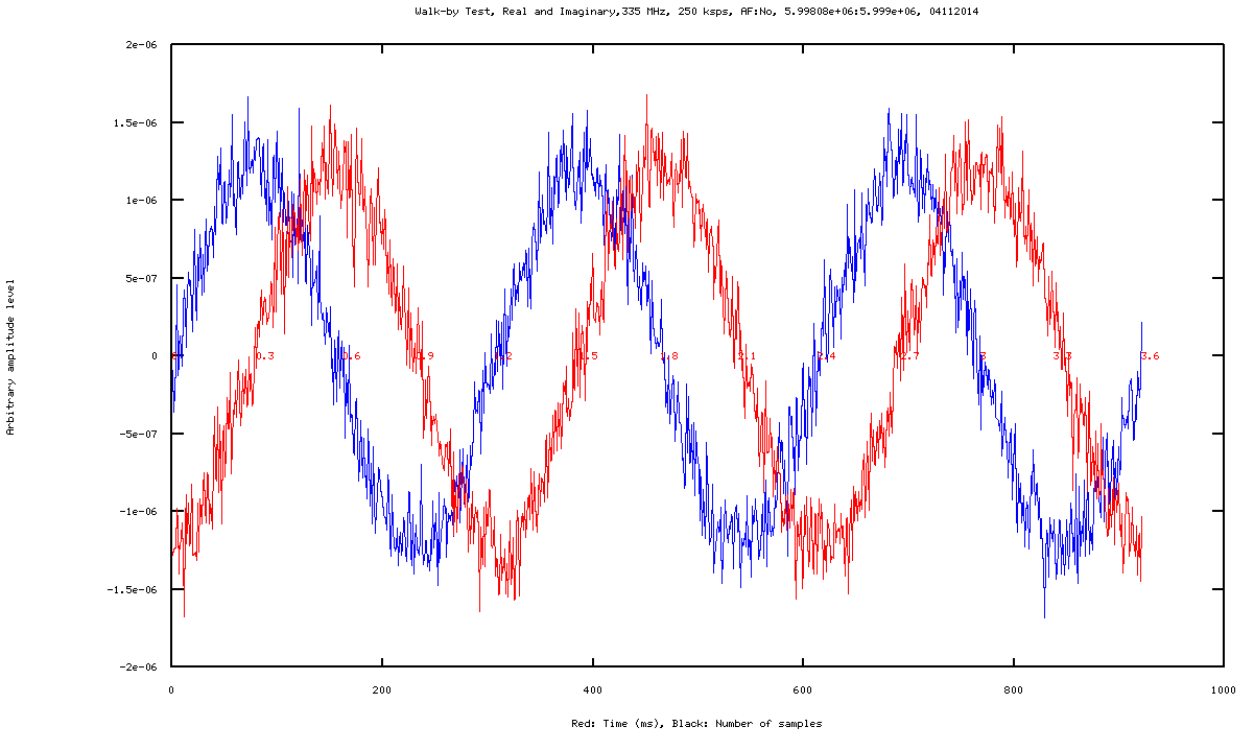

Figure 8.28. Sinusoidal correlation pattern. Real and imaginary components (335 MHz)

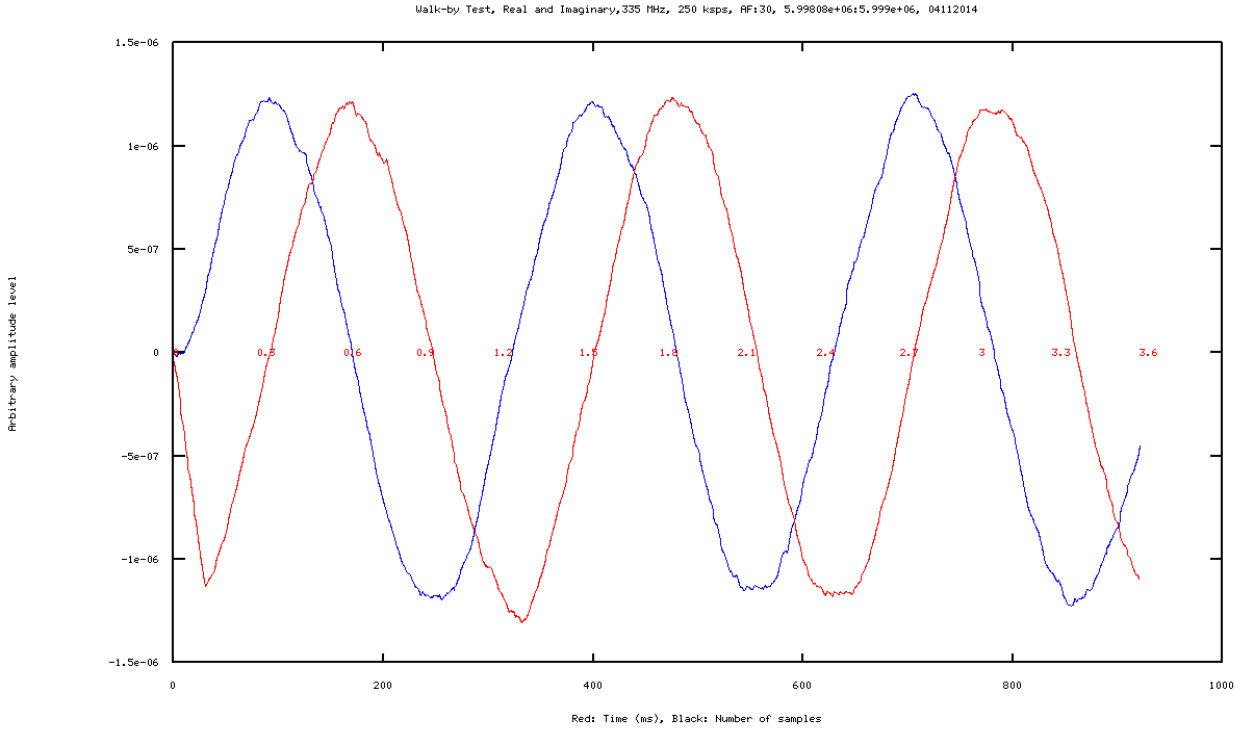

Figure 8.29. Sinusoidal correlation pattern. Real and imaginary component averaged (335 MHz)

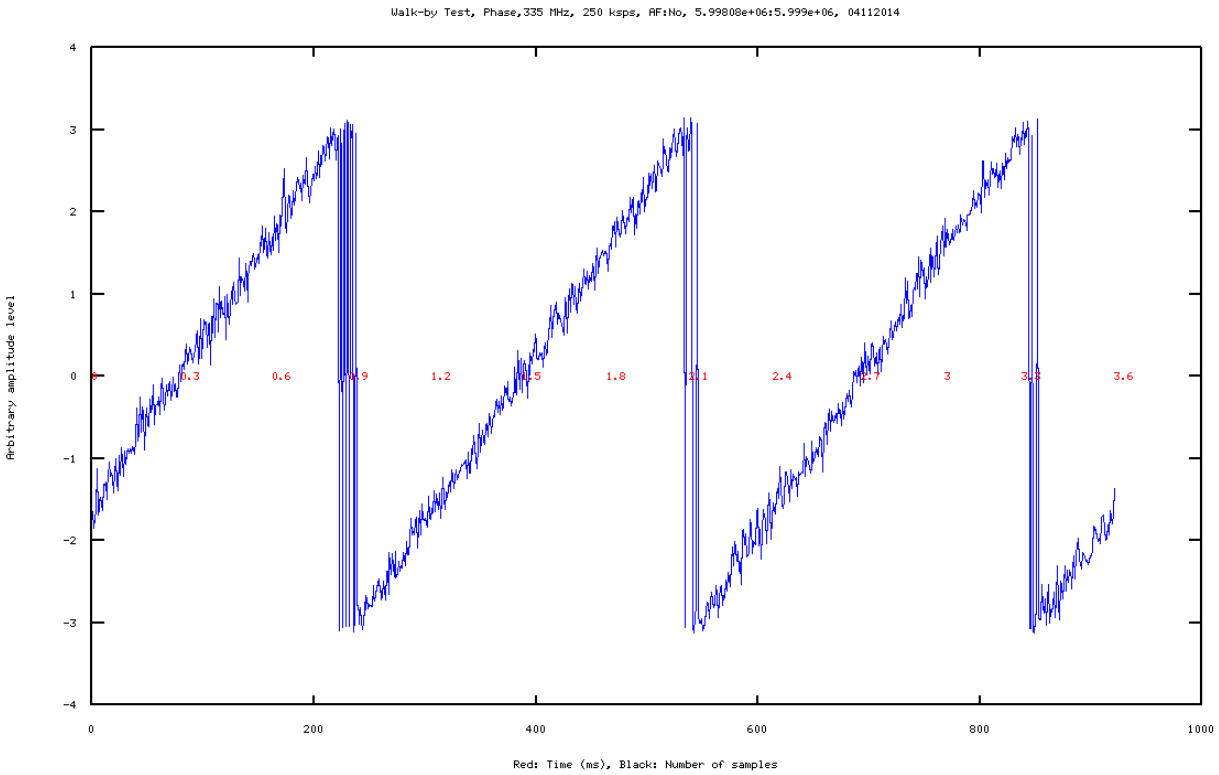

Figure 8.30. Sinusoidal correlation pattern. Phase component (335 MHz)

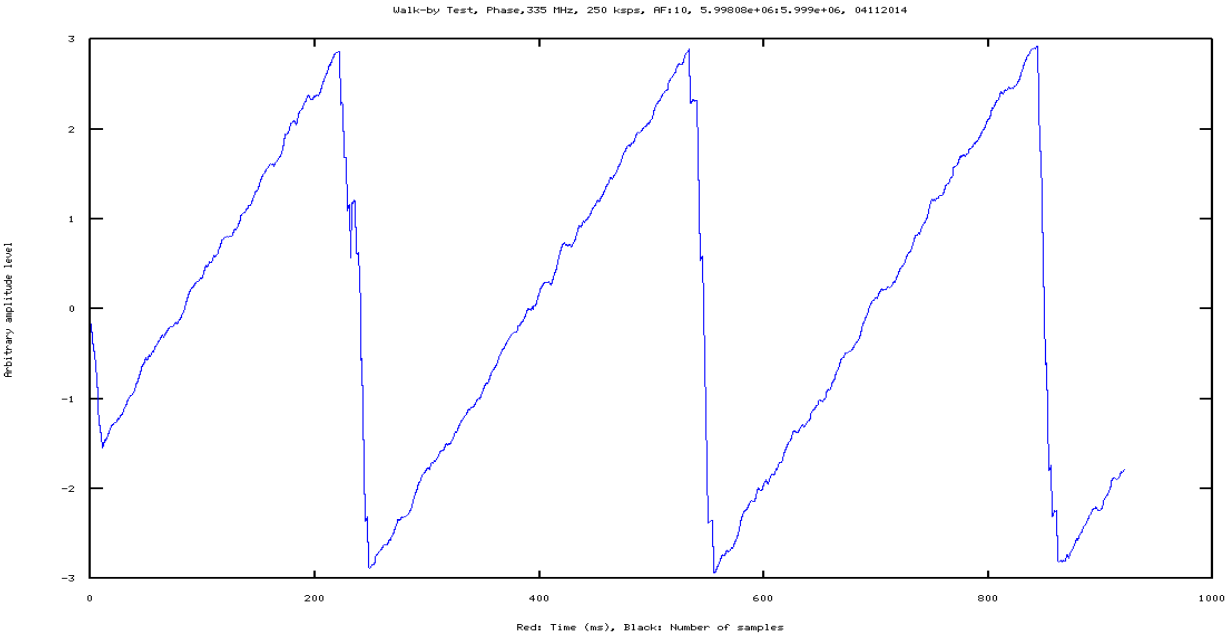

Figure 8.31. Sinusoidal correlation pattern. Phase component averaged (335 MHz)

8.4. Sensitivity Comparison Test

The USRP device has several analog stages (AGC, amplifiers, etc.) which affect the signal-to-noise ratio (SNR) before it is passed to the analog-to-digital converter (ADC) [52]. The purpose of this test was to compare the SNR of the MITRA Back-End with that of a spectrum analyzer. The test setup for this exercise is shown Figure 8.32.

A dipole antenna was connected to a signal generator (433 MHz) in order to radiate RF to the MITRA antennas. The transmitting antenna was at a fixed location. The level of the output signal from the signal generator was set to +13 dBm. A 2-way splitter was inserted at the output of the fibre RX. One output of the splitter was connected to the spectrum analyzer to monitor the received signal shown in Figure 8.33. The SNR ratio from the spectrum analyzer reading was calculated as:

$$SNR = -74.6 - (-90) = 15.4\,\text{dB} \tag{8.1}$$

The other output of the splitter was connected to the RF input of the IF stage. The IF output was connected to the USRP system. Figure 8.34 shows the plot of the power component of the recorded data, calculated as magnitude squared. The averaged version of this power plot is shown in Figure 8.35. The SNR from the averaged power plot can be calculated as:

$$SNR = \frac{7.5\text{x}10^{-8}}{1\text{x}10^{-8}} = 7.5 = 8.8\,\text{dB} \tag{8.2}$$

The USRP system gives a SNR which is 6.6 dB below that provided by the spectrum analyzer with a resolution bandwidth of 300 kHz on the spectrum analyzer.

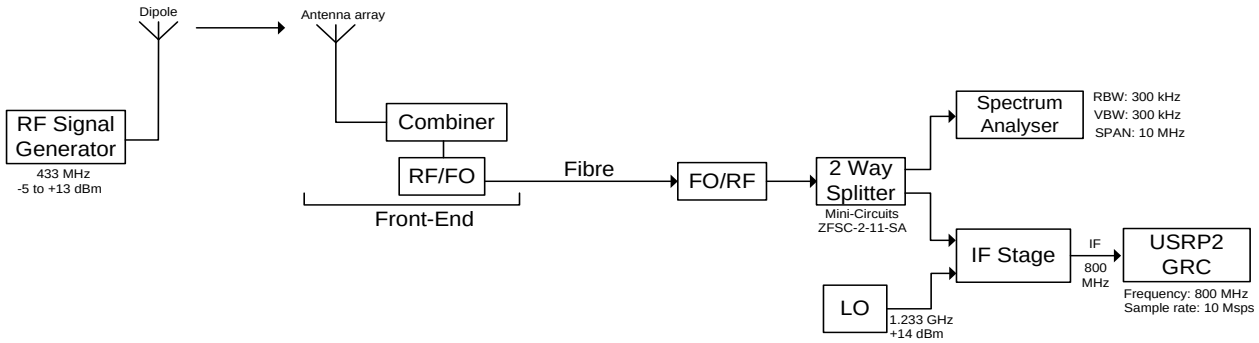

Figure 8.32. Simulation setup for sensitivity comparison

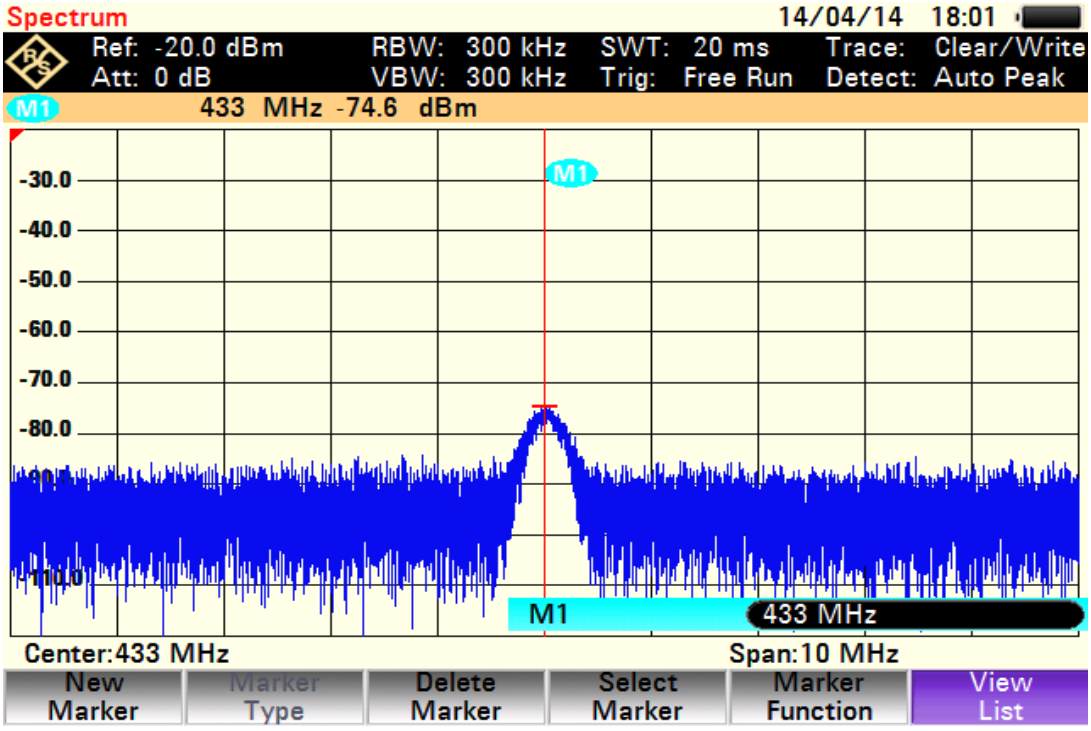

Figure 8.33. Detected signal with the signal generator set to +13 dBm

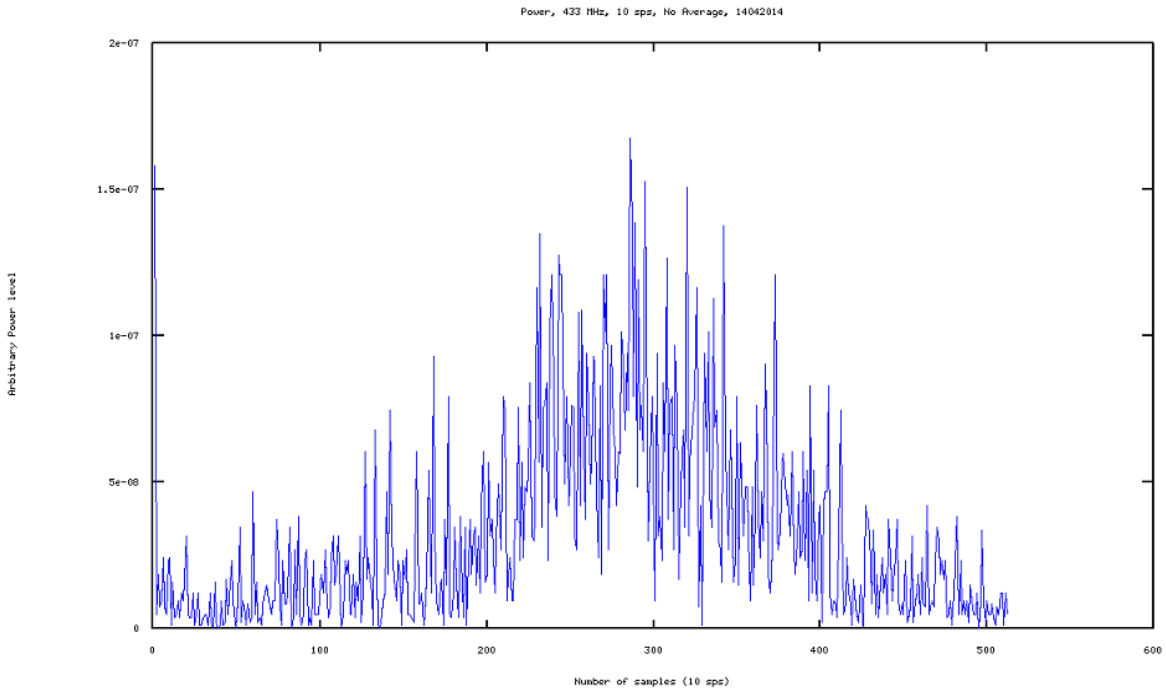

Figure 8.34. Sensitivity Test (Power plot)

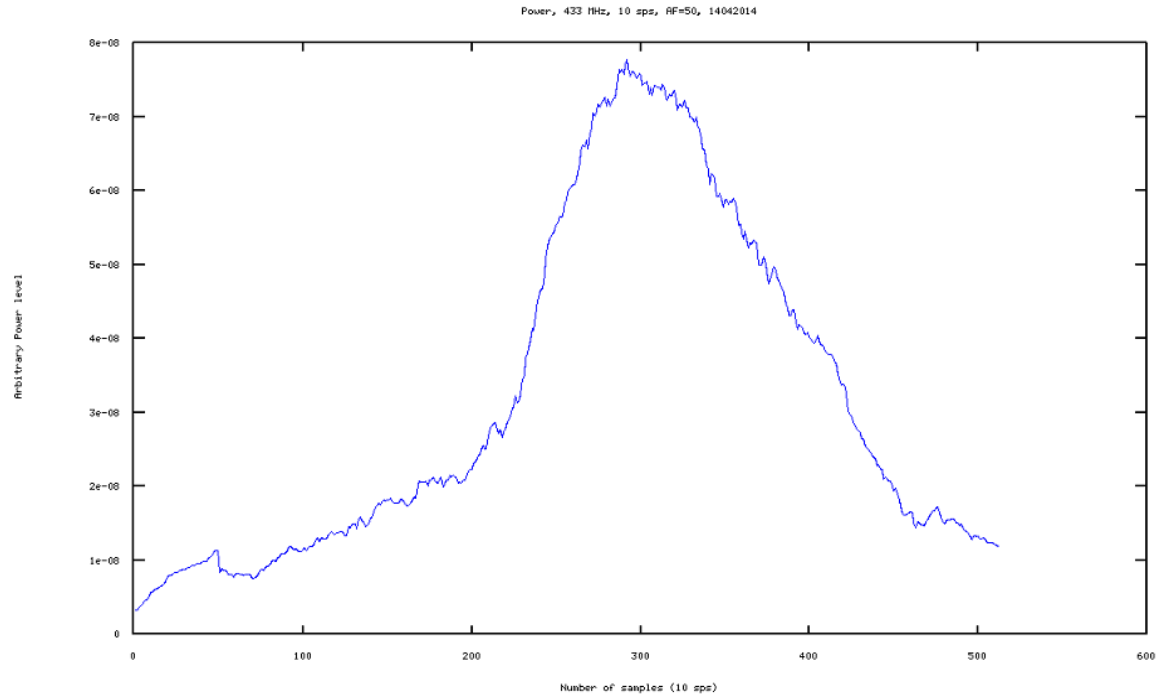

Figure 8.35. Sensitivity Test (Power plot averaged)

Chapter 9: Final Conclusion and Recommendations

As discussed in Chapter 1, the purpose of this research study was to develop the Durban station of the MITRA Radio Telescope at the Durban University of Technology. A project of this scope required a background in engineering as well as radio astronomy. A considerable amount of research was conducted in order to understand the proposal and the specifications of the project.

The major objectives of the study that were achieved included the following:

1. Design and construction of the dual-polarized LPDA arrays.
2. Design and construction of the receiver Analogue Front end and Digital Back-End in SDR.
3. Implementing the multiplying correlator in Gnu-radio, and data analysis using Octave.

As in any radio astronomy station, the antenna is a critical element in the MITRA station. The concept of dual-polarization in the context of a LPDA was not easy to design and to implement mechanically. Although the performance of the dual-polarized LPDA was optimized, the design of this antenna was challenging. The software (LPCAD and 4Nec2) used in this project was only able to design a single-polarized LPDA. The simulated results reported in this research were therefore obtained from a single-polarized antenna design. After the initial tests conducted at DUT a single dual-polarized MITRA antenna was taken to the South African National Antenna Test Range at Paardefontein for further testing. The positive results from the measurements made were able to validate the design and construction processes applied in the MITRA antennas.

The two MITRA antenna arrays, arranged in an East-West configuration with an 8 m baseline, successfully demonstrated the operation of a 2 element correlating interferometer using an RF generator to simulate an astronomical source.

As shown in Figure 4.1, the full MITRA digital Back-End was meant to have 4 USRP devices to be configured in a 4x4 system (see Figure 4.3). At this stage, the MITRA station is running with 2 USRP devices in a 2x2 configuration (see Figure 4.2.). The USRP used in the MITRA Back-End can run up to a data rate of 100 Msps. However the computer used in the Back-End could only achieve 10 Msps. Hence the measured result showed a maximum bandwidth of 10 MHz.

Although attempts were made to detect fringes from the Sun and Sagittarius A at the centre of the Milky Way galaxy these proved inconclusive. At a frequency of 350 MHz the baseline of 8 m results in a fringe width of 6.3°. A source moving at 4° per minute requires approximately 25 minutes of observation time to produce a single fringe. The extremely high levels of in-band RFI experienced with long observation times at the Durban site precluded the possibility of detecting a low amplitude fringe.

In light of the above the following recommendations are made.

1. If the MITRA project is to produce any useful science the Durban station will have to be relocated to a site that is relatively free of RFI in the VHF and UHF bands.
2. The baseline distance needs to be increased significantly to improve the angular resolution of the telescope.
3. The Back-End computer should be replaced with a more powerful unit. This will allow the receiver bandwidth to be increased with an associated increase in sensitivity.

At the time of writing the DUT MITRA station is already a useful working instrument. Various important radio astronomy concepts can be demonstrated including receiver design, implementation of mathematical operations using embedded systems, programming (Linux, Python, Matlab, etc.) and data analysis of large dataset.

The MITRA Radio telescope could be evaluated in terms of short, medium, and long term goals. The research and developmental stage could be regarded as the short term or phase 1 of the project, where the primary objective was to get the station up and running in order to prove the concept behind this research. This has been achieved. Appropriate tests and measurements were conducted to verify the response of each stage in the signal chain of the MITRA station. The results from the walk-by and the sensitivity tests were adequate to demonstrate that, from an engineering point of view, the research and development of the MITRA station at DUT has proved to be successful.

References

[1] A. Joseph and J. R. Angelo, *Encyclopedia of Space and Astronomy*: Facts on File Inc., 2006.

[2] NRA0. (17 January 2013). *How Radio Telescopes Work*. Available: www.nrao.edu/index.php/learn/radioastronomy/radiotelescopes.

[3] J. J. Condon and S. M. Ramson. (2010, October 2012). *Essential Radio Astronomy*. Available: www.cv.nrao.edu/course/astr534/ERA.shtml.

[4] J. Daintith and W. Gould, *The Facts On File Dictionary of Astronomy*, 5 ed. Facts On File, Inc., 2006.

[5] B. F. Burke and F. Graham-Smith, *An Introduction to Radio Astronomy*, 2nd ed. Cambridge, UK: Cambridge University Press, 2002.

[6] S. Odenwald. (2010, 30 October 2013). *The Most Important Equation in Astronomy!* [Space Math VI]. Available: http://spacemath.gsfc.nasa.gov/SMBooks/SMBook6.pdf.

[7] M. J. Gaylard, "Practical Radio Astronomy: A High-Math Introduction," *Unpublished,* 2006.

[8] R. M. Prestage, K. T. Constantikes, T. R. Hunter, L. J. King, R. J. Lacasse, F. L. Lockman*, et al.*, "The Green Bank Telescope," *IEEE Proceedings,* vol. 97, pp. 1382-1390, August 2009.

[9] J. D. Romney. (2012). *Very Long Baseline Array Observational Status Summary*. Available: www.vlba.nrao.edu/astro/obstatus/current/obssum_120106.html.

[10] A. Joshi and R. Shrikumar, "The Low-Frequency Radio Universe: Scientifique Programme and Book of Abstracts," *NCRA-TIFR,* 8-18 December 2008.

[11] G. Beeharry, "Mauritius-South Africa Multi-frequency Interferometer Telescope for Radio Astronomy (MITRA): The Friendship Telescope," *Unpublished,* 28 October 2010.

[12] D. G. K. Ingala and S. D. MacPherson, "An Overview of the MITRA Radio Telescope Signal Chain," in *IEEE Africon 2013*, Port-Louis, Mauritius, 2013, pp. 1319-1323.

[13] H. J. Visser, *Array and Phased array antenna basics*: Wiley, 2005.

[14] W. L. Stutzman and G. A. Thiele, *Antenna Theory and Design*, 2nd ed.: Wiley, 1998.

[15] Y. Huang and K. Boyle, *Antennas: From Theory to Practice*: Wiley, 2008.

[16] L. Martin. (2011, 12 January 2013). *Log Periodic Dipole Array*. Available: http://www.articpeak.com/antennapages/LPDA.html.

[17] R. Cox. (2012, May 2012). *LPCAD - Log Periodic CAD*. Available: http://wb0dgf.com/LPCAD.htm.

[18] A. Voors. *NEC Based Antenna Modeler and Optimizer*. Available: www.qsl.net/4nec2.

[19] J. J. Condon and S. M. Ramson. (2010, October 2012). *Antenna Fundamentals (NRA0 ed.)* [Book: Essential Radio Astronomy]. Available: www.cv.nrao.edu/course/astr534/AntennaTheory.html.

[20] G. R. Jessop, *VHF/UHF Manual*: RSGB, 1983.

[21] D. Baker. (2010). *User Manual for the VHF/UHF Range of the NATR at Paardefontein* [Report for Gerotek]. Available: www.paardefontein.co.za/images/paardefontein_VHF_UHF_Range_Manual.pdf.

[22] A. O. Michael, "On the Antenna Gain Formula," *International Journal of Applied Science and Technology,* vol. 3, No. 1, pp. 43-49, January 2013.

[23] B. Woestenburg. (2008, May 2012). *Definition of Array Receiver Gain and Noise Temperature.* [SKA, Memo:98]. Available: www.skatelescope.org/publications.

[24] J. F. White, *High Frequency Techniques: An Introduction to RF and Microwave Engineering*: IEEE Press, Wiley, 2004.
[25] J. D. Kraus, *Radio Astronomy*, 2nd ed. Durham, N.H.: Cygnus-Quasar Books, 1986.
[26] J. F. Heagy, J. Iams, and J. M. Ralston, "Very High Frequency (VHF) and Ultrahigh Frequency (UHF) Band Sky Noise Estimates From Analysis of 34.5 MHz and 408 MHz Sky Surveys," *Institute For Defense Analyses,* 1998.
[27] F. Leferink, F. Silva, J. Catrysse, S. Batterman, V. Beauvois, and A. Roc'h, "Man-Made Noise in Our Living Environments," *Radio Science Bulletin,* vol. 334, URSI, pp. 49-57, Septembre 2010.
[28] A. R. Thompson, J. M. Moran, and G. W. Swenson, *Interferometry and synthesis in radio astronomy*, 2nd ed. New York, N.Y.: Wiley, 2001.
[29] D. M. Pozar, *Microwave Engineering*, 4th ed. Wiley, 2012.
[30] K. Rohlfs and T. L. Wilson, *Tools of radio astronomy*, 4th ed. Berlin: Springer, 2004.
[31] Ettus_Research™. *USRP N200/N210 Networked Series* [Datasheet]. Available: https://www.ettus.com/content/files/07495_Ettus_N200-210_DS_Flyer_HR.pdf.
[32] Ettus_Research™. *UHD-USRP-Synchronisation* [Application Note].
[33] Ettus_Research™. *Synchronisation and MIMO Capability with USRP Devices* [Application Note]. Available: https://www.ettus.com/content/files/kb/mimo_and_sync_with_usrp.pdf.
[34] Ettus_Research™. *Selecting an RF Daughterboard* [Application Note]. Available: https://www.ettus.com/content/files/kb/Selecting_an_RF_Daughterboard.pdf.
[35] Symmetricom®. (2012, February 2013). *MHM 2010™ Active Hydrogen Maser* [Datasheet]. Available: www.symmetricom.com/link.cfm?lid=8200.
[36] Precision-Test-Systems™, "GPS10RBN 10 MHz Disciplined Rubidium Frequency/Time Standard," PTS™, Instruction Manual, 2012.
[37] T. J. Rouphael, *RF and Digital Signal Processing for Software-Defined Radio: A Multi-Standard Multi-Mode Approach*: Elsevier, 2009.
[38] R. H. Hosking. (2013, 07-11-2013). *Software Defined Radio Handbook (Pentek ed.)*. Available: http://www.pentek.com/sftradhandbook/SftRadHandbook.cfm.
[39] Ronan Farrell, Magdalena Sanchez, and G. Corley, "Software-defined radio demonstrators: An example and future trends," *International Journal of Digital Multimedia Broadcasting,* vol. 2009, ID 547650, p. 12, 2009.
[40] M. Ewing, *The ABCs of Software Defined Radio*: ARRL, 2012.
[41] Gnu_Radio. (2011, February 2012). *Welcome to Gnu Radio*. Available: http://gnuradio.org/redmine/projects/gnuradio/wiki.
[42] Ettus_Reaserch™. (February 2012). *USRP1 Bus Series* [Datasheet]. Available: https://www.ettus.com/content/files/07495_Ettus_USRP1_DS_Flyer_HR.pdf.
[43] Ettus_Reaserch. (February 2012). *UHD - General Application Notes* [Application Notes]. Available: http://files.ettus.com/uhd_docs/manual/html/general.html.
[44] Ettus_Reaserch. (February 2012). *UHD - Device Identification Notes* [Application Notes]. Available: http://files.ettus.com/uhd_docs/manual/html/identification.html.
[45] R. Gandhiraj, R. Ram, K. P. Soman, and CERG, "Analog and Digital Modulation Toolkit for Software Defined Radio," *Proceedia Engineering,* vol. 30, pp. 1155-1162, 2012.

[46] Ettus_Reaserch. (February 2012). *USRP2 Card Burner GUI*. Available: htt://ettus-apps.sourcerepo.com/redmine/ettus/projects/uhd/repository/revisions/master/changes/host/utils/usrp2_card_burner_gui.py.
[47] Ettus_Reaserch. (February 2012). *Master Images*. Available: http:/files.ettus.com/binaries/master_images
[48] Ubuntu_help. (Februray). *Network Configuration*. Available: https://help.ubuntu.com/10.04/serverguide/network-configuration.html.
[49] S. C. Bloch, *Excell for Engineers and Scientists*: Wiley, 2000.
[50] J. J. Condon and S. M. Ramson. (2010, October 2012). *Interferometers I* [Book: Essential Radio Astronomy]. Available: www.cv.nrao.edu/course/astr534/Interferometers1.html.
[51] A. R. Thompson, J. M. Moran, and G. W. Swenson, *Interferometry and synthesis in radio astronomy* vol. 1, 1986.
[52] GnuRadio. (2014, February 2014). *Frequently Asked Question*. Available: www.gnuradio.org/redmine/projects/gnuradio/wiki/FAQ.
[53] D. G. K. Ingala, "MITRA Radio Telescope: Proof of Concept," presented at the RTA Durban, South Africa, 2014.

Annexure 1: Antenna ETS-Lindgren 3142 D

ETS·LINDGREN
An ESCO Technologies Company

EMC Antennas

BiConiLog™

Model 3142D

FEATURES:

- **26 MHz - 6 GHz Frequency Range**
- **Avg. 2:1 VSWR Above 50 MHz**
- **Emissions Testing:**
  - **-- ANSI C63.4**
  - **-- FCC-15 and FCC-18**
  - **-- EN 55022**
- **Immunity Testing:**
  - **-- IEC 61000-4-3**
- **Flexible Mounting Systems**

ETS-Lindgren's EMCO Model 3142D BiConiLog Antenna

ETS-Lindgren's EMCO Model 3142D BiConiLog is a hybrid antenna that combines innovative design, compact size, and excellent performance. This antenna enables users to measure a frequency range of 26 MHz to 6 GHz in one sweep, negating the need for multiple antennas and time-consuming equipment setup. Accuracy and repeatability are improved, while time and money are saved.

This BiConiLog is designed as a dual-purpose antenna that can be used for both immunity and emission testing. From 26 MHz to 60 MHz, the Model 3142D antenna with optional end plates exhibits an average 5.5 dB gain improvement vs. typical hybrid antennas. At some frequencies, a 10 dB gain improvement is achieved.

This model replaces the EMCO Model 3142C, and includes a new stinger mount as standard equipment. Individual antenna calibration data is provided for emission testing.

FEATURES

Frequency Range

The Model 3142D increases the upper frequency limit to accommodate the new upper limit of 6 GHz included in the IEC 61000-4-3 standard.

VSWR Levels

The average VSWR is 2:1 above 50 MHz, an excellent level at this low frequency for an antenna this size.

Emissions Testing

The 3142 is ideal for emissions testing, since it cover the entire range of typical emissions measurements.

Immunity Testing

For immunity measurements, the 3142D covers the typical 80 MHz to 6 GHz range, as well as the 26 MHz to 6 GHz used for testing medical equipment.

Individually Calibrated

The 3142D is individually calibrated at 10 m per ANSI C63.5 and calibrations at 1m and 3m per SAE ARP 958.

Flexible Mounting System

The 3142D antenna includes both a Classic EMCO mount and a rear "stinger" mount.

APPLICATIONS

- Emissions
  - -- ANSI C63.4
  - -- FCC-15 and FCC-18
  - -- EN 55022
- Immunity
  - -- IEC 61000-4-3

www.ets-lindgren.com

ETS-LINDGREN
An ESCO Technologies Company

EMC Antennas
BiConiLog
Model 3142D

STANDARD CONFIGURATION

- Antenna
- Individually calibrated:
  -- 10 m per ANSI C63.5
  -- 3 m per SAE ARP 958
  -- 1 m per SAE ARP 958
- Actual antenna factors and a signed Certificate of Calibration Conformance included in manual
- Manual

OPTIONS

- ETS-Lindgren offers several non-metallic, non-reflective tripods. For easy horizontal and vertical polarization changes, the 7-TR tripod is recommended

Electrical Specifications

MODEL	FREQUENCY RANGE	MAXIMUM CONTINUOUS POWER	IMPEDANCE (NOMINAL)	VSWR RATIO (AVG)	CONNECTORS
3142D	26 MHz – 60 MHz 60 MHz – 600 MHz 600 MHz – 1 GHz 1 GHz – 6 GHz	500 W 1 kW 500 W 200 W	50 Ω	2:1	Type N female (1)

Physical Specifications

MODEL	WIDTH	DEPTH	HEIGHT	WEIGHT
3142D	133.9 cm 52.7 in	168.1 cm 66.2 in	76.2 cm 30.0 in	7.7 kg 17.0 lb

Antenna Factor and Gain Typical Measured Data Performance

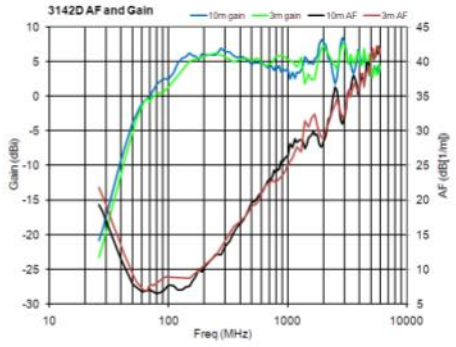

VSWR Typical Measured Data Performance

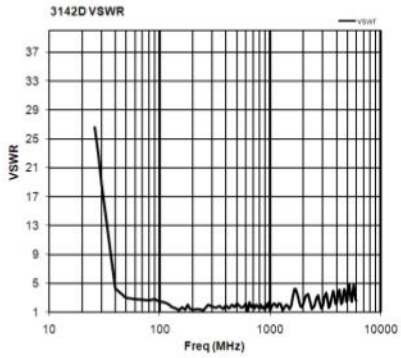

Beamwidth Typical Measured Data Performance

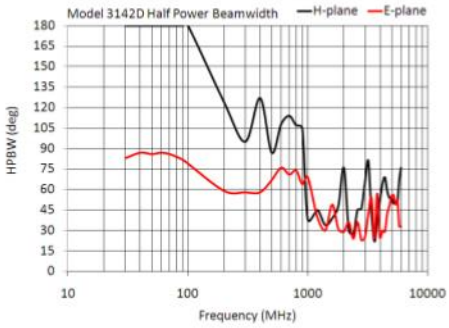

ETS-LINDGREN
An ESCO Technologies Company

EMC Antennas
BiConiLog
Model 3142D

E-Plane 30 MHz to 900 MHz
Typical Measured Data Performance

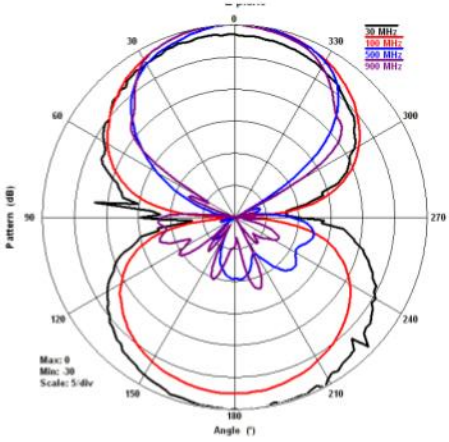

H-Plane 30 MHz to 900 MHz
Typical Measured Data Performance

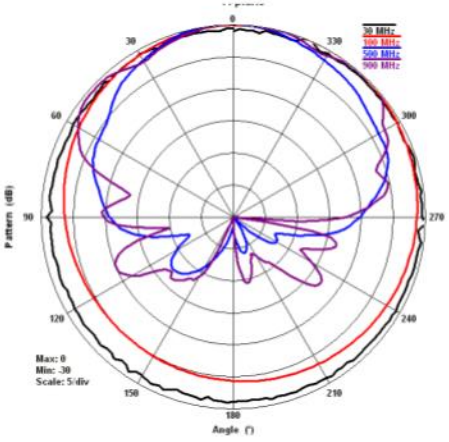

E-Plane 2 to 6 GHz
Typical Measured Data Performance

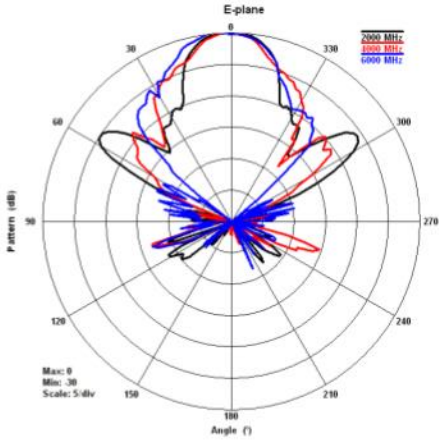

H-Plane 2 to 6 GHz
Typical Measured Data Performance

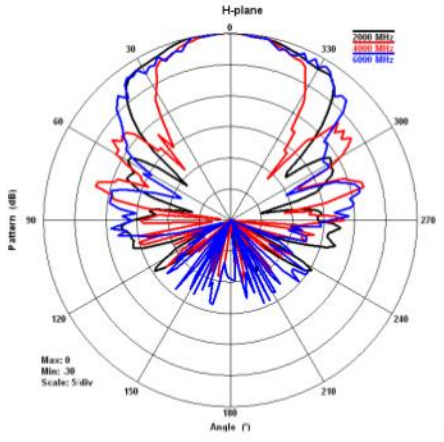

Phone + 1.512.531.6400 ● info@ets-lindgren.com ● www.ets-lindgren.com
Offices in the US, Finland, UK, France, Singapore, India, Japan, China, Taiwan

Annexure 2: Antenna Schaffner CBL6143A

X-Wing® BiLog® Antenna 30MHz - 3GHz CBL 6143

- **Compact size for compact chambers**
- **Reduced chamber coupling**
- **Up to 30% test time saved**
- **Ultra-broadband immunity and emission antenna**

CBL 6143 mounted on optional tripod CTP 6097A

The X-Wing® BiLog® for RF EMC immunity and emission testing in compact chambers

Immunity Testing
The combination of BiLog® technology with novel low frequency, folded elements (X-Wings®) allows low frequency power to be efficiently projected forward without significantly affecting the high frequency performance and, at the same time, reduces the chamber coupling effects. The CBL 6143 has a unique matching network which will allow powers of up to 300 watts CW to be transmitted, making it suitable for most immunity measurements requiring fields of 10V/m, or even greater.

Emission Testing
The innovative geometry of the log periodic section of the CBL 6143 has been created using advanced modelling techniques of the University of York. This shape optimises the gain performance over conventional log periodic antennas at frequencies above 700MHz and extends the useful operating range to 3GHz. This improvement is invaluable in measurement systems using receiving instruments with high noise floors at high frequencies, saving pre-amplification which is not always desirable or practical when measuring high level signals or broadband impulsive noise.

Individual Calibration
All CBL 6143 antennas are supplied individually calibrated with data providing the free space antenna factor and gain using our custom designed software on our UKAS test range.
All calibrations are traceable to national standards.

Alternative calibration methods can be offered if requested at time of order.

Options

UKAS Calibration

Schaffner EMC Systems is UKAS accredited for antenna calibration and can offer a UKAS calibration as an additional costed option.

UKAS calibration provides reduced measurement uncertainties and additional data includes the voltage reflection coefficient for calculation of measurement uncertainties. Data is provided on disk as well as in graphic and tabulated format as hard copy.

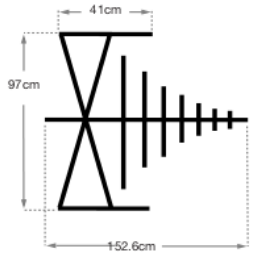

11

- Immunity testing to 300 watts
- Excellent symmetry ±1dB (typically better than ±0.5dB)
- Improved high frequency gain
- No rotational offsets

Typical Antenna Factor

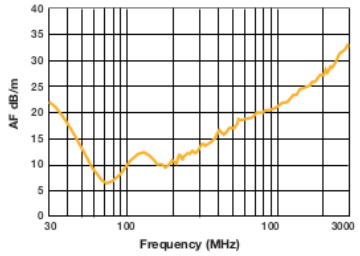

Typical VSWR

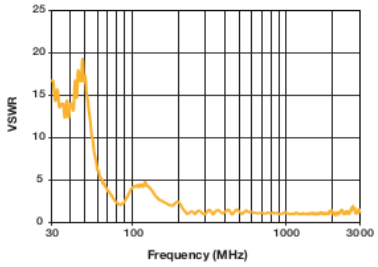

Typical Balance

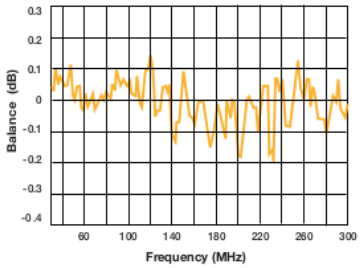

Gain dB

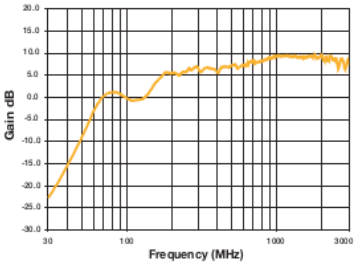

Gain Ratio

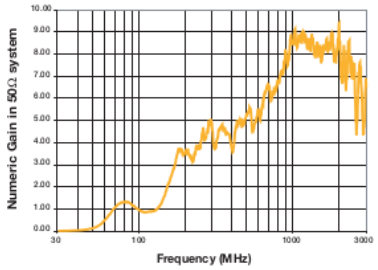

10V/m Power Requirement

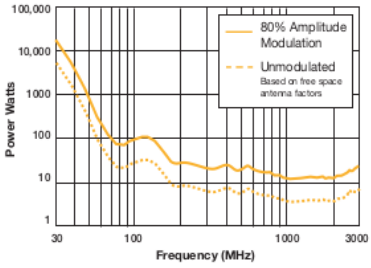

Typical Polar Plot
Horizontal

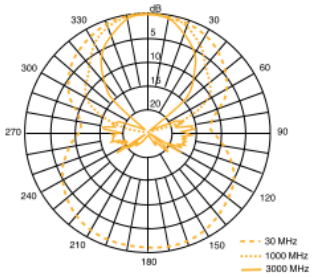

Technical Specifications	CBL 6143
Frequency range	30MHz - 3GHz
Impedance (nominal)	50Ω
Typical gain	6dB (200MHz-3GHz) / 8dB (700MHz-2.5GHz)
Connector	N type female
VSWR	Average 2:1
Max transmit power	300W CW
Size L x H x W cm	152.6 x 97 x 41
Weight	4.2kg

Annexure 3: RF-to-Fibre Converter RFoF-2G

RF Optic
Optical RF Test Equipment

RF over Fiber - RFoF-2.4GHz

Applications:

- *Telecommunication – Antenna remoting , long RF links via fiber*
- *Satcom*
- *GPS*
- *Radio Telescopes*
- *Distributed Antenna*

Key features:

- *Best Cost Performance*
- *Frequency Range: 0.05-2.4 GHz*
- *Compact unit*
- *Can be installed also in 1U*
- *Lightweight and small size*

RFOptic's analog RFoF compact modules convert RF signals to optical signals and back. One unit has an optical transmitter (Tx) converts RF to Optical signal, and second receiver unit (Rx) converts Optical to RF signal. The two units are connected by an optical fiber of the customer.

RFOptic's RF over Fiber modules (RFoF) are suitable for telecommunications and radar applications. Satellite, Point-to-Point antennas can be connected from several meters to many kilometers away from the control room. Base stations can be connected through fiber to remote sector antennas. Broadcasters can easily distribute their full RF streams over fiber to remote locations, therefore eliminating the need for complex equipment to be installed in far and hard to reach locations. With our wide-band units, cable operators can centrally locate their broadcasting equipment, and connect the RF through fiber to the remote location, thus reducing significantly the CAPEX and OPEX of their networks. Radar system houses can easily connect remote antenna elements using economical fiber. Phased array antennas can also use fiber to connect to their RF systems.

For further information, please visit our website: www.RFOptic.com

RF over Fiber - RFoF-2.4GHz

Table below describes the typical specifications of the RFoF-2.4GHz product.

Parameter	Unit	Specification (typical)
RF Tx-Rx link		
Frequency Range [1]	MHz	50 – 2,400
RF Gain	dB	7.5
Gain Flatness [1]	dB	+/-1.5
1dB input compression point	dBm	-5
VSWR	-	2:1
RF input signal range	dBm	(-65) - (-5)
Maximum input level	dBm	10
Noise Figure [2]	dB	28
Spurious signals [3]	dB	-70
Input and output impedance	Ohm	50
Optical and Electrical (Tx,Rx)		
Laser diode operating wavelength	µm	1.31±0.01
Receiver Photodiode operating wavelength	µm	1.2 – 1.65
Optical Power	dBm	1.5
Optical Connectors	-	FC/APC
RF input and output connectors	-	SMA
Electrical connectors [4]		DB9
Power [4]	VDC	5
Current consumption at 5VDC (Tx unit)	A	0.1
Current consumption at 5VDC (Rx unit)	A	0.05
LED status indicators (Tx./Rx.)	-	Green
Mechanical and Environmental (Tx,Rx)		
Dimensions of Transmitter	mm	80*55*22
Dimensions of Receiver	mm	80*55*22
Operating temperature range (Trans./ Rec.)	^{0}C	-10 to 55
Storage Temperature range (Trans./Rec.)	^{0}C	-40 to +85

[1] Maximum frequency is 2700 MHz
(2) Can be improved by high gain pre amplifier
[3] Excluding in-band harmonics.
[4] DB-9 pin layout table below.
[5] DB-9 female adaptor to 110/220 D AC adaptor is optional.

Pin Number	*Value*	*Usage*
1+2	*+5 VDC*	*operating voltage for RFoF Tx and Rx*
3	*NC*	*Not Connected*
4+5	*0*	*Ground*
6	*EN(TX)*	*for turn off externally the RFoF unit by +5VDC input*
7	*LED OUT*	*for customer's external LED (useful for integrators)*
8+9	*NC*	*Not connected*

D9 Male Layout

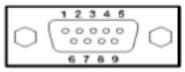

Annexure 4: Combiner Mini-Circuits ZFSC-8-43+

Coaxial

Power Splitter/Combiner

8 Way-0° 50Ω 10 to 1000 MHz

ZFSC-8-43+
ZFSC-8-43

BNC version shown
CASE STYLE: R29

Connectors	Model	Price	Qty.
BNC	ZFSC-8-43+	$138.95	(1-9)
SMA	ZFSC-8-43-S(+)	$163.95	(1-9)

+ RoHS compliant in accordance with EU Directive (2002/95/EC)

The +Suffix identifies RoHS Compliance. See our web site for RoHS Compliance methodologies and qualifications.

Maximum Ratings

Operating Temperature	-55°C to 100°C
Storage Temperature	-55°C to 100°C
Power Input (as a splitter)	1W max.
Internal Dissipation	0.62W max.

Coaxial Connections

SUM PORT	S(COM)
PORT 1,2,3,4,5,6,7,8	1,2,3,4,5,6,7,8

Features

- wideband, 10 to 1000 MHz
- good isolation, 25 dB typ.
- rugged shielded case

Applications

- VHF/UHF
- cellular
- signal processing
- communication systems

Outline Drawing

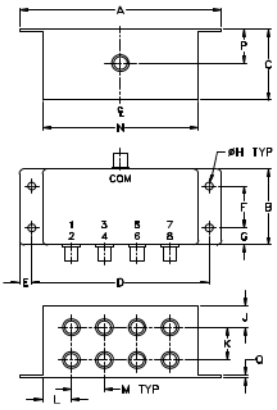

Outline Dimensions (inch / mm)

A	B	C	D	E	F	G	H
4.06	1.60	2.125	3.56	.25	.88	.36	.160
103.12	40.64	53.98	90.42	6.35	22.35	9.14	4.06

J	K	L	M	N	P	Q	R	wt.
.40	.69	.58	.66	3.13	.80	.06	.33	grams
10.16	17.53	14.73	16.76	79.50	20.32	1.52	8.38	350

Electrical Specifications

FREQ. RANGE (MHz)	ISOLATION (dB)						INSERTION LOSS (dB) ABOVE 9.0 dB						PHASE UNBALANCE (Degrees)			AMPLITUDE UNBALANCE (dB)		
	L		M		U		L		M		U		L	M	U	L	M	U
f_L-f_U	Typ.	Min.	Typ.	Min.	Typ.	Min.	Typ.	Max.	Typ.	Max.	Typ.	Max.	Max.	Max.	Max.	Max.	Max.	Max.
10-1000	23	20	25	20	26	20	1.0	1.6	1.4	2.1	2.1	2.9	5	10	20	0.4	0.4	0.7

L = low range [f_L to 10 f_L] M = mid range [10 f_L to f_U/2] U = upper range [f_U/2 to f_U]

Typical Performance Data

Freq. (MHz)	Insertion Loss (dB)						Amp. Unbal. (dB)	Isolation (dB)				Phase Unbal. (deg.)	VSWR S	VSWR 1	VSWR 8
	S-1	S-2	S-3	S-4	S-6	S-8		1-2	1-7	3-4	5-7				
10.00	9.95	9.94	9.95	9.94	9.89	9.89	0.07	27.78	52.68	27.78	27.70	0.12	1.34	1.26	1.25
26.00	9.86	9.86	9.86	9.86	9.85	9.85	0.02	31.14	51.33	31.16	31.08	0.21	1.17	1.23	1.23
42.00	9.83	9.84	9.84	9.83	9.83	9.83	0.01	31.95	48.73	31.96	31.83	0.18	1.14	1.22	1.22
100.00	9.84	9.84	9.84	9.85	9.85	9.85	0.02	31.74	43.64	31.80	31.64	0.34	1.13	1.22	1.21
160.00	9.89	9.89	9.89	9.89	9.89	9.89	0.02	30.68	40.72	30.81	30.56	0.54	1.15	1.21	1.20
220.00	9.95	9.95	9.96	9.96	9.96	9.96	0.03	29.66	38.76	29.83	29.55	0.78	1.17	1.20	1.19
280.00	9.99	10.00	10.00	10.00	10.00	9.99	0.04	28.77	37.34	28.96	28.65	0.98	1.16	1.19	1.18
380.00	10.04	10.03	10.05	10.05	10.04	10.03	0.06	27.86	36.10	28.11	27.79	1.37	1.11	1.19	1.17
500.00	10.12	10.11	10.16	10.12	10.12	10.09	0.12	26.96	35.80	27.27	27.02	1.77	1.08	1.19	1.16
620.00	10.22	10.21	10.27	10.24	10.24	10.17	0.17	25.42	36.97	25.78	25.71	2.16	1.21	1.20	1.17
740.00	10.24	10.23	10.33	10.27	10.27	10.18	0.25	23.45	39.94	23.83	23.91	2.68	1.34	1.21	1.17
840.00	10.29	10.28	10.40	10.37	10.35	10.21	0.31	22.13	43.13	22.49	22.67	3.18	1.33	1.20	1.17
920.00	10.40	10.37	10.53	10.48	10.45	10.30	0.39	21.60	41.79	21.97	22.23	3.68	1.23	1.18	1.16
960.00	10.43	10.40	10.58	10.52	10.49	10.32	0.43	21.52	39.68	21.88	22.19	4.09	1.15	1.18	1.16
1000.00	10.52	10.46	10.67	10.60	10.56	10.39	0.48	21.57	37.66	21.93	22.30	4.41	1.09	1.18	1.16

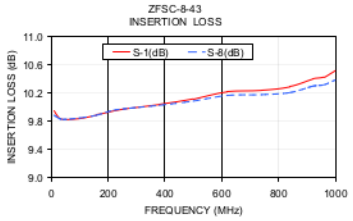

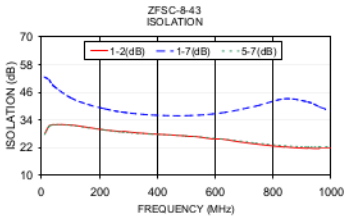

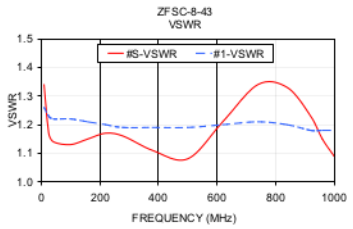

electrical schematic

Mini-Circuits®
ISO 9001 ISO 14001 CERTIFIED

ALL NEW minicircuits.com

REV. C
M113397
ZFSC-8-43
HY/TD/CP/AM
071022

P.O. Box 350166, Brooklyn, New York 11235-0003 (718) 934-4500 Fax (718) 332-4661 For detailed performance specs & shopping online see Mini-Circuits web site

The Design Engineers Search Engine Provides ACTUAL Data Instantly From MINI-CIRCUITS At: www.minicircuits.com

RF/IF MICROWAVE COMPONENTS

Annexure 5: Low-Pass Filter Mini-Circuits VLF-800

Coaxial

Low Pass Filter

VLF-800+
VLF-800

50Ω *DC to 800 MHz

Maximum Ratings

Operating Temperature	-55°C to 100°C
Storage Temperature	-55°C to 100°C
RF Power Input*	10W max. at 25°C
DC Current Input to Output	0.5A max. at 25°C

** Passband rating, derate linearly to 3.5W at 100°C ambient.*
Permanent damage may occur if any of these limits are exceeded.

Features

- rugged uni-body construction, small size
- 7 sections
- excellent power handling, 10W
- temperature stable
- low cost
- protected by U.S. Patent 6,943,646

CASE STYLE: FF704

Connectors	Model	Price	Qty.
SMA	VLF-800(+)	$21.95 ea.	(1-9)

+RoHS Compliant
The +Suffix identifies RoHS Compliance. See our web site for RoHS Compliance methodologies and qualifications

Applications

- harmonic rejection
- transmitters/receivers
- lab use

Outline Drawing

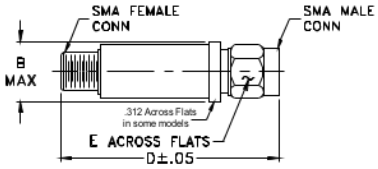

Outline Dimensions (inch / mm)

B	D	E	wt
.410	1.43	.312	grams
10.41	36.32	7.92	10.0

Electrical Specifications at 25°C

PASSBAND (MHz) (loss < 1 dB) Max.	fco, MHz Nom. (loss 3 dB) Typ.	STOP BAND (MHz) (loss, dB) f 20 Min.	30 Typ.	fr 20 Typ.	VSWR (:1) Stopband Typ.	Passband Typ.	NO. OF SECTIONS
*DC-800	1075	1275	1350-4850	5100	20	1.2	7

** Not for use with DC voltage at input and output ports*

typical frequency response

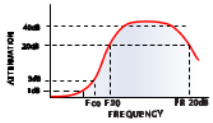

electrical schematic

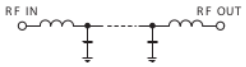

Typical Performance Data at 25°C

Frequency (MHz)	Insertion Loss (dB)	VSWR (:1)
10	0.06	1.01
100	0.14	1.06
300	0.26	1.10
600	0.46	1.14
800	0.71	1.13
1000	1.66	1.29
1075	3.38	1.88
1120	7.07	3.86
1170	14.92	8.72
1275	29.63	18.30
1350	32.29	23.18
2000	38.01	48.26
3000	48.80	54.29
4850	47.41	57.91
5100	31.24	49.64

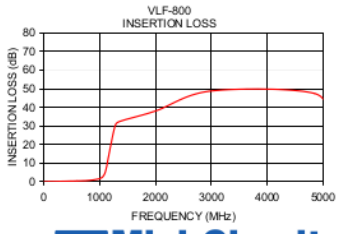

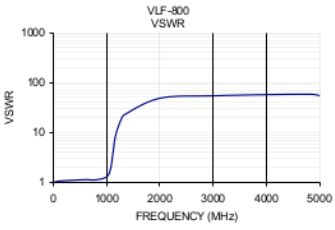

For detailed performance specs & shopping online see web site

Mini-Circuits®
ISO 9001 ISO 14001 AS9100 CERTIFIED

P.O. Box 350166, Brooklyn, New York 11235-0003 (718) 934-4500 Fax (718) 332-4661 *The Design Engineers Search Engine* Provides ACTUAL Data Instantly at minicircuits.com

IF/RF MICROWAVE COMPONENTS

REV. H
M129173
VLF-800
EDR-6608
RVN/AD/CP/AM
130117

Annexure 6: Low-Noise Amplifier Mini-Circuits Zx60-33 LN+

Coaxial

Low Noise Amplifier

ZX60-33LN+

50Ω 50 to 3000 MHz

Features

- wide bandwidth, 50 to 3000 MHz
- low noise figure 1.1 dB typ.
- output power, up to 17.5 dBm typ.
- protected by US patent 6,790,049

Applications

- front-end amplifier
- cellular
- GPS
- bluetooth
- lab
- instrumentation
- test equipment

Case Style: GC957

Connectors	Model	Price	Qty.
SMA	ZX60-33LN-S+	$79.95 ea.	(1-9)

+RoHS Compliant

The +Suffix identifies RoHS Compliance. See our web site for RoHS Compliance methodologies and qualifications

Electrical Specifications at 25°C

Parameter	Condition(MHz)	Min	Typ.	Max.	Units
Frequency	–	50	–	3000	MHz
Noise Figure		–	1.1	1.9	dB
Gain	100 1000 2000 3000	– – 13 –	21.9 18.8 14.5 11.9	– – – –	dB
Gain Flatness		–	–	–	dB
Output Power at 1dB compression		14.5	16.5	–	dBm
Output third order intercept point		–	+32	–	dBm
Input VSWR		–	2.0	–	:1
Output VSWR		–	1.6	–	:1
Active Directivity		–	–	–	dB
DC Supply Voltage		–	5	–	V
Supply Current		–	70	80	mA

Outline Drawing

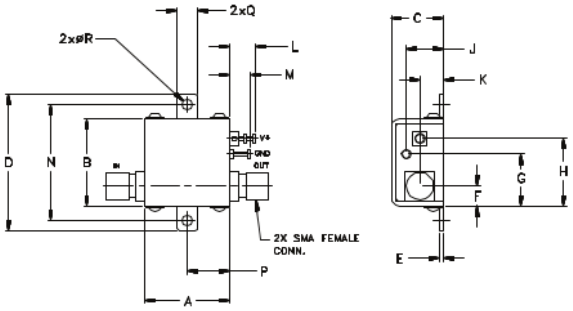

Maximum Ratings

Parameter	Ratings
Operating Temperature	-40°C to 85°C Case
Storage Temperature	-55°C to 100°C
DC Voltage	5.5 V
Input RF Power (no damage)	+13 dBm
Power Dissipation	0.44W

Permanent damage may occur if any of these limits are exceeded.

Outline Dimensions (inch / mm)

A	B	C	D	E	F	G	H	J	K	L	M	N	P	Q	R	wt
.74	.75	.46	1.18	.04	.17	.45	.59	.33	.21	.22	.18	1.00	.37	.18	.106	grams
18.80	19.05	11.68	29.97	1.02	4.32	11.43	14.99	8.38	5.33	5.59	4.57	25.40	9.40	4.57	2.69	23.0

Notes

A. Performance and quality attributes and conditions not expressly stated in this specification document are intended to be excluded and do not form a part of this specification document.
B. Electrical specifications and performance data contained in this specification document are based on Mini-Circuit's applicable established test performance criteria and measurement instructions.
C. The parts covered by this specification document are subject to Mini-Circuits standard limited warranty and terms and conditions (collectively, "Standard Terms"); Purchasers of this part are entitled to the rights and benefits contained therein. For a full statement of the Standard Terms and the exclusive rights and remedies thereunder, please visit Mini-Circuits' website at www.minicircuits.com/MCLStore/terms.jsp

Mini-Circuits®
www.minicircuits.com P.O. Box 35166, Brooklyn, NY 11235-0003 (718) 934-4500 sales@minicircuits.com

REV. A
M116867
ZX60-33LN+
ED-12875/2
MM/CP/AM
130710
Page 1 of 2

Typical Performance Data/Curves **ZX60-33LN+**

FREQUENCY (MHz)	GAIN (dB)		DIRECTIVITY (dB)		VSWR IN (:1)		VSWR OUT (:1)		NOISE FIGURE (dB)		POUT at 1dB COMPR. (dBm)		IP3 (dBm)	
	3V	5V	3V	5V	3V	5V	3V	5V	3V	5V	3V	5V	3V	5V
50.00	21.75	21.99	5.60	5.48	1.89	1.93	1.26	1.27	1.26	1.60	16.47	17.63	28.47	31.95
100.00	21.65	21.94	5.12	4.98	1.78	1.85	1.15	1.12	0.96	1.11	16.67	17.55	28.75	32.29
200.00	21.54	21.84	5.05	4.95	1.77	1.85	1.08	1.07	1.09	0.97	16.68	17.71	29.11	32.08
300.00	21.34	21.63	5.24	5.24	1.79	1.88	1.05	1.11	0.90	0.98	16.66	17.66	29.31	32.09
400.00	21.06	21.32	5.64	5.74	1.83	1.93	1.03	1.16	0.92	0.99	16.93	17.86	29.63	32.27
500.00	20.71	20.94	6.09	6.37	1.88	1.99	1.04	1.22	0.92	1.01	16.83	17.87	29.86	32.51
600.00	20.28	20.47	6.67	7.17	1.94	2.05	1.07	1.28	0.94	1.04	16.94	17.88	29.59	32.48
700.00	19.61	19.76	7.73	8.45	1.87	1.98	1.14	1.35	1.20	1.30	16.80	17.87	29.35	32.33
800.00	19.37	19.46	7.82	8.83	2.03	2.16	1.15	1.40	0.95	1.04	16.79	17.80	29.32	32.03
900.00	19.11	19.19	8.08	9.32	1.78	1.90	1.20	1.42	0.95	1.03	16.61	17.66	29.23	31.29
1000.00	18.80	18.82	8.35	9.88	1.97	2.09	1.22	1.48	0.87	0.96	16.72	17.56	29.10	30.95
1500.00	16.71	16.54	10.35	13.28	2.16	2.27	1.42	1.76	0.85	0.95	15.92	16.91	28.04	30.66
2000.00	14.79	14.51	11.49	14.99	2.14	2.18	1.62	2.01	1.05	1.20	15.62	16.63	27.99	28.58
2500.00	13.42	13.11	11.42	14.60	2.00	1.94	1.75	2.15	1.03	1.18	16.37	16.83	27.92	28.55
3000.00	12.22	11.90	11.12	13.78	1.75	1.63	1.76	2.17	1.20	1.33	16.50	16.95	28.16	28.14

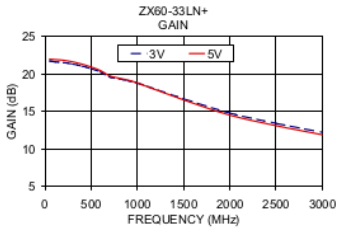

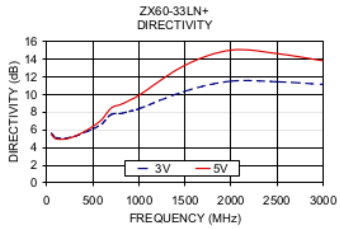

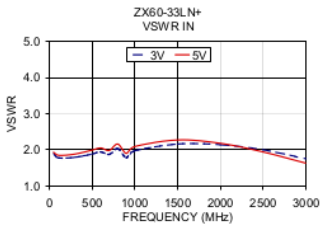

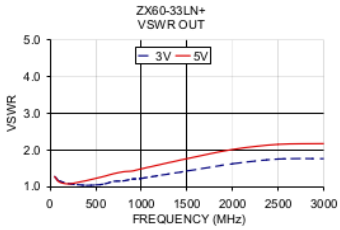

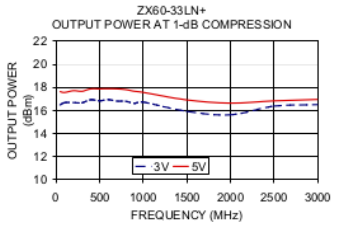

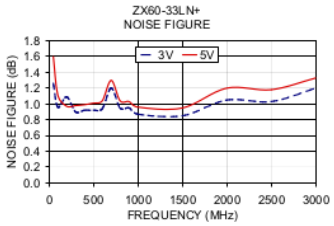

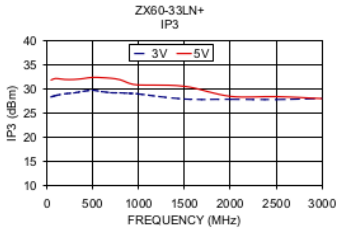

Notes
A. Performance and quality attributes and conditions not expressly stated in this specification document are intended to be excluded and do not form a part of this specification document.
B. Electrical specifications and performance data contained in this specification document are based on Mini-Circuit's applicable established test performance criteria and measurement instructions.
C. The parts covered by this specification document are subject to Mini-Circuits standard limited warranty and terms and conditions (collectively, "Standard Terms"); Purchasers of this part are entitled to the rights and benefits contained therein. For a full statement of the Standard Terms and the exclusive rights and remedies thereunder, please visit Mini-Circuits' website at www.minicircuits.com/MCLStore/terms.jsp

Annexure 7: Line Amplifier Mini-Circuits ZFL-1000 LN+

Coaxial

Low Noise Amplifier

ZFL-1000LN+

50Ω 0.1 to 1000 MHz

Features
- low noise figure, 2.9 dB typ.
- wideband, 0.1 to 1000 MHz
- protected by US Patent 6,943,629

Applications
- VHF/UHF
- cellular
- small signal amplifier

Case Style: Y460

Connectors	Model	Price	Qty.
SMA	ZFL-1000LN+	$89.95 ea.	(1-9)
BRACKET (OPTION "B")		$5.00	(1+)

+RoHS Compliant
The +Suffix identifies RoHS Compliance. See our web site for RoHS Compliance methodologies and qualifications

Electrical Specifications

Parameter	Frequency (MHz)	Min.	Typ.	Max.	Units
Frequency Range		0.1		1000	MHz
Noise Figure	0.1-1000	—	2.9	—	dB
Gain	0.1-1000	20	—	—	dB
Gain Flatness	0.1-1000	—	—	±0.5	dB
Output Power at 1 dB compression	0.1-1000	—	+3	—	dBm
Output third order intercept point	0.1-1000	—	+14	—	dBm
Input VSWR	0.1-1000	—	1.5	—	:1
Output VSWR	0.1-1000	—	2.0	—	:1
DC Supply Voltage		—	15	—	V
Supply Current		—	—	60	mA

Open load is not recommended, potentially can cause damage.
With no load derate max input power by 20 dB

Outline Drawing

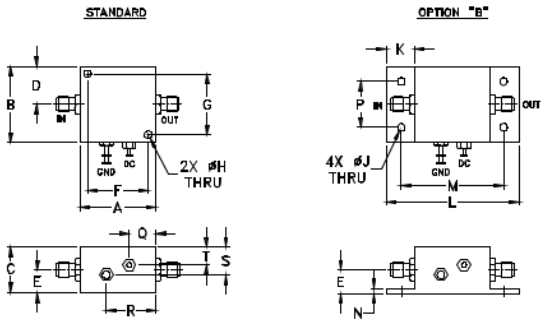

Maximum Ratings

Parameter	Ratings
Operating Temperature	-20°C to 71°C
Storage Temperature	-55°C to 100°C
DC Voltage	17V
Input RF Power (no damage)	+5 dBm

Permanent damage may occur if any of these limits are exceeded.

Outline Dimensions (inch / mm)

A	B	C	D	E	F	G	H	J	K	L	M	N	P	Q	R	S	T	wt.
1.25	1.25	.75	.63	.36	1.000	1.000	.125	.125	.46	2.18	1.688	.06	.750	.50	.80	.45	.29	grams
31.75	31.75	19.05	16.00	9.14	25.40	25.40	3.18	3.18	11.68	55.37	42.88	1.52	19.05	12.70	20.32	11.43	7.37	38

Notes
A. Performance and quality attributes and conditions not expressly stated in this specification document are intended to be excluded and do not form a part of this specification document.
B. Electrical specifications and performance data contained in this specification document are based on Mini-Circuit's applicable established test performance criteria and measurement instructions.
C. The parts covered by this specification document are subject to Mini-Circuits standard limited warranty and terms and conditions (collectively, "Standard Terms"); Purchasers of this part are entitled to the rights and benefits contained therein. For a full statement of the Standard Terms and the exclusive rights and remedies thereunder, please visit Mini-Circuits' website at www.minicircuits.com/MCLStore/terms.jsp

Mini-Circuits®
www.minicircuits.com P.O. Box 35166, Brooklyn, NY 11235-0003 (718) 934-4500 sales@minicircuits.com

REV. C
M121747
ZFL-1000LN+
131015
Page 1 of 2

FREQUENCY (MHz)	GAIN (dB)			DIRECTIVITY (dB)			VSWR (:1)		NOISE FIGURE (dB)	POUT at 1 dB COMPR. (dBm)
	12V	15V	16V	12V	15V	16V	IN	OUT	15V	15V
0.10	19.66	23.31	23.96	29.30	27.50	27.90	1.28	1.19	—	4.76
0.70	19.90	23.56	24.24	28.80	27.10	26.90	1.11	1.13	—	4.95
7.90	19.89	23.55	24.21	28.60	27.10	27.20	1.11	1.13	—	5.02
95.70	19.91	23.50	24.14	28.50	27.20	26.70	1.11	1.14	2.98	4.91
384.70	19.69	23.21	23.81	25.90	24.80	24.10	1.07	1.26	3.07	6.08
487.20	20.16	23.42	23.97	25.00	23.50	22.80	1.08	1.30	3.09	6.60
615.40	20.48	23.49	24.02	22.80	21.30	21.30	1.09	1.36	3.08	7.14
743.60	20.81	23.65	24.11	21.30	19.80	19.30	1.05	1.45	3.05	7.47
871.80	20.79	23.50	23.96	19.50	18.20	17.40	1.03	1.57	3.07	7.43
1000.00	20.84	23.32	23.66	18.10	16.60	16.20	1.06	1.71	3.11	7.00

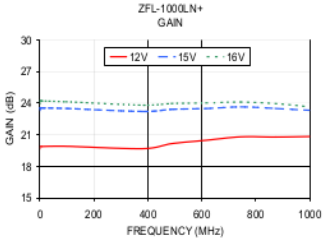

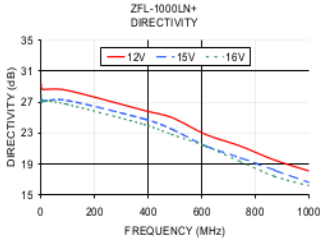

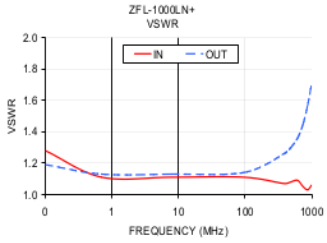

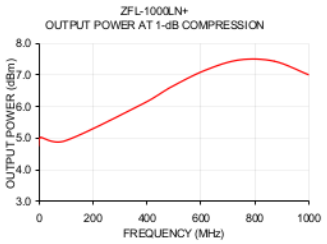

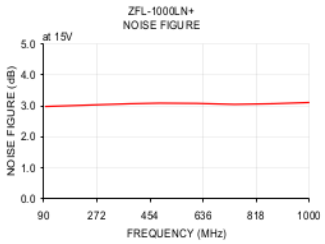

Notes
A. Performance and quality attributes and conditions not expressly stated in this specification document are intended to be excluded and do not form a part of this specification document.
B. Electrical specifications and performance data contained in this specification document are based on Mini-Circuit's applicable established test performance criteria and measurement instructions.
C. The parts covered by this specification document are subject to Mini-Circuits standard limited warranty and terms and conditions (collectively, "Standard Terms"); Purchasers of this part are entitled to the rights and benefits contained therein. For a full statement of the Standard Terms and the exclusive rights and remedies thereunder, please visit Mini-Circuits' website at www.minicircuits.com/MCLStore/terms.jsp

Annexure 8: Mixer Mini-Circuits Zx-05-11x

Coaxial

Frequency Mixer

ZX05-11X+
ZX05-11X

Level 7 (LO Power +7 dBm) 10 to 2000 MHz

CASE STYLE: FL905

Connectors	Model	Price	Qty.
SMA	ZX05-11X-S(+)	$37.95 ea.	(1-24)

+ RoHS compliant in accordance with EU Directive (2002/95/EC)

The +Suffix identifies RoHS Compliance. See our web site for RoHS Compliance methodologies and qualifications.

Maximum Ratings

Operating Temperature	-40°C to 85°C
Storage Temperature	-55°C to 100°C
RF Power	50mW
IF Current	40mA

Coaxial Connections

LO	1
RF	2
IF	3

Features

- rugged construction
- small size
- low convesion loss
- high L-R isolation
- protected by US Patents 6,133,525 and 6,790,049

Applications

- cellular
- PCS
- instrumentation
- satellite communication

Outline Drawing

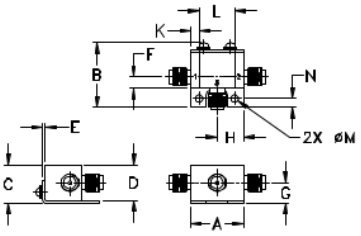

Outline Dimensions (inch / mm)

A	B	C	D	E	F	G
.74	.90	.54	.50	.04	.16	.29
18.80	22.86	13.72	12.70	1.02	4.06	7.37

H	J	K	L	M	N	wt
.37	--	.122	.496	.106	.122	grams
9.40	--	3.10	12.60	2.69	3.10	20.0

Electrical Specifications (T_{AMB}=25°C)

FREQUENCY (MHz)		CONVERSION LOSS (dB)				LO-RF ISOLATION (dB)						LO-IF ISOLATION (dB)						IP3 at center band (dBm)
		Mid-Band m			Total Range	L		M		U		L		M		U		
LO/RF f_L-f_U	IF	$\overline{X}$	σ	Max.	Max.	Typ.	Min.	Typ.	Min.	Typ.	Min.	Typ.	Min.	Typ.	Min.	Typ.	Min.	Typ.
10-2000	5-1000	7.1	0.1	8.2	9.8	62	45	36	20	27	18	60	45	37	20	38	20	9

1 dB COMP.: +1 dBm typ.

L = low range [f_L to 10 f_L] M = mid range [10 f_L to f_U/2] U = upper range [f_U/2 to f_U]
m = mid band [2f_L to f_U/2]

Typical Performance Data

Frequency (MHz)		Conversion Loss (dB)	Isolation L-R (dB)	Isolation L-I (dB)	VSWR RF Port (:1)	VSWR LO Port (:1)
RF	LO	LO +7dBm	LO +7dBm	LO +7dBm	LO +7dBm	LO +7dBm
10.10	40.10	6.84	74.97	78.47	1.03	2.59
50.10	80.10	6.84	61.40	64.93	1.03	2.58
100.10	130.10	6.91	55.74	58.48	1.04	2.52
206.16	236.16	6.98	51.92	52.08	1.12	2.54
318.28	288.28	7.08	48.10	48.28	1.20	2.58
430.40	400.40	7.13	44.07	45.47	1.38	2.53
542.52	512.52	7.20	40.20	43.42	1.60	2.54
654.65	624.65	7.32	38.92	41.99	1.84	2.66
766.77	736.77	7.40	35.90	39.98	2.01	2.62
878.89	848.89	7.26	35.13	37.69	1.99	2.63
1000.10	970.10	7.11	33.55	36.59	1.90	2.90
1103.13	1073.13	7.02	30.72	35.49	1.80	2.94
1215.25	1185.25	7.15	29.08	34.26	1.81	2.84
1327.37	1297.37	7.25	29.09	33.25	1.67	2.90
1439.49	1409.49	7.22	31.00	33.11	1.43	2.90
1551.62	1521.62	7.31	33.01	33.10	1.21	2.64
1663.74	1633.74	7.52	30.60	34.88	1.05	2.63
1775.86	1745.86	7.90	27.23	36.31	1.12	2.57
1887.98	1857.98	8.28	25.73	34.43	1.37	2.53
2000.10	1970.10	8.81	26.34	34.73	1.68	3.08

Electrical Schematic

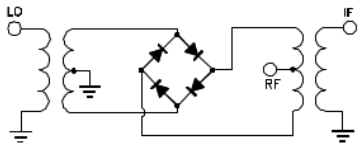

Mini-Circuits®
ISO 9001 ISO 14001 CERTIFIED
ALL NEW minicircuits.com
P.O. Box 350166, Brooklyn, New York 11235-0003 (718) 934-4500 Fax (718) 332-4661 For detailed performance specs & shopping online see Mini-Circuits web site
The Design Engineers Search Engine Provides ACTUAL Data Instantly From MINI-CIRCUITS At: www.minicircuits.com
RF/IF MICROWAVE COMPONENTS
REV. C
M98898
ZX05-11X
RVN/TD/CP/AM
070430
Page 1 of 2

Performance Charts

ZX05-11X
at IF Freq of 30 MHz CONVERSION LOSS

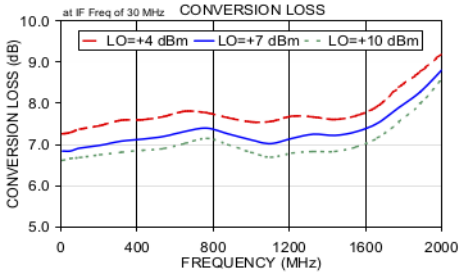

ZX05-11X
L-R ISOLATION

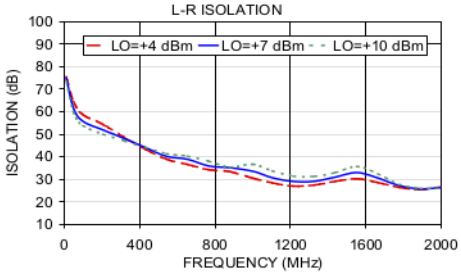

ZX05-11X
L-I ISOLATION

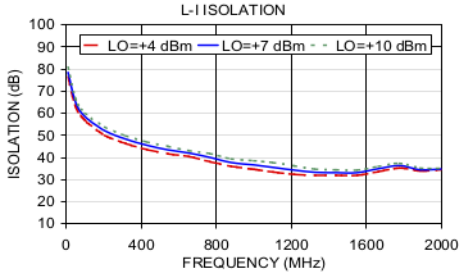

ZX05-11X
RF VSWR

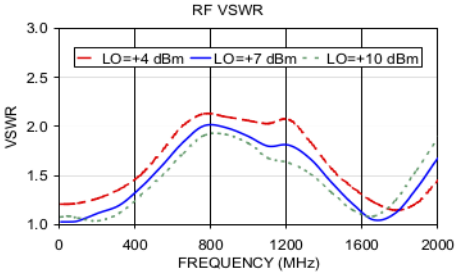

ZX05-11X
LO VSWR

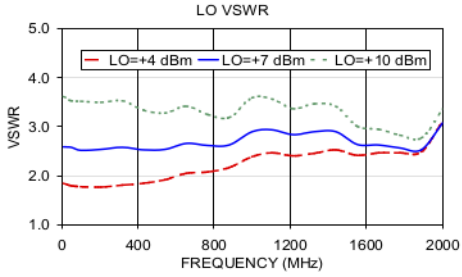

ZX05-11X
IF VSWR

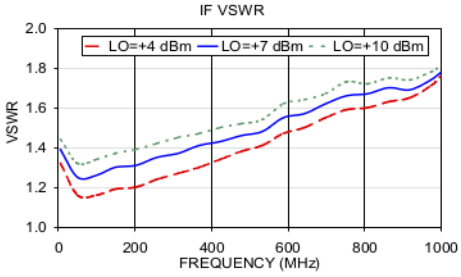

ZX05-11X
IP3

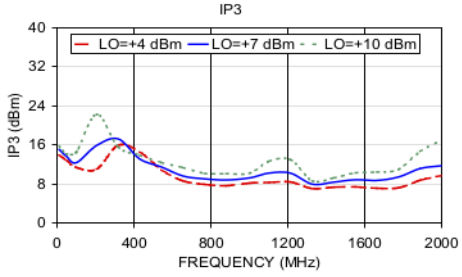

Annexure 9: USRP Network Devices

Ettus Research™

USRP™ N200/N210 NETWORKED SERIES

FEATURES:

- Use with GNU Radio, LabVIEW™ and Simulink™
- Modular Architecture: DC-6 GHz
- Dual 100 MSPS, 14-bit ADC
- Dual 400 MSPS, 16-bit DAC
- DDC/DUC with 25 mHz Resolution
- Up to 50 MHz GigE Streaming
- Fully-Coherent MIMO Capability
- Gigabit Ethernet Interface to Host
- 2 Gbps Expansion Interface
- Spartan 3A-DSP 1800 FPGA (N200)
- Spartan 3A-DSP 3400 FPGA (N210)
- 1 MB High-Speed SRAM
- Auxiliary Analog and Digital I/O
- 2.5 ppm TCXO Frequency Reference
- 0.01 ppm w/ GPSDO Option

N200/N210 PRODUCT OVERVIEW:

The Ettus Research™ USRP™ N200 and N210 are the highest performing class of hardware of the USRP (Universal Software Radio Peripheral) family of products, which enables engineers to rapidly design and implement powerful, flexible software radio systems. The N200 and N210 hardware is ideally suited for applications requiring demanding RF streaming performance including those covering advanced physical layer design and prototyping, dynamic spectrum access and cognitive radio, spectrum monitoring and signal intelligence, record and playback, and even network deployment.

The Networked Series products offer MIMO and high bandwidth/high dynamic range capabilities, in addition to higher speed and higher resolution ADCs/DACs, to meet the requirements for more demanding applications, enhance measurement sensitivity and dynamic range. The GigE interface serves as the connection between the N200/N210 and the host computer enables the user to realize real-time bandwidth 50 MHz in the receive and 25 MHz in the transmit directions simultaneously (full duplex).

The Networked Series MIMO connection is located on the front panel of each unit. Two Networked Series units may be connected to realize a complete 2x2 MIMO configuration using the optional MIMO cable. The N200 and N210 are largely the same, except that the N210 features a larger FPGA than the N200 for those customers wanting to extend the FPGA-based signal processing capabilities.

The USRP Hardware Driver™ is the official driver for all Ettus Research products. The USRP Hardware Driver supports Linux, Mac OSX, Windows, NetBSD and FreeBSD.

USRP™ N200/N210 NETWORKED SERIES

SPECIFICATIONS

Spec	Typ.	Unit
POWER		
DC Input	6	V
Current Consumption	1.3	A
w/ WBX Daughterboard	2.3	A
CONVERSION PERFORMANCE AND CLOCKS		
ADC Sample Rate	100	MSPS
ADC Resolution	14	bits
ADC Wideband SFDR	88	dBc
DAC Sample Rate	400	MSPS
DAC Resolution	16	bits
DAC Wideband SFDR	80	dBc
Sample Rate to/from Host (8b/16b)	50/25	MSPS
Frequency Accuracy	2.5	ppm
w/ GPSDO Reference	0.01	ppm

Spec	Typ.	Unit
RF PERFORMANCE (W/ WBX)		
SSB/LO Suppression	35/50	dBc
Phase Noise(1.8 Ghz)		
10 kHz	-80	dBc/Hz
100 kHz	-100	dBc/Hz
1 MHz	-137	dBc/Hz
Power Output	15	dBm
IIP3	0	dBm
Receive Noise Figure	5	dB
PHYSICAL		
Operating Temperature	0 to 55°	C
Dimensions (l x w x h)	22 x 16 x 5	cm
Weight	1.2	kg

* All specifications are subject to change without notice.

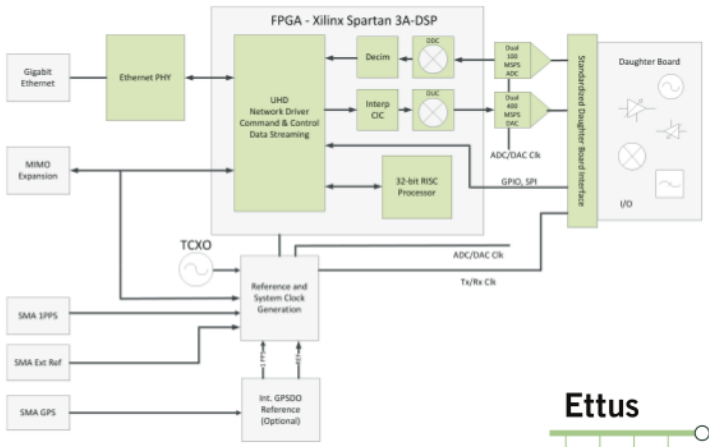

Ettus Research™

ABOUT ETTUS RESEARCH:

Ettus Research is an innovative provider of software defined radio hardware, including the original Universal Software Radio Peripheral (USRP) family of products. Ettus Research products maintain support from a variety of software frameworks, including GNU Radio. Ettus Research is a leader in the GNU Radio open-source community, and enables users worldwide to address a wide range of research, industry and defense applications. The company was founded in 2004 and is based in Mountain View, California. As of 2010, Ettus Research is a wholly owned subsidiary of National Instruments.

1043 North Shoreline Blvd
Suite 100
Mountain View, CA 94043

P 650.967.2870 www.ettus.com
F 866.807.9801

Annexure 10: Rubidium GPS10RBN

Precision Test Systems

GPS10RBN: 10 MHz, GPS Disciplined, Rubidium Frequency Standard

Key Features

- Completely self-contained unit. No extra P.C needed. Full information available via LCD.
- Rubidium Oscillator locked to GPS satellite signal. Accuracy to parts in 10^{-13} (Stratum 1 performance)
- Free run mode. Rubidium still gives an accurate output without a GPS satellite signal (Stratum 1)
- Two 1 pps time outputs. Typical error < 20 ns compared to UTC. Jitter < 300 ps
- Low Phase Noise, e.g. -135 dBc/Hz at 10Hz
- Multiple 10 MHz Outputs plus other outputs
- Windows software with full control and monitoring of the GPS10RBN via RS232, USB, Ethernet or the web.
- 19" 2U high rack mountable case.
- Very Low Microphonics
- Many options. See list of options in this brochure.
- Custom built options available upon request
- High quality design

General Description

The GPS10RBN is a 10 MHz, GPS disciplined, ultra low phase noise, rubidium frequency standard. It combines the short-term stability of an atomic rubidium oscillator with the long-term stability and traceability of the Global Positioning Service (GPS) set of satellites. The GPS10RBN achieves short and long-term frequency accuracy of parts in 10^{-13}. Thus the GPS10RBN exceeds the requirements of a Stratum 1 level frequency standard.

Options for the GPS10RBN include 5 to 20 isolated sinewave outputs, an antenna amplifier or fiber optic GPS link, enabling the antenna to be placed up to 1 km from the GPS10RBN, various fixed high frequency outputs, alarm relay outputs, redundancy, battery backup supply, time code outputs and a variable frequency output.

Ultra Low Phase Noise

The GPS10RBN has very low phase noise. Phase noise is -95 dBc/Hz at a 1 Hz offset with a -162 dBc/Hz noise floor. Low phase noise is a very important parameter. A typical plot of the phase noise is shown below. This phase noise can even be improved further with the ultra low phase noise option (option 26).

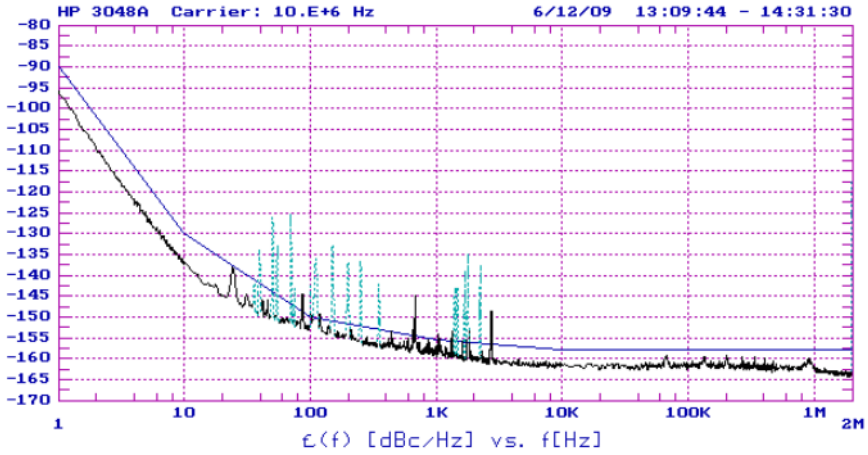

Accurate Timing Outputs

There are two 1 pps (pulse per second) outputs that are derived from the GPS receiver or the rubidium oscillator. The leading edge of the GPS 1 pps signal is aligned to UTC time ± 20 ns. The Rb 1 pps output signal has very low jitter of < 300 ps. These outputs can drive TTL levels into 50 Ω.

Keyboard Control and LCD Display

A 16-way keyboard is used to interface to three microprocessors that control the GPS10RBN. The LCD display's over 50 different menus. These menus show all the relevant information including time, position (longitude, latitude, height), number of satellite tracked, health of each satellite and the status of the rubidium oscillator.

Multiple Frequency Outputs

The GPS10RBN has many different output options. These outputs are:

Buffered 10 MHz sinewave outputs. Each output is fully isolated from each other. The amplitude of each output can be individually adjusted from 0 dBm to +13 dBm. Reverse isolation of each output is 130 dB and channel to channel isolation is typically 90 dB. Five outputs as standard. Up to 20 outputs can be optionally installed. Optional output level to +20 dBm is available. By connecting more distribution amplifiers, up to 1000 outputs can be realized, all delivering a low phase noise output.

- Optional square wave output that can drive TTL levels into a 50 Ω load impedance. The frequency of the square wave can be set to 10, 5, 2, 1, 0.1 MHz and 1 pps via the front panel keyboard.
- Dual one pulse per second outputs aligned to UTC, as mentioned above.
- Optional high frequency outputs can be specified at the time of ordering. These fixed high frequency outputs can be as high at 10 GHz (higher frequencies available upon special request) and are phase locked to the main frequency reference. Note: this option only generates one fixed frequency.

- Optional DDS Output enables the GPS10RBN to produce a sinewave and squarewave output that is locked to the GPS10RBN. The frequency range of this output is 1 µHz to 80 MHz (1 µHz steps).

- 10µHz to 1640 MHz (10 µHz steps). This option can be used to generate the popular 2048 kHz and 13 MHz frequencies as well as any frequency in the range 1 µHz to 80 MHz or 10 µHz to 1640 MHz.

- Optional Time Code Output. This option generates the industry standard IRIG-B, IRIG-E, SMPTE, NTP etc. Also a 48 bit BCD time code can be generated with option 16.

Free Run Mode. Ideal for portable applications

The GPS10RBN is normally operated with the Rubidium oscillator's 10 MHz output, locked to the GPS satellite system. In the event of a failure of the GPS signal for any reason, the GPS10RBN will automatically switch over to free run mode. In this mode, the GPS10RBN's Rubidium Oscillator still achieves Stratum 1 performance over a 72 hour period.

Also the GPS10RBN can be used for portable applications where a satellite signal is not available, or the time required to lock the GPS10RBN is not available. When the GPS10RBN is powered up it can be set to the free run mode. The Rubidium Oscillator "remembers" the last known good frequency setting and adjusts itself to this frequency. Thus an accurate 10 MHz is available within a few minutes of switch on. This mode is ideal for setting up GSM base stations that require an accurate time base for frequency measurement.

RS232 and USB Interface

The RS232 interface allows complete control and interrogation of the GPS10RBN. Optional USB or Ethernet adapters allows the GPS10RBN to be controlled via the USB port of the PC or from a network.

GPS10RBN Rear panel

Options

The GPS10RBN has many options enabling it to work in varied applications. Not all options can be installed at the same time. Some options require a separate case. Some of the options are listed below:

Option 01 and 02: Second Frequency Output, 0 to 500 MHz spot frequency and 500 to 1 GHz spot frequency
This option gives a second frequency output. The frequency is fixed and cannot be changed. The spot frequency must be advised by the customer prior to manufacture. The frequency can be in the range 0 to 1 GHz. Some examples are shown below:

01A	500 MHz Square x 1	01E	10.24 MHz Sine x 5	01J	5 MHz Sine x 5	01N
01B	100 MHz Sine x 1	01F	8.0 MHz Sine x 5	01K	1 MHz Sine x 5	01P
01C	10.23 MHz Sine x5	01G	100 MHz Sine ULN	01L	100 kHz Sine x 5	01Q
01D	10.24 MHz Sine x 1	01H	16 MHz Sine ULN	01M	5 MHz x 5 LN	01R

Option 02Aand option 02B. : Second Variable Frequency Output, 780 to 820 MHz or 800 to 1200 MHz.
This option gives a second frequency output. The frequency is variable and can be changed from 780 MHz to 820 MHz or 800 - 1200 MHz in 100 kHz steps. The frequency output has good phase noise and low spurious.

Option 03: Second Frequency Output, 1 GHz to 3.2 GHz spot frequency
This option gives a second frequency output. The frequency is fixed and cannot be changed. The spot frequency must be advised by the customer prior to manufacture. The frequency can be in the range 1 GHz to 3.2 GHz.

Option 03A: Second Variable Frequency Output, 2.25 GHz to 2.65 GHz
This option gives a second frequency output. The frequency is variable and can be changed from 2.25 GHz to 2.65 GHz in 100 kHz steps. The frequency output has good phase noise and low spurious.

Option 04 and Option 35: Antenna Amplifier /Fiber Optic Link
These options can be used to extend the range between the GPS antenna and the GPS10RBN. Up to 300 m (1000 feet) can be realized with a cable and amplifier, up to 1 km (3200 feet) with a fiber optic GPS link.

Option 05, 05A and 05B: DDS Signal Generator
Option 05 adds a DDS (direct digital synthesis) signal output to the GPS10RBN. The DDS output has a squarewave and sinewave output. The frequency of this output is adjustable from 1 µHz to 80 MHz in steps of 1 µHz.

Option 06: RS232 Cable
The RS232 cable connects the GPS10RBN to a PC enabling control and interrogation of the GPS10RBN.

Option 07, 07A and 07B: Alarm Relay/TTL Output
This option adds an alarm output. Option 07 and 07A add a dual changeover relay that is activated in the event of an alarm. Each relay contact is rated at 30 VDC and 1 Amp (5A for Option 07A). Option 07B is a TTL output signal only.

Option 08: Redundancy
Option 08 adds redundancy. With this option, two GPS10RBN's can be configured into a redundancy set-up with five main 10 MHz outputs (up to 20 outputs optionally available). Normally one unit will supply the 10 MHz outputs (locked to the GPS satellite). In the event of failure of this unit, the 10 MHz outputs will be automatically switched to the second GPS10RBN unit. The second GPS10RBN unit will then supply the 10 MHz outputs, locked to the GPS system.

Even if both GPS antennas are disconnected, and one unit completely fails, there will still be a 10 MHz from the second unit running from the rubidium oscillator. Both units are identical; there is no master or slave. Simply, whatever unit is healthy will supply the 10 MHz output. System status is available via the RS232 interface. This option is ideal for applications that require extra security. Extra 10 MHz outputs can be added if required.

Option 09: IRIG-B Output
This option gives the industry standard IRIG-B or IRIG-E time code output. The output can be internally set to give an AM modulated signal or TTL output.

Option 11: Clock / Date Display Unit
Option 11 provides a remote Clock / Date display. The display consists of a 6 digit 25 mm high digital LED display that can be read from a distance of 10 meters.

Option 12: Additional sinewave outputs
The GPS10RBN has five isolated 10 MHz sinewave outputs. Option 12 adds a further outputs up to 20 in total.

Option 12A: 10.23 MHz Outputs
This option changes the five sinewave outputs to 10.23 MHz. A rear panel input connector allows the DDS option (option 05) to generate 10.230 MHz and be available on these five isolated outputs.

Option 13: Mute Sinewave Outputs in the event of an alarm
This option disables all the sinewave outputs in the event of an alarm or error.

Option 14: Service manual. The service manual has service information and realignment procedures.

Option 15: Windows Software

This windows software operates on Windows 2000/XP/Vista. It allows all the main parameters of the GPS10RBN to be monitored and recorded by the PC.

Option 16: BCD Time Code Output
This option gives a 48 bit BCD time code output. The time output is in the format HH:MM:SS.sssssss. The fractional seconds have a resolution of 100 ns. The output is updated every 100 ns and is accurate to UTC to within 200 ns.

Option 18: Ethernet Port
This option adds an Ethernet port. This allows the GPS10RBN to be controlled and monitored via an Ethernet network or internet.

Option 19: +24VDC Input or Option 19B: +12 VDC input
This option allows the GPS10RBN to be externally powered by a +12 or +24 VDC supply. In the event of AC power being lost, the GPS10RBN will instantly switch over to the external DC supply.

Option 20: 2.048 MHz G703:10 output
This option gives the popular 2.048 MHz output. The output is a squarewave with amplitude of ± 1.2 V in 75 Ω

Option 21: Lightening Protection
This option adds lightening protection to the antenna input. The protection is placed close to the GPS antenna.

Option 22: 0 to 1640 MHz DDS Output
This option adds a DDS output. The output can be set anywhere from 0 to 1640 MHz in 10 µHz steps.

Option 23: GSM Interface
This option enables the GPS10RBN to send a SMS (short message service) or text to ten GSM mobile phones in the event of an error.

Option 24: Frequency Change to 5 MHz (also requires option 12 additional 5 outputs to be installed)
This option changes all sinewave outputs to 5 MHz instead of 10 MHz. A 10 MHz output is still available.

Option 25: USB Adapter. Allows GPS10RBN to be controlled from a USB port of a PC.

Option 26: Ultra Low Phase Noise: Phase noise is -113 dBc/Hz at 1 Hz with a -170 dBc/Hz noise floor.

Option 28: Control of GPS10RBN over the internet: Ideal for remote monitoring of the GPS10RBN.

Option 30, 30A, 30B: Squarewave and Pulse Outputs
Opt 30: Squarewave Output. Gives a TTL output switchable in frequency to 10, 5, 2, 1, 0.1 MHz and 1 pps.
Opt 30A: 5 x squarewave outputs at 1 MHz (other frequencies available)
Opt 30B: Pulse Output. 5 x pulse outputs, each can be individually set to 1 PPS, 10 PPS, 100 PPS, 1k PPS or 10k PPS

Option 32: Slave Output.
Adds a slave 10 MHz output. This can be used to connect further distribution amplifiers to the GPS10RBN.

Option 33: Carrying Case. A plastic carrying case with foam insert is used to carry and protect the GPS10RBN

Option 34: High Power Outputs. The 10 MHz output levels are increased to a maximum of +20 dBm.

Option 35: Fiber Optic Link for Antenna: Allows GPS Antenna to be located up to 1 km away from GPS10RBN.

Option 36: Fiber Optic 10 MHz Output
This option adds a fiber optic output together with a fiber optic receiver. This allows the 10 MHz output to be routed over very long distances using fiber optic cable.

Option 37: Guaranteed Phase Noise Specifications: Phase noise plots of every output included.

Option 38: NTP Server: NTP Server Output via the Ethernet.

Option 39: 2nd RS232 Port: A second RS232 port to be used with various options, freeing up original interface.

Option 40A and 40 B External Locking Inputs: Allows GPS10RBN to be locked to external 10 MHz or 1 pps signals

Option 42: Different Connectors: The standard BNC connectors can be replaced with TNC, SMA or other types

Applications

Applications of the GPS10RBN include, but are not limited to, the following examples:

- Reference frequency source in a calibration or standards laboratory
- Portable frequency standard
- Calibration of GSM Base Station Clocks
- Reference Frequency and Time source for the electricity generating industry
- Synchronizing of telecommunication and computer networks
- Space Measurements.

High Quality of Construction

The GPS10RBN is made to the highest standards. A purpose built aluminum 19" rack mount case houses all the circuits inside the GPS10RBN. The GPS10RBN is CE marked for sale within the EEC.

Active Antenna Supplied as Standard

The GPS10RBN is supplied with an active antenna. This small unit can be easily fitted to buildings, roofs etc.

GPS10RBN Specifications

Description	Specification	Remarks
10 MHz Outputs		
Connector	Rear panel BNC socket	
Frequency	10 MHz	
Accuracy	Refer to Allan Deviation section	
Signal Type / Amplitude	Sine wave @ 0 dBm to + 13 dBm	Internally adjustable
Harmonic Distortion / Spurious	-30 dBc / - 120 dBc (> 0.5 MHz)	
Return Loss	> 23 dB @ 10 MHz	
Reverse / Channel to Channel Isolation	> 130 dB / 90 dB	
Squarewave Output (Option 30 required)		
Frequency	10, 5, 2, 1, 0.1 MHz and 1 pps	
Accuracy	Refer to Allan Deviation section	Selectable by keyboard
Amplitude (open circuit / 50 ohm)	0 to 5 V / 2.7 V , TTL Compatible	
1 PPS Outputs		
Connector	Rear panel BNC socket	
Frequency	1 pulse per second	
Amplitude (open circuit)	0 to 5 V, TTL Compatible	
Amplitude (50 ohm)	0 to > 2.5 V, TTL Compatible	
Accuracy to UTC time (GPS 1 pps output)	< 20 ns (6 sigma)	
Jitter of Rubidium Osc. 1 pps output	< 300 ps	After cable delays taken into account
Slave Output (Option 32 required)		
Connector	Rear panel BNC socket	
Frequency	10 MHz	
Accuracy	Refer to Allan Deviation section	
Signal Type	Sine wave	
Amplitude	> 3 dBm	Fixed level output
Harmonic Distortion	- 20 dBc	Typically -40 dBc

Phase Noise Response (Typical). 10 MHz Outputs		
At 1 Hz Offset	-95 dBc/Hz	
At 10 Hz Offset	-135 dBc/Hz	
At 100 Hz Offset	-152 dBc/Hz	
At 1 kHz Offset	-157 dBc/Hz	
At 10 kHz Offset	-162 dBc/Hz-	
At 100 kHz Offset	-162 dBc/Hz	
Allan Deviation when locked to GPS Satellites (typical)		
Observation Time 1 / 10 seconds	$<2 \times 10^{-11}$ / $< 1 \times 10^{-11}$	GPS10RBN in full lock for > 1 week. > 3
Observation Time 100 / 1000 seconds	$< 2 \times 10^{-12}$ / $< 7 \times 10^{-13}$	satellites in view. Ambient temperature
Observation Time 10k / 100k seconds	$< 6 \times 10^{-13}$ / $< 7 \times 10^{-13}$	0 °C to +50 °C. Temperature change less
Observation Time 1 week	$< 2 \times 10^{-13}$ /	than 3 °C per hour
Rubidium Drift when GPS10RBN NOT Locked to GPS Satellites		
Drift due to aging	$< 5 \times 10^{-11}$ per month	After 30 days operation
Drift due to temperature	$< 5 \times 10^{-11}$	0 °C to +50 °C
GPS Receiver		
Number of Channels / Frequency	12 parallel / 1575.42 MHz	Simultaneous operation / L1 Frequency
Acquisition Time / Positioning Accuracy	< 50 s typical / < 25 m	With current position / time data. No SA
Jamming Immunity	-79 dBm @ 1575.42 MHz	Measured at active antenna input
Antenna	Active micro strip patch	Powered by GPS10RBN
Miscellaneous		
Operating Temperature	0 °C to +50 °C	
Storage Temperature	-20 °C to +60°C	
Magnetic Field	$< 2 \times 10E^{-10}$ for 1 Gauss field reverse	
AC Power Inlet with switch	IEC320 power cord	Rear Panel
AC Voltage Range	100 - 240 VAC (usable 90-260 VAC)	Automatic switchover
Power consumption	50 watts typical operating, 100W warm-up	Warm up period is < 10 minutes at +20 °C
Fuse rating	3.15A, 250 VAC slow blow type	
Dimensions Width x Depth	482.6 mm x 323 mm	
Height and weight	88 mm and 7 kg	
Supplied Accessories		
Antenna	Active type, 5V @ 20 mA	
Power cord	IEC320 type	
Instruction manual		
Option 05: DDS Generator Output		
Overall Frequency Range / Step Size	1 µHz to 80 MHz in 1 µHz steps	Usable to 90 MHz
Frequency Accuracy	± 300 µHz plus main 10 MHz error	Subject to jitter specification
Sinewave Frequency Range	10 kHz to 80 MHz	
Sinewave Output level	> 0 dBm into 50 Ω	
Spurious and Harmonic Output	-40 dBc and -20 dBc respectively	Option > +10 dBm available (opt 05A)
Squarewave Frequency Range	1 µHz to 80 MHz	
Squarewave Output Level	0V to 3V nominal into open circuit	Use 50 ohm termination above 1 MHz
Allan deviation (100 second)	2.5×10^{-12}	> 0 dBm into 50 Ω (10 kHz – 80 MHz)
Output 09: IRIG Time Code Output		
Output types	IRIG-B or IRIG-E or ESE TC-90	Internally selectable
Mark – Space Ratio (IRIG-B)	3.3 to 1	
Output type (IRIG-B) / Impedance	TTL or AM. 2.7 V p-p / 600 Ω	Internally selectable
All other options		
Consult Precision Test Systems for further details of other options. Not all options can be fitted at the same time.		

Head Office - UK	South Africa	USA
Precision Test Systems LTD	Precision Test Systems cc	Precision Test Systems
The Studio, Whitehouse Farm	Gauteng	14781 Memorial Dr, Suite # 981
New Hall Lane, Mundon	South Africa	Houston
Maldon, Essex, CM9 6PJ, UK.	Fax: 08651 58198	Texas, 77079, USA
Tel: +44 (0) 870 368 9608	Email: sasales@ptsyst.com	Tel: 1 888 876 4804
Fax: +44 (0) 1245 330030	Web: www.ptsyst.com	Fax: 1 832 201 6564
Email: uksales@ptsyst.com		Email: usasales@ptsyst.com
Web: www.ptsyst.com		Web: www.ptsyst.com

Annexure 11: 5-way Splitter Mini-Circuits ZFSC-5-1

Coaxial

Power Splitter/Combiner

5 Way-0° 50Ω 1 to 300 MHz

ZFSC-5-1+
ZFSC-5-1

BNC version shown
CASE STYLE: G1170

Connectors	Model	Price	Qty.
BNC	ZFSC-5-1(+)	$99.95	(1-9)
SMA	ZFSC-5-1-S(+)	$99.95	(1-9)
BRACKET (OPTION "B")		$5.00	(1+)

+ RoHS compliant in accordance with EU Directive (2002/95/EC)

The +Suffix identifies RoHS Compliance. See our web site for RoHS Compliance methodologies and qualifications.

Maximum Ratings

Operating Temperature	-55°C to 100°C
Storage Temperature	-55°C to 100°C
Power Input (as a splitter)	1W max.
Internal Dissipation	0.5W max.

Permanent damage may occur if any of these limits are exceeded.

Coaxial Connections

SUM PORT	S
PORT 1	1
PORT 2	2
PORT 3	3
PORT 4	4
PORT 5	5

Features

- low insertion loss, 0.6 dB typ.
- excellent amplitude unbalance, 0.3 dB typ.
- rugged shielded case

Applications

- VHF
- instrumentation
- communications system

Outline Drawing

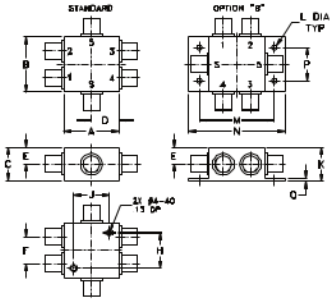

Outline Dimensions (inch / mm)

A	B	C	D	E	F	G	H
1.25	1.25	.75	.63	.38	.61	--	.80
31.75	31.75	19.05	16.00	9.65	15.49	--	20.32

J	K	L	M	N	P	Q	wt
.80	.76	.125	1.688	2.18	.75	.07	grams
20.32	19.30	3.18	42.88	55.37	19.05	1.78	85.0

Electrical Specifications

FREQ. RANGE (MHz)	ISOLATION (dB)						INSERTION LOSS (dB) ABOVE 7.0 dB						PHASE UNBALANCE (Degrees)			AMPLITUDE UNBALANCE (dB)		
	L		M		U		L		M		U		L	M	U	L	M	U
f_L-f_U	Typ.	Min.	Typ.	Min.	Typ.	Min.	Typ.	Max.	Typ.	Max.	Typ.	Max.	Max.	Max.	Max.	Max.	Max.	Max.
1-300	25	20	23	18	20	17	0.2	0.5	0.6	1.0	1.5	2.0	2	4	8	0.2	0.3	0.6

L = low range [f_L to 10 f_L] M = mid range [10 f_L to f_U/2] U= upper range [f_U/2 to f_U]

Typical Performance Data

Freq. (MHz)	Total Loss[1] (dB)					Amp. Unbal. (dB)	Isolation (dB)				Phase Unbal. (deg.)	VSWR S	VSWR OUTPUTS
	S-1	S-2	S-3	S-4	S-5		1-2	2-3	2-5	3-4			
1.00	7.14	7.14	7.15	7.15	7.14	0.00	51.33	51.91	37.56	49.97	0.07	1.08	1.10
2.60	7.13	7.13	7.13	7.13	7.14	0.01	51.90	51.80	39.59	51.00	0.04	1.06	1.08
4.20	7.13	7.14	7.14	7.14	7.14	0.01	50.50	50.57	39.90	49.85	0.04	1.06	1.07
7.00	7.14	7.14	7.14	7.15	7.15	0.00	48.39	48.53	39.74	47.90	0.04	1.06	1.07
10.00	7.16	7.16	7.15	7.16	7.16	0.01	46.46	46.75	39.40	46.14	0.07	1.06	1.07
46.00	7.24	7.24	7.23	7.24	7.24	0.01	36.33	36.72	35.07	36.29	0.24	1.10	1.06
82.00	7.29	7.29	7.28	7.28	7.28	0.01	32.10	32.52	32.12	32.16	0.29	1.16	1.06
118.00	7.40	7.39	7.38	7.37	7.40	0.03	29.53	29.93	30.08	29.63	0.43	1.21	1.07
138.00	7.43	7.41	7.40	7.40	7.41	0.03	28.52	28.95	29.27	28.63	0.52	1.24	1.07
150.00	7.43	7.41	7.41	7.40	7.42	0.03	28.02	28.43	28.86	28.13	0.51	1.25	1.08
202.00	7.61	7.58	7.56	7.55	7.59	0.06	26.36	26.81	27.56	26.48	0.78	1.30	1.11
254.00	7.68	7.63	7.62	7.60	7.64	0.08	25.44	25.94	27.07	25.58	0.98	1.31	1.15
284.00	7.82	7.77	7.76	7.73	7.78	0.09	24.91	25.38	26.83	25.00	1.09	1.31	1.18
292.00	7.78	7.73	7.71	7.68	7.75	0.10	24.72	25.17	26.71	24.79	1.18	1.31	1.18
300.00	7.70	7.65	7.62	7.61	7.67	0.10	24.51	24.95	26.55	24.56	1.18	1.31	1.19

1. Total Loss = Insertion Loss + 7dB splitter loss.

ZFSC-5-1
TOTAL LOSS

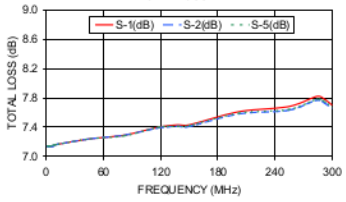

ZFSC-5-1
ISOLATION

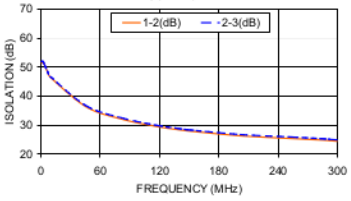

ZFSC-5-1
VSWR

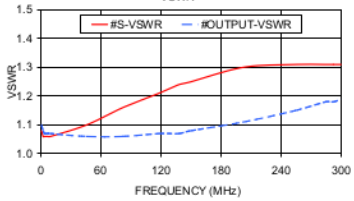

electrical schematic

Mini-Circuits®
ISO 9001 ISO 14001 AS9100 CERTIFIED

For detailed performance specs & shopping online see web site

P.O. Box 350166, Brooklyn, New York 11235-0003 (718) 934-4500 Fax (718) 332-4661 *The Design Engineers Search Engine Provides ACTUAL Data Instantly at* minicircuits.com

IF/RF MICROWAVE COMPONENTS

Notes: 1. Performance and quality attributes and conditions not expressly stated in this specification sheet are intended to be excluded and do not form a part of this specification sheet. **2.** Electrical specifications and performance data contained herein are based on Mini-Circuit's applicable established test performance criteria and measurement instructions. **3.** The parts covered by this specification sheet are subject to Mini-Circuits standard limited warranty and terms and conditions (collectively, "Standard Terms"); Purchasers of this part are entitled to the rights and benefits contained therein. For a full statement of the Standard Terms and the exclusive rights and remedies thereunder, please visit Mini-Circuits' website at www.minicircuits.com/MCLStore/terms.jsp.

REV. B
M127604
ZFSC-5-1
HY/TD/CP
120306

Annexure 12: 4-way Splitter Mini-Circuits ZMSC-4-2+

Coaxial

Power Splitter/Combiner

4 Way-0° 50Ω 0.002 to 20 MHz

ZMSC-4-2+
ZMSC-4-2

CASE STYLE: N24

Connectors	Model	Price	Qty.
SMA	ZMSC-4-2(+)	$76.95	(1-9)
BRACKET (OPTION "B")		$5.00	(1+)
BRACKET (OPTION "BR")		$1.50	(1+)

+ RoHS compliant in accordance with EU Directive (2002/95/EC)

The +Suffix identifies RoHS Compliance. See our web site for RoHS Compliance methodologies and qualifications.

Maximum Ratings

Operating Temperature	-55°C to 100°C
Storage Temperature	-55°C to 100°C
Power Input (as a splitter)	1W max.
Internal Dissipation	0.250W max.

Permanent damage may occur if any of these limits are exceeded.

Coaxial Connections

SUM PORT	S
PORT 1	1
PORT 2	2
PORT 3	3
PORT 4	4

Features

- high isolation, 33 dB typ.
- rugged shielded case

Applications

- HF
- amateur radio

Outline Drawing

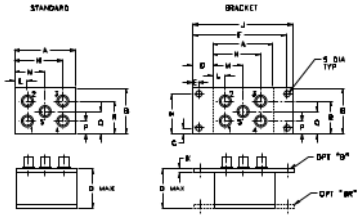

Outline Dimensions (inch / mm)

A	B	C	D	E	F	G	H	J
1.50	1.13	1.00	.50	.155	2.345	.138	.987	2.50
38.10	28.70	25.40	12.70	3.94	59.56	3.51	25.07	63.50

K	L	M	N	P	Q	R	S	wt
.10	.32	.75	1.18	.31	.56	.81	.150	grams
2.54	8.13	19.05	29.97	7.87	14.22	20.57	3.81	45.0

Electrical Specifications

FREQ.* RANGE (MHz)	ISOLATION (dB)						INSERTION LOSS (dB) ABOVE 6.0 dB						PHASE UNBALANCE (Degrees)			AMPLITUDE UNBALANCE (dB)		
	L		M		U		L		M		U		L	M	U	L	M	U
f_L-f_U	Typ.	Min	Typ.	Min	Typ.	Min	Typ.	Max.	Typ.	Max.	Typ.	Max.	Max.	Max.	Max.	Max.	Max.	Max.
0.002-20	30	20	33	25	33	25	0.45	0.75	0.3	0.5	0.7	1.0	4	6	8	0.15	0.20	0.25

L = low range [f_L to 10 f_L] M = mid range [10 f_L to f_U/2] U= upper range [f_U/2 to f_U]
* At low range frequency band (f_L to 10 f_L), linearly derate maximum power by 13dB.

Typical Performance Data

Freq. (MHz)	Total Loss[1] (dB)				Amp. Unbal. (dB)	Isolation (dB)			Phase Unbal. (deg.)	VSWR S	VSWR 1	VSWR 2	VSWR 3	VSWR 4
	S-1	S-2	S-3	S-4		1-2	2-3	3-4						
0.002	6.440	6.440	6.410	6.410	0.030	28.370	24.590	29.080	0.320	1.580	1.860	1.860	1.920	1.920
0.005	6.260	6.260	6.260	6.260	0.010	29.820	30.590	29.890	0.200	1.410	1.360	1.360	1.380	1.380
0.010	6.230	6.230	6.230	6.220	0.000	30.090	35.540	30.080	0.110	1.380	1.210	1.210	1.220	1.220
0.014	6.220	6.220	6.220	6.220	0.000	30.110	37.820	30.110	0.080	1.380	1.180	1.180	1.180	1.180
0.020	6.220	6.220	6.220	6.220	0.000	30.120	39.980	30.110	0.060	1.370	1.150	1.150	1.150	1.150
0.142	6.220	6.220	6.220	6.220	0.000	30.110	44.600	30.110	0.020	1.370	1.130	1.130	1.130	1.130
0.265	6.220	6.220	6.220	6.220	0.000	30.100	44.820	30.120	0.040	1.370	1.130	1.130	1.130	1.130
0.510	6.220	6.220	6.220	6.220	0.000	30.120	44.840	30.140	0.050	1.370	1.130	1.130	1.130	1.130
1.000	6.220	6.220	6.230	6.220	0.000	30.190	44.690	30.200	0.090	1.370	1.130	1.130	1.120	1.120
5.000	6.320	6.320	6.320	6.320	0.010	31.240	42.390	31.090	0.280	1.390	1.110	1.110	1.110	1.110
10.000	6.410	6.410	6.420	6.410	0.010	32.480	39.090	31.850	0.530	1.400	1.090	1.090	1.090	1.090
12.000	6.440	6.440	6.450	6.440	0.010	32.970	38.030	32.080	0.630	1.390	1.090	1.090	1.090	1.090
15.000	6.480	6.480	6.480	6.480	0.010	33.770	36.690	32.420	0.780	1.380	1.080	1.080	1.080	1.080
18.000	6.510	6.510	6.520	6.520	0.010	34.700	35.550	32.820	0.920	1.360	1.070	1.070	1.070	1.070
20.000	6.530	6.530	6.540	6.540	0.010	35.410	34.890	33.160	1.030	1.350	1.070	1.070	1.070	1.060

1. Total Loss = Insertion Loss + 6dB splitter loss.

ZMSC-4-2
TOTAL LOSS

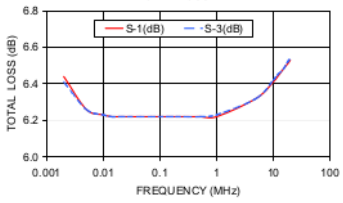

ZMSC-4-2
ISOLATION

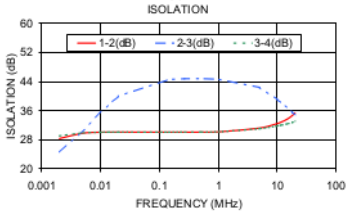

ZMSC-4-2
VSWR

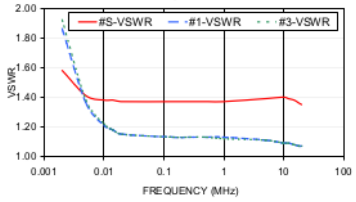

electrical schematic

Mini-Circuits®
ISO 9001 ISO 14001 AS 9100 CERTIFIED

For detailed performance specs & shopping online see web site

P.O. Box 350166, Brooklyn, New York 11235-0003 (718) 934-4500 Fax (718) 332-4661 *The Design Engineers Search Engine Provides ACTUAL Data Instantly at* minicircuits.com

IF/RF MICROWAVE COMPONENTS

REV. B
M128050
ZMSC-4-2
HY/TD/CP/AM
100719

Notes: 1. Performance and quality attributes and conditions not expressly stated in this specification sheet are intended to be excluded and do not form a part of this specification sheet. **2.** Electrical specifications and performance data contained herein are based on Mini-Circuit's applicable established test performance criteria and measurement instructions. **3.** The parts covered by this specification sheet are subject to Mini-Circuits standard limited warranty and terms and conditions (collectively, "Standard Terms"); Purchasers of this part are entitled to the rights and benefits contained therein. For a full statement of the Standard Terms and the exclusive rights and remedies thereunder, please visit Mini-Circuits' website at www.minicircuits.com/MCLStore/terms.jsp.

Annexure 13: USRP-1 Device

Ettus Research™

USRP-1 BUS SERIES

FEATURES:

- Use with GNU Radio, LabVIEW™ and Simulink™
- Modular Architecture: DC-6 GHz
- Connectivity for Two, Complete Tx/Rx chains
- Two Dual 64 MSPS, 12-bit ADC's
- Two Dual 128 MSPS, 14-bit DAC's
- DDC/DUC with 15 mHz Resolution
- Up to 64 MHz Signal Processing
- Up to 16 MHz USB Streaming
- USB 2.0 Interface to Host
- Auxiliary Digital and Analog I/O
- 25 ppm TCXO Frequency Reference

USRP-1 PRODUCT OVERVIEW:

The Ettus Research™ USRP-1 is the original hardware of the USRP™ (Universal Software Radio Peripheral) family of products, which enables engineers to rapidly design and implement powerful, flexible software radio systems. The USRP-1 provides an entry-level platform with built in MIMO expansion and a modular design allowing the hardware to operate from DC to 6 GHz. The architecture includes an Altera Cyclone FPGA, 64 MSPS dual ADC, 128 MSPS dual DAC and USB 2.0 connectivity to provide data-to-host processors.

The USRP-1 includes connectivity for two daughtercards, enabling two complete transmit/receive chains. This feature makes the USRP-1 ideal for applications that require high isolation between transmit and receive chains, or dual-band dual transmit/receive operation. The USRP-1 can stream up to 16 MHz of RF bandwidth to host applications, with 15 mHz resolution, and simplified filtering requirements with on-board DDC's and DUC's.

The USRP Hardware Driver™ is the official driver for all Ettus Research products, and supports rapid development in a comprehensive environment. The USRP Hardware Driver supports Linux, Mac OSX, Windows, NetBSD and FreeBSD.

USRP-1
BUS SERIES

SPECIFICATIONS

Spec	Typ.	Unit
POWER		
DC Input	6	V
Current Consumption	0.7	A
w/ WBX Daughterboard	1.7	A
CONVERSION PERFORMANCE AND CLOCKS		
ADC Sample Rate	64	MSPS
ADC Resolution	12	bits
ADC Wideband SFDR	85	dBc
DAC Sample Rate	128	MSPS
DAC Resolution	14	bits
DAC Wideband SFDR	83	dBc
Sample Rate to/from Host	8/16	MSPS
Frequency Accuracy	2.5	ppm
w/ GPSDO Reference	0.01	ppm

Spec	Typ.	Unit
RF PERFORMANCE (W/ WBX)		
SSB/LO Suppression	35/50	dBc
Phase Noise(1.8 Ghz)		
10 kHz	-80	dBc/Hz
100 kHz	-100	dBc/Hz
1 MHz	-137	dBc/Hz
Power Output	15	dBm
IIP3	0	dBm
Receive Noise Figure	5	dB
PHYSICAL		
Operating Temperature	0 to 55°	C
Dimensions (l x w x h)	18x21 x5.5	cm
Weight	0.7	kg

* All specifications are subject to change without notice.

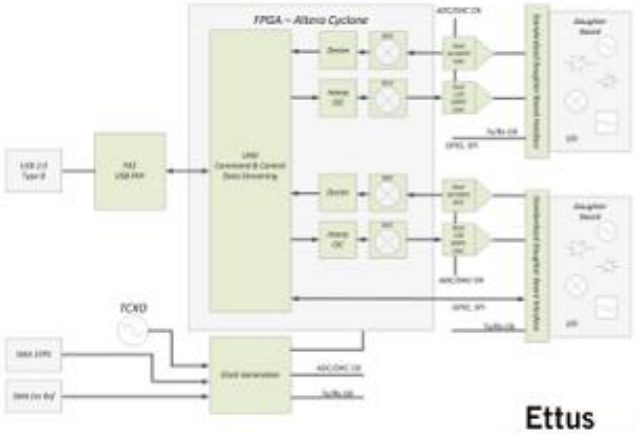

Ettus Research™

ABOUT ETTUS RESEARCH:

Ettus Research is an innovative provider of software defined radio hardware, including the original Universal Software Radio Peripheral (USRP) family of products. Ettus Research products maintain support from a variety of software frameworks, including GNU Radio. Ettus Research is a leader in the GNU Radio open-source community, and enables users worldwide to address a wide range of research, industry and defense applications. The company was founded in 2004 and is based in Mountain View, California. As of 2010, Ettus Research is a wholly owned subsidiary of National Instruments.

1043 North Shoreline Blvd
Suite 100
Mountain View, CA 94043

P 650.967.2870 www.ettus.com
F 866.807.9801

Annexure 14: Band-Pass Filter Mini-Circuits VBFZ-780

Coaxial

Bandpass Filter

VBFZ-780+

50Ω 710 to 850 MHz

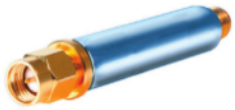

Maximum Ratings

Operating Temperature	-55°C to 100°C
Storage Temperature	-55°C to 100°C
RF Power Input*	7W at 25°C

*Passband rating, derate linearly to 3W at 100°C ambient. Permanent damage may occur if any of these limits are exceeded.

Features

- Good Rejection, 30dB up to 16GHz
- Low insertion loss
- Excellent power handling, 7W
- Temperature stable LTCC internal structure
- Rugged stainless steel unibody
- Protected by US Patent 6,943,646

Application

- Harmonic rejection
- Transmitters/receivers
- Lab use
- Test instrumentation

CASE STYLE: FF1145

Connectors	Model	Price	Qty.
SMA	VBFZ-780-S+	$39.95 ea.	(1-9)

+RoHS Compliant
The +Suffix identifies RoHS Compliance. See our web site for RoHS Compliance methodologies and qualifications

Outline Drawing

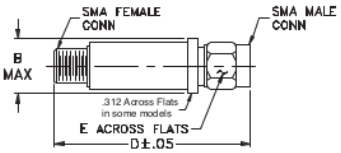

Outline Dimensions (inch / mm)

B	D	E	wt.
.410	1.91	.312	grams
10.41	48.51	7.92	11.8

Bandpass Filter Electrical Specifications (T_{AMB}= 25°C)

CENTER FREQ. (MHz)	PASSBAND (MHz) (Loss < 2.5dB)	STOPBANDS (MHz) (Loss > 20dB)		(Loss 30dB Typ)		VSWR (:1) Passband		VSWR (:1) Stopband
Fc	F1 - F2	F3	F4	F5	F6	Typ.	Max.	Typ.
780	710 - 850	460	1300	440	1320 - 16000	1.6	2.3	20

Typical Frequency Response

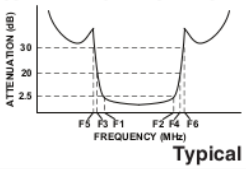

Functional Schematic

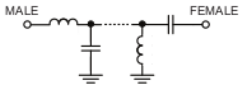

Typical Performance Data at 25°C

Frequency (MHz)	Insertion Loss (dB)	VSWR (:1)
10	79.73	6806.77
80	65.09	2913.45
250	57.62	233.19
440	33.58	40.34
460	29.32	33.32
510	19.74	19.36
542	14.26	12.39
595	6.78	4.72
643	3.19	2.14
710	1.87	1.42
780	1.76	1.55
850	2.01	1.86
1052	3.95	2.08
1105	7.91	3.31
1158	15.43	5.32
1300	30.97	14.04
1320	31.84	15.36
3000	76.71	66.69
8000	47.70	8.93
16000	45.21	19.38

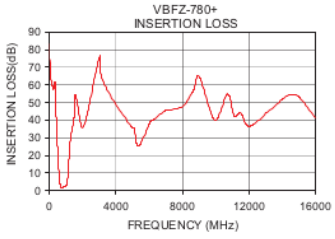

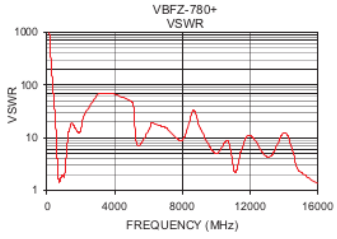

REV. B
M131793
EDR-9444U
VBFZ-780+
URJ/RAV
121016
Page 1 of 1

Annexure 15: 4-way Splitter Mini-Circuits ZC4PD-18-S+

Coaxial

Power Splitter/Combiner

4 Way-0° 50Ω 1000 to 1800 MHz

ZC4PD-18+
ZC4PD-18

CASE STYLE: Z184

Connectors	Model	Price	Qty.
SMA	ZC4PD-18-S(+)	$91.95	(1-9)

+ RoHS compliant in accordance with EU Directive (2002/95/EC)

The +Suffix identifies RoHS Compliance. See our web site for RoHS Compliance methodologies and qualifications.

Maximum Ratings

Operating Temperature	-55°C to 100°C
Storage Temperature	-55°C to 100°C
Power Input (as a splitter)	10W max.
Internal Dissipation	0.375W max.

Permanent damage may occur if any of these limits are exceeded.

Coaxial Connections

SUM PORT	S
PORT 1	1
PORT 2	2
PORT 3	3
PORT 4	4

Features

- wideband, 1000 to 1800 MHz
- high isolation, 32 dB typ.
- up to 10W power input as splitters
- good VSWR, 1.10:1 typ.

Applications

- GPS
- communication systems

Outline Drawing

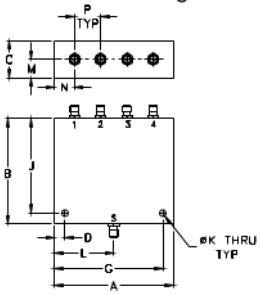

Outline Dimensions (inch / mm)

A	B	C	D	G	J
2.26	2.00	.70	.200	2.060	1.800
57.40	50.80	17.78	5.08	52.32	45.72

K	L	M	N	P	wt
.125	1.13	.35	.38	.500	grams
3.18	28.70	8.89	9.65	12.70	59

Electrical Specifications

FREQ. RANGE (MHz)	ISOLATION (dB)		INSERTION LOSS (dB) ABOVE 6.0 dB		PHASE UNBALANCE (Degrees)	AMPLITUDE UNBALANCE (dB)	VSWR (:1)			
							S		OUT	
f_L-f_U	Typ.	Min.	Typ.	Max.	Max.	Max.	Typ.	Max.	Typ.	Max.
1000-1800	32	18	0.3	0.8	6	0.40	1.05	1.55	1.08	1.45

Typical Performance Data

Freq. (MHz)	Total Loss[1] (dB)				Amp. Unbal. (dB)	Isolation (dB)			Phase Unbal. (deg.)	VSWR S	VSWR 1	VSWR 2	VSWR 3	VSWR 4
	S-1	S-2	S-3	S-4		1-2	2-3	3-4						
1000.00	6.35	6.34	6.35	6.34	0.01	26.64	34.99	27.84	0.31	1.19	1.13	1.13	1.12	1.12
1100.00	6.31	6.34	6.35	6.32	0.03	35.48	40.94	38.87	0.25	1.08	1.09	1.09	1.09	1.09
1140.00	6.25	6.28	6.31	6.26	0.05	43.36	39.59	48.11	0.25	1.08	1.08	1.08	1.08	1.09
1200.00	6.32	6.34	6.34	6.32	0.03	45.51	36.37	39.28	0.30	1.15	1.08	1.08	1.08	1.09
1240.00	6.29	6.32	6.33	6.32	0.04	38.82	34.55	35.71	0.30	1.12	1.06	1.07	1.07	1.08
1300.00	6.32	6.33	6.35	6.34	0.03	34.79	32.55	33.06	0.32	1.17	1.06	1.06	1.06	1.06
1340.00	6.35	6.36	6.39	6.38	0.04	33.40	31.61	32.09	0.26	1.10	1.08	1.08	1.08	1.09
1400.00	6.37	6.36	6.40	6.37	0.03	32.13	30.71	31.22	0.34	1.10	1.03	1.03	1.04	1.04
1440.00	6.39	6.38	6.42	6.39	0.04	31.72	30.35	30.88	0.38	1.07	1.07	1.07	1.08	1.09
1500.00	6.41	6.38	6.44	6.40	0.06	31.74	30.20	30.91	0.34	1.03	1.04	1.04	1.05	1.06
1540.00	6.37	6.36	6.40	6.38	0.04	32.43	30.30	31.37	0.37	1.04	1.04	1.05	1.07	1.07
1600.00	6.41	6.40	6.45	6.42	0.05	34.57	30.99	32.74	0.60	1.02	1.03	1.04	1.06	1.06
1640.00	6.38	6.37	6.40	6.38	0.03	35.90	31.69	33.09	0.56	1.05	1.05	1.06	1.09	1.08
1700.00	6.42	6.43	6.46	6.44	0.04	32.54	33.47	30.46	0.55	1.08	1.04	1.05	1.07	1.07
1800.00	6.52	6.54	6.53	6.50	0.04	24.16	38.22	23.50	0.60	1.23	1.10	1.11	1.14	1.13

1. Total Loss = Insertion Loss + 6dB splitter loss.

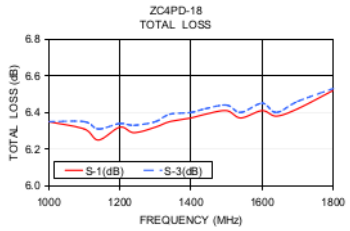

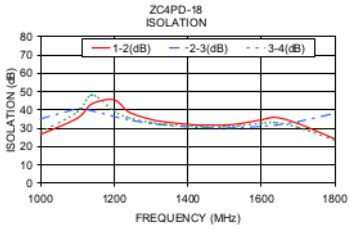

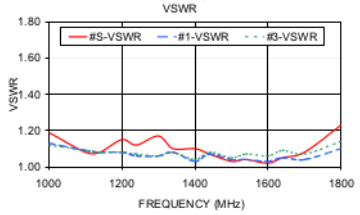

electrical schematic

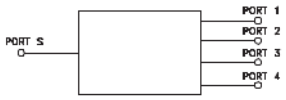

Mini-Circuits®
ISO 9001 ISO 14001 AS 9100 CERTIFIED

For detailed performance specs & shopping online see web site

P.O. Box 350166, Brooklyn, New York 11235-0003 (718) 934-4500 Fax (718) 332-4661 *The Design Engineers Search Engine Provides ACTUAL Data Instantly at* minicircuits.com

IF/RF MICROWAVE COMPONENTS

REV. B
M134941
ZC4PD-18
HY/TD/CP/AM
111207

Annexure 16: Adding and Multiplying Correlator spread sheet

A (V)	f (Hz)	t	ϕ (varying)	v1(t)	v2(t)	Added	Multiplied	Correlated	Smoothed	(Added)^2
1	2,5	0,01	0	0,156434465	0,156434	0,3128689	0,02447174			0,09788697
		0,02	4	0,309016994	0,287808	0,5968248	0,08893752			0,35619989
		0,03	8	0,4539905	0,413955	0,8679454	0,18793161	0,100447		0,75332928
		0,04	12	0,587785252	0,532585	1,1203703	0,31304562	0,196638	0,100446955	1,25522955
		0,05	16	0,707106781	0,641544	1,3486507	0,45364005	0,318206	0,10525652	1,8188587
		0,06	20	0,809016994	0,738853	1,54787	0,59774465	0,45481	0,115903982	2,39590159
		0,07	24	0,891006524	0,822745	1,7137518	0,73307145	0,594819	0,132849288	2,93694539
		0,08	28	0,951056516	0,891697	1,8427539	0,84805463	0,72629	0,15594776	3,39574202
		0,09	32	0,987688341	0,944457	1,9321455	0,93282934	0,837985	0,184464884	3,73318631
		0,1	36	1	0,980067	1,9800666	0,98006658	0,920317	0,217140897	3,92066365
		0,11	40	0,987688341	0,997879	1,9855673	0,98559343	0,966163	0,252299694	3,94247755
		0,12	44	0,951056516	0,997571	1,9486274	0,94874631	0,971469	0,287992865	3,79714883
		0,13	48	0,891006524	0,979148	1,8701545	0,87242723	0,935589	0,322166661	3,49747785
		0,14	52	0,809016994	0,942945	1,7519617	0,7628583	0,861344	0,352837777	3,06936985
		0,15	56	0,707106781	0,889619	1,5967253	0,62905531	0,75478	0,378263086	2,5495318
		0,16	60	0,587785252	0,820138	1,4079231	0,48206492	0,62466	0,397088946	1,9822474
		0,17	64	0,4539905	0,735764	1,1897547	0,33402997	0,481717	0,408467474	1,41551634
		0,18	68	0,309016994	0,63803	0,9470469	0,19716209	0,337752	0,412129937	0,89689787
		0,19	72	0,156434465	0,52871	0,6851441	0,08270841	0,204633	0,408411056	0,46942244
		0,2	76	-3,2157E-16	0,409789	0,4097885	-1,318E-16	0,09329	0,398222178	0,16792664
		0,21	80	-0,15643447	0,283426	0,1269916	-0,0443376	0,01279	0,382975578	0,01612687
		0,22	84	-0,30901699	0,151917	-0,1571	-0,0469449	-0,03043	0,364466312	0,02468044
		0,23	88	-0,4539905	0,017649	-0,436341	-0,0080125	-0,0331	0,344721621	0,19039384
		0,24	92	-0,58778525	-0,11694	-0,704724	0,06873516	0,004593	0,325830623	0,49663662
		0,25	96	-0,70710678	-0,2494	-0,956511	0,17635531	0,079026	0,309768721	0,91491301

		0,26	100	-0,80901699	-0,37734	-1,186357	0,30527445	0,183455	0,298231584	1,40744285
		0,27	104	-0,89100652	-0,49842	-1,38943	0,44409883	0,308576	0,292492754	1,93051653
		0,28	108	-0,95105652	-0,61046	-1,561513	0,58057882	0,443317	0,293296926	2,43832351
		0,29	112	-0,98768834	-0,7114	-1,699093	0,70264579	0,575774	0,300797948	2,88691599
		0,3	116	-1	-0,79943	-1,799434	0,79943364	0,694219	0,314546774	3,23796143
		0,31	120	-0,98768834	-0,87295	-1,860634	0,86219862	0,788093	0,333530406	3,46196028
		0,32	124	-0,95105652	-0,93061	-1,881663	0,88505949	0,848897	0,35625852	3,54065616
		0,33	128	-0,89100652	-0,97137	-1,862375	0,86549553	0,870918	0,380890457	3,46844014
		0,34	132	-0,80901699	-0,99449	-1,803508	0,80456013	0,851705	0,405391828	3,25264113
		0,35	136	-0,70710678	-0,99955	-1,706662	0,70679194	0,792283	0,427707489	2,91269356
		0,36	140	-0,58778525	-0,98647	-1,574253	0,5798311	0,697061	0,445936241	2,47827199
		0,37	144	-0,4539905	-0,95547	-1,409458	0,43377302	0,573465	0,458492482	1,98657096
		0,38	148	-0,30901699	-0,90712	-1,216133	0,28031441	0,431306	0,464241125	1,47898063
		0,39	152	-0,15643447	-0,84229	-0,998728	0,13176373	0,28195	0,462594378	0,99745749
		0,4	156	2,41951E-15	-0,76218	-0,762175	-1,844E-15	0,137359	0,453562178	0,58091115
		0,41	160	0,156434465	-0,66822	-0,511782	-0,1045321	0,009077	0,437752038	0,26192111
		0,42	164	0,309016994	-0,56212	-0,253107	-0,1737059	-0,09275	0,416318296	0,06406321
		0,43	168	0,4539905	-0,44582	0,0081666	-0,2023998	-0,16021	0,390865081	6,6694E-05
		0,44	172	0,587785252	-0,32143	0,2663573	-0,1889306	-0,18835	0,363311197	0,07094624
		0,45	176	0,707106781	-0,1912	0,5159116	-0,1351954	-0,17551	0,335728365	0,26616481
		0,46	180	0,809016994	-0,05749	0,7515265	-0,0465108	-0,12355	0,310166518	0,56479209
		0,47	184	0,891006524	0,077258	0,9682647	0,06883751	-0,03762	0,288480913	0,93753647
		0,48	188	0,951056516	0,210604	1,1616604	0,20029616	0,074208	0,272175723	1,34945479
		0,49	192	0,987688341	0,340125	1,3278135	0,33593769	0,20169	0,262277318	1,76308879
		0,5	196	1	0,46347	1,4634702	0,46347022	0,333235	0,259247975	2,14174509
		0,51	200	0,987688341	0,578399	1,5660874	0,57127805	0,456895	0,262947311	2,45262989